1-10-2013 12:00 AM

Variability in Characteristics of Ground Motions Across North America

Alireza Babaie Mahani, *The University of Western Ontario*

Supervisor: Dr. Gail M. Atkinson, *The University of Western Ontario*

A thesis submitted in partial fulfillment of the requirements for the Doctor of Philosophy degree in Geophysics

VARIABILITY IN CHARACTERISTICS OF GROUND MOTIONS ACROSS NORTH AMERICA

(Thesis format: Integrated Article)

by

Alireza Babaie Mahani

Graduate Program in Geophysics

A thesis submitted in partial fulfillment
of the requirements for the degree of
Doctor of Philosophy

The School of Graduate and Postdoctoral Studies
The University of Western Ontario
London, Ontario, Canada

THE UNIVERSITY OF WESTERN ONTARIO
School of Graduate and Postdoctoral Studies

CERTIFICATE OF EXAMINATION

Supervisor

Dr. Gail M. Atkinson

Supervisory Committee

Dr. Kristy F. Tiampo

Dr. Robert Shcherbakov

Examiners

Dr. Martin Chapman

Dr. Hesham ElNeggar

Dr. Kristy F. Tiampo

Dr. Robert Shcherbakov

The thesis by

Alireza Babaie Mahani

entitled:

Variability in characteristics of ground motions across North America

is accepted in partial fulfillment of the
requirements for the degree of
Doctor of Philosophy

Date

Chair of the Thesis Examination Board

Abstract

In this study, ground motions from earthquakes in North America with moment magnitude (**M**) 3.0 to 6.0 were investigated to reveal regional differences in ground motion amplitudes.

First, we examined several attenuation forms to evaluate their ability to describe the decay of response spectral amplitudes in different regions across North America. Linear, bi-linear and tri-linear regression forms with different combinations of geometric spreading coefficients were tested to assess their ability to describe spectral amplitude decay from 0.33 to 10 Hz in the distance range from 10 to 400 km. We found that the linear model has steeper slope in the west (~1.3) than in the east (~1), and may not extend well over large distances. The bi-linear form offers a good compromise between simplicity and the ability to model amplitude decay appropriately at both near and regional distances. Although tri-linear models are a better fit to the data in some regions (Eastern North America), they may have no practical advantage over simpler models.

In the second step, a simple and robust approach to estimate moment magnitude (**M**) for events of **M**<6 was presented from regional seismographic observations (vertical component), recorded in the distance range from 100 to 400 km. **M** can be estimated from 1-Hz response spectral amplitudes for events in North America with an uncertainty (standard deviation of residuals) of <0.2 units in most regions, using the simple relationships provided herein.

Finally, regional differences in amplitudes across North America were investigated. Ratios of log-averaged response spectral amplitudes in each region to those in Southern California were examined to identify the effects of magnitude, frequency and distance on regional differences. For the horizontal component, differences due to site effects were considered by correcting all amplitudes to equivalent values for B/C boundary site conditions. It was assumed that site effects on the vertical component are negligible. We find that most of the observed amplitude differences appear to be attributable to complex frequency-dependent differences in regional attenuation. For example, the change in the slope of apparent geometric spreading due to the transition from direct body waves to surface waves occurs at closer distances in Eastern Canada/Northeastern United States than other regions, and may be

frequency-dependent. Regional differences in ground-motion amplitudes across North America show a clear frequency and distance dependence. This dependency is especially significant between ground motions in Eastern North America versus Southern California.

Keywords: Attenuation, moment magnitude, site conditions, geometric spreading, North America

Co-Authorship Statement

The materials present in chapters 2, 3, and 4 of this thesis have been previously published or submitted for publication to the peer-reviewed journal of *Bulletin of Seismological Society of America*. This thesis contains only the original results of research conducted by the candidate under supervision of his mentor. The original contributions are summarized as follows:

Catalogue/waveform acquisition from CNSN, POLARIS, LD, SLU, CERI, and UW networks for earthquakes with M > 3.0 from 1990-2011; Data processing of the earthquake waveforms for Eastern Canada/Northeastern United States, Central United States, and Pacific Northwest/British Columbia; Calculation/tabulation of ground-motion parameters including peak ground acceleration, peak ground velocity and response spectral ordinates (PSA); Regression analysis and obtaining ground motion prediction equations; Statistical analysis such as analysis of residuals and AIC; Moment magnitude estimation from 1-Hz PSA at regional distances; Point source stochastic simulations; Analysis of ground-motion amplitudes to reveal regional differences across north America including ground motion binning, ratio analysis of binned ground motions, and H/V analysis.

Professor Atkinson was my co-author in two of the articles presented in this thesis (chapters 2 and 4). She is the first author for the article presented in chapter 3.

Acknowledgments

I would like to thank my supervisor Dr. Gail M. Atkinson for her continuous support throughout the completion of this research. I would also like to extend my gratitude to Dr. Karen Assatourians. His help in processing of earthquake waveforms is appreciated.

Table of Contents

List of Tables

List of Figures

List of Appendices

List of frequently-used symbols and acronyms

AIC	Akaike Information Criterion
b	Geometric spreading coefficient
β	Shear-wave velocity
CUS	Central United States
ENA	Eastern North America
f	Frequency in Hz
g	Anelastic attenuation coefficient
GMPE	Ground Motion Prediction Equation
H/V ratio	Ratio of the horizontal to the vertical component of ground motion
MAICE	Minimum AIC Estimate
M	Moment magnitude
NEHRP	National Earthquake Hazard Reduction Program
NGA	Next Generation Attenuation
Northeast	Eastern Canada/Northeastern United States
PGA	Peak Ground Acceleration
PGV	Peak Ground Velocity
PSA	Pseudo-Spectral Acceleration
PNW/BC	Pacific Northwest/British Columbia
Q	Quality factor

Vs30	Time-averaged shear-wave velocity over top 30 m
WNA	Western North America

Chapter 1

1 Introduction

1.1 Purpose and significance of the study

The purpose of this study is to understand regional differences in ground motion characteristics across North America. This goal is important since it is helpful in developing ground-motion models, and in the development of ground motion prediction equations (GMPEs) in regions with sparse recorded ground-motion data (e.g. eastern Canada). Such process models and GMPEs are important in engineering seismology, and play a major role in seismic hazard assessment. If we can understand regional differences in ground motions, we can transfert knowledge gained in regions with a rich ground-motion database to other regions. In this study, we examine regional differences in ground-motion amplitudes for eathquakes with moment magnitude from 3.0 to 6.0. This study covers the regions of Eastern Canada/Northeastern United States, Central United States, including the New Madrid Seismic Zone, the Pacific Northwest/British Columbia (PNW/BC), Offshore PNW/BC, and California.

1.2 Organization of thesis

The study is presented in 5 Chapters in this thesis. Chapter 1 introduces the work and provides background material relevant to the subject. Chapter 2 focuses on attenuation of response spectral amplitudes for small-to-moderate earthquakes across North America. Different functional forms of attenuation were tested to derive a conclusion on what functional form of attenuation best fits response spectral amplitudes. Chapter 3 presents a simple yet practical method for estimation of moment magnitude from 1-Hz (vertical) response spectral amplitudes at regional distances, in order to facilitate determination of consistent moment magnitudes for study events in all regions. Chapter 4 compares the ground motion amplitudes for events across regions in different moment magnitude-distance bins. Finally, Chapter 5 lists overall conclusions and suggestions for future work. It is noted that Chapters 2 and 3 have been accepted for publication in *Bull. Seism. Soc. Am.*; Chapter 4 has been submitted for publication in *Bull. Seism. Soc. Am.* (Dec.

2012). The thesis also includes two appendices. Database of ground motion amplitudes for each region in presented in Appendix A, while Appendix B contains the supplementary materials.

1.3 Characteristics of earthquake ground motions

Ground motions are the outcome of released strain energy during earthquakes. This generates seismic waves that are propagated through the earth in the manner of wave transmission (Dutton, 1904). The ground motion signal recorded at a receiver, after having travelled from the source to the recording station, is the convolution of several complicated functions with different space (amplitude) and time (period) characteristics (Figure 1.1). These functions can be divided into four main categories of source, path, site, and instrument. The overall factors influencing source, path and site may vary from one geographic region to another.

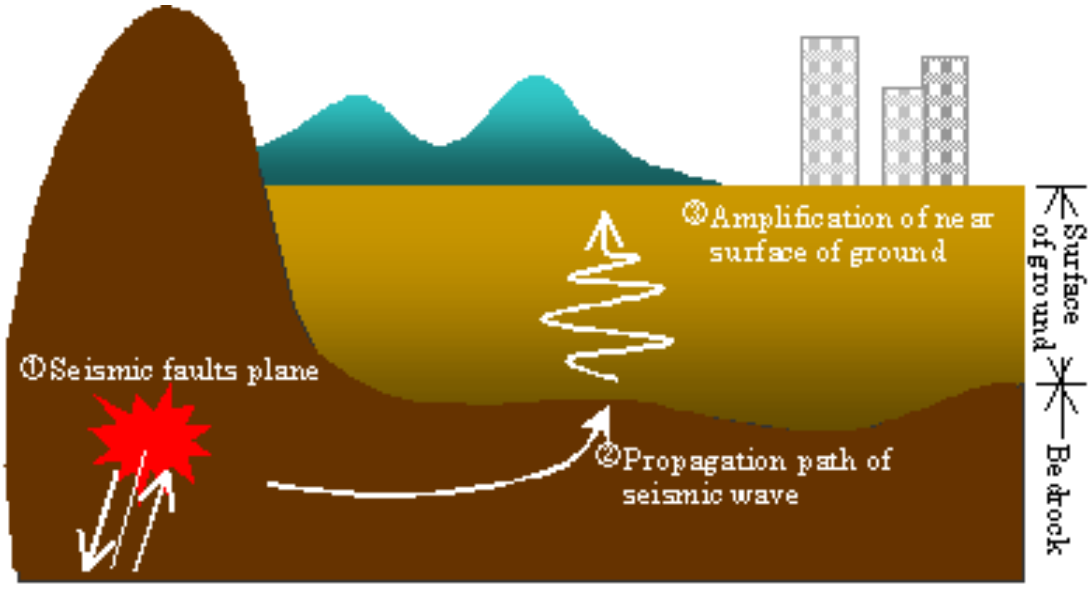

Figure 1.1 Schematic of seismic wave propagation through earth.

1.4 Source

The source spectrum is controlled by seismic moment and stress drop. The low frequency portion of the source spectrum is controlled by the seismic moment while stress drop controls the high frequency level (Stein and Wysession, 2003). Figure 1.2 shows the effect of these two parameters on the spectrum.

Figure 1.2 Source spectrum and its dependence on seismic moment (M_0) and stress drop ($\Delta\sigma$). From Boore (2003).

The source characteristics of an earthquake may be dependent on its tectonic setting. In North America, there are several distinct tectonic settings: crustal earthquakes in

California occur in an active tectonic setting; in the Pacific Northwest, there are both active crustal tectonics and subduction processes; in the Central United States and Northeast there are crustal earthquakes in distinct moderate-seismicity clusters. It is not well-known to what extent the source spectra of earthquakes of a given moment magnitude differ amongst these regions, although there are standard guidelines and expectations. For example, it is widely held that earthquake stress drops are higher in inactive as compared to active regions (e.g. Kanamori and Anderson, 1975; Atkinson and Boore, 1990).

1.5 Path

As waves travel through the earth they undergo significant transformation due to the path effects. Among these effects are geometrical spreading and anelastic attenuation. In a homogenous elastic earth, strain energy carried through waves loses its intensity in proportion to distance. For body waves (P and S waves), energy is propagated on a sphere with surface area of $4\pi R^2$ while for surface waves, energy propagates as an expanding cylinder which, for unit height, has area of $2\pi R$, where R is the distance from the source to any point on the sphere or cylinder. Therefore, energy loss for body waves can be related to $1/R^2$ while for surface waves it is 1/R. Since energy is related to the square of amplitudes, the amplitude loss for body and surface waves becomes proportional to 1/R and $1/\sqrt{R}$, respectively. This phenomenon is called geometrical spreading or elastic attenuation as the energy in propagating wave is conserved (Stein and Wysession, 2003). Elastic attenuation also includes a scattering component.

Anelastic attenuation, on the other hand, is called intrinsic attenuation as the seismic energy transforms into heat (Stein and Wysession, 2003). Anelastic attenuation is usually described by the Quality factor, which is the inverse of anelastic attenuation. This means that a higher Quality factor corresponds to lesser attenuation and vice versa. Anelastic attenuation, as opposed to geometrical spreading, is frequency dependent (Benz et al., 1997; Fatehi and Herrmann, 2008; Zandieh and Pezeshk, 2010).

1.6 Site

Site condition plays a major role in the amplitude and frequency content of recorded ground motions (e.g. Mexico City during the 1985 Michoacan earthquake, Singh et al., 1988a, Campillo et al., 1989). Seismic energy can both attenuate and amplify by the near surface materials. The attenuation of seismic waves within the near surface materials is described by kappa (κ) or f_{max} (Hough, et al., 1984; Hanks and McCuire, 1981). Ground motions are also amplified as the result of the differences in physical properties of the bedrock and soil column (Scherbaum, 1987; Williams et al., 1993; Field and Jacob, 1995).

The effects of site condition may depend on both the frequency and the amplitude of the incoming signal, as soils respond non-linearly when amplitudes exceed a certain threshold (Hartzell, 1998; Cultrera, 1999). However, in this study we consider weak motions that are generally below the threshold for non-linear behaviour, simplifying the treatment of site response.

1.7 References

Atkinson G., and D. Boore (1990). Recent Trends in Ground Motion and Spectral Response Relations for North America, *Earthquake Spectra,* **6,** 15-36.

Benz, H., A. Frankel, and D. Boore (1997). Regional Lg attenuation for the continental United States, *Bull. Seism. Soc. Am.,* **87,** 606-619.

Boore, D. M. (2003). Simulation of Ground Motion Using the Stochastic Method, *Pure Appl. Geophys.* **160,** 635-676.

Campillo, M., J. C. Gariel, K. Aki, and F. J. Sanchez-Sesma (1989). Destructive Strong Ground Motion in Mexico City: Source, Path, and Site Effects During Great 1985 Michoacan Earthquake, *Bull. Seism. Soc. Am.* **79,** 1718-1735.

Chiou, B., R. Youngs, N. Abrahamson, and K. Addo (2010). Ground-Motion Attenuation Model for Small-To-Moderate Shallow Crustal Earthquakes in California and Its

Implications on Regionalization of Ground-Motion Prediction Models, *Earthquake Spectra* **26,** 907- 926.

Cultrera, G., D. M. Boore, W. B. Joyner, C. M. Dietel (1999). Nonlinear Soil Response in the Vicinity of the Van Norman Complex Following the 1994 Northridge, California, Earthquake, *Bull. Seism. Soc. Am.* **89,** 1214-1231.

Dutton, C. E. (1904). Earthquakes in the Light of the New Seismology, *G. P. Putnam's Sons, New York*, 314 pages.

Fatehi, A., and R. B. Herrmann (2008). High-Frequency Ground-Motion Scaling in the Pacific Northwest and in Northern and Central California, *Bull. Seism. Soc. Am.,* **98,** 709-721.

Field, E. H., and K. H. Jacob (1995). A Comparison and Test of Various Site-Response Estimation Techniques, Including Three that Are Not Reference-Site Dependent, *Bull. Seism. Soc. Am.* **85,** 1127-1143.

Hanks, T. C., and R. K. McGuire (1981). The character of High-Frequency Strong Ground Motion, *Bull. Seism. Soc. Am.* **71,** 2071-2095.

Hartzell, S. (1998). Variability in Nonlinear Sediment Response During the 1994 Northridge, California, Earthquake, *Bull. Seism. Soc. Am.* **88,** 1426-1437.

Hough, S. E., J. G. Anderson, J. Brune, F. Vernon III, J. Berger, J. Fletcher, L. Haar, L. Hanks, and L. Baker (1984). Attenuation Near Anza, California, *Bull. Seism. Soc. Am.* **78,** 672-691.

Kanamori, H., and D. L. Anderson (1975). Theoretical Basis of Some Empirical Relations in Seismology, *Bull. Seism. Soc. Am.,* **65,** 1073-1095.

Scherbaum, F. (1987). Seismic Imaging of the Site Response Using Microearthquake Recordings. Part I. Method, *Bull. Seism. Soc. Am.* **77,** 1905-1923.

Singh, S. K., E. Mena, and R. Castro (1988a). Some Aspects of Source Characteristics of the 19 September 1985 Michoacan Earthquake and Ground Motion Amplification in and Near Mexico City from Strong Motion Data, *Bull. Seism. Soc. Am.* **78,** 451-477.

Stein S., and M. Wysession (2003). An Introduction to Seismology, Earthquakes, and Earth Structure, *Blackwell Publishing Ltd, UK,* 498 pages.

Williams, R. R., K. W. King, J. C. Tinsley (1993). Site Response Estimates in Salt Lake Valley, Utah, from Borehole Seismic Velocities, *Bull. Seism. Soc. Am.* **83,** 862-889.

Zandieh, A., and S. Pezeshk (2010). Investigation of Geometrical Spreading and Quality Factor Functions in the New Madrid Seismic Zone, *Bull. Seism. Soc. Am.,* **100,** 2185-2195.

Chapter 2

2 Evaluation of functional forms for the attenuation of small-to-moderate-earthquake response spectral amplitudes in North America[1]

2.1 Introduction

Ground Motion Prediction Equations (GMPEs) are key parameters in seismic hazard assessment (e.g. Green and Hall, 1994; Scherbaum et al. 2009; Atkinson and Goda, 2011). These relationships describe the attenuation of ground-motion amplitudes for a given magnitude, distance and site condition. An important element of GMPE development, especially in regions of sparse data, concerns the shape of the attenuation function that is used to parameterize the decay of amplitudes with distance. These forms typically include simple linear decay models over all distances (e.g. Joyner and Boore, 1981), hinged bi-linear forms (e.g. Street and Turcotte, 1977; Boatwright and Seekins, 2011), and hinged tri-linear forms (e.g. Atkinson and Mereu, 1992; Atkinson, 2004; Allen et al. 2007). Different models have been used in different regions to model the overall attenuation features. In general, ground-motion amplitudes decrease with increasing distance from the source of the earthquakes because of the energy loss due to geometric spreading of the wave fronts and anelastic energy losses. For body waves in a homogeneous whole space, the loss of amplitude due to geometric spreading occurs at the rate of 1/R, while for surface waves in a half space the loss is at a lower rate of $1/\sqrt{R}$ (where R is hypocentral distance). At distances of around 70 km, waves which impinge on the Moho discontinuity at an angle more than the critical angle may result in strong post-critical reflections, with an increase in amplitudes (Burger et al. 1987). At regional distances, more than ~140 km, the decreases of amplitudes goes as $1/\sqrt{R}$, as waves are comprised of multiple reflections and refractions and propagate as surface waves (Ou and

[1] A version of this chapter has been published. Babaie Mahani, A., and G. M. Atkinson (2012). Evaluation of Functional Forms for the Attenuation of Small-to-Moderate-Earthquake Response Spectral Amplitudes in North America, *Bull. Seism. Soc. Am.* **102,** 2714-2726.

Herrmann, 1990). Potentially then, the attenuation might be modeled with linear, bi-linear or tri-linear forms, with the latter forms being used to incorporate the effect of the Moho bounce and surface wave spreading at regional distances.

The purpose of this study is to evaluate the ability of different attenuation shapes (linear, bi-linear, and tri-linear) to fit the decay of ground-motion amplitudes in different regions across North America, including Eastern Canada/Northeastern United States (Northeast), the Central United States, including New Madrid (CUS), the Pacific Northwest/British Columbia (PNW/BC), Northern California (N. California) and Southern California (S. California). To enable inter-regional comparisons, we restrict our analysis to small-to-moderate-magnitude events, for which data are available in all regions. We use response spectra (5% damped pseudo-acceleration, PSA) amplitudes for events of M 3 to 5 at distances to 400 km in Northeast, CUS, and PNW/BC, and to 200 km in California (where M is the magnitude scale reported in the catalogs).

We are evaluating PSA attenuation, but note that PSA attenuates in a similar way to Fourier spectra with some distinctions. Specifically, the decay rate may be faster for PSA at small magnitudes due to the non-stationarity of oscillator response for short-duration signals. At larger magnitudes, finite fault effects cause a slowing of the apparent attenuation at small source-receiver distance due to geometric effects; these effects are particularly pronounced if the distance metric is fault distance (rather than hypocentral distance, which is used in this study). These effects tend to cause a magnitude dependence in attenuation (e.g. see Atkinson, 2012). Thus when comparing response spectra attenuation across regions, it is important to use a common magnitude range and to check for any potential magnitude-dependent attenuation effects.

2.2 Database for analysis

We used acceleration and velocity ground-motion data from Canadian and U.S. networks, for events of M 3 to 5. Events from offshore and volcanic activities (e.g. Mt. Saint Helens tremors) were excluded from the database. In particular, we excluded a very rich cluster of 200 small-magnitude events (3 to 3.8) in a ~1 by ~2 km region near Mt. Saint Helens, to avoid potential bias (the attenuation from this particular source would

exert undue influence because of the large number of events). Figures 2.1 and 2.2 show the location of the selected earthquakes and stations across North America.

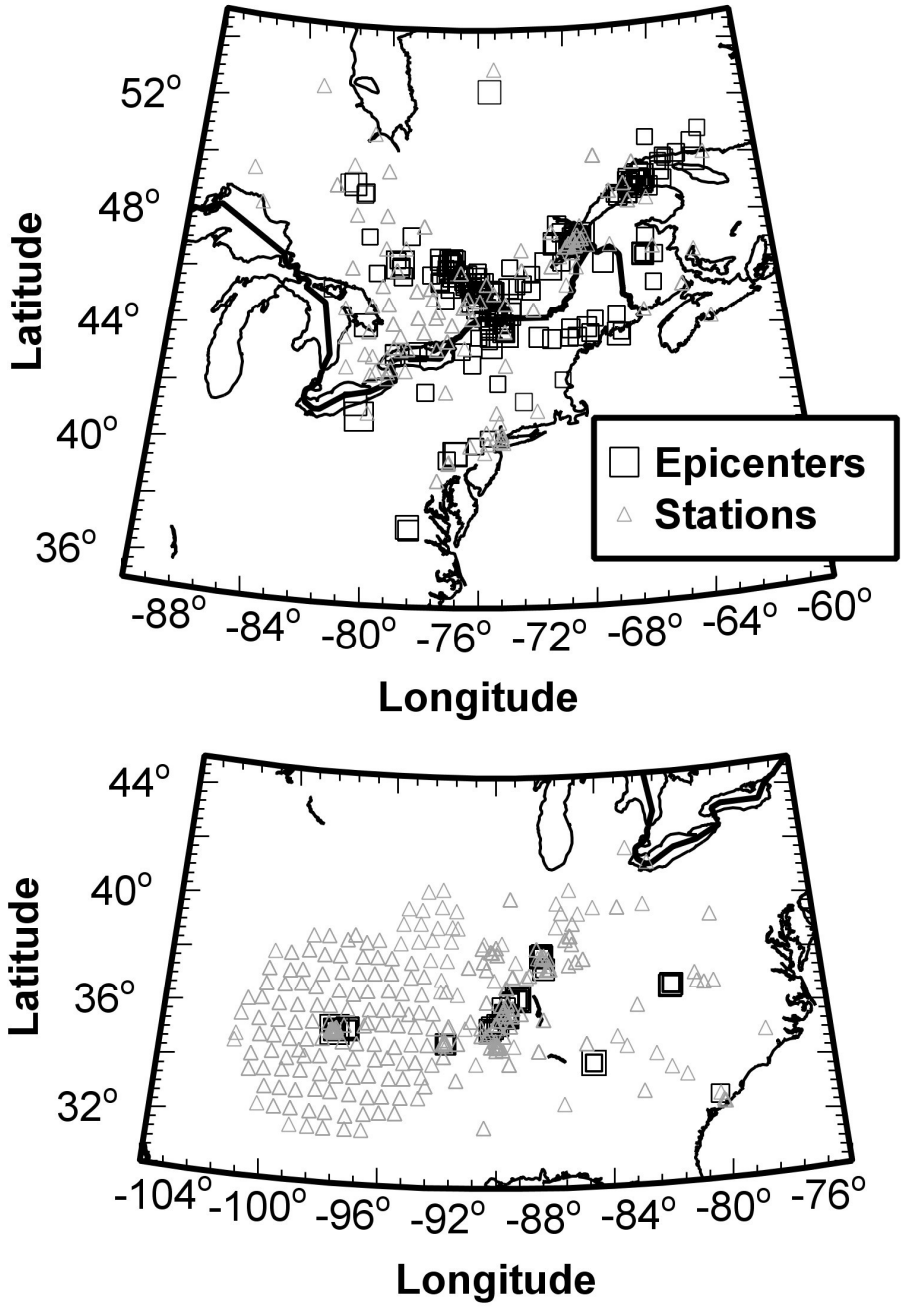

Figure 2.1 Distribution of earthquakes and stations in Eastern North America (top: Eastern Canada/Northeastern United States; bottom: Central United States). The size of epicenters corresponds to the magnitude of the events.

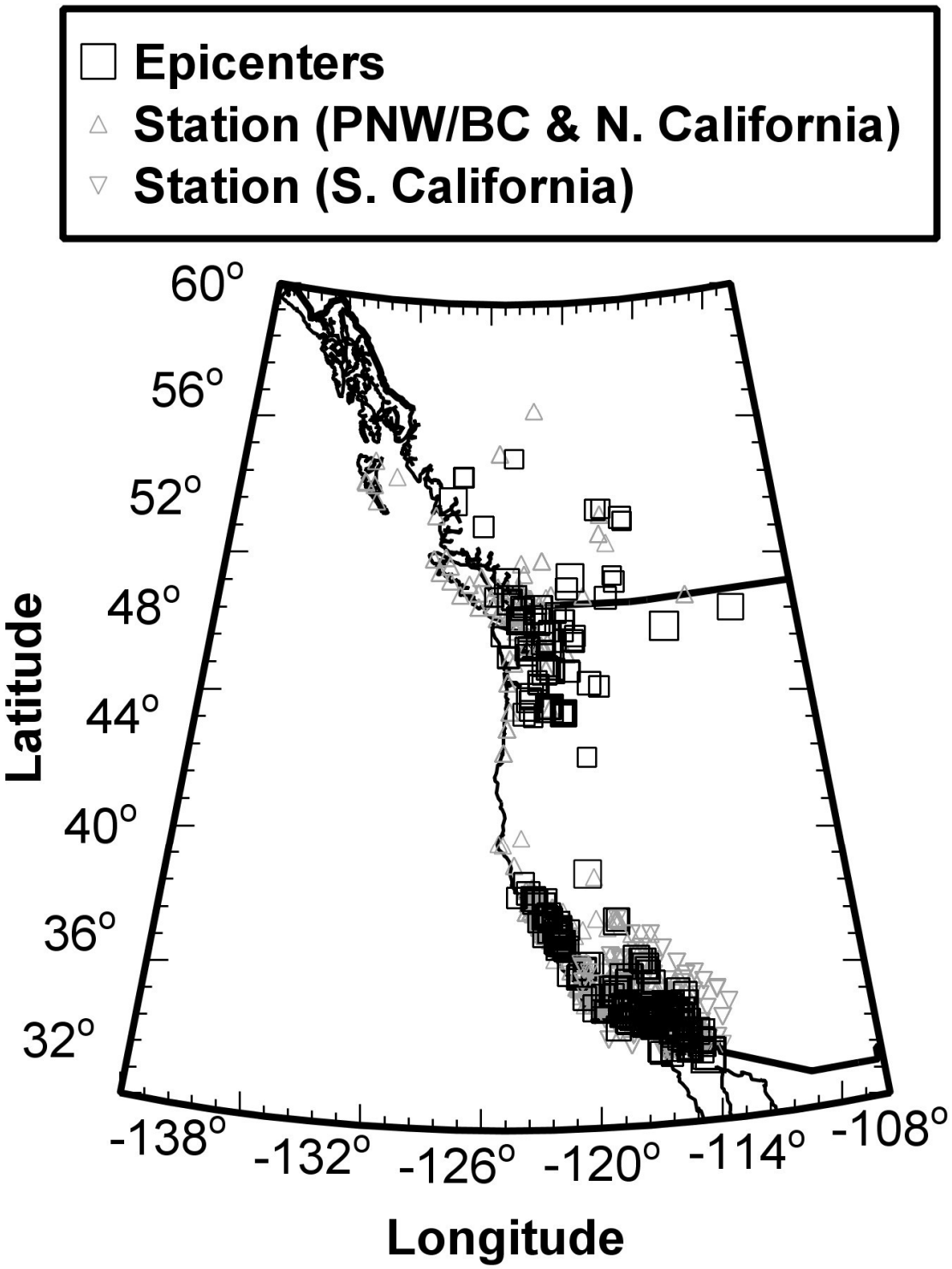

Figure 2.2 Distribution of earthquakes and stations in Western North America. The size of epicenters corresponds to the magnitude of the events.

For the PNW/BC, the events were sub-divided into crustal and in-slab groups based on the depth of the events reported in the catalogs. Events with depth less than 30 km were considered as crustal, while those with depth more than 30 km were considered as in-slab events. The depth distribution of the crustal and in-slab events is shown in Figure 2.3. For other regions, all events are crustal events. For each event, waveforms at distances up to 1000 km were downloaded; these are predominantly velocity records from regional broadband seismographic stations. Qualitative analysis of the waveforms shows a high level of noise for distances more than 400 km. Therefore, waveforms from distances more than 400 km were not considered in the analysis.

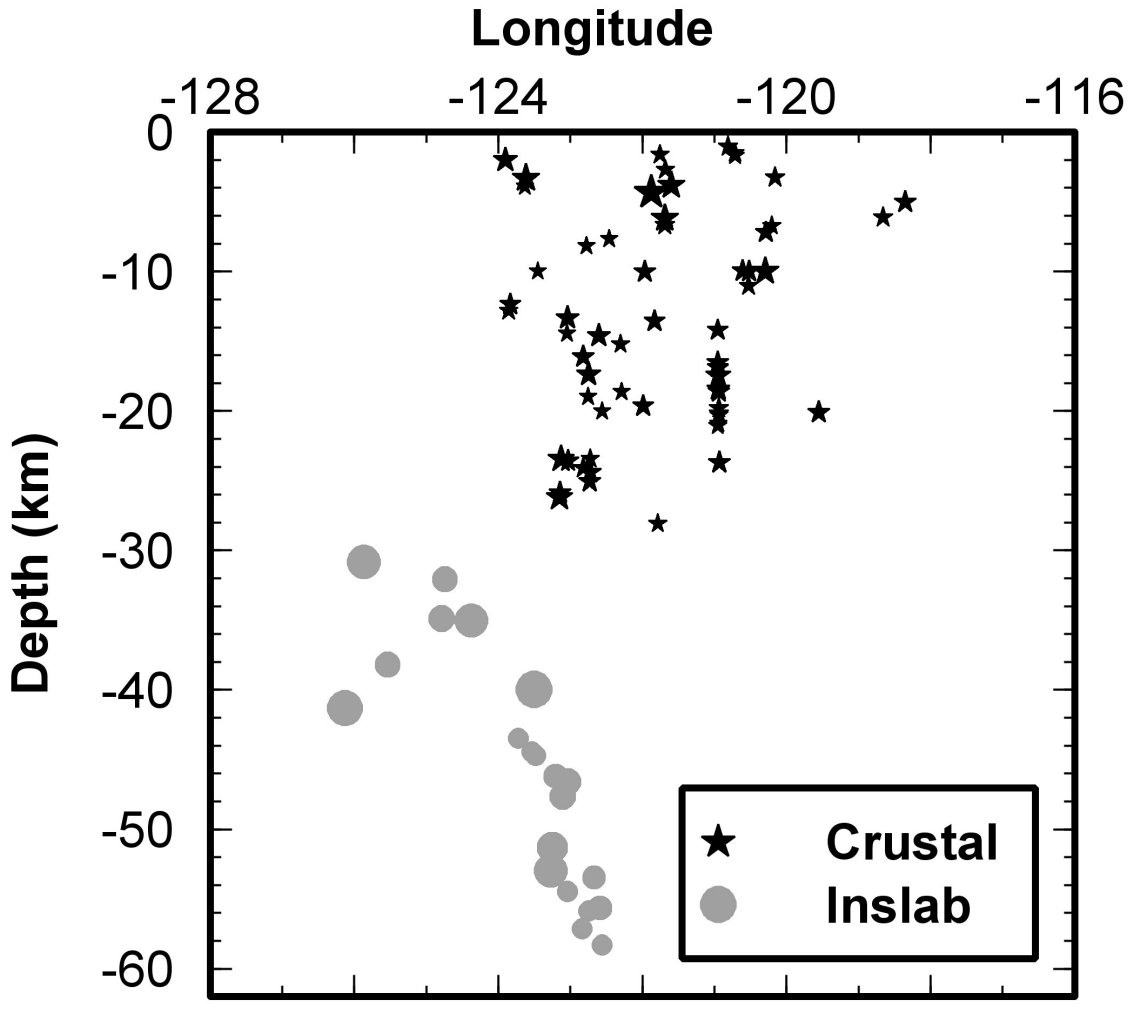

Figure 2.3 Depth distributions of the earthquakes in Pacific Northwest/British Columbia. The size of symbols corresponds to the magnitude of the events.

We initially compiled our own database for all regions except California. However, during the revision of this manuscript, the NGA-East database of PSA amplitudes for periods 0.1 to 10 sec became available. The NGA-East database contains more data for the CUS region than the one we had compiled, but not as rich as ours for the Northeast. Therefore, we decided to use the NGA-East database for the CUS; this did not change our preliminary results for the CUS significantly, but did make them more statistically robust. Similarly, we checked that use of the NGA-East database would not change the results that we obtained for the Northeast. Since our compiled database had more data for the Northeast, we retained it in preference to the NGA-East database for this region.

Processing of the waveforms was performed in several steps. The waveforms were windowed from the event origin time to the end of the S-wave coda, then checked for instrumental glitches or trends. Glitches were considered as steps or spikes in a 20-point window. A cosine window with tapering width of 0.02 (fractional width relative to the length of the signal) was applied to the waveforms prior to the Fourier Transform. A 4^{th}-order Butterworth bandpass filter with low- and high-cut frequencies of 0.1 to 50 Hz, respectively, was applied in the frequency domain. Instrument correction of velocity data was performed in the frequency domain using the Seismotoolbox software (www.seismotoolbox.ca). We chose 50 Hz as the default high-cut frequency for filtering, since the majority of stations have a sampling rate of 100 samples per second; however the high-cut was reduced to the Nyquist frequency for those stations with lower sample rates. Peak Ground Acceleration (PGA), Peak Ground Velocity (PGV), and 5% damped PSA for 200 logarithmically distributed frequencies from 0.1 to 50 Hz were calculated. We restricted our focus in the analysis that follows to the frequency range from 0.33 Hz to 10 Hz (and the distance range of <400km), to mitigate the need to look carefully at each signal to judge the useable frequency range.

For California, we used the ShakeMap database prepared by Brian Chiou (written communication, November 2011) rather than repeating the data processing. We note that the ShakeMap dataset includes PSA at 3 frequencies (0.33, 1 and 3.3 Hz), PGA and PGV. Plots of the observed data for both N. and S. California show that the low-frequency amplitudes (PSA at 0.33 Hz) do not decay after some distance, especially for smaller

magnitudes (M<4), revealing data-quality issues. We therefore restrict analysis of these data (0.33 Hz) to within the following limits: to 60 km for 3.0<M<3.6; to 100 km for 3.6<M<4; and to 200 km for M >4. For higher frequencies (more than 0.33 Hz), no such problems are apparent. With the frequency and distance restrictions as noted above for each region, the signals used for the analysis are of reasonable quality, as indicated by spot-checking of the behavior of the Fourier spectra.

The magnitudes reported in the catalog vary from region to region, and even within regions. $M_{N,}$ Nuttli magnitude (Nuttli, 1973), is the magnitude most frequently reported for events in Northeast while the local magnitude M_L, is the dominant scale in British Columbia. For the U.S. Pacific Northwest, the coda wave magnitude, M_c, is often used. Events from CUS and California are either moment magnitude, **M,** or converted to this from local scales (Brian Chiou, written communication, November 2011). In general it is preferred to convert all magnitudes to a common scale. However, in this study the source term for each event is calculated in the regression procedure (we are using the first step of a 2-step regression as described by Joyner and Boore, 1993), and we are only interested in the attenuation shape. Therefore the magnitude measures for the events are unimportant.

2.3 Characterization of site conditions

The importance of site condition in affecting ground-motion amplitudes is well known (e.g. Molnar, et al. 2004). The most commonly-used site parameter is the time-averaged shear-wave velocity in the top 30 m, Vs30 (Borcherdt, 1994). For example, the National Earthquake Hazards Reduction Program (NEHRP) classifies sites based on Vs30: (A, greater than 1500 m/s; B, between 760 and 1500 m/s; C, between 360 and 760 m/s; D, between 180 and 360 m/s; and E, less than 180 m/s). Incorporation of the effect of site geology on GMPEs, based on Vs30 classification, has been the topic of several studies (Boore et al. 1993, 1994 and 1997; Power et al. 2008). In Northeast, most seismographic stations used in this study (81 stations) are located on hard rock (Vs30 ≥ 1500 m/s) so the NEHRP site class is A (Atkinson, 2004). There are also 13 stations in category B, 11 stations in category C, 4 stations in category D and 1 station in category E. For the CUS (including New Madrid), 25 stations are in NEHRP site class B, 146 stations are in C,

107 stations are in D, and 3 stations are in category E (Chris Cramer; written communication, July 2010). For those stations in the CUS for which there is no measured Vs30 available, Wald and Allen's method (2007) was used to estimate the site condition based on topographic slope. In the PNW/BC, site conditions include NEHRP site class A (55 stations), C (16 stations) and D (1 station). British Columbia stations are generally on hard rock with NEHRP site class A (Atkinson and Morrison, 2009). In the U.S. Pacific Northwest, Wald and Allen's topographic slope method was used to estimate the site conditions of the seismographic data having no available Vs30 data. Wong et al. (2011), using the Spectral-Analysis-of-Surface-Waves (SASW) technique, obtained velocity profiles for the strong-motion sites in and around the Puget Sound region. Their Vs30 values calculated from actual velocity profiles match the Vs30 values from Wald and Allen's method well, providing confidence in the use of the Wald and Allen method. For N. California, stations are mostly in the categories C (173 stations) and D (95 stations), along with 2 stations in site class B and 3 stations in site class E. In S. California, the stations are in classes C (248 stations) and D (281stations), along with 9 stations in the B category (from Chiou et al. 2010). Figure 2.4 shows the magnitude-distance distribution of the ground-motion amplitudes for each region/site class.

2.4 Attenuation model/functional form and regression

An empirical prediction model of ground-motion amplitudes is developed by regression analysis of amplitudes against distance, magnitude and site conditions, for each frequency. Model parameters can be estimated using two-stage or maximum likelihood methods (e.g. Joyner and Boore, 1993; Brillinger and Preisler, 1984). A general form of attenuation from which ground motion parameters of source, site and path is estimated can be written as:

$$\log(Y_{ij}) = \log(S_i) + b\log(R_{ij}) + gR_{ij} + \log(I_j) + \varepsilon_{ij} \tag{2.1}$$

where Y_{ij} is the ground-motion amplitude at a specific frequency for earthquake i and station j, S_i is the source term for event i, R_{ij} is hypocentral distance and I_j is the site term for station j. The coefficients b and g are the geometric spreading and anelastic attenuation coefficients, respectively. The coefficient b is independent of frequency,

while g may be frequency dependent. Log is the base 10 logarithm. The above equation can be considered as the first step of a two-step regression in which the distance dependence is determined, along with a source term for each earthquake and a station term for each station or site category (Joyner and Boore, 1993). The residual errors in log units (ε) which are the difference between observed and predicted values, have zero mean and a standard deviation of σ (Joyner and Boore, 1993).

We can express this equation in the form $\mathbf{d} = \mathbf{Gm}$ where $\mathbf{d}$ is the data vector, $\mathbf{m}$ is the model parameters vector and $\mathbf{G}$ is the kernel or model matrix. The kernel matrix relates the data vector and model parameters vector in an analytical form, such as that of Equation (2.1). Data values (observed PSA amplitudes at a specific frequency) are stored in vector $\mathbf{d}$. The vector $\mathbf{m}$ (the output of the regression) includes a source term for each event ($log(S_i)$), the geometric spreading coefficient (b), an anelastic attenuation coefficient for each frequency (g), and a site term for each soil category (for each frequency ($log(I_j)$)). The matrix $\mathbf{G}$ includes dummy variables for each event (e.g. 1 for event i, 0 otherwise), distance vectors (in forms of R or $log\ R$) and dummy variables for each soil type (e.g. 1 for station j, 0 otherwise). We followed Menke (1989) for solving this inverse problem using the least squares approach, in which $\mathbf{m}$ can be calculated by multiplying $[\mathbf{G}^\mathbf{T}\mathbf{G}]^{-1}\mathbf{G}^\mathbf{T}$ by $\mathbf{d}$. Here, the $\mathbf{T}$ and -1 superscripts refer to the transpose and inverse of the matrix, respectively.

The site condition terms were calculated relative to a reference soil type in each region, chosen as the stiffest soil condition for which there is a reasonable sample of data. For Northeast, the reference site is soil category A; therefore 4 relative site terms were calculated, for site classes B, C, D, and E. For the CUS, site terms were calculated for site classes C, D, and E relative to a reference site class of B, because there are no rock sites (site class A) with which to anchor a reference condition. For the PNW/BC, site terms for C and D were determined with reference to A. For both N. and S. California, site class C was considered as the reference and relative site terms were determined for site classes B, D and E for N. California, and B and D for S. California. The choice of reference site class is not important in this study as our main objective is to look at the shape of the attenuation function with distance, rather than its level. Three trial functional forms of

linear, bi-linear and tri-linear attenuation were tested in this study. The bi-linear and tri-linear forms are hinged at a distance point where the slope of the line (geometric spreading) changes. There is one transition and two transitions for the bi-linear and tri-linear forms, respectively, which are defined as follows.

Linear form

The simplest attenuation model form is:

$$\log(Y_{ij}) = \log(S_i) + b\log(R_{ij}) + gR_{ij} + \log(I_j) + \varepsilon_{ij} \quad (2.2)$$

with terms as given for Equation (2.1). Here, ε is the intra-event (record-to-record) error term. The geometric spreading coefficient (b) is either set to -1 or is determined from the regression.

Bi-linear form

$$\log(Y_{ij}) = \log(S_i) + b_1 \log(R_{ij}) + b_2 \log(R_{ij} / R_t) + gR_{ij} + \log(I_j) + \varepsilon_{ij} \quad (2.3)$$

The bi-linear form is similar to the linear form, except that the slope of the geometric spreading changes after a transition distance (R_t). Three alternative transition distances of 50, 70 and 100 km were considered. Here, the near-distance geometric spreading coefficient (b_1) is either set to the fixed value of -1 or is determined from the regression, while the geometric spreading associated with the surface waves (b_2) is fixed to -0.5.

Tri-linear form

$$\log(Y_{ij}) = \log(S_i) + b_1 \log(R_{ij}) + b_2 \log(R_{ij} / R_{t1}) + b_3 \log(R_{ij} / R_{t2}) + gR_{ij} + \log(I_j) + \varepsilon_{ij} \quad (2.4)$$

The tri-linear form has two transition distances (R_{t1} and R_{t2}). Six transition zones of 50-70, 50-100, 50-140, 70-100, 70-140 and 100-140 km were tested. The geometric spreading coefficients b_1 and b_2 are either fixed to -1 and 0, respectively, or they are determined from the regression. b_3 is set to -0.5. In all cases (Equations 2.2-2.4), the anelastic coefficient, g, is determined for each frequency, while the geometric spreading coefficients are independent of frequency. Overall, there are 32 combinations of these

three forms fitted for each of databases, as summarized in Table 2.1. In this table, each of the forms is numbered; the absolute numbers (1, 2, and 3) refer to the linear, bi-linear, and tri-linear forms, respectively, while the decimal numbers refer to the subcategory. For example, 1.1 is the linear form with b_1 set to -1 and 3.15 refers to the tri-linear form with transition zone 50-70 km, b_1 = free (to be determined), b_2 = 0, and b_3 = -0.5.

Table 2-1 Parameters for the 32 scenarios of linear, bi-linear and tri-linear attenuation forms.

Form	ID	Transition distance/zone (km)	b_1	b_2	b_3	Total number of forms
Linear	1.1, 1.2	NA	-1, free	NA	NA	2
Bi-linear	2.1, 2.2, 2.3, …, 2.6	50, 70, 100	-1, free	-0.5	NA	6
Tri-linear	3.11, 3.13, 3.15, …, 3.57	50-70, 50-100, 50-140, 70-100, 70-140, 100-140	-1,free	0, free	-0.5	24

2.5 Results

We applied a common regression analysis technique using all of the 32 trial forms shown in Table 2.1 to the PSA data from each region. The data for Northeast, CUS, PNW/BC (Crustal), N. California and S. California allow regression to all 32 forms. However, note that for in-slab data in the PNW/BC, as shown in Figure 2.4, the closest distance is always larger than 50 km; therefore we consider only the linear form, and a bi-linear form with the first transition distance set >50 km. Figure 2.5 shows the near-distance geometric spreading coefficients (b_1) calculated from each of the 32 trial forms. For the linear form, b_1 is the geometric spreading coefficient for the entire distance range, but for bi-linear and tri-linear forms b_1 is the geometric spreading coefficient before the first transition distance. The majority of the candidate forms have b_1 values between -0.8 to -1.8 in all regions, with b_1 values becoming more negative (steeper) as we move from linear to bi-linear to tri-linear forms.

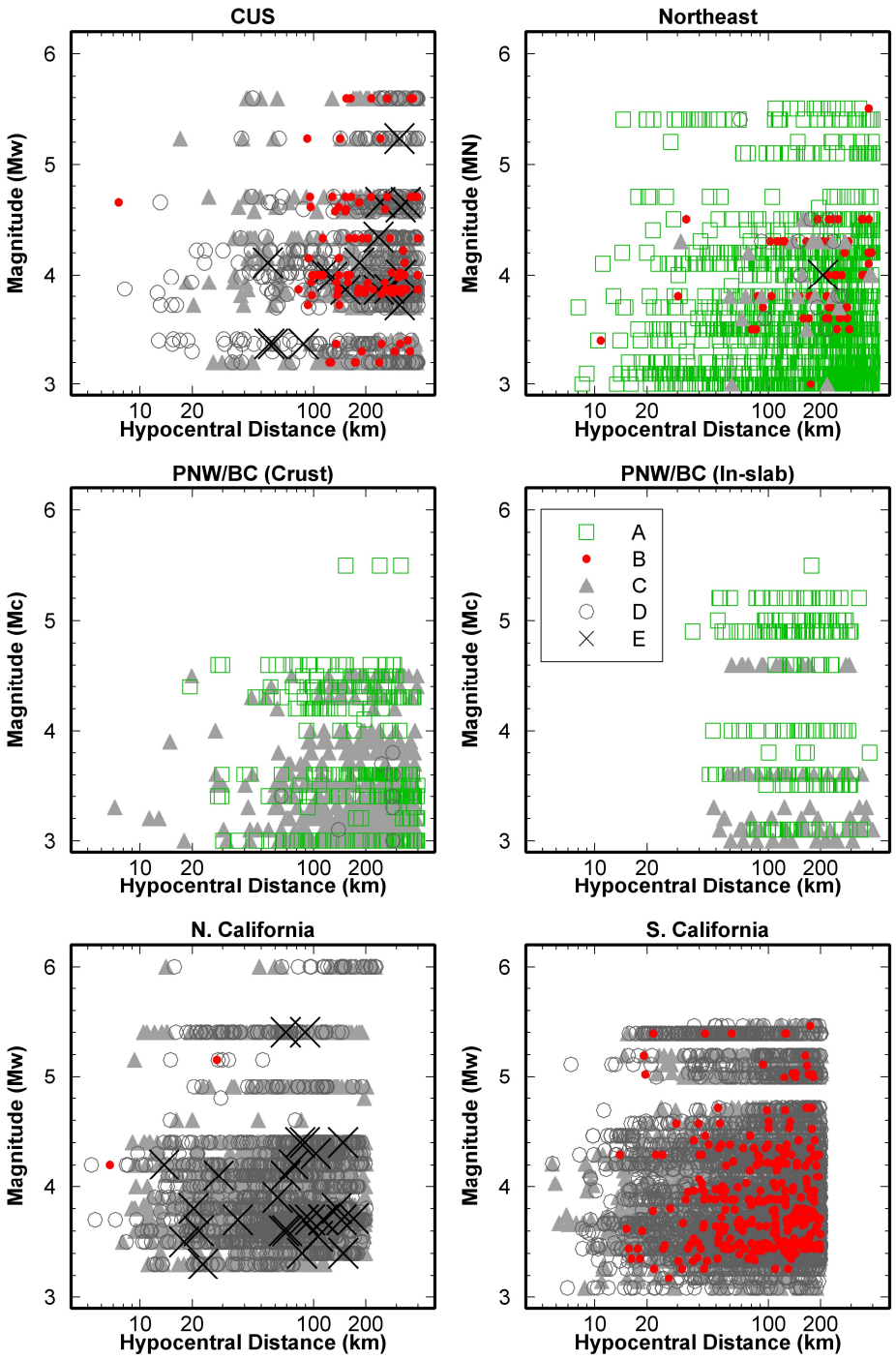

Figure 2.4 Magnitude and distance distribution of the ground-motion amplitudes (PSA, PGA and PGV) for each site class. Site classes are defined as NEHRP site categories A to E.

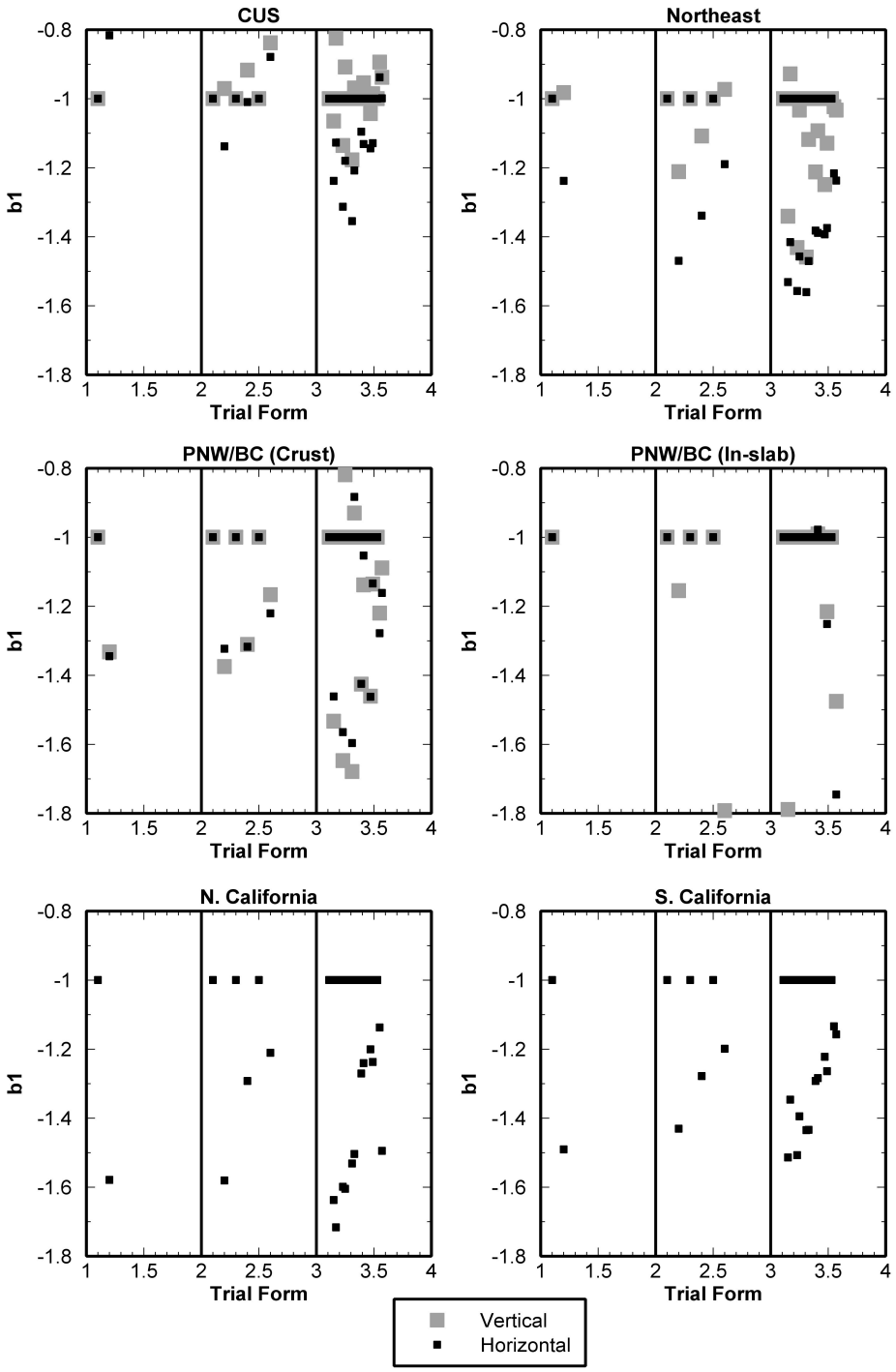

Figure 2.5 Near-distance geometric spreading coefficient (b_1) obtained for different trial function forms for vertical component and geometric mean of the horizontal components, as listed in Table 2.1. For in-slab events the tri-linear, although plotted here, is discarded due to paucity of data.

In order to assess which forms have a better fit to the data in each region, we performed an AIC, Akaike Information Criterion (Akaike, 1974), test on the candidate forms. This test allows us to compare the goodness of fit for a group of several models which are applied to the same data set, by considering the amount of information loss from each model (Sakamoto, et al, 1986). The model which has the lowest information loss is the optimum fit. The AIC can be calculated as:

AIC = 2 (number of free parameters of the model) – 2 (maximum log likelihood of the model)

(Sakamoto, et al, 1986). The preferred model is the one with the Minimum AIC Estimate (MAICE). Note that the AIC value, by itself, is not interpretable. The AIC differences among the models, $D_i = AIC_i - AIC_{min}$ where i refer to each candidate form, are, however, important and useful. The best model is that with $D_i = 0$ (Burnham and Anderson, 2002). As an example, the bi-linear form 2.2 (for geometric mean of the horizontal components) in the CUS has AIC = -177.6 when averaged over the entire frequency range. The minimum of the AICs for this dataset is that for the tri-linear form 3.17, with AIC = -451.7. Therefore $D_{2.2} = AIC_{2.2} - AIC_{3.17} = 274.1$.

The AIC difference for form 3.17 is obviously zero. Table 2.2 presents the AIC results, when averaged over the entire frequency range considered, with the MAICE highlighted in bold. Note that there is little consistency among the best forms according to the MAICE, nor among the coefficients, even for horizontal versus vertical coefficients within a single region. We conclude that the MAICE criterion is of limited usefulness, due to its general inability to clearly identify a single preferred model, and that there are several alternative models that could reasonably be considered.

In presenting the attenuation results in Table 2.2, we have chosen to convert the anelastic attenuation coefficients (g) to the more familiar inverse form that is based on the regional Quality factor Q (see Discussion for further comments on Q). We note that because we are modeling PSA rather than Fourier spectra, this is not exactly equal to Q, though it will be similar. We define the parameter Q' in terms of the anelastic coefficient (g) as:

$$Q' = [log(e)\pi f]/[g\beta] \quad (2.5)$$

(Atkinson and Mereu, 1992), where β is the shear wave velocity, and regress it against frequency to obtain the coefficients of the usual exponential form:

$$Q' = Q_0' f^{\eta'} \quad (2.6)$$

Table 2-2 Best-fit parameters for the best forms for each of the linear, bi-linear and tri-linear cases, based on the average of the AICs for the entire frequency range (0.33 to 10 Hz in CUS, Northeast, and PNW/BC; 0.33 to 3.33 Hz in California). [1]Crustal [2]In-slab

Region	Comp.	Form	R_{t1}	R_{t2}	b_1	b_2	b_3	AIC	AIC_D	σ	Q_0'	η'
CUS	H	1.1	NA	NA	-1	NA	NA	36.6	488.27	0.3	879	0.6
CUS	H	2.2	50	NA	-1.14	-0.5	NA	-177.6	274.0	0.3	369	0.6
CUS	**H**	**3.17**	**50**	**70**	**-1.13**	**-0.41**	**-0.5**	**-451.7**	**0**	**0.3**	**413**	**0.5**
CUS	**V**	**1.2**	**NA**	**NA**	**-0.79**	**NA**	**NA**	**-1664.6**	**0**	**0.3**	**798**	**0.3**
CUS	V	2.4	70	NA	-0.92	-0.5	NA	-157.7	1506.9	0.3	461	0.5
CUS	V	3.25	50	100	-0.91	-0.65	-0.5	-507.5	1157.1	0.3	695	0.2
Northeast	H	1.2	NA	NA	-1.24	NA	NA	18.2	110.7	0.2	664	1.4
Northeast	**H**	**2.4**	**70**	**NA**	**-1.34**	**-0.5**	**NA**	**-92.5**	**0**	**0.2**	**457**	**0.5**
Northeast	H	3.39	70	100	-1.38	0	-0.5	-91.5	1	0.2	362	0.4
Northeast	V	1.2	NA	NA	-0.99	NA	NA	-455.7	2756.9	0.2	631	0.6
Northeast	V	2.2	50	NA	-1.21	-0.5	NA	-72.9	3139.8	0.2	467	0.3
Northeast	**V**	**3.11**	**50**	**70**	**-1**	**0**	**-0.5**	**-3212.7**	**0**	**0.2**	**358**	**0.5**
PNW/BC(C)[1]	H	1.2	NA	NA	-1.34	NA	NA	-34.5	2414.1	0.4	687	0.7
PNW/BC (C)	H	2.6	100	NA	-1.22	-0.5	NA	-73.1	2375.5	0.4	235	0.7

PNW/BC (C)	**H**	**3.55**	**100**	**140**	**-1.28**	**0**	**-0.5**	**-2448.6**	**0**	**0.4**	**209**	**0.7**
PNW/BC (C)	V	1.2	NA	NA	-1.33	NA	NA	-177.7	4130.5	0.4	483	0.8
PNW/BC (C)	V	2.4	70	NA	-1.31	-0.5	NA	-242.1	4066.1	0.4	244	0.6
PNW/BC (C)	**V**	**3.19**	**50**	**100**	**-1**	**0**	**-0.5**	**-4308.2**	**0**	**0.4**	**187**	**0.7**
PNW/BC(I)^2	H	1.1	NA	NA	-1	NA	NA	2.9	605.2	0.3	158	0.7
PNW/BC (I)	**H**	**2.3**	**70**	**NA**	**-1**	**-0.5**	**NA**	**-602.2**	**0**	**0.3**	**104**	**0.8**
PNW/BC (I)	V	1.1	NA	NA	-1	NA	NA	19.5	349.6	0.3	220	0.6
PNW/BC (I)	**V**	**2.3**	**70**	**NA**	**-1**	**-0.5**	**NA**	**-330.1**	**0**	**0.3**	**125**	**0.7**
N. California	H	1.1	NA	NA	-1	NA	NA	-131	5258.2	0.3	115	1
N. California	H	2.4	70	NA	-1.29	-0.5	NA	-1624.7	3764.5	0.3	100	0.9
N. California	**H**	**3.47**	**70**	**140**	**-1.20**	**0**	**-0.5**	**-5389.3**	**0**	**0.3**	**72**	**0.9**
S. California	H	1.1	NA	NA	-1	NA	NA	-443.6	18565.3	0.3	240	1.1
S. California	**H**	**2.2**	**50**	**NA**	**-1.43**	**-0.5**	**NA**	**-19009**	**0**	**0.3**	**118**	**0.8**
S. California	H	3.27	50	140	-1	0	-0.5	-4166.5	14842.5	0.3	70	0.9

To understand the attenuation results, Figures 2.6 and 2.7 plot the mean residuals in distance bins of 0.1 log units, for PSA at 3.3 Hz, for the best candidate forms in each of the linear, bi-linear and tri-linear cases, based on the minimum of the AIC values, for the vertical component and the geometric mean of horizontal components.

Table 2.3 shows the parameters of the forms presented in Figures 2.6 and 2.7. As can be seen from these figures, one cannot make a clear qualitative distinction between the three functional form shapes in any region. Furthermore, all the residuals show similar trends. Overall, a simple linear model appears to fit the data relatively well in every

region. However, as we can see in Figure 2.5, the linear model has a steeper slope (*b* value) in the west (~1.3), as compared to that in the east (~1).

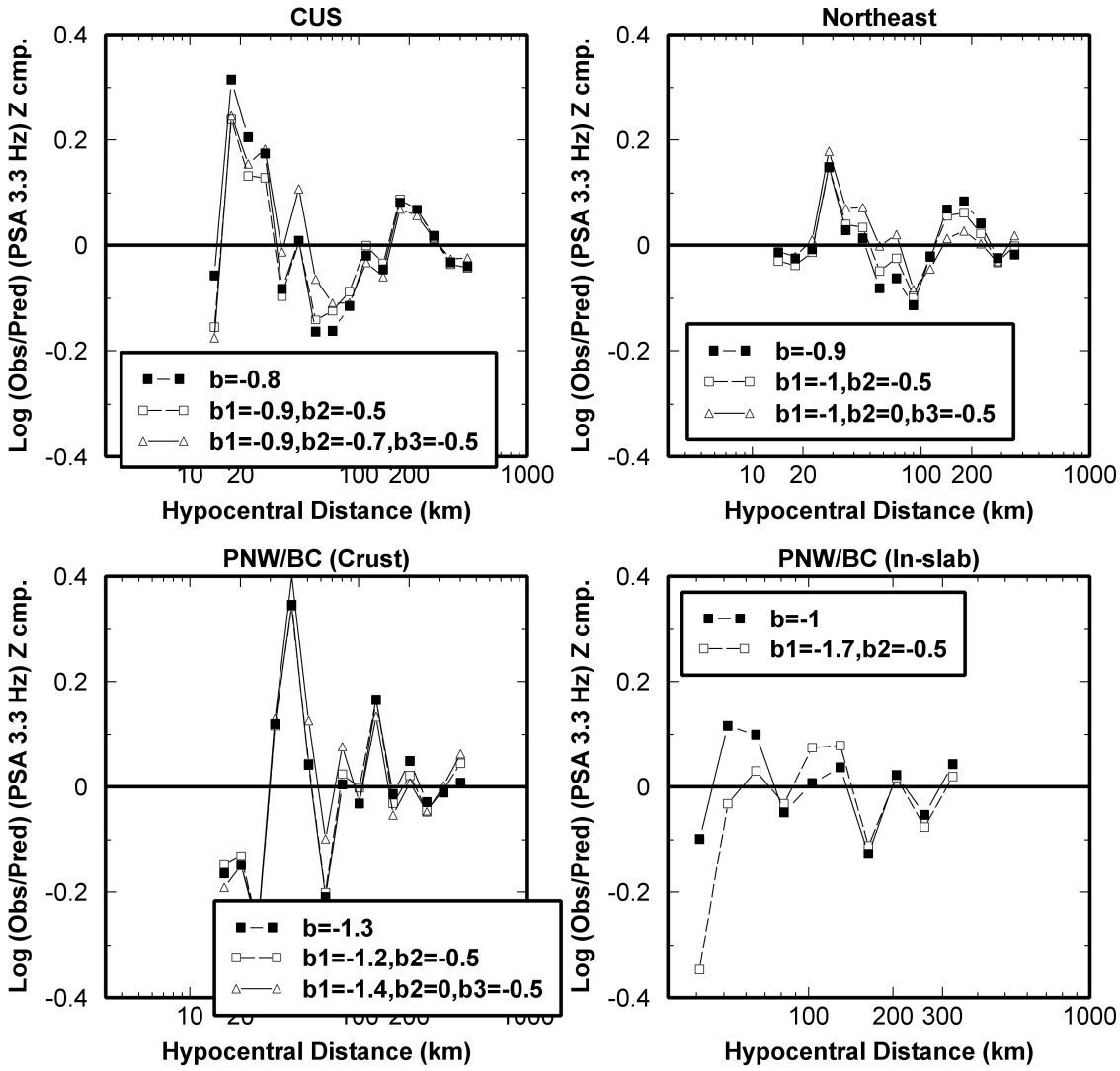

Figure 2.6 Mean residuals of the best of the candidate forms in each region for each distance bin for PSA at 3.3 Hz (vertical component) for linear, bi-linear, and tri-linear forms. Parameters of these forms are given in Table 2.3.

2.6 Discussion

The reason for the similarity of the residual trends for all of the attenuation forms can be appreciated by examining Figures 2.8 and 2.9. These figures show the shapes of the best linear, bi-linear and tri-linear models for PSA at frequency 3.3 Hz, for the vertical

and geometric mean of horizontal components in each region. The source-and-site-corrected amplitudes (based on the linear model with geometric spreading -1 in each region) are overlaid by the best of the linear, bi-linear and tri-linear shapes. All of the models were plotted in such a way as to normalize amplitudes at a fixed distance of 200 km (at the value of the linear model at this distance). This distance is chosen as it reflects the weight of the data distribution in most regions.

Table 2-3 Best-fit parameters for the best forms of Figures 2.6 and 2.7 for each of the linear, bi-linear and tri-linear cases, based on the minimum of the AIC values at 3.3 Hz. [1]Crustal [2]In-slab

Region	Comp.	Form	R_{t1}	R_{t2}	b_1	b_2	b_3	Q_0'	η'
CUS	H	1.1	NA	NA	-1	NA	NA	879	0.63
CUS	H	2.2	50	NA	-1.1	-0.5	NA	369	0.61
CUS	H	3.25	50	100	-1.2	-0.3	-0.5	422	0.38
CUS	V	1.2	NA	NA	-0.8	NA	NA	798	0.32
CUS	V	2.4	70	NA	-0.9	-0.5	NA	461	0.54
CUS	V	3.25	50	100	-0.9	-0.7	-0.5	695	0.23
Northeast	H	1.1	NA	NA	-1	NA	NA	1025	0.58
Northeast	H	2.2	50	NA	-1.4	-0.5	NA	398	0.57
Northeast	H	3.33	50	100	-1.4	-0.4	-0.5	400	0.58
Northeast	V	1.2	NA	NA	-0.9	NA	NA	631	0.64
Northeast	V	2.3	70	NA	-1	-0.5	NA	470	0.35

Northeast	V	3.43	70	140	-1	0	-0.5	293	0.54
PNW/BC (C)[1]	H	1.2	NA	NA	-1.3	NA	NA	687	0.66
PNW/BC (C)	H	2.4	70	NA	-1.3	-0.5	NA	211	0.70
PNW/BC (C)	H	3.29	50	140	-1	-1.3	-0.5	306	0.59
PNW/BC (C)	V	1.2	NA	NA	-1.3	NA	NA	483	0.77
PNW/BC (C)	V	2.6	100	NA	-1.2	-0.5	NA	273	0.57
PNW/BC (C)	V	3.39	70	100	-1.4	0	-0.5	227	0.62
PNW/BC (I)[2]	H	1.1	NA	NA	-1	NA	NA	158	0.72
PNW/BC (I)	H	2.5	100	NA	-1	-0.5	NA	110	0.79
PNW/BC (I)	V	1.1	NA	NA	-1	NA	NA	220	0.58
PNW/BC (I)	V	2.6	100	NA	-1.7	-0.5	NA	161	0.67
N. California	H	1.2	NA	NA	-1.6	NA	NA	1174	-0.61
N. California	H	2.4	70	NA	-1.3	-0.5	NA	100	0.92
N. California	H	3.47	70	140	-1.2	0	-0.5	72	0.93
S. California	H	1.2	NA	NA	-1.5	NA	NA	253	1.07
S. California	H	2.2	50	NA	-1.4	-0.5	NA	118	0.78
S. California	H	3.57	100	140	-1.1	-0.2	-0.5	137	0.70

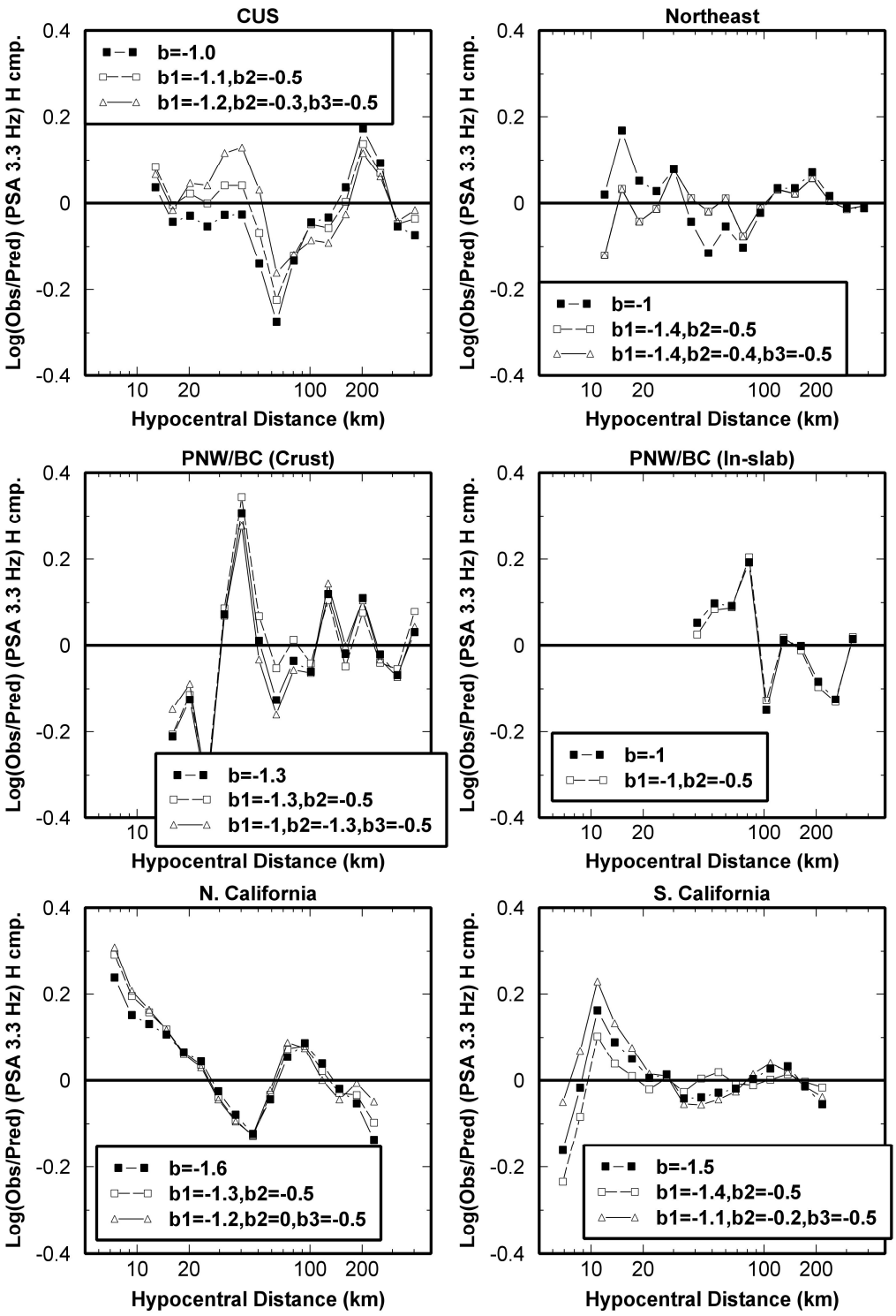

Figure 2.7 Mean residuals of the best of the candidate forms in each region for each distance bin for PSA at 3.3 Hz (geometric mean of the horizontal components) for linear, bi-linear, and tri-linear forms. Parameters of these forms are given in Table 2.3.

The figures reveal that the differences between the models are subtle in comparison to the large data scatter. The large scatter may be attributable to the use of simple site and attenuation models to parameterize complicated amplitude decay processes, applied over a wide range of distances and site conditions. This makes it difficult to pick a single functional form as the "best" fit to the data. The bi-linear form may be a good practical choice, as it incorporates the decay of both body waves and surface waves from near to regional distances in a reasonable way. This is especially important in the eastern and central regions.

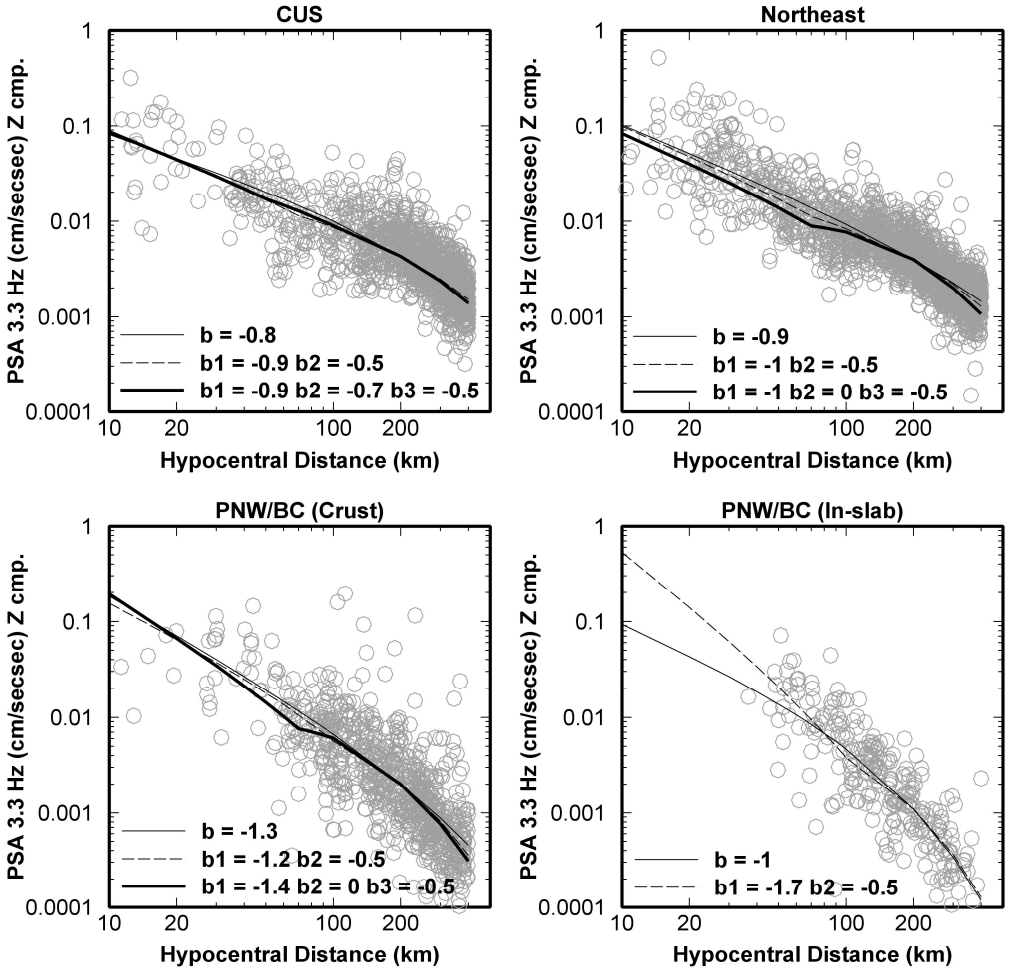

Figure 2.8 Shapes of the best attenuation models based on the minimum of the AIC value for PSA 3.3 Hz (vertical component). The shapes are normalized to have a fixed value at 200 km.

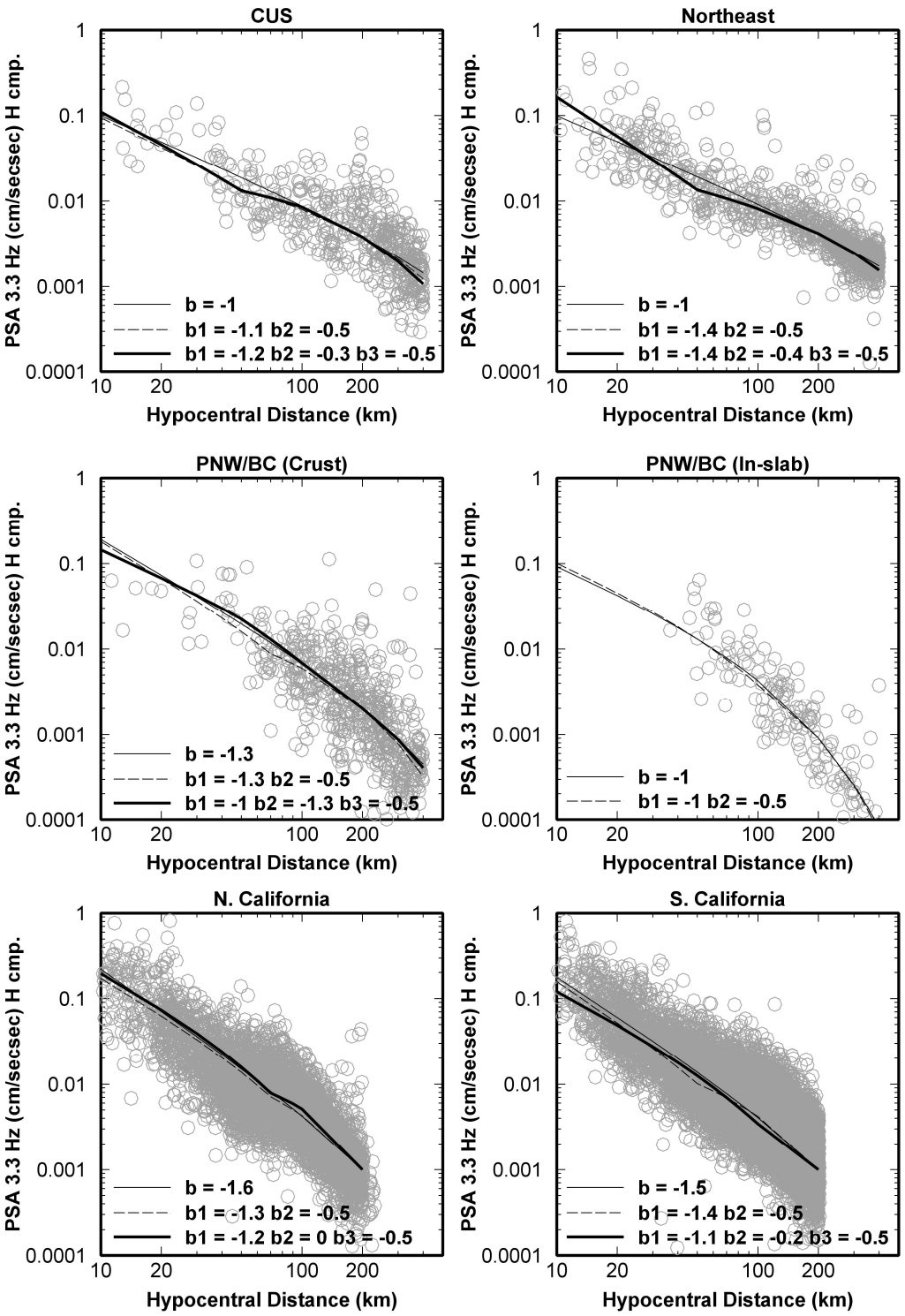

Figure 2.9 Shapes of the best attenuation models based on the minimum of the AIC value for PSA 3.3 Hz (geometric mean of the horizontal components). The shapes are normalized to have a fixed value at 200 km.

The AIC technique provides an objective measure to compare the different models as applied to each dataset. However, the best-fit model is sensitive to frequency. The AIC differences were estimated for 6 PSA frequencies (0.33, 0.5, 1, 3.3, 5, and 10 Hz), in Northeast, CUS, and PNW/BC, and for 3 PSA frequencies (0.33, 1 and 3.3 Hz), for N. and S. California. The best model in each region is not consistent over all frequencies based on the AIC values. In Figure 2.10, we show how the parameters of the best-fit model, and even its basic shape, appear to change with frequency. In this figure, we can see the fluctuations of the best trial forms based on the MAICE with frequency in each region, for the vertical component and geometric mean of the horizontal components. These fluctuations are more significant in the west than in the east, as the best trial forms in the west range from linear to tri-linear, while for the east the forms are mostly tri-linear at all frequencies. While the tri-linear forms are statistically preferred in many cases, we conclude based on Figures 2.8 and 2.9 that the differences between the forms are not sufficiently significant to prefer one over another. The linear form has advantages due to its simplicity, while the bi-linear form offers a good compromise between simplicity and the ability to describe the combination of relative steep attenuation of body waves near the source, transitioning to slower attenuation of surface waves at regional distances.

There are different statistical tests, other than AIC, such as F-test and T-test to evaluate the goodness-of-fit of a model. Even though the results indicate one model may be statistically better, none show any significance over another regarding their residuals. We have thus not further pursued the use of such tests to distinguish between models.

Since the linear and bi-linear forms appear to be good practical choices in describing the attenuation of the ground-motion amplitudes, we defined a linear and bi-linear form to fit the PSA ground-motion amplitudes at all frequencies for each region. We chose these forms based on the average MAICE over the entire frequency range (0.33 to 10 Hz for most regions, 0.33 to 3.33 Hz for California), as presented in Table 2.2. We note that the obtained Q' factors are not the same for the vertical component and the geometric mean of the horizontal components. However, it is reasonable to expect that anelastic attenuation, which determines this parameter, should be common to the horizontal and vertical components. We therefore chose to force a common anelastic attenuation

coefficient, using the Q' model obtained from whichever component provided a more stable trend of Q' versus frequency (based on the data within each region). This was the vertical component in Northeast and the PNW/BC and the horizontal component in the CUS; we used the horizontal component in California because it was the only component available. Then, the anelastic coefficients implied by the adopted Q' model (Equation 2.6) were used as a regression constraint, and the remaining coefficients determined (for both the vertical and horizontal component regressions). In other words, we repeat the regression of the linear and bi-linear forms presented in Table 2.2, to estimate the geometric spreading coefficient while the anelastic attenuation coefficient is held fixed. Tables 2.4 and 2.5 show the parameters of these linear and bi-linear forms, along with the confidence limits on the slope b_1. Note that b_1 is not well-constrained for the bi-linear form, due to the paucity of data at <100 km. Figure 2.11 shows the b_1 slopes and their confidence limits for each of the regions. Generally the attenuation appears to be similar for both vertical and geometric mean of the horizontal components; although there are some apparent differences in b_1 slopes, there are no consistent significant trends that carry across both the linear and bi-linear models.

Table 2-4 Parameters of linear forms for each region which fit the PSA ground-motion amplitudes in all frequencies for vertical component and geometric mean of the horizontal components. Columns $b_{1,L}$ and $b_{1,U}$ refer to lower and upper 95% confidence intervals for b_1 estimates, respectively.

Region	Comp.	Form	R_{t1}	R_{t2}	b_1	$b_{1,L}$	$b_{1,U}$	b_2	σ	Q_0'	η'
CUS	H	Linear	NA	NA	-0.87	-0.95	-0.79	NA	0.28	879	0.6
CUS	V	Linear	NA	NA	-0.82	-0.89	-0.75	NA	0.26		
Northeast	H	Linear	NA	NA	-0.88	-0.92	-0.85	NA	0.22	631	0.6
Northeast	V	Linear	NA	NA	-0.84	-0.85	-0.82	NA	0.22		
PNW/BC(Crustal)	H	Linear	NA	NA	-1.15	-1.22	-1.09	NA	0.40	483	0.8

PNW/BC (Crustal)	V	Linear	NA	NA	-1.13	-1.18	-1.07	NA	0.40		
PNW/BC(In-slab)	H	Linear	NA	NA	-1.31	-1.41	-1.22	NA	0.31	220	0.6
PNW/BC (In-slab)	V	Linear	NA	NA	-1.09	-1.18	-1.01	NA	0.34		
N. California	H	Linear	NA	NA	-1.10	-1.15	-1.06	NA	0.30	115	1.0
S. California	H	Linear	NA	NA	-1.15	-1.18	-1.13	NA	0.29	240	1.1

Table 2-5 Parameters of bi-linear forms for each region which fit the PSA ground-motion amplitudes in all frequencies for vertical component and geometric mean of the horizontal components. Columns $b_{1,L}$ and $b_{1,U}$ refer to lower and upper 95% confidence intervals for b_1 estimates respectively.

Region	Comp.	Form	R_{t1}	R_{t2}	b_1	$b_{1,L}$	$b_{1,U}$	b_2	σ	Q_0'	η'
CUS	H	Bi-linear	50	NA	-1.16	-1.39	-0.92	-0.5	0.28	369	0.6
CUS	V	Bi-linear	70	NA	-0.88	-1.04	-0.72	-0.5	0.26		
Northeast	H	Bi-linear	70	NA	-1.20	-1.27	-1.13	-0.5	0.22	467	0.3
Northeast	V	Bi-linear	50	NA	-1.08	-1.14	-1.03	-0.5	0.22		
PNW/BC (Crustal)	H	Bi-linear	100	NA	-1.11	-1.24	-0.98	-0.5	0.40	244	0.6
PNW/BC (Crustal)	V	Bi-linear	70	NA	-1.24	-1.38	-1.09	-0.5	0.39		
PNW/BC (In-slab)	H	Bi-linear	70	NA	-1	NA	NA	-0.5	0.30	125	0.7
PNW/BC (In-slab)	V	Bi-linear	70	NA	-1	NA	NA	-0.5	0.30		

N. California	H	Bi-linear	70	NA	-1.28	-1.33	-1.22	-0.5	0.30	100	0.9
S. California	H	Bi-linear	50	NA	-1.43	-1.48	-1.38	-0.5	0.28	118	0.8

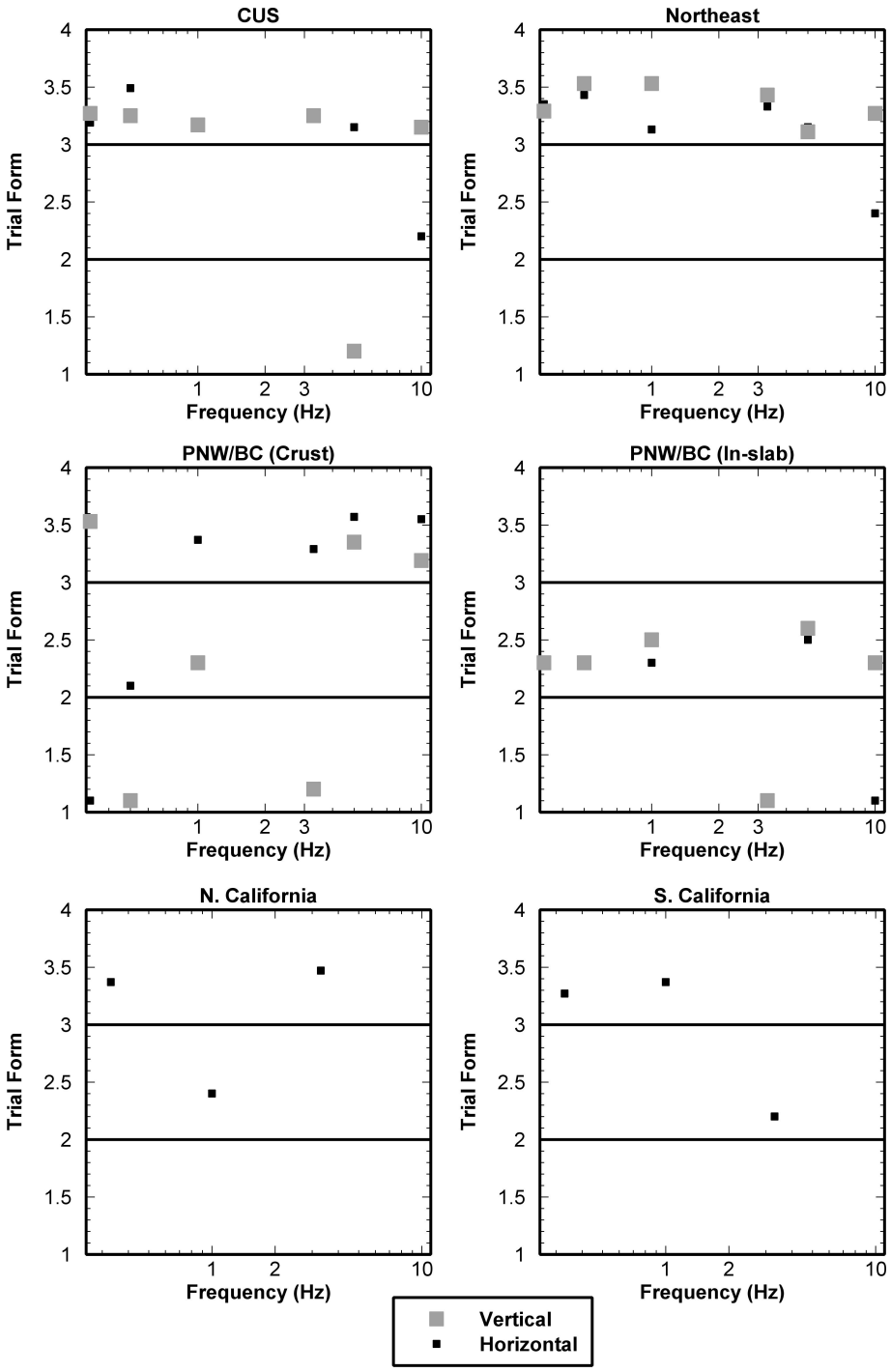

Figure 2.10 Fluctuations of the best trial forms based on the MAICE with frequency for vertical component and geometric mean of the horizontal components for each region, where the trial forms are as listed in Table 2.1. The tri-linear form was not use for the PNW/BC due to the paucity of data.

We observe on Figure 2.11 that the geometric spreading coefficient is clearly more negative (steeper) in the west as compared to the east, especially when considering the linear form. This is perhaps not surprising due to the known lesser attenuation in eastern regions compared to the west. Of particular interest is the comparison of the near-distance slope amongst regions for the bilinear model. (Note: for the in-slab data in the PNW/BC, the near-distance geometric spreading is set to -1 as data are not available at distances less than 50 km). Based on the bi-linear model, a b_1 coefficient in the range of -1.1 to -1.3 appears to be reasonable for most regions (both vertical and horizontal components), with the vertical component of CUS having a somewhat slower attenuation, and Southern California having a faster attenuation.

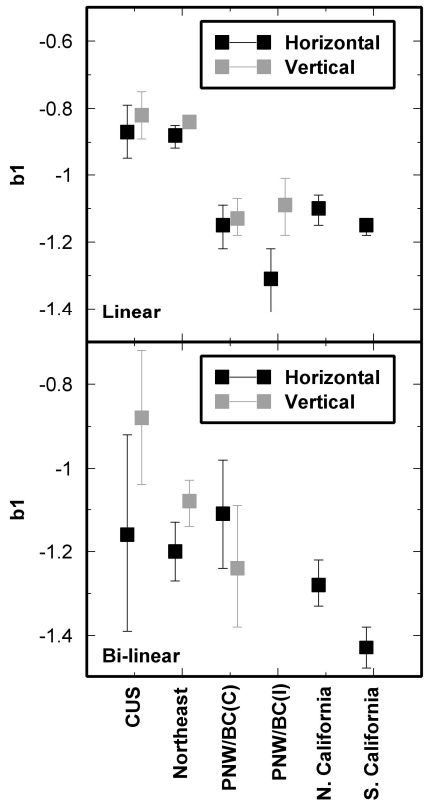

Figure 2.11 Plot of b_1 slopes and their confidence intervals from linear and bi-linear forms presented in Tables 2.4 and 2.5 for the vertical component and geometric mean of the horizontal components. The b_1 slopes for the bi-linear form in in-slab PNW/BC was not shown because they were set to -1 and not determined from the bi-linear model. See Table 2.4 and 2.5 for parameters of the models.

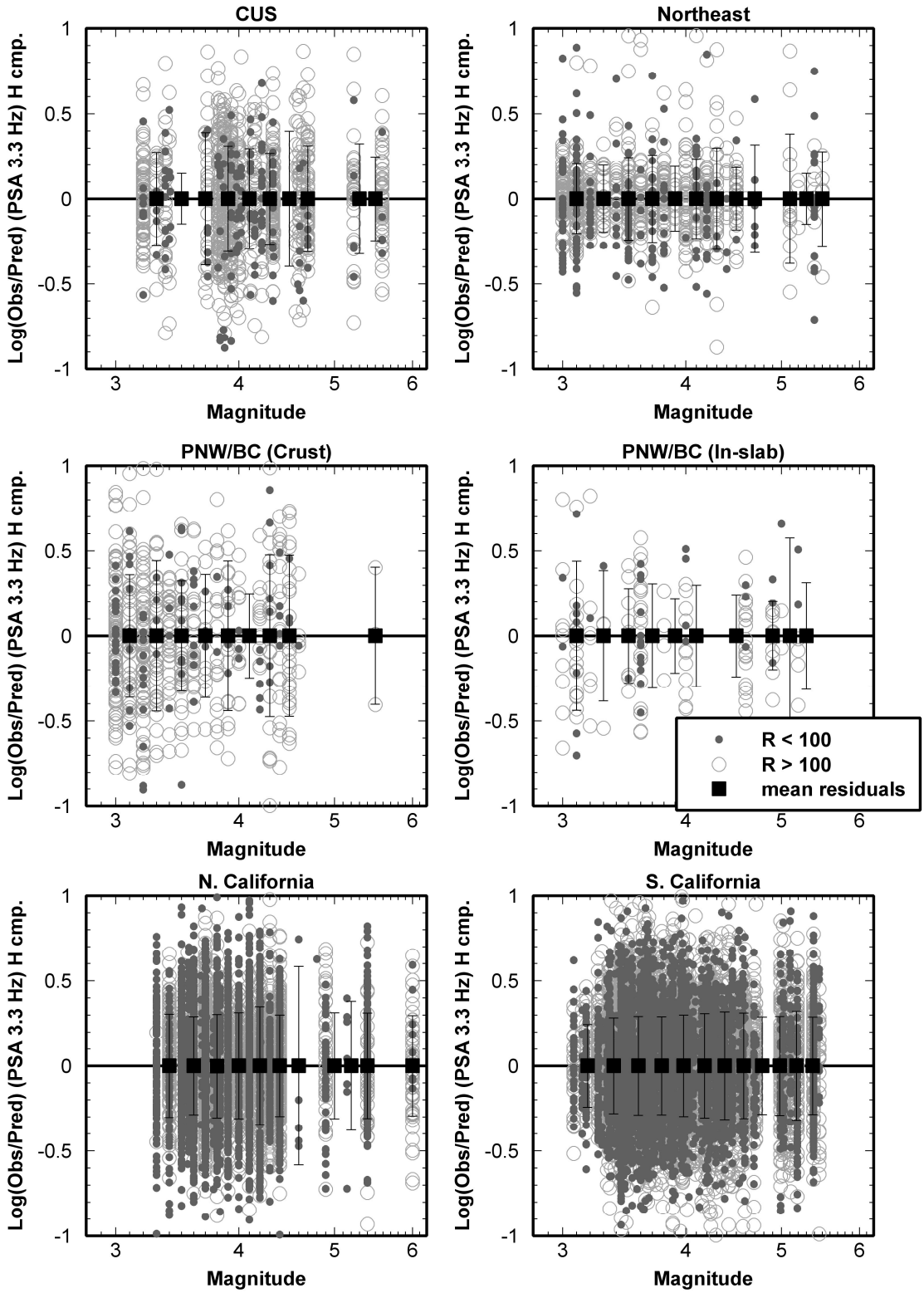

Figure 2.12 Residuals of the linear form presented in Table 2.4 against magnitude, for geometric mean of the horizontal components of PSA 3.3 Hz in each region.

Finally, we test whether the attenuation results obtained here for PSA in various regions show any dependence on magnitude, in the range of these data (due to possible effects of oscillator response on the apparent attenuation rate, as noted earlier, and discussed by Atkinson, (2012).

Figure 2.12 shows the residuals of the linear form presented in Table 2.4, against catalog magnitude (M) for the geometric mean of the horizontal components of PSA 3.3 Hz in each region. (Graphs for other frequencies, not shown, have similar appearance). The residuals do not show any trends, confirming that there is no magnitude dependency of the attenuation forms obtained for PSA, at least in the magnitude range from 3 to 5.

2.7 Conclusions

Thirty-two alternative combinations of linear, bi-linear and tri-linear attenuation shapes were evaluated to assess their ability to describe the decay of amplitudes in 5 regions: Northeast, the CUS (including New Madrid), the PNW/BC, N. California and S. California. The residual plots for alternative shapes do not show any apparent significant differences between them, making it difficult to conclude which is the best model for each region. An AIC test was performed to see if statistical analyses reveal whether one model is superior to the others. The best AIC values are not consistent over frequency; nevertheless, we tabulate the best model on average (0.33 to 10 Hz) from each of the three trial forms of linear, bi-linear and tri-linear, for each region. We note that a simple linear form with geometric spreading ~1 in the East and ~1.3 in the West is a reasonable "first-order" description of the attenuation within 300 km across North America, and works as well as more complex models in describing regional attenuation. However, there may be advantages to using at least a bi-linear form to distinguish between direct-wave and surface-wave spreading regimes. Near-source geometric spreading under the bi-linear model appears to be in the range of $R^{-1.1}$ to $R^{-1.3}$ for most regions, with the CUS (including New Madrid) showing slower attenuation, and Southern California showing faster attenuation. Tri-linear models are a better fit to the data in some regions (Northeast), but may have no practical advantage over simpler models. These conclusions may be used to inform alternative choices for input attenuation forms in the development of ground-motion prediction models and other applications.

2.8 References

Akaike, H. (1974). A New Look at the Statistical Model Identification. *IEEE Transactions on Automatic Control,* Vol. **19**, No. 6, 716-723.

Allen, T. I., P. R. Cummins, T. Dhu, and J. F. Schneider (2007). Attenuation of Ground-Motion Spectral Amplitudes in Southeastern Australia, *Bull. Seism. Soc. Am.* **97,** 1279-1292.

Assatourians, K., and G. Atkinson (2010). Database of Processed Time Series and Response Spectra Data for Canada: An Example Application to Study of 2005 MN 5.4 Riviere du Loup, Quebec, Earthquake, *Seism. Res. Lett.* **81**, 1013-1031.

Atkinson, G. M. (2004). Empirical Attenuation of Ground-Motion Spectral Amplitudes in Southeastern Canada and the Northeastern United States, *Bull. Seism. Soc. Am.* **94,** 1079-1095.

Atkinson, G. M., and R. Mereu (1992). The shape of Ground Motion Attenuation curves in Southeastern Canada, *Bull. Seism. Soc. Am.* **82,** 2014-2031.

Atkinson, G. M., and M. Morrison (2009). Observations on Regional variability in Ground-Motion Amplitudes for Small-to-Moderate Earthquakes in North America, *Bull. Seism. Soc. Am.* **99,** 2393-2409.

Atkinson, G. M. (2012). Evaluation of Attenuation models for the Northeastern United States/Southeastern Canada, *Seism. Res. Lett.* **83,** 166-178.

Atkinson, G. M., and K. Goda (2011). Effects of Seismicity Models and New Ground-Motion Prediction Equations on Seismic Hazard Assessment for Four Canadian Cities. *Bull. Seism. Soc. Am.* **101,** 176-189.

Boatwright, J., L. Seekins (2011). Regional Spectral Analysis of three moderate earthquakes in northeastern North America, *Bull. Seism. Soc. Am.* **101,** 1769-1782.

Boore, D. M., W. B. Joyner, and T. E. Fumal (1993). Estimation of Response Spectra and Peak Accelerations from Western North American Earthquakes: An Interim Report, *U.S. Geol. Surv.* Open-File Rept. 93-509, 72 pp.

Boore, D. M., W. B. Joyner, and T. E. Fumal (1994). Estimation of response spectra and peak accelerations from western North American earthquakes: an interim report, Part 2, *U.S. Geol. Surv.* Open-File Rept. 94-127, 40 pp.

Boore, D. M., W. B. Joyner, and T. E. Fumal (1997). Equations for estimating horizontal response spectra and peak accelerations from Western North American earthquakes: a summary of recent work, *Seism. Res. Lett.* **68,** 128–153.

Borcherdt, R. D. (1994). Estimates of site-dependent response spectra for design (methodology and justification), *Earthquake Spectra* **10,** 617–654.

Brillinger, D. R., and H. K. Preisler (1984). An exploratory analysis of the Joyner-Boore attenuation data, *Bull. Seism. Soc. Am.* **74,** 1441-1450.

Burger, R., P. Somerville, J. Barker, R. Herrmann, and D. Helmberger (1987). The Effect of crustal structure on strong ground motion attenuation relations in eastern North America, *Bull. Seism. Soc. Am.* **77,** 420-439.

Burnham, K. P., and D. R. Anderson (2002). Model Selection and Multimodel Inference; A Practical Information-Theoretic Approach, Second Edition. *Springer*, 488 pages, New York.

Chiou, B., R. Youngs, N. Abrahamson, and K. Addo (2010). Ground-Motion Attenuation Model for Small-To-Moderate Shallow Crustal Earthquakes in California and Its Implications on Regionalization of Ground-Motion Prediction Models, *Earthquake Spectra* **26,** 907- 926.

Green, R. A., and W. J. Hall (1994). An Overview of the Selected Seismic Hazard Analysis Methodologies. *Civil Engineering Studies, Structural Research Series,* No. **592,** ISSN: 0069-4274, 102 pages.

Joyner, W. B., and D. M. Boore (1981). Peak Horizontal Acceleration and Velocity from Strong-Motion Records including records from the 1979 Imperial Valley, California, Earthquake, *Bull. Seism. Soc. Am.* **71,** 2011-2038.

Joyner, W. B., and D. M. Boore (1993). Methods for Regression Analysis of Strong Motion Data, *Bull. Seism. Soc. Am.* **83,** 469-487.

Menke, W. (1989). Geophysical data analysis: discrete inverse theory. *Academic Press, Inc,* 289 pages, San Diego, CA.

Molnar, S., J. F. Cassidy, and S. E. Dosso (2004). Site Response in Victoria, British Columbia, from Spectral Ratios and 1D Modeling, *Bull. Seism. Soc. Am.* **94,** 1109-1124.

Nuttli, O. (1973). Seismic Wave Attenuation and Magnitude Relations for Eastern North America, *J. Geophys. Res.* **78,** 876-885.

Ou, G., and R. Herrmann (1990). A statistical model for peak ground motion from local to regional distances, *Bull. Seism. Soc. Am.* **80,** 1397-1417.

Power, M., N. Abrahamson, Y. Bozorgnia, T. Shantz, and C. Roblee (2008). An Overview of the NGA Project, *Earthquake Spectra* **24,** 3-21.

Sakamoto, Y., M. Ishiguro, and G. Kitagawa (1986). Akaike Information Criterion Statistics. *KTK Scientific Publishers/Tokyo,* 290 pages.

Scherbaum, F., E. Delavaud, and C. Riggelsen (2009). Model Selection in Seismic Hazard Analysis: An Information-Theoretic Perspective. *Bull. Seism. Soc. Am.* **99,** 3234-3247

Street, R, and F. Turcotte (1977). A Study of Northeastern North American Spectral Moments, Magnitudes, and Intensities, *Bull. Seism. Soc. Am.* **67,** 599-614.

Wald, D. J., and T. I. Allen (2007). Topographic Slope as a Proxy for Seismic Site Conditions and Amplification, *Bull. Seism. Soc. Am.* **97,** 1379-1395.

Wong, I. G., K. H. Stokoe II, B. R. Cox, Y. Lin, and F. Menq (2011). Shear-wave velocity profiling of strong motion sites that recorded the 2001 Nisqually, Washington, earthquake, *Earthquake Spectra* **77,** 183-212.

Chapter 3

3 Estimation of moment magnitude from ground motions at regional distances[2]

3.1 Introduction

An important task for the characterization and assessment of seismic hazard is the development of regional earthquake catalogs using a consistent magnitude scale. Moment magnitude (**M**), as defined by Hanks and Kanamori (1979), is the magnitude scale of choice for a number of reasons: (i) it provides a measure of the physical size of the earthquake; (ii) it is the magnitude scale used in Ground Motion Prediction Equations, facilitating use of catalog data products in seismic hazard assessments; (iii) it works well over a wide range of magnitudes because it does not "saturate" at high magnitudes; and (iv) it provides a consistent magnitude metric for event comparisons across different regions. Thus the assessment of moment magnitude for events is a high-priority task. Moment tensors are routinely assessed on a global basis for moderate-to-large events (**M**>5) by the Global Centroid Moment Tensor project using global waveform modeling techniques. There are also regional centers, such as that led by R.B. Herrmann at Saint Louis, that provide moment tensors for selected moderate events having sufficient recordings (generally events of **M**~3.5 to 5), based on regional waveform modeling. However, for the majority of moderate events that occur, **M** must be estimated using simple conversions from other catalog scales (see Sonley and Atkinson, 2005; Fereidoni et al., 2012; Petersen et al., 2008, for examples). These conversions vary depending on the magnitude scales used, the region, the practices of the observatories determining the magnitudes, and even with time (e.g. Bent, 2011). This results in ambiguity and lack of confidence in using **M** estimates based on conversions from other magnitude scales.

---

[2] A version of this chapter has been accepted for publication. Atkinson, G. M., and A. Babaie Mahani (2013). Estimation of Moment magnitude from Ground Motions at Regional Distances, *Bull. Seism. Soc. Am.* (in press).

In this note, we develop a direct and simple procedure for estimating **M** for small-to-moderate regional events (**M** 3 to 6) from network ground-motion observations, which can be consistently applied across different regions. The reference ground-motion parameter for the method is 1-Hz response spectral amplitude, which is particularly convenient as it is a downloadable "ShakeMap" parameter, making moment magnitude estimation simple in regions that support this common ground-motion tool. We develop the method using ground-motion observations for events in Eastern North America (ENA), considering the regions of Eastern Canada/Northeastern United States (called the "Northeast" hereafter) and the region of the Central United States surrounding the New Madrid seismic zone (called the "CUS" hereafter). The method is motivated by the observation that ground motion amplitudes at regional distances, beyond ~100 km, behave in a stable and robust way, providing a good measure of source strength (Herrmann and Kijko, 1983a,b; Ou and Herrmann, 1990). At regional distances, complications in attenuation due to interactions between seismic phases and crustal structure effects have been homogenized by multi-pathing. The ground motions, which are comprised of multiply reflected and refracted shear waves, have frequency-domain amplitudes that decay smoothly according to the overall geometric and anelastic processes associated with spreading of waves trapped within the crustal waveguide (Kennett, 1986; Benz, et al., 1997). Vertical-component amplitudes are particularly well behaved, as they have minimal influence from the site effects that are often prominent on the horizontal component (Lermo and Chavez-Garcia, 1993). This allows attenuation at regional distances (for a given frequency) to be represented by a simple decay curve, with the level of the curve being correlated with the strength of the source at that frequency. The concept is illustrated in Figure 3.1, which shows the attenuation of vertical-component 1-Hz pseudo acceleration amplitudes (PSA, 5% damped) at regional distances for three example ENA earthquakes. A significant advantage to the use of regional data to characterize source strength is that they are relatively plentiful, even in sparsely-instrumented ENA.

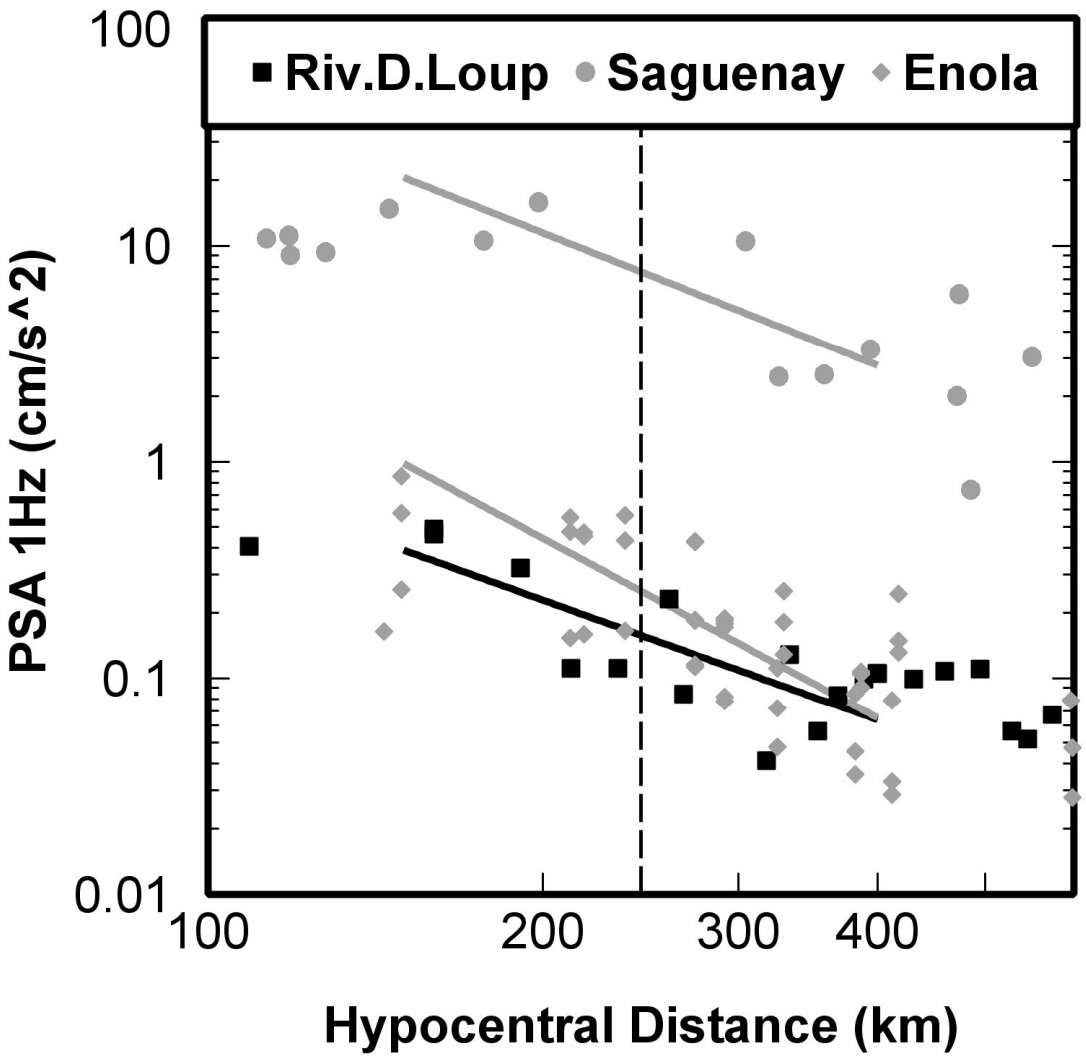

Figure 3.1 Example of attenuation of 1-Hz PSA amplitudes (vertical) for the 2005 **M**4.7 Riviere du Loup, Quebec earthquake (Riv.D.Loup), the 1988 **M**5.8 Saguenay, Quebec earthquake (Saguenay), and the 2001 **M**4.3 Enola, AR earthquake (Enola). The regional amplitudes are fitted over the distance range from 150 to 400 km by straight line segments, whose mid-points (dashed line) are used to define the reference amplitude A245 for each event.

3.2 Methodology and data used

We base our moment magnitude estimation methodology for ENA on vertical-component ground motions in the distance range from 150 to 400 km, due to the stability of these ground-motion observations as illustrated in Figure 3.1. The choice of distance

range (D_1 = 150 to D_2 = 400 km) was made after examining the behavior and availability of data for many events. D_1 and D_2 were chosen to maximize available data, while providing stable amplitude decay. We tested the robustness of the results to the selected distance range, and found that this range is not critical. Similar results are obtained using slightly different distance ranges (e.g. 200 to 600 km), as long as D_1 is beyond the "Moho bounce" range (>100km), and D_2 is not so distant as to introduce much noisier records. The selected ground-motion parameter is the vertical-component 1-Hz PSA (PSA_{1v}), 5% damped. This is convenient because PSA_{1v} is a "ShakeMap" ground-motion parameter that is readily available (or can be easily calculated) in many regions. The signal filtering provided by the oscillator response function tends to smooth amplitudes over a limited frequency range up to that of the oscillator frequency, which damps ground-motion amplitude variability. The frequency of 1 Hz is a good choice because it is low enough to be controlled mostly by seismic moment (for small-to-moderate events), but not so low as to be overly contaminated by noise. Specifically, 1 Hz is near or below the corner frequency for ENA earthquakes of **M**<5.5, and is thus indicative of the "flat displacement" amplitude portion of the Fourier spectrum (e.g. Atkinson, 2004). Another possible choice for the ground-motion parameter would be PSA at 0.33 Hz (also a ShakeMap parameter), but small-magnitude events are significantly contaminated at frequencies less than 0.5 Hz by a microseism tremor peak (Douglas and Boore, 2011).

We fit PSA_{1v} using the data for a specific event, in the distance range from D_1=150 km to D_2=400 km, by a simple straight-line segment in log-log space:

$$log(\,PSA_{1v}) = a + b\,log(R) + \varepsilon \qquad (3.1)$$

where R is hypocentral distance, a and b are the coefficients of the line segment, and ε is the error term (residual). The amplitude of the line segment at the mid-point of the fitted distance range (=245 km in log space), referred to as A245, is taken as the measure of the source strength of the event. This process is illustrated in Figure 3.1. The use of a simple straight-line segment for the attenuation function allows us to fit a segment for each earthquake of interest, with a minimum of observations being needed to define the function. To ensure robust results, we require a minimum of 5 points to fit the line

segment. Furthermore, we accept solutions only for those events for which the fitted segment has a slope that is in a reasonable range, relative to other events in the region. Specifically, by inspection of amplitude data from dozens of ENA events, we note that 1-Hz PSA slopes for this distance range are almost always in the range from -0.5 to -3.0, for events having sufficient data to determine a slope with confidence. Therefore we consider only events having apparent attenuation slopes (150 to 400 km) within this range (-0.5 to -3.0). If the slope falls outside this range, it is most likely due to poor resolution of the slope due to sparse observations and/or data errors. By imposing these constraints, we ensure that the mid-point amplitude, A245, is a stable and robust representation of the overall 1-Hz amplitude level produced by the source.

The study events for calibration of the technique are those ENA events with a known moment magnitude from global or regional moment tensor solutions, and having sufficient ground-motion data available in the regional distance range. We obtained PSA data for events in the Northeast from the ground-motion databases of the Engineering Seismology Toolbox. The processing of the regional data to obtain these response spectra was described by Assatourians and Atkinson (2010). In brief, the PSA amplitudes were calculated for waveforms which were windowed from the event origin time to the end of the S-wave coda, and corrected as required for instrument response. For events in the CUS, PSA data were obtained from the NGA-East (Next Generation Attenuation-East) project database (Chris Cramer, written communication, May 2012). We used only records with high-pass filter corner <0.5 Hz and low-pass filter corner >2 Hz. The magnitude scale reported in the NGA-East database for events in the CUS is moment magnitude (though it is not always clear how this value was obtained; many values may be estimates). In the Northeast only a small percentage of available events have a determined moment magnitude. The common magnitude scale for seismicity catalogs for this region is MN (Nuttli magnitude; Nuttli, 1973). Moment magnitude estimates were obtained from the Saint Louis regional moment tensor website, supplemented by some additional moment tensor estimates from the literature as reported in the Composite Seismicity Catalog (CCSC) by Fereidoni et al. (2012). Figures 3.2 and 3.3 plot the locations of study events for the Northeast and CUS, while Figure 3.4 shows the distribution of PSA_{1v} observations in magnitude-distance space. Note that the data

distribution is richest at distances beyond 100 km, which is a key advantage to using regional data to define source parameters.

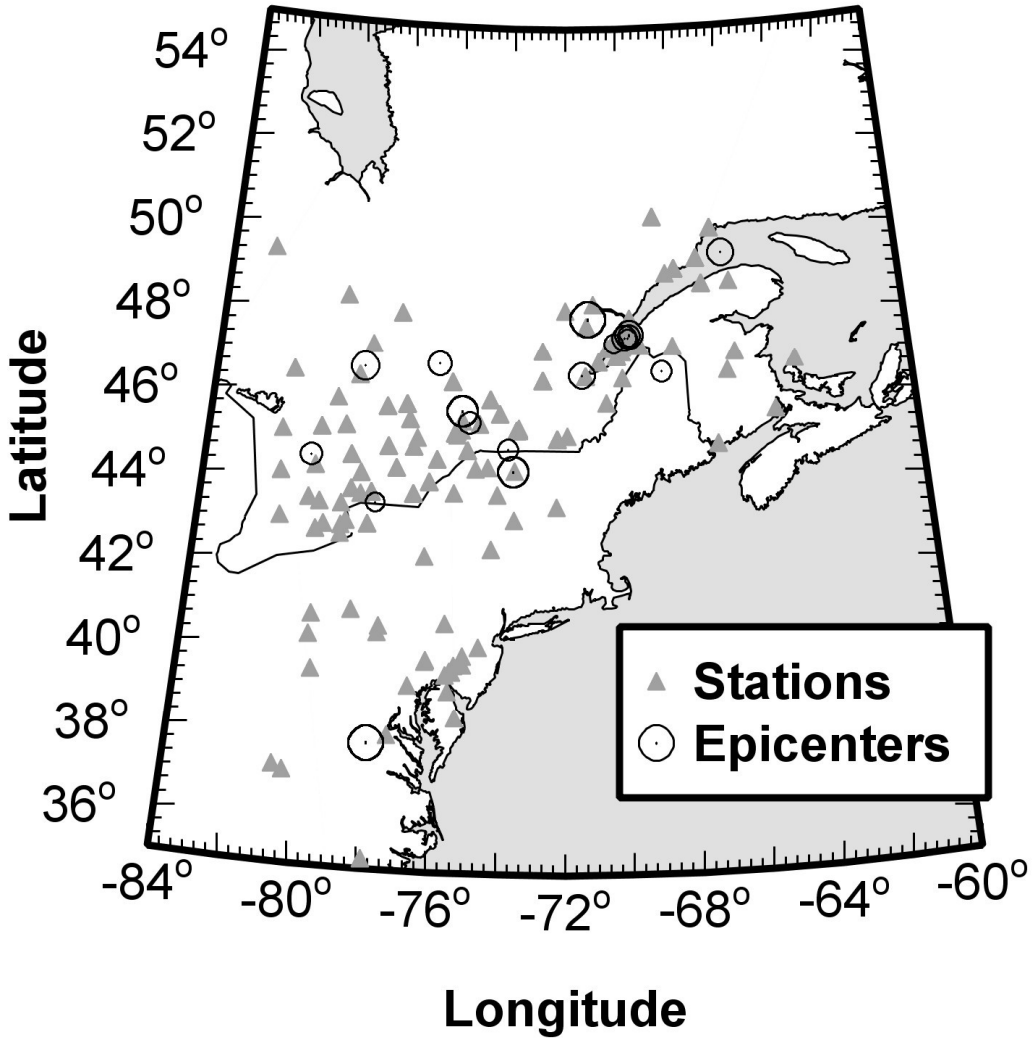

Figure 3.2 Location of study events (those with known **M**) and recording stations, for the Northeast region. The size of epicenters corresponds to the magnitude of the events.

3.3 Results

The amplitudes at the reference distance (D_{ref} = 245 km) are plotted on Figure 3.5, for both the Northeast and CUS regions. It is apparent that these data follow a single trend, with a straight-line fit being appropriate for both regions. We can estimate **M** for events in the Northeast and CUS regions by:

$$\boldsymbol{M} = 5.20(\pm 0.06) + 0.78(\pm 0.04)\ log(A245) \qquad (3.2)$$

where A245 is in units of cm/s^2. The standard deviation of the residuals is 0.16 units, providing an excellent estimate of **M** for events for which we can define A245.

The main improvement of this method, in comparison to estimates of **M** based on catalog magnitudes such as MN, is that the estimate can be made directly from ShakeMap ground-motion database parameters, and consistently determined across regions regardless of the magnitude scales in use in regional catalogs. As we show in the next section, the method also facilitates interpretation of the ground motions in the context of simple seismological models of ground-motion processes.

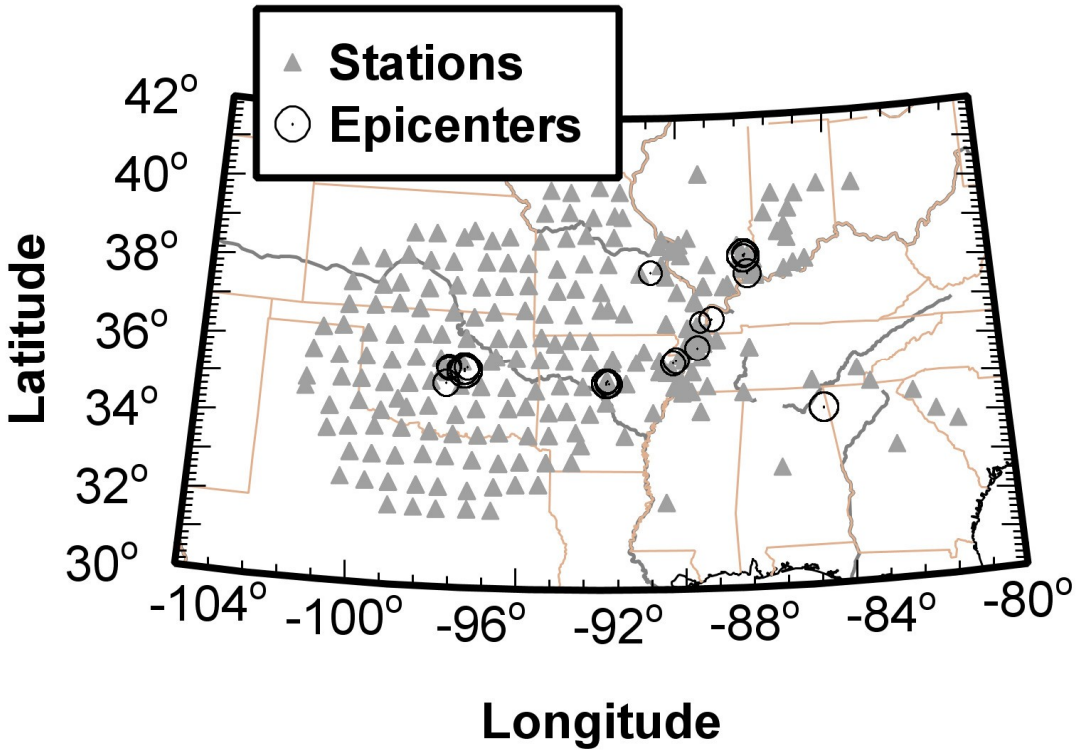

Figure 3.3 Location of study events (those with known **M**) and recording stations, for the CUS region. The size of epicenters corresponds to the magnitude of the events.

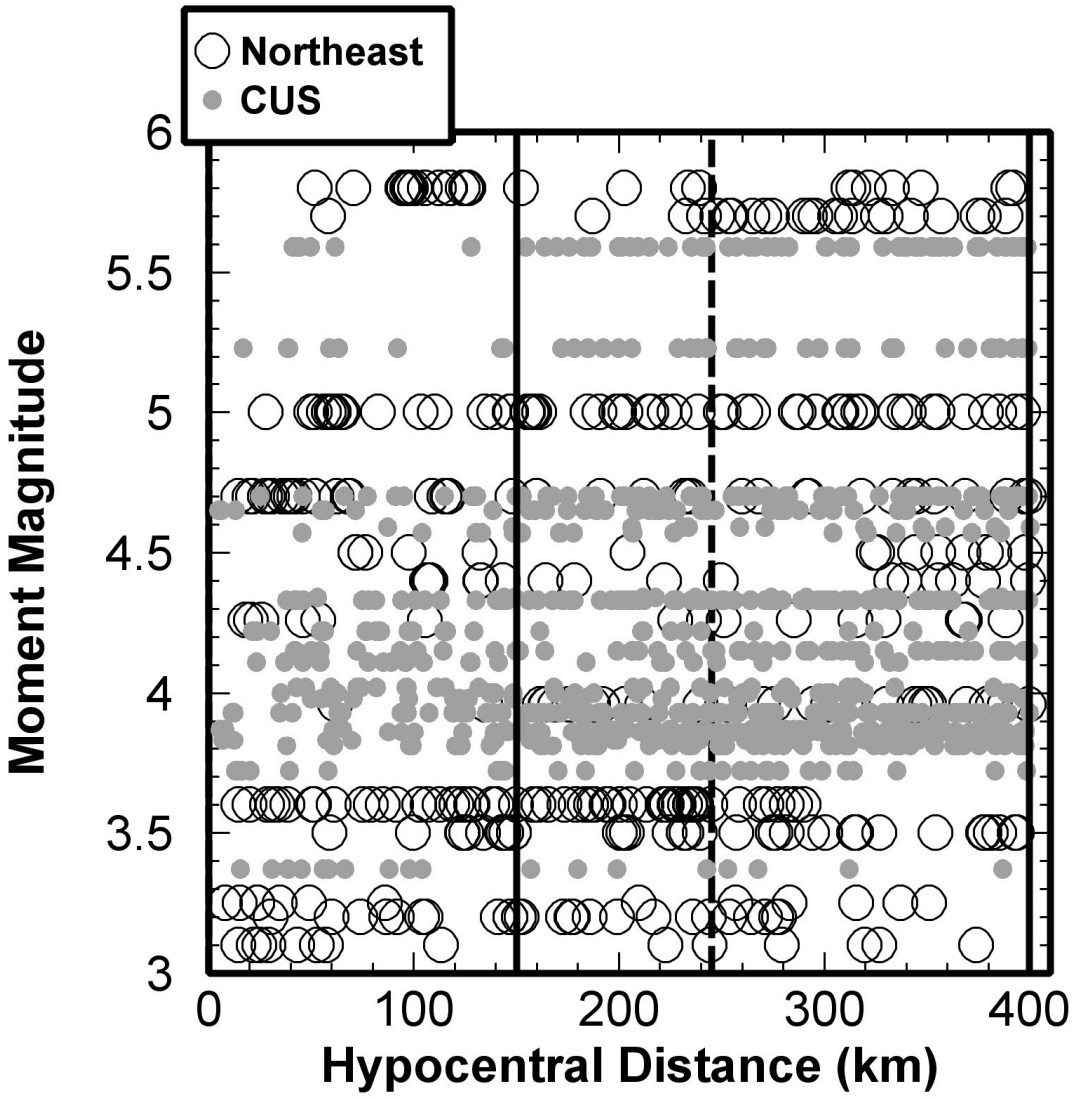

Figure 3.4 Distribution of PSA1v in magnitude and distance. The distance range from 150 to 400 km and the 245 km midpoint is indicated with the solid and dash lines, respectively.

3.4 Comparison with predictions from point-source simulations

The empirical relationship between **M** and 1-Hz PSA amplitude (Equation 3.2) can be compared with what we would predict based on a stochastic point-source model. Assuming a single-corner Brune (1970, 1971) point-source model for an event of the specified moment, we use the SMSIM program (Boore, 2003; 2009) to produce simulated

acceleration time series at a distance of 245 km, from which PSA are calculated (average PSA is calculated for 800 trials). The input attenuation model is a bi-linear model, having geometric spreading slope given by b_1=-1 to a transition distance (R_t) of 70 km, then a slope of b_2= -0.5 beyond. The anelastic attenuation is given by Q=470 $f^{0.3}$. The duration is assumed to increase with distance as 0.05R; physical constants are as given in Atkinson and Boore (2006). The selected attenuation model has been shown to provide a reasonable match to PSA amplitudes in ENA (e.g. Atkinson, 2012; Babaie Mahani and Atkinson, 2012), and is similar to other recent ENA attenuation models (e.g. Boatwright and Seekins, 2011). Amplitudes at 1-Hz are insensitive to stress drop – which is the only free parameter controlling spectral level- for small to moderate magnitudes. This is illustrated in Figure 3.6, which plots the observed relationship between A245 and **M** with the stochastic point-source predictions, for stress drops ranging from 50 to 500 bars. We note that the observations agree well with the simulation model; this consistency is expected, as the selected attenuation model parameters for the simulation were inferred from a very similar database by Babaie Mahani and Atkinson (2012).

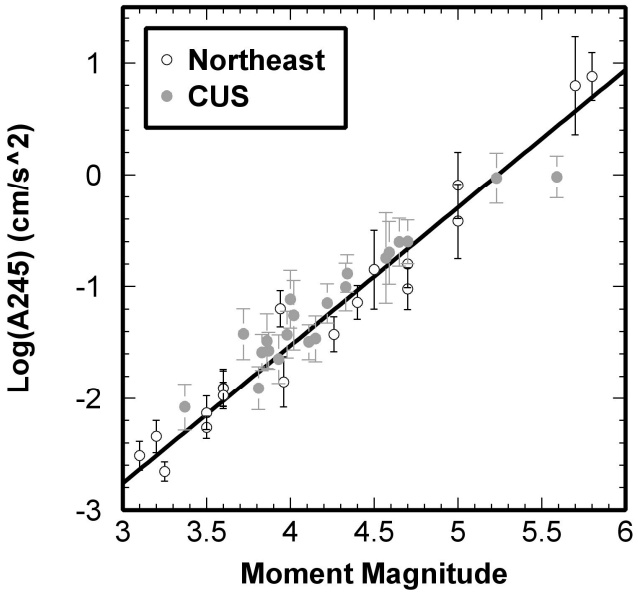

Figure 3.5 Calibration line of **M** versus A245 (PSA1v at the reference distance of 245 km). Error bars show standard deviation of A245 (residual term in Equation 3.1) for each event.

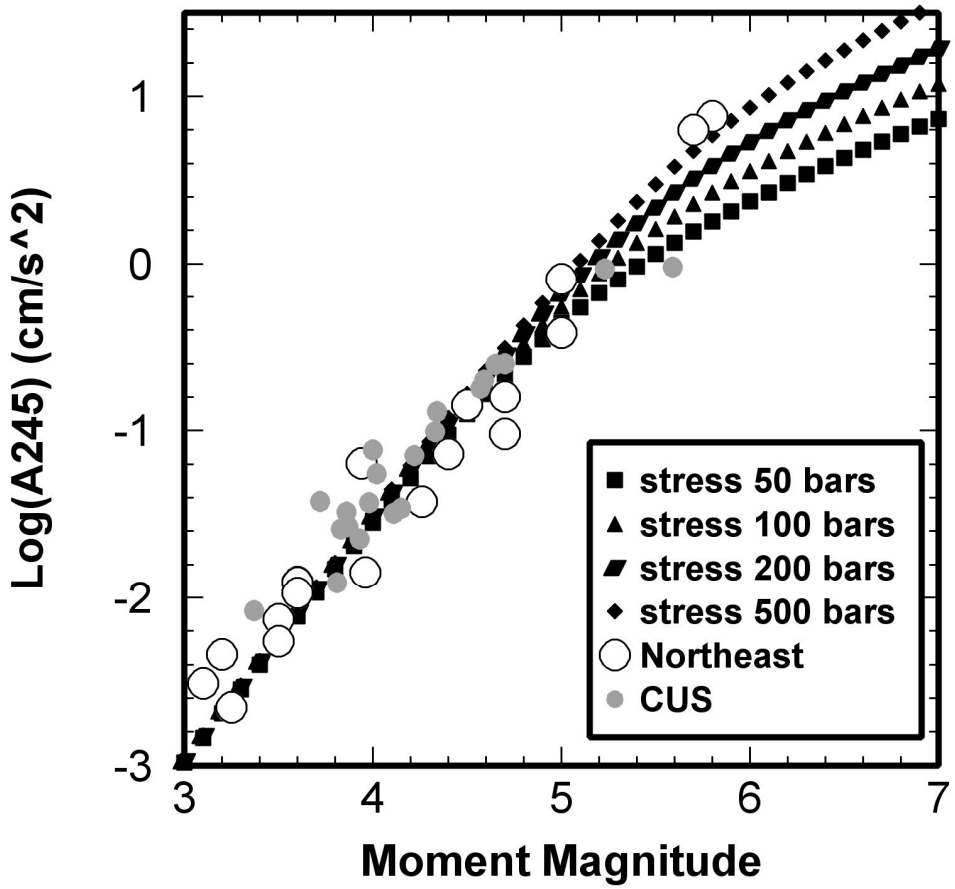

Figure 3.6 Comparison of predicted relationship between A245 and **M** from stochastic point source model and observations, for stress drops from 50 to 500 bars. (b_1=-1, b_2=-0.5, Rt=70km, Q=470 f0.3, path duration 0.05R).

Although the relationship between A245 and **M** for the simulations is insensitive to stress drop, it does show significant sensitivity to attenuation. This is illustrated in Figure 3.7, which shows that the level of the predicted relationship is very sensitive to b1, the geometric spreading slope within 70 km. Other sensitivities were also explored, but are not illustrated with plots, for the sake of brevity. We find that the relationship is sensitive to Q (assuming a fixed geometric spreading coefficient of 0.5 beyond 70 km) only if a very low value of 1-Hz Q (near 100) is selected; for Q values consistent with those reported in the literature for ENA (Q>400 at 1 Hz), the relationship is insensitive to Q. Similarly, the relationship is also insensitive to path duration, at least for path durations up to 0.1R.

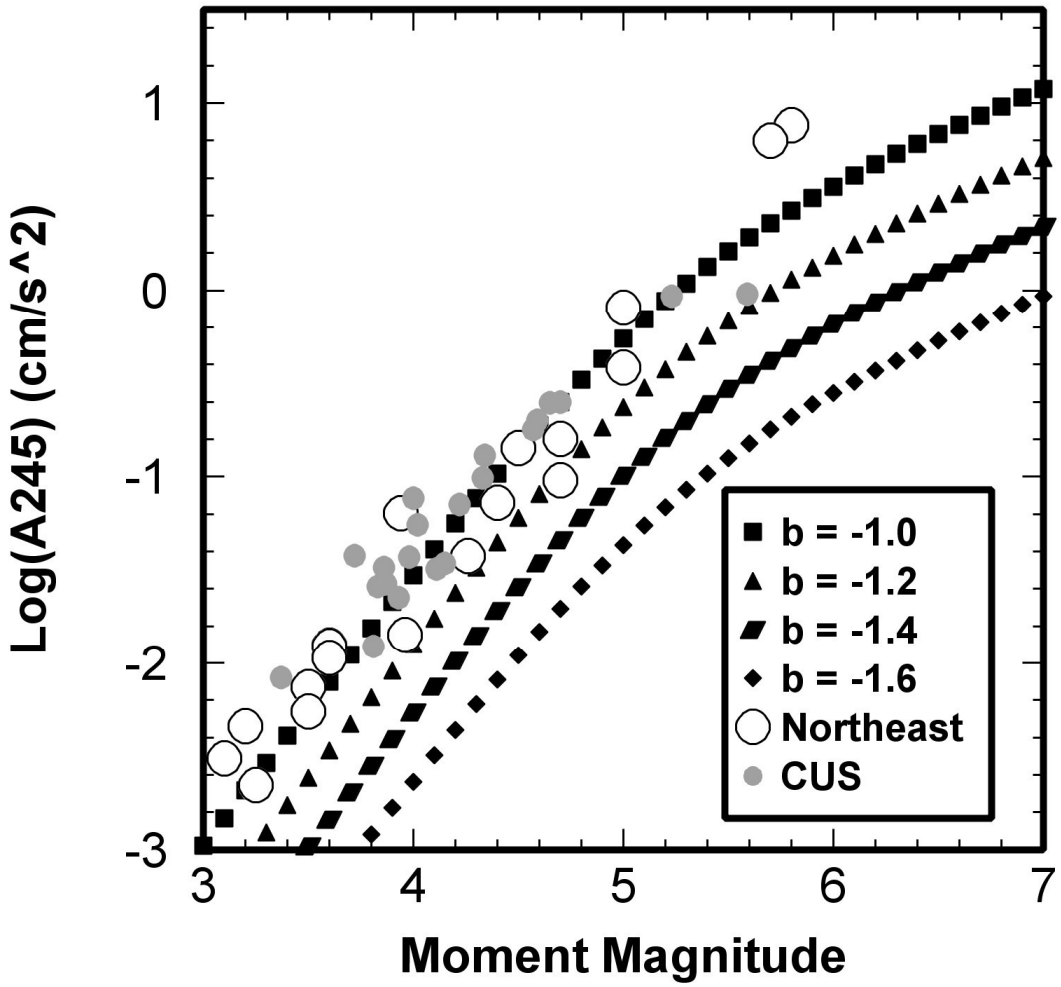

Figure 3.7 Comparison of predicted relationship between A245 and **M** from stochastic point source model and observations, for geometric spreading coefficients (at R<70 km) from -1.0 to -1.6 (stress = 100 bars, b_2 = -0.5, Rt = 70 km, Q = $470f^{0.3}$, path duration = 0.05R).

It is important to recognize that the sensitivity to geometric spreading places constraints on the total amount of attenuation from the source to 245km, but not the actual shape of the attenuation curve. Specifically, the prediction line provided in Figure 3.7 for a bilinear model to 70 km with b_1=-1 gives a total attenuation from 1 km to 245 km of 2.12 log units due to geometric spreading (e.g. log(70) + 0.5 log (245/70)). The same amount of attenuation could be obtained with a different attenuation model shape. For example, if we assume the trilinear model of Atkinson (2004), with b_1=-1.3 to 70 km,

then a transition slope of +0.2 to 140 km, and impose a near-source saturation from 1 to 10 km (e.g. as in Atkinson and Assatourians, 2010), we would predict almost the same amount of attenuation, and therefore the same prediction line. Thus it is the total attenuation that is constrained, not the shape of the decay function.

Figure 3.7 suggests that comparing the results of stochastic modeling with the actual observations can help put constraints on the coefficient of geometric spreading, which was the topic of Chapter 2. Based on the results from Figure 3.7 the best form of attenuation for the Northeast and CUS would be a bi-linear model with R_t = 70km, b_1 = -1.0 and b_2 = -0.5.

The sensitivity of predicted ground-motion amplitudes at regional distances to poorly-constrained geometric spreading functions at near distances, for a given value of **M**, highlights a key advantage of our proposed approach of using regional observations to determine **M,** namely that it is independent of near-source attenuation. By contrast, alternative methods of estimating **M** from regional displacement spectral amplitudes, corrected to the source with an attenuation model (e.g. Atkinson, 1993, 2004), are very sensitive to the choice of attenuation model.

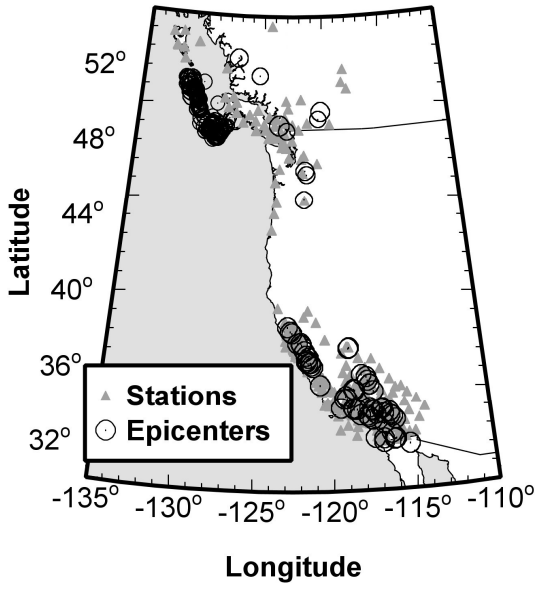

Figure 3.8 Location of study events (those with known **M**) and recording stations, for WNA. The size of epicenters corresponds to the magnitude of the events.

3.5 Application to other regions

In order to assess the validity of the moment magnitude estimation method to other regions, we applied the same technique to three regions in Western North America (WNA), including crustal events in the Pacific Northwest/British Columbia (PNW/BC), crustal offshore events in PNW/BC (Offshore), and California. For the Offshore and PNW/BC, we used the Engineering Seismology Toolbox database as our source for 1-Hz PSA amplitudes, while for California the NGA-West2 database was used. The reported catalog magnitude for events that we used in the offshore region is moment magnitude. For California and PNW/BC, the database reports a variety of magnitudes. For PNW/BC, these include **M** (for some events), ML (local magnitude), and Mc (coda magnitude), while for California, moment magnitude, along with a converted (or estimated) value of **M** and an unknown magnitude (UK) was reported. For the Offshore and PNW/BC, the **M** values (where available) came directly from the Engineering Seismology Toolbox catalog, while for California they came from the NGA-West2 database. Figure 3.8 plots the locations of the study events in WNA. Figure 3.9 shows the distribution of PSA_{1v} observations in magnitude-distance space for Offshore, PNW/BC, and California. We repeated the analysis given by Equation 3.1 for these three regions. However, the distance ranges (D_1 and D_2) for which the amplitudes were fitted were adjusted as appropriate for the region. For the Offshore and California, we used D_1=100 and D_2=300 km (thus the mid-point D_{ref}=173 km). For the PNW/BC, we chose D_1=100 km and D_2=400 km (thus D_{ref}=200km). As was the case for ENA, we chose the distances to maximize available data while maintaining the desired stability of amplitude decay, after inspecting numerous attenuation plots. Figure 3.10 shows the amplitudes at the reference distance versus known moment magnitude for these three regions. **M** can be obtained for WNA from an equation that follows the form for ENA (Equation 3.2) as follows:

$$\text{PNW/BC: } \mathbf{M} = 5.09(\pm 0.16) + 0.52(\pm 0.09)\log(A200) \tag{3.3}$$

with standard deviation of residuals = 0.11.

$$\text{Offshore: } \mathbf{M} = 5.92(\pm 0.05) + 0.68(\pm 0.03)\log(A173) \tag{3.4}$$

with standard deviation of residuals = 0.24.

California: **M** = 5.13(±0.05) + 0.75(±0.03) log(A173) (3.5)

with standard deviation of residuals = 0.14.

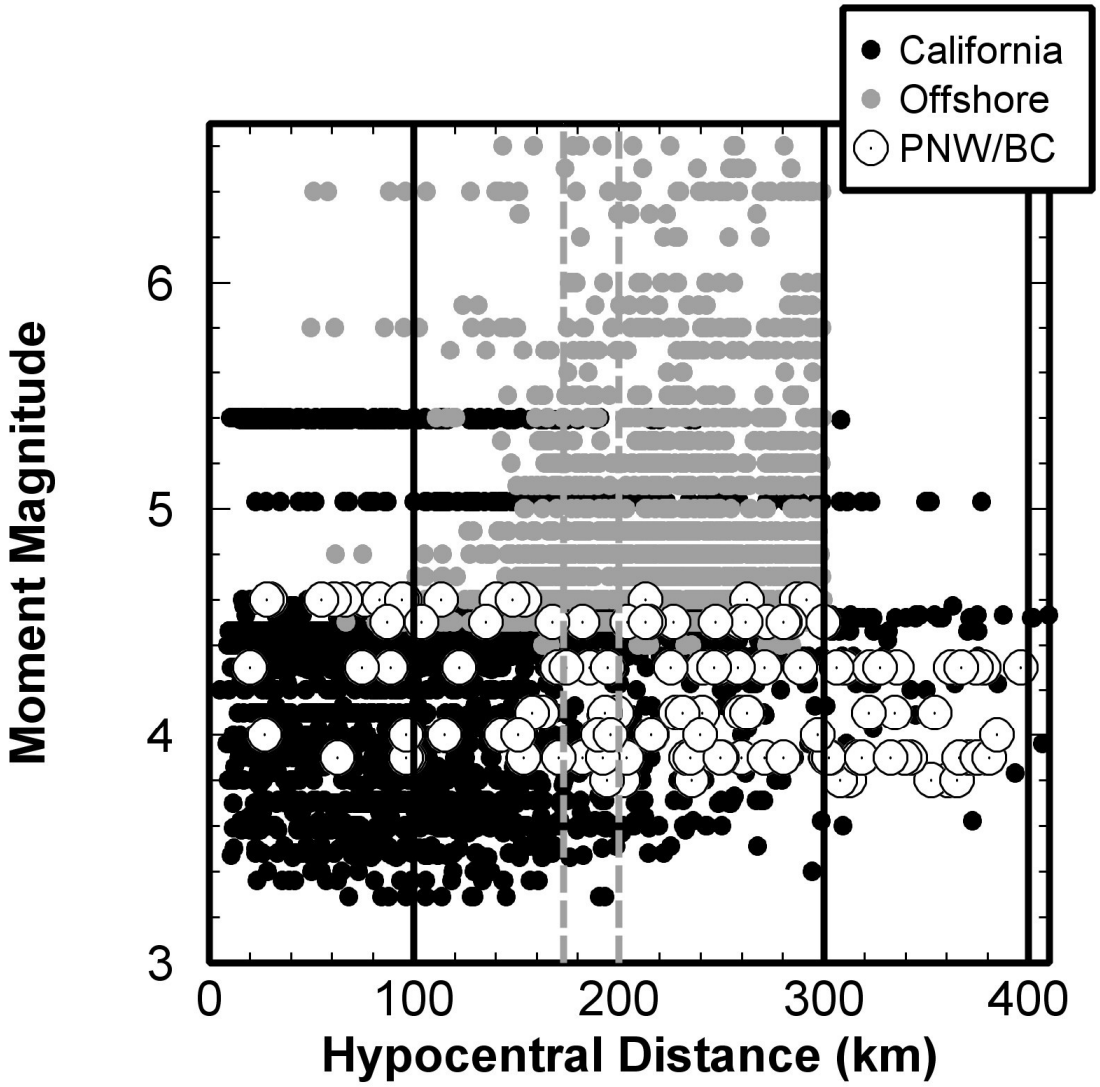

Figure 3.9 Distribution of PSA1v in magnitude and distance. The distance range from D_1 to D_2 in km and the D_{ref} midpoint is indicated with the solid and dash lines, respectively. D_1, D_2, and D_{ref} are 100, 300, and 173 km for California and Offshore and 100, 400, and 200 km for PNW/BC.

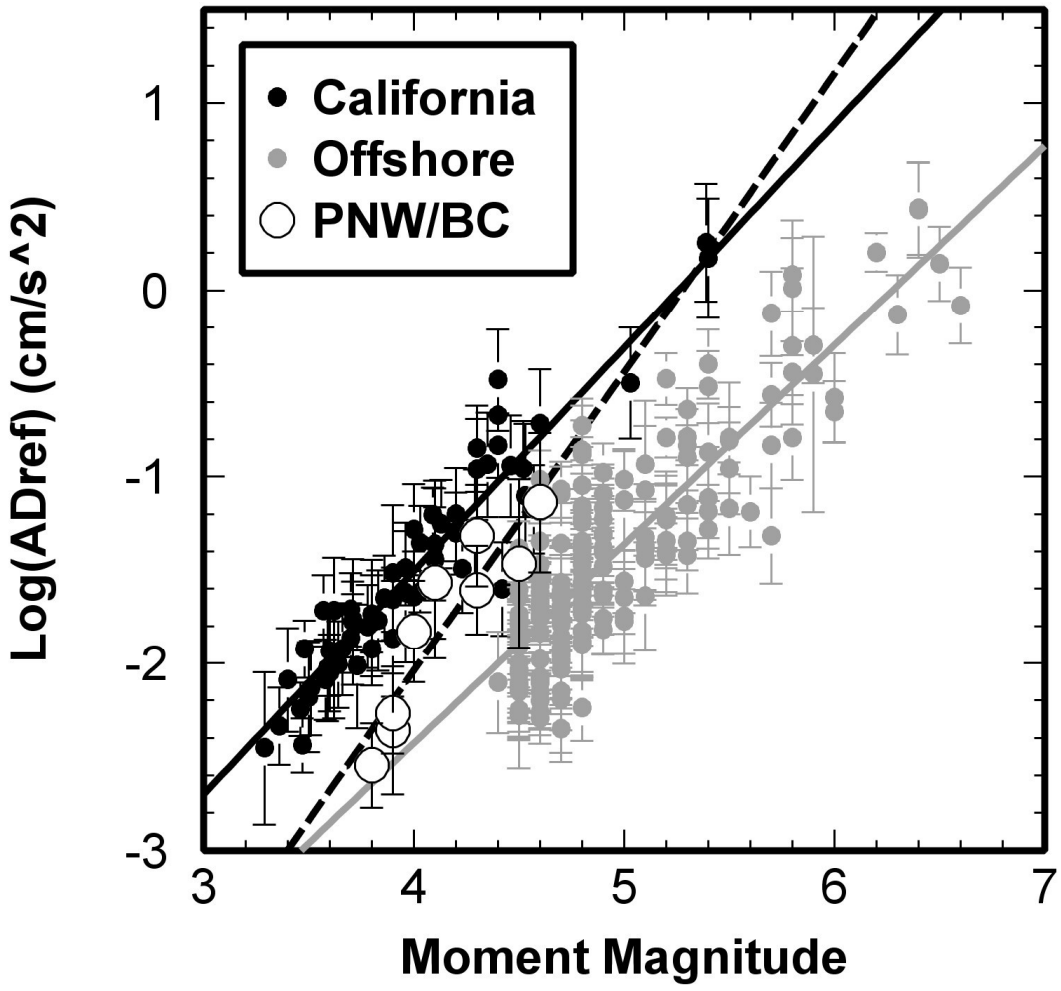

Figure 3.10 Calibration of M versus PSA1v at the reference distance (AD_{ref}) for WNA. Error bars show standard deviation of AD_{ref} for each event (residual term in Equation 3.1). D_{ref} is 173 km for California and Offshore and 200 km for PNW/BC.

Figure 3.11 shows a plot of catalog magnitudes versus the estimated moment magnitude for the considered regions in WNA. This plot shows much variability in PNW/BC, especially for Mc, compared to other magnitude pairs in other regions, perhaps due to the complicated geological setting of this region. Earthquakes in PNW/BC occur in a variety of settings and include both shallow crustal events and in-slab events (e.g. Atkinson, 2005). The different event types likely have a different relationship between **M** and regional ground-motion amplitudes due to differences in both source and attenuation processes, but the available data are not sufficient at this time to resolve these differences

and define separate relationships. Further work, requiring more events with known moment, is required in order to better define the relationship between PSA_{1v} and moment for events in the PNW/BC region.

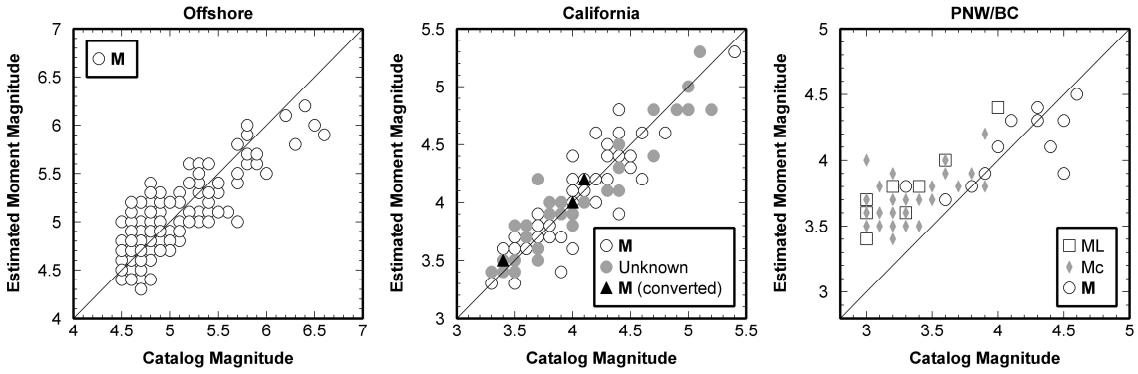

Figure 3.11 Plot of catalog magnitude versus the estimated moment magnitude for WNA.

3.6 Conclusions

Moment magnitude can be estimated for events in North America of **M**<6 from regional 1-Hz response spectral amplitudes (vertical component), with an uncertainty of <0.2 units (standard deviation of residuals) in most regions, using the relationships provided in Equations 3.2 to 3.5. The relationship between **M** and PSA_{1v} is robust and reliable for events having as few as 5 observations in the distance range from 100 to 400 km (100 to 300 km for Offshore and California; 100 to 400 km for PNW/BC; 150 to 400 km for Northeast and CUS). The empirical relationship for the Northeast and CUS is consistent with the predictions of a stochastic point-source model for a typical regional attenuation model for ENA.

3.7 References

Assatourians, K., and G. Atkinson (2010). Database of Processed Time Series and Response Spectra Data for Canada: An Example Application to Study of 2005 MN 5.4 Riviere du Loup, Quebec, Earthquake, *Seism. Res. Lett.* **81**, 1013-1031.

Atkinson, G. M. (2012). Evaluation of Attenuation Models for the Northeastern United States/Southeastern Canada, *Seism. Res. Lett.* **83**, 166-178.

Atkinson, G. M., and K. Assatourians (2010). Attenuation and Source Characteristics of the 23 June 2010 M 5.0 Val-des-Bois, Quebec, Earthquake, *Sesim. Res. Lett.* **81**, 849-860.

Atkinson, G. M. (2005). Ground Motions for Earthquakes in Southwestern British Columbia and Northwestern Washington: Crustal, In-slab, and Offshore Events, *Bull. Seism. Soc. Am.* **95**, 1027-1044.

Atkinson, G. M. (2004). Empirical Attenuation of Ground-Motion Spectral Amplitudes in Southeastern Canada and the Northeastern United States, *Bull. Seism. Soc. Am.* **94**. 1079-1095.

Atkinson, G. M. (1993). Earthquake Source Spectra in Eastern North America, *Bull. Seism. Soc. Am.* **83**. 1778-1798.

Atkinson, G. M., and D. M. Boore (2006). Earthquake Ground-Motion Prediction Equations for Eastern North America, *Bull. Seism. Soc. Am.* **96**, 2185-2205.

Atkinson, G. M. (2004). Empirical Attenuation of Ground-Motion Spectral Amplitudes in Southeastern Canada and the Northeastern United States, *Bull. Seism. Soc. Am.* **94**, 1079-1095.

Babaie Mahani, A., and G. M. Atkinson (2012). Evaluation of Functional Forms for the Attenuation of Small-To-Moderate-Earthquake Response Spectral Amplitudes in North America, *Bull. Seism. Soc. Am.* **102,** 2714-2726.

Bent, A. (2011). Moment Magnitude (MW) Conversion Relations for Use in Hazard Assessment in Eastern Canada, *Seism. Res. Lett.* **82**, 984-990.

Benz, H. M., A., Frankel, and D. M. Boore (1997). Regional Lg Attenuation for the Continental United States, *Bull. Seism. Soc. Am.* **87**, 606-619.

Boatwright, J., and L. Seekins, (2011). Regional Spectral Analysis of Three Moderate Earthquakes in Northeastern North America, *Bull. Seism. Soc. Am.* **101,** 1769-1782.

Boore, D. M. (2003). Simulation of Ground Motion Using the Stochastic Method, *Pure appl. geophys.* **160,** 635–676.

Boore, D. M. (2009). Comparing Stochastic Point-Source and Finite-Source Ground-Motion Simulations: SMSIM and EXSIM, *Bull. Seism. Soc. Am.* **99**, 3202-3216.

Brune J. N. (1970). Tectonic Stress and the Spectra of Seismic Shear Waves From Earthquakes, *J. Geophys. Res.* **75** 4997–5009.

Brune, J. (1971). Correction, *J. Geophys. Res.* **76**, 5002.

Douglas, J., and D. M. Boore (2011). High-Frequency Filtering of Strong-Motion Records, *Bull Earthquake Eng* **9**, 395–409.

Fereidoni, A., G. M. Atkinson, M. Macias, and K. Goda (2012). CCSC: A Composite Seismicity Catalog for Earthquake Hazard Assessment in Major Canadian Cities, *Seism. Res. Lett.* **83**, 179-189.

Hanks, T. C., and H. Kanamori (1979). A Moment Magnitude Scale, *J. Geophys. Res.* **84** (B5): 2348–2350.

Herrmann, R. B., and A. Kijko (1983a). Modeling Some Empirical Vertical Component Lg Relations, *Bull. Seism. Soc. Am.* **73**, 157-171.

Herrman, R. B., and A. Kijko (1983b). Short-Period Lg Magnitudes: Instrument, Attenuation, and Source Effects, *Bull. Seism. Soc. Am.* **73**, 1835-1850.

Kennett, B. (1986). Lg waves and structural boundaries. Bull. Seism. Soc. Am., **76**,1133-1141.

Lermo, J., and F. J. Chavez-Garcia (1993). Site Effect Evaluation Using Spectral Ratios With Only One Station, *Bull. Seism. Soc. Am.* **83**, 1574-1594.

Nuttli, O. (1973). Seismic Wave Attenuation and Magnitude Relations for Eastern North America, *J. Geophys. Res.* **78,** 876-885.

Ou, G. B., and R. B. Herrmann (1990). A Statistical Model for Ground Motion Produced by Earthquakes at Local and Regional Distances, *Bull. Seism. Soc. Am.* **80**, 1397-1417.

Petersen, M., A. Frankel, S. Harmsen, C. Mueller, K. Haller, R. Wheeler, R. Wesson, Y. Zeng, O. Boyd, D. Perkins, N. Luco, E. Field, C. Wills, and K. Rukstales (2008). Documentation for the 2008 Update of the United States National Seismic Hazard Maps, *USGS Open-File Report* 2008-1128, 61 pp.

Sonley, E., and G. M. Atkinson (2005). Empirical Relationship between Moment magnitude and Nuttli Magnitude for Small-magnitude Earthquakes in Southeastern Canada, *Seism. Res. Lett.* **76**, 752-755.

Chapter 4

4 Regional differences in ground-motion amplitudes of small-to-moderate earthquakes across North America[3]

4.1 Introduction

One of the challenges in engineering seismology is characterizing regional variability in ground-motion amplitudes. This issue is relevant for the development and calibration of Ground Motion Prediction Equations (GMPEs). If we can understand regional differences in ground motions, then we can more readily transfer information or lessons learned from data in one region to make inferences about expected ground motions in another region. Regional differences in observed amplitudes are difficult to disentangle, as they may be caused by regional variations in source, attenuation or site processes, or a combination of all of these factors.

Regional differences in ground-motion amplitudes between southern California and northern California (or more correctly, central California, based on geographic region of the study data) were studied by Chiou et al. (2010). They found significant amplitude differences that depended on spectral period and earthquake magnitude; differences appeared to diminish at longer periods and for larger magnitudes (**M** > 6.0). Atkinson and Morrison (2009) performed a similar study, finding that ground-motion amplitudes in northern California are lower on average than those for southern California, for events of small-to-moderate magnitude, at distances >50 km. They also concluded that ground motions in the Pacific Northwest and British Columbia are similar to, or less than, those for northern California (and therefore less than those for southern California at distances>50km). In this study, we take advantage of recent ground-motion databases to systematically compare response spectral amplitudes from small-to-moderate earthqaukes across different regions of North America. We compare amplitudes for crustal events in

[3] A version of this chapter has been submitted for publication. Babaie Mahani, A., and G. M. Atkinson (2012). Regional Differences in Ground-Motion Amplitudes of Small-to-Moderate Earthquakes across North America, *Bull. Seism. Soc. Am.*

magnitude-distance bins, for both the horizontal component (geometric mean) and vertical components of motion, for five regions: Eastern Canada/Northeastern United States (which we call the Northeast), Central United States (including the New Madrid region, which we refer to as CUS), the Pacific Northwest/southwestern British Columbia (which we refer to as PNW/BC; only crustal events are considered), Northern (N.) California (which includes Central California), and Southern (S.) California. Following Atkinson and Morrison (2009), we use southern California as a reference region due to its abundance of observations in a range of magnitude-distance bins. Comparisons are made by taking the ratio of amplitudes in each region to the corresponding values for S. California. Our aim is to improve understanding of regional differences in frequency-dependent source and attenuation effects on observed ground motions. Characterizing the differences empirically is an important step in developing such an understanding.

4.2 Database

We used databases of ground-motion amplitudes, from events with moment magnitde (**M**) 3.0 to 6.0, for Peak Ground Acceleration (PGA), Peak Ground Velocity (PGV) and PSA (5% damped pseudo-acceleration) at 6 frequencies: 0.33, 0.5, 1, 3.3, 5, and 10 Hz, considering the vertical-component and the geometric mean of the two horizontal components. For the Northeast, CUS and PNW/BC regions we used the database of ground-motion amplitudes as described by Babaie Mahani and Atkinson (2012). The NGA (Next Generation Attenuation)-West2 database (for small-to-moderate magnitudes) was used for California. The depth of all study events is less than 30 km, so all are crustal events. The databases contain different magnitude scales across the regions, including Nuttli magnitude (MN, used in the Northeast), local magnitude (ML, used in the CUS, PNW/BC and California), coda magnitude (Mc, used mostly in the PNW/BC), and moment magnitude (**M**). Moment magnitude (Hanks and Kanamori, 1979) is the scale of choice, as it is the basis for modern GMPEs, and measures the physical size of earthquakes. To make meaningful comparisons of events of a given size, we consider only those events for which **M** is known or for which a reliable estimate can be made. For the Northeast, CUS, and PNW/BC, **M** is available for many events from moment tensor solutions while for California **M** is reported in the NGA-West2 database. For events with

unknown moment, we used the method of Atkinson and Babaie Mahani (2012) to provide a robust estimate based on the vertical 1-Hz PSA at regional distances. In brief, Atkinson and Babaie Mahani (2012) used vertical 1-Hz PSA amplitudes at regional distances (from about 150 to 400 km) to fit a simple linear attenuation line (in log-log). The amplitude at the midpoint of this line segment (in log space), A_{Dref}, provides an estimate of **M**:

$$\boldsymbol{M} = a + b \times log(A_{Dref}) \tag{4.1}$$

where the coefficients *a* and *b* were determined for each region by calibration against events with known **M** (Atkinson and Babaie Mahani, 2012). Figure 4.1 illustrates the method, showing $\log(A_{Dref})$ versus moment magnitude for events in the Northeast and CUS.

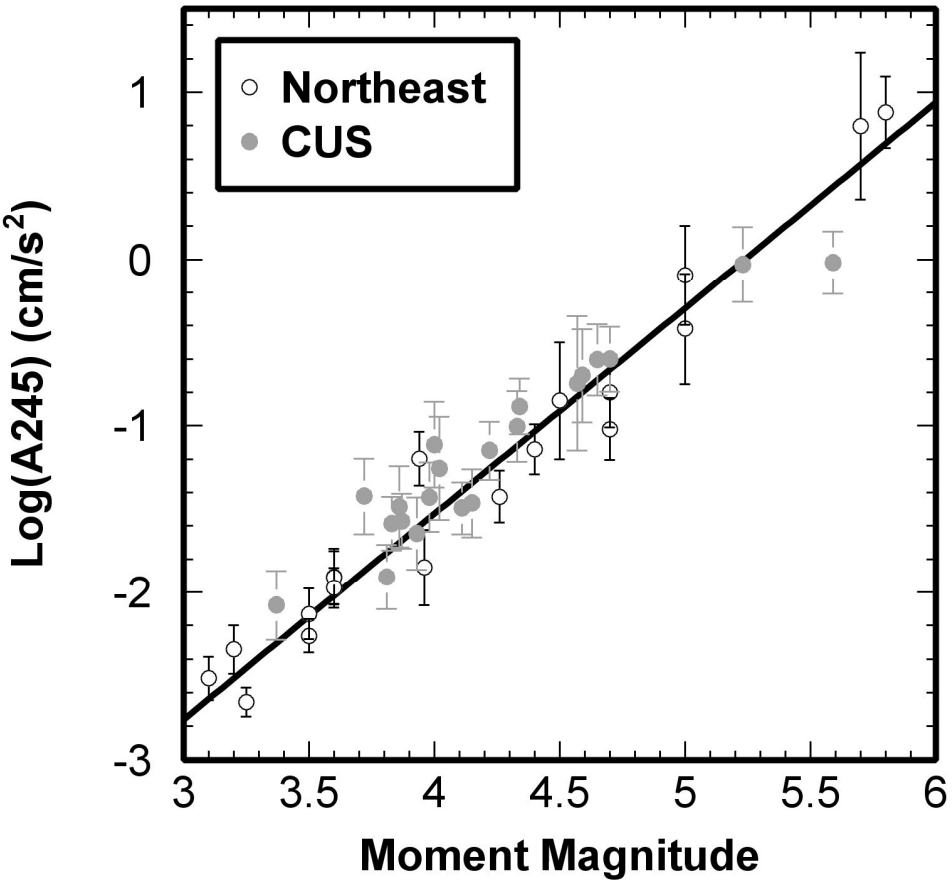

Figure 4.1 Plot of vertical 1-Hz PSA estimated at regional distances versus known moment magnitude for ENA. A245 refers to PSA amplitude (cm/s^2) at 245 km. (from Atkinson and Babaie Mahani, 2012).

Figures 4.2 and 4.3 show the locations of the study events across North America. Figure 4.4 shows the distribution of the regional databases by NEHRP (National Earthquake Hazard Reduction Program) site class (Dobry et al., 2000). Information on site class comes from measured or inferred values of Vs30 (the time-averaged shear-wave velocity over the top 30m of the deposit) as documented by several studies: Atkinson (2004), Atkinson and Morrison (2009), Wong et al. (2011), Chris Cramer (written communication, July 2010) or Wald and Allen (2007). In the Northeast, the majority of records are for site class A (Vs30>1500 m/s), while C (Vs30 360 to 760 m/s) is the dominant site class in other regions. Accounting for these regional differences in predominant site class is important when comparing ground-motion amplitudes across regions.

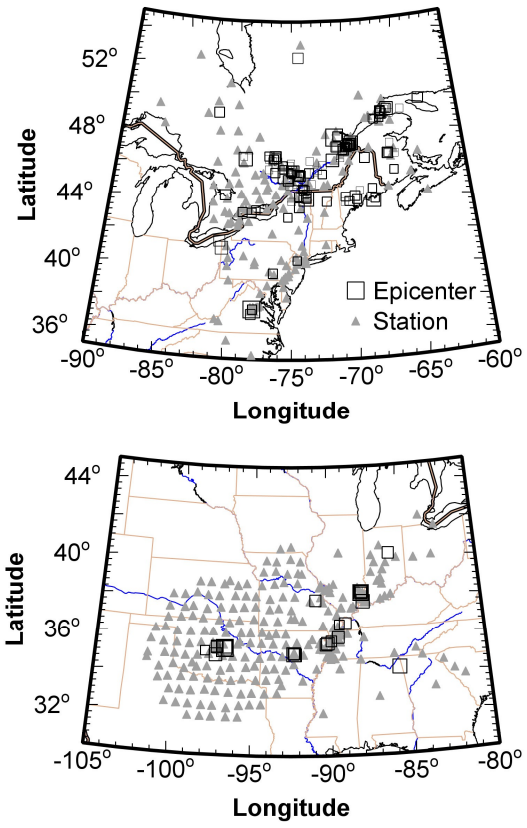

Figure 4.2 Location of earthquakes with moment magnitude (known and estimated) in ENA (top: Northeast; bottom: CUS). The size of epicenters corresponds to the magnitude of the events.

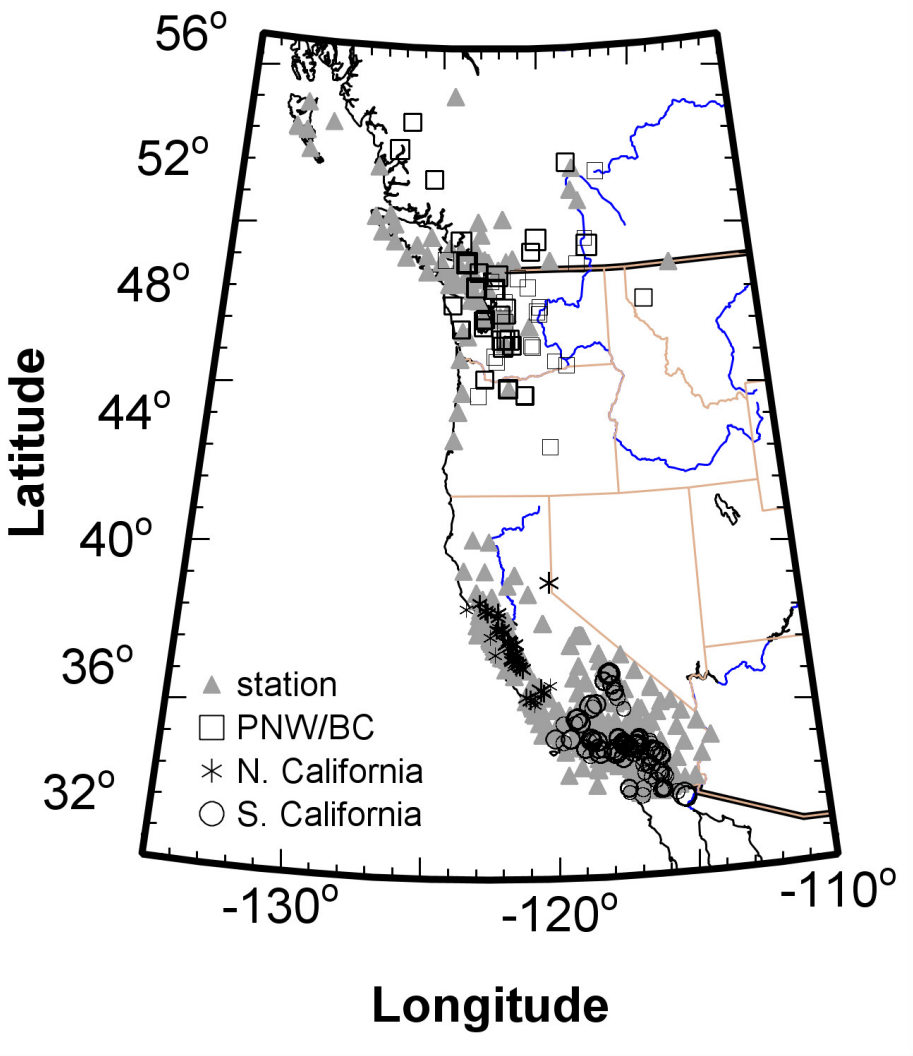

Figure 4.3 Location of earthquakes with moment magnitude (known and estimated) in WNA. The size of epicenters corresponds to the magnitude of the events.

Figure 4.5 shows the magnitude and distance distribution of ground-motion amplitudes available for the comparisons in each region. Overall there are 563 earthquakes in our database with over 18000 records. Table 4.1 shows the number of events and records in each region and their relative percentages within the database. Ground-motion amplitudes in each region are fairly well distributed across a number of events - in other words, they are not biased toward a specific event. However, for the CUS the database is relatively sparse compared to that available for the other regions.

The availability of data, particularly in the CUS, will be a limiting factor in our ability to draw conclusions.

Table 4-1 Number of events and records used in this study. V and H refer to vertical component and geometric mean of the horizontal components, respectively. The number in parentheses are the relative percentages of events and records within the database.

Region	events	V	H
Northeast	202 (36)	1972 (20)	1041(12)
CUS	30 (5)	1294 (13)	1219 (14)
PNW/BC	87 (15)	756 (8)	577 (7)
N. California	105 (19)	2296 (23)	2296 (27)
S. California	139 (25)	3478 (36)	3478 (40)
Total	563 (100)	9796 (100)	8611(100)

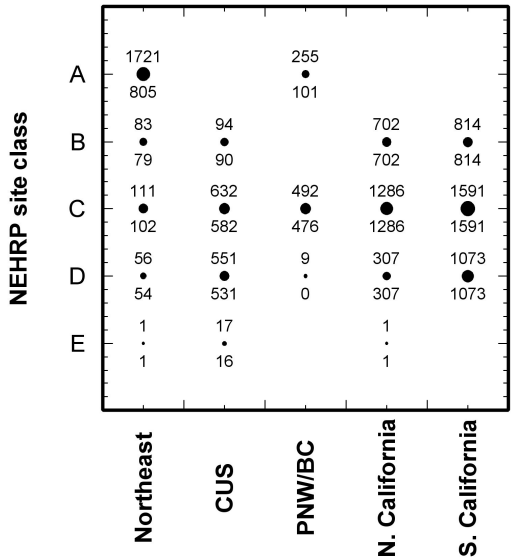

Figure 4.4 Plot of records in each region by NEHRP site class for vertical component (upper digit) and geometrical mean of the horizontal components (lower digit). The size of circles indicates the relative number of records, for the vertical component.

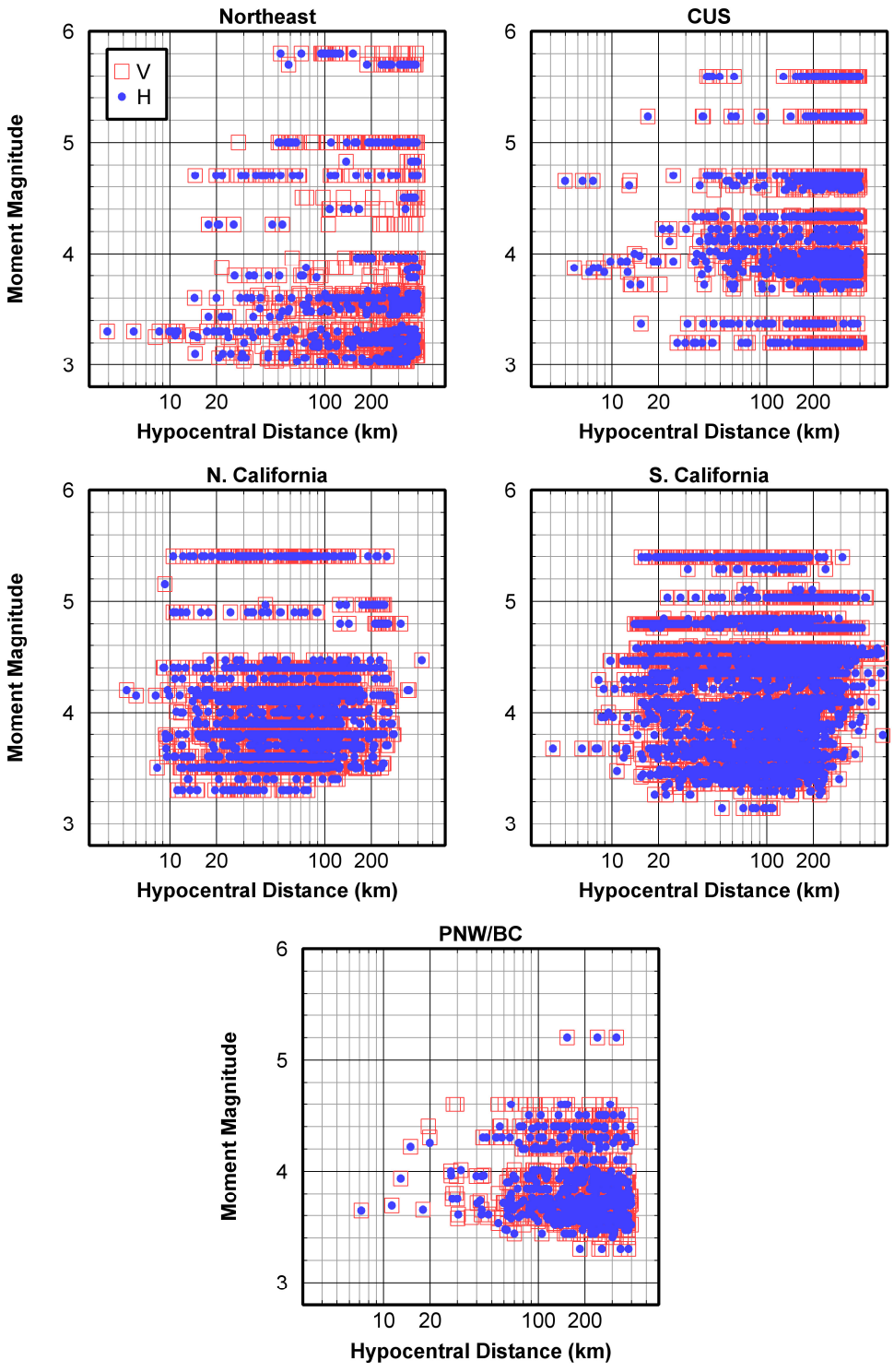

Figure 4.5 Magnitude and Distance distribution of ground-motion amplitudes for vertical component (V) and geometrical mean of the horizontal components (H) in each region. Magnitude is **M**, when available, otherwise estimated **M** was used.

4.3 Regional differences in ground-motion amplitudes across North America

The ground-motion amplitude measures in each region were grouped into magnitude and distance bins to facilitate comparisons. The magnitudes were binned into 0.3 units in width; **M** 3.0-3.3 (3.15), 3.3-3.6 (3.45), 3.6-3.9 (3.75), and so on, where the number in parentheses indicates the center of the bin. The distance bins considered were 0.1 log units in width; 0.1 (1.26 km), 0.2 (1.58 km), and so on. For vertical-component motions, it is assumed that site effects do not have a significant effect on the observed amplitudes; this is in accordance with a number of studies in the literature to this effect (e.g. Nakamura, 1989; Lermo and Chavez Garcia, 1993). However, the horizontal-component motions are expected to be significantly influenced by soil stiffness, with soil sites incorporating larger amplification effects than rock sites. In order to make best use of the available data, we use an empirical correction for the horizontal-component (geometric mean), to allow all comparisons to be made for the equivalent of B/C boundary site conditions (Vs30=760 m/s). The correction factor for site condition is made as follows. For the hard-rock (A class) sites (mostly in the Northeast, with some in the PNW/BC), we use the coefficients provided by Atkinson and Boore (2011, Table 2) to correct horizontal-component amplitudes to equivalent values for B/C site conditions. For other site classes, we use the site correction coefficients of Boore and Atkinson (2008, Table 3), assuming that site response is in the linear range due to the low amplitudes considered in this study.

Figures 4.6 and 4.7 provide an example comparison of PSA-1Hz and PGA amplitudes versus hypocentral distance for the vertical component, and for the geometric mean of the horizontal components in two magnitude bins for which the data are relatively abundant: **M**= 3.45 (3.3-3.6) and **M**= 4.95 (4.8-5.1) for S. California and Northeast. Similar figures are provided for each of the other regions in the appendices of this thesis (for CUS and PNW/BC, **M**= 3.75 (3.6-3.9) and **M**= 4.65 (4.5-4.8) are plotted). The number of events varies with magnitude bins and regions; the smaller magnitude bins (3.45 and 3.75) have 7 to 9 events, while the larger magnitude bins (4.65 and 4.95) generally have 3 or more events. The fact that we see similar trends for the horizontal and vertical components

suggests that the applied site correction factors are reasonable. An initial observation from Figures 4.6 and 4.7 is that regional differences in observed amplitudes vary with distance, frequency and magnitude; this makes the task of characterizing the differences difficult. It should be noted that PGA in the Northeast is a different parameter than PGA in S. California. The reason is that if the Fourier amplitude spectrum is band-limited by attenuation at some frequency (fh), then PSA tends to become constant for oscillator frequencies greater than fh, whereas the Fourier amplitudes continue to decay as a function of increasing frequency. Because the value of fh in the Northeast corresponds to higher frequencies than in the S. California, the PGA in the Northeast would be representative of the Fourier acceleration amplitude at higher frequencies (Atkinson and Hanks, 1995; Atkinson, 2004).

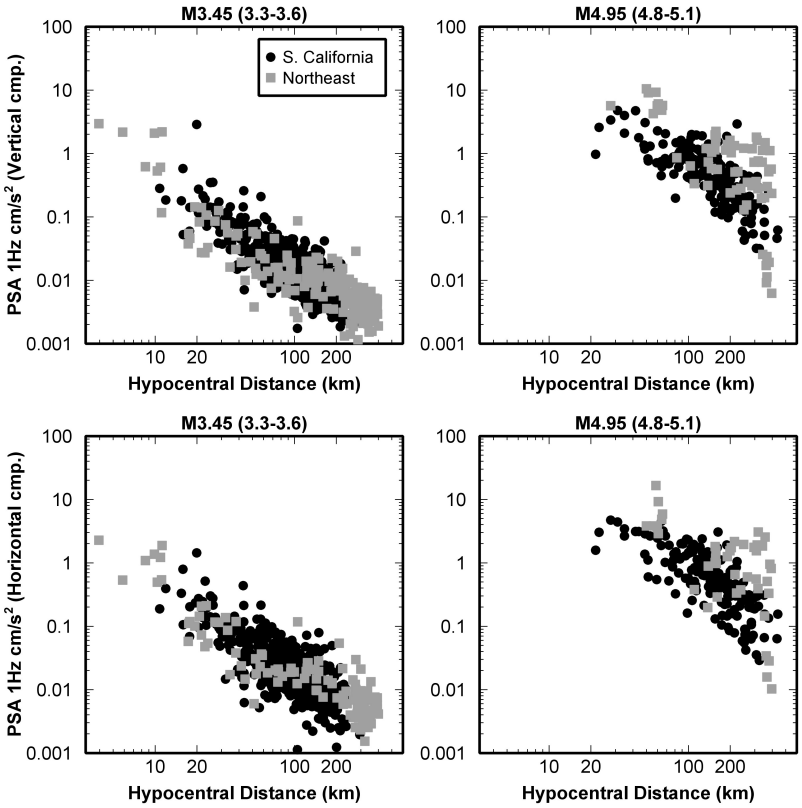

Figure 4.6 Plot of PSA-1Hz (cm/s^2) versus hypocentral distance for the vertical component and geometrical mean of horizontal components in two magnitude bins, **M=** 3.45 and 4.95 for S. California and Northeast (all for B/C site condition).

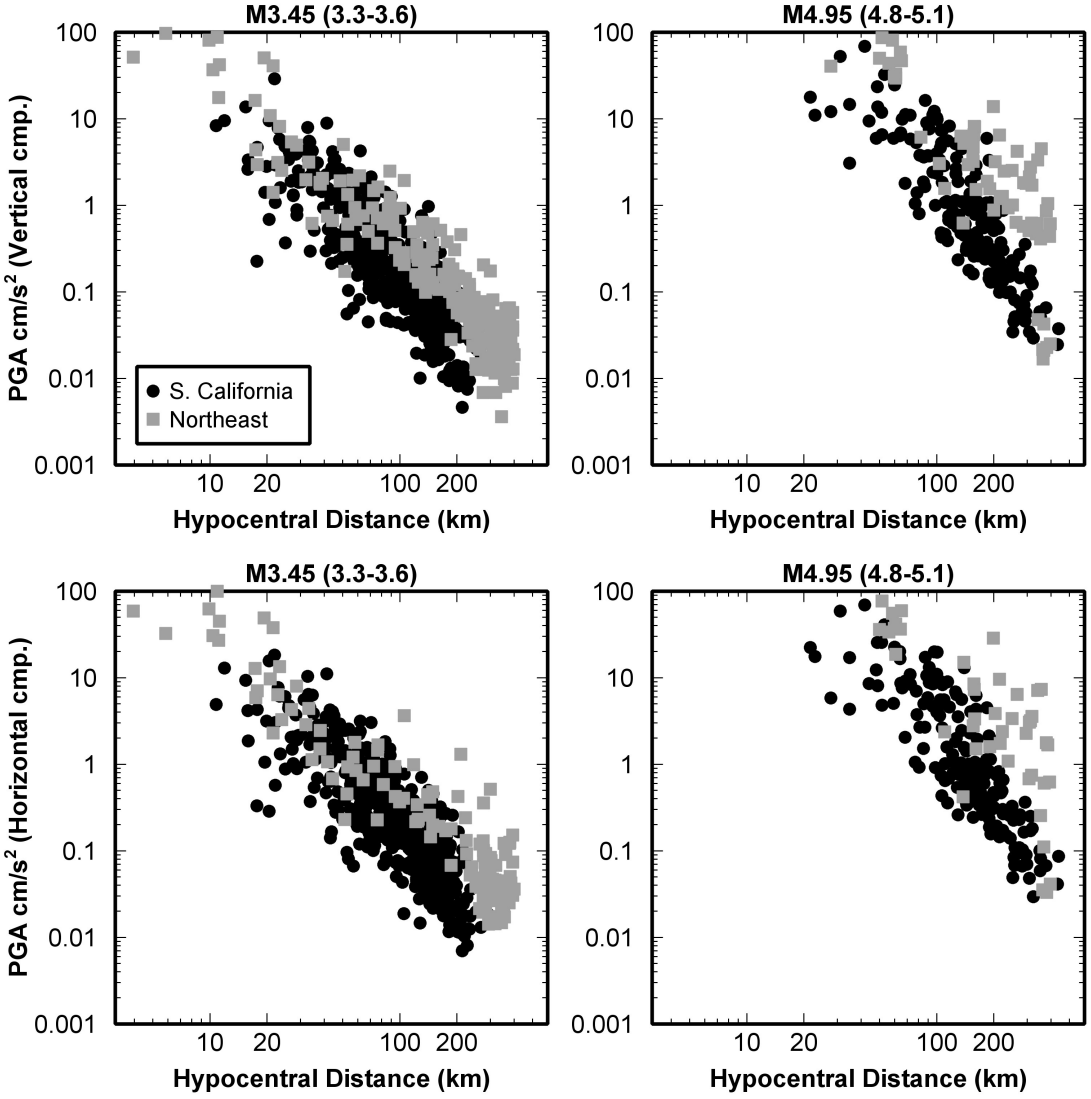

Figure 4.7 Plot of PGA (cm/s^2) versus hypocentral distance for the vertical component and geometrical mean of horizontal components in two magnitude bins, **M**= 3.45 and 4.95 for S. California and Northeast (all for B/C site condition).

It is well known that attenuation in eastern North America differs from that in the west at regional distances. Anelastic losses of high-frequency energy are less in the east than in the west, due to the higher regional Quality factor (Q); the effects of Q on regional attenuation across North America have been well-documented (e.g. Benz et al., 1997). Furthermore, in the east, a pronounced wave train of multiply-reflected and refracted shear waves develops at distances beyond about 70 to 150 km (the Lg phase) (Kennett,

1986; Atkinson, 2012). However, while attenuation differences at large distances are known, there has been a lack of information on regional attenuation differences at distances less than 70 km, and in particular regional differences in geometric spreading at close distances. This issue is particularly important for GMPE development, and for seismic hazard analysis. We use the data of this study to obtain estimates of apparent geometric spreading at close distances in each region, using cut-off distances 40, 50, 60, and 70 km (so that we can see the effect of distance range on the results). To isolate the effects of geometric spreading from those of anelastic attenuation, we first correct all amplitudes for anelastic absorption effects (Q factor), using typical values of Q from the literature for each region. Q is inversely related to the anelastic attenuation coefficient (γ) (Atkinson and Mereu, 1992):

$$\gamma = (-\pi f/Q\beta) \tag{4.2}$$

where f is frequency and β *is* shear-wave velocity (in km/s); ground-motion amplitudes decay from anelastic effects as exp(-γ D) (in which D is distance). We can therefore correct the amplitudes for anelastic effects by multiplying them by exp(γ D); this correction is relatively minor for short distances, growing more important as distance increases.

For the Northeast and CUS, we used the frequency-dependent Q model assumed by Atkinson and Boore (2006) to correct the amplitudes for anelastic attenuation: Q=893 $f^{0.32}$ (with a minimum Q of 1000). For PNW/BC, the Q model determined by Atkinson (2005) was used: Q=229 $f^{0.60}$, while for California, we used Q = 280 $f^{0.50}$ from Fatehi and Herrmann (2008).

We regress the Q-corrected amplitudes, all for B/C site conditions, to obtain an estimate of geometric spreading, using:

$$Log(A) = a + blog(R) \tag{4.3}$$

where A is the PSA at a certain frequency and R is the hypocentral distance. b is the geometric spreading coefficient to be determined from regression and a is the intercept which is the average of all source terms in the regression. We repeated the regression for

different cut-off distances (from 40 to 400 km with 10 km interval). Table B-1 in the Appendices shows the parameters of Equation (4.3) in each region (for each frequency).

Figure 4.8 shows how the obtained values of apparent geometric spreading vary across the regions. The near-source (less than 70 km) geometric spreading coefficient is frequency-dependent in all regions. Overall, S. California has a steeper (more negative) geometric spreading coefficient than other regions. The change in the slope of geometric spreading (transition from direct waves to refracted waves) occurs at closer cut-off distances in the Northeast (50 km) than in other regions. In PNW/BC and CUS, the availability of data in the first 60 km is poorer than for the other regions, therefore, the slope is not well defined at close distances. The apparent geometric spreading at distances <50 km is steeper than 1/R in all regions except possibly the CUS, and shows some frequency dependence. In California and the CUS, the attenuation appears to be slower at low frequencies, possibly reflecting contributions of surface waves. By contrast, in the northeast the apparent geometric attenuation, after removal of anelastic effects, is less at high frequencies than at low frequencies.

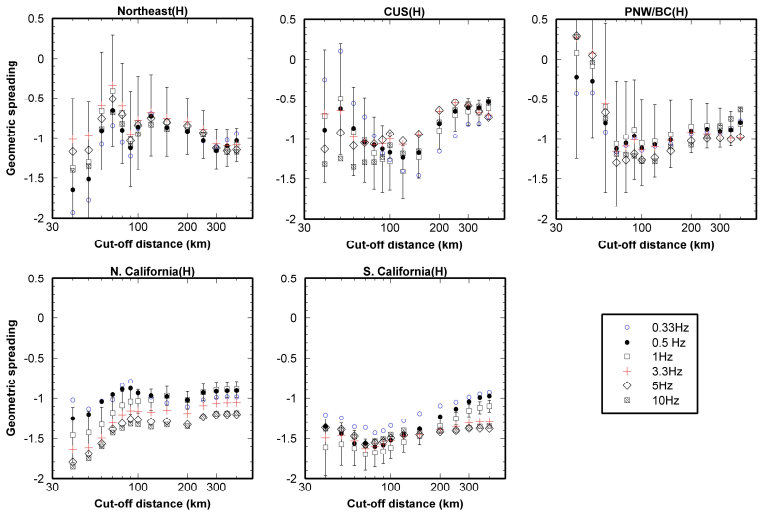

Figure 4.8 Apparent geometric spreading coefficient (horizontal component, geometric mean), after correction for regional Q, for different cut-off distances (with respect to distance from the source). Error bars are plotted for coefficient at 1Hz (Error bars are similar for other frequencies).

Figures 4.9 and 4.10 show the log-averaged PSA-1Hz and PGA (in cm/s^2) versus hypocentral distance for the vertical component and geometric mean of the horizontal components in two example magnitude bins, **M=** 3.45 and **M=** 4.95 for N. California and the Northeast in comparison to S. California. Points are plotted only if at least 3 events, each of which has at least 3 records, are included in a bin. For bins with many observations, the standard error of the mean is quite small, even though variability is significant (as indicated by the symbols), enabling confident distinction of average amplitude differences. We observe that there is a more complex transition to regional attenuation in the Northeast than in California; note the flat portion of the attenuation curve from about 50 to 150 km. At regional distances, high-frequency attenuation is markedly slower in the Northeast than in California, as expected. However, regional attenuation differences, even at large distances, are not readily apparent at 1 Hz. Additional figures of this type are shown for the other regions and other ground-motion parameters in the appendices of this thesis. Our overall interpretation of these figures is that the regional attenuation in eastern North America is slower than S. California, but mostly at > 100 km. In the CUS, the trend is visible at both low and high frequencies while it is only apparent at high frequency in the Northeast. For the PNW/BC, attenuation is faster than S. California over all distances and all frequencies. The results for N. California are frequency-dependent, with the low frequency amplitudes being higher than those for S. California at distances more than ~40 km. At high frequency, however, the ground motions from S. California become higher at all distances. We also note that very similar trends are seen for the site-corrected horizontal component as are seen for the vertical component. This suggests that the implemented site corrections are effective in removing the gross site effects. Looking at such figures is a good way to visualize the regional differences in ground-motion amplitudes, but does not provide a statistical conclusion.

To put the results of the amplitude comparisons on a more statistical footing, we performed a standard t-test between ground-motion amplitudes (in magnitude and distance bins) in each region in comparison to those in S. California. The t-test results for the Northeast (geometric mean of the horizontal components) are shown in Figure 4.11 (with all amplitudes corrected to B/C site class). The results show that the regional

differences between the Northeast and S. California are clearly significant at larger distances (more than ~100 km), but are of marginal significance at closer distances (no consistent differences pop out across magnitude-distance bins). Significant differences are especially noted at higher frequencies (PSA10Hz and PGA). This confirms the inferences drawn from inspection of Figures 4.9 and 4.10 concerning the slower attenuation of motions in the Northeast at high frequencies. The results of statistical t-test for the CUS, N. California, and PNW/BC are presented in the appendices of this thesis, for both the horizontal and vertical components. Overall, the differences are concentrated at regional distances in the CUS at all frequencies. In N. California, the results of t-test show differences at distances beyond 20 km for all frequencies. The differences between southern and northern California are most obvious at low magnitudes, but appear to persist to higher magnitude levels. For PNW/BC, the differenes exist at all frequencies with differences at low frequency being most significant. Similar conclusions are drawn by inspection of either the horizontal or vertical components.

To examine the size of regional differences in ground-motion amplitudes in a quantitative manner, we used the ratios of ground-motion amplitudes in each region over those for the reference region of S. California. For each region the log-averaged ground-motion amplitudes (e.g. PSA 0.33 Hz) in each magnitude-distance bin were divided by the corresponding value in S. California (R = X/Y where X and Y are the log-averaged ground-motion amplitudes (for a specific frequency) in a magnitude-distance bin for a region and S. California, respectively). The propagation of error due to division was then calculated from Equation (4.4):

$$\Delta R = \sqrt{(\Delta X / X)^2 + (\Delta Y / Y)^2} \tag{4.4}$$

where ΔR refers to the error of ratio (R), and ΔX, and ΔY are the standard error of the log-averaged ground motions in each magnitude-distance bin for each region and S. California, respectively.

Figures 4.12 to 4.15 show examples of the the ratios of ground-motion amplitudes (PSA 1Hz and PGA, respectively) in each region to S. California for the vertical component and geometric mean of the horizontal components. The weighted average of

ratios in each distance bin (for all magnitudes) is also plotted, where the weights are based on the number of observations. Table B2 and additional figures in the appendices of this thesis show these ratios for PSA0.33Hz, PSA1Hz, PSA3.3Hz, and PGA.

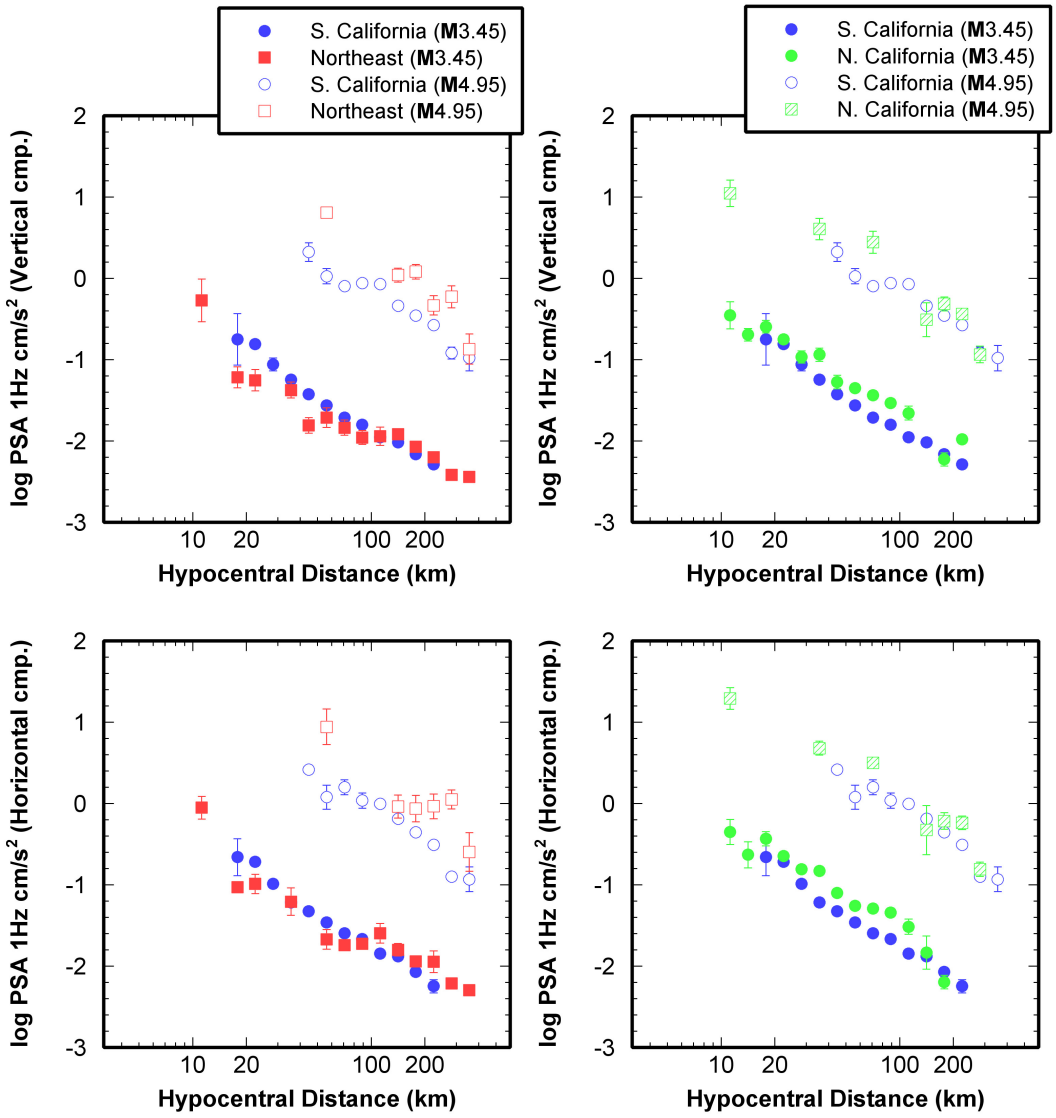

Figure 4.9 Plot of log-averaged PSA-1Hz (cm/s^2) versus hypocentral distance for the vertical component and geometric mean of the horizontal components in two magnitude bins, **M**= 3.45 and 4.95, for Northeast and N. California, in comparison to S. California. All amplitudes corrected to site class B/C. Error bars show the standard error of the average of the ground motions in each magnitude-distance bin. Points are plotted only if at least 3 events, each of which has at least 3 records, are included in a bin.

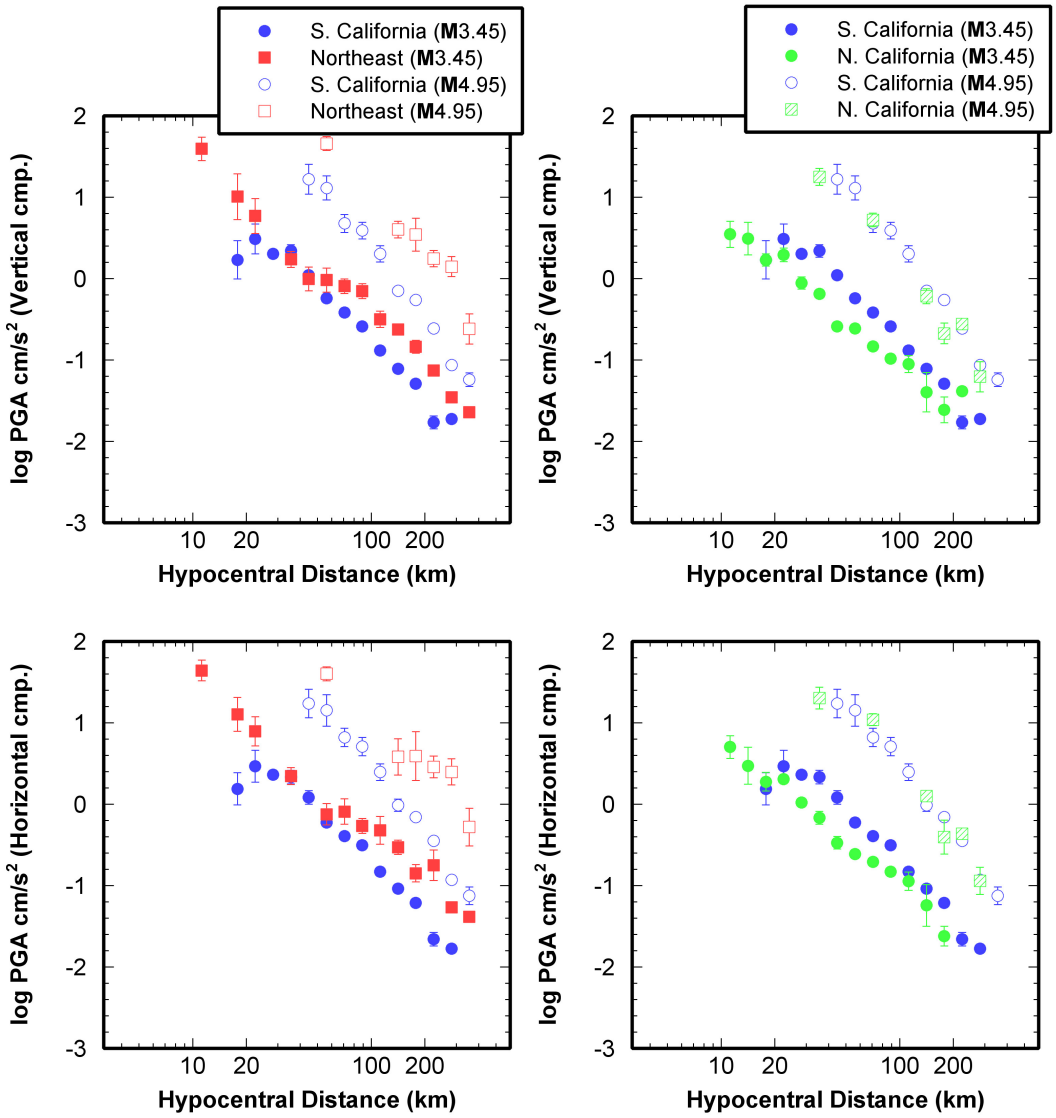

Figure 4.10 Plot of log-averaged PGA (cm/s^2) versus hypocentral distance for the vertical component and geometric mean of the horizontal components in two magnitude bins, **M**= 3.45 and 4.95 for Northeast and N. California, in comparison to S. California. All amplitudes corrected to site class B/C. Error bars show the standard error of the average of ground motions in each magnitude-distance bin. Points are plotted only if at least 3 events, each of which has at least 3 records, are included in a bin.

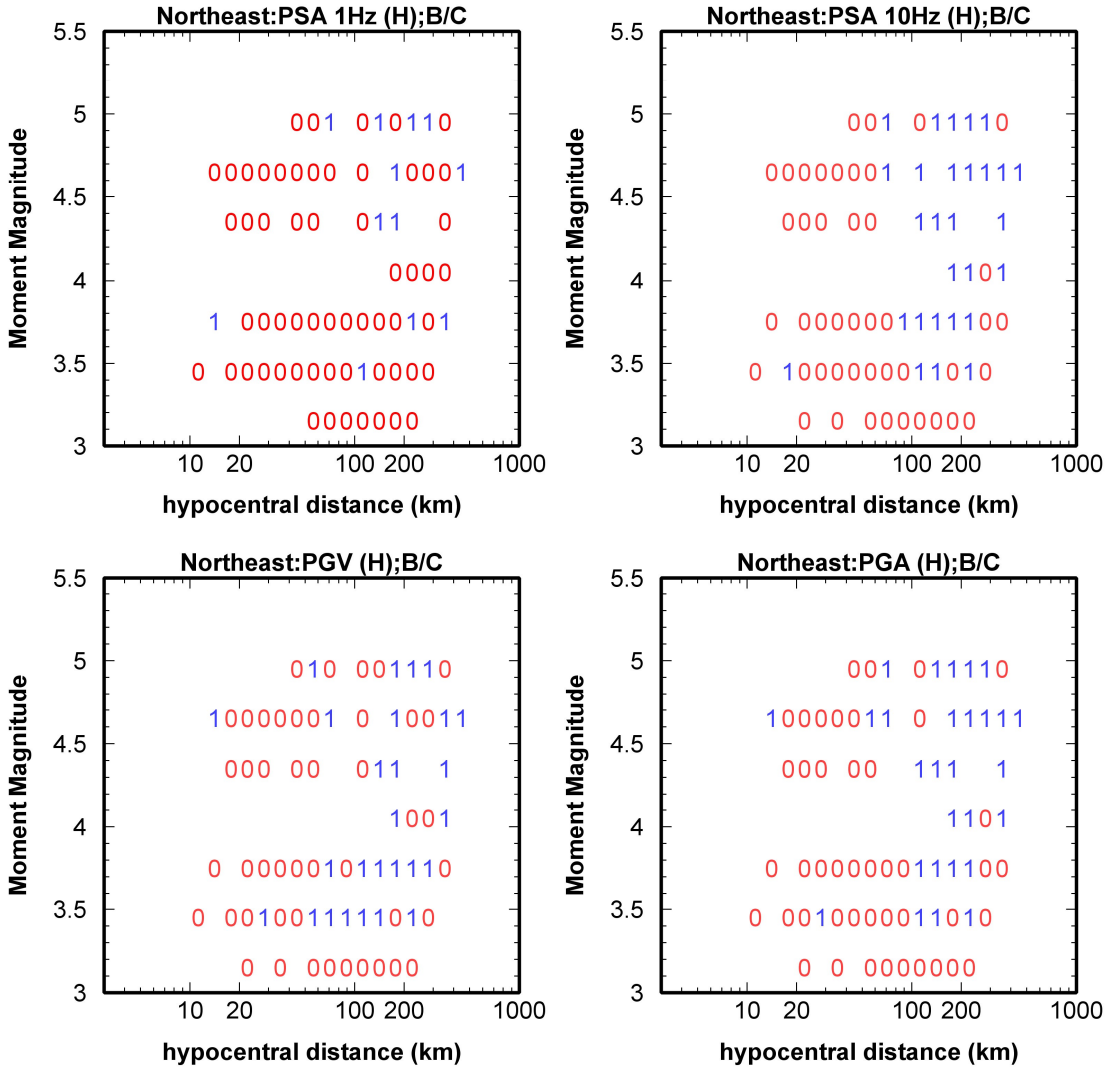

Figure 4.11 Results of statistical t-test for the binned horizontal ground motions (all records corrected to site class B/C) in Northeast and S. California. h = 1 is for the case where the difference in ground motions are statistically significant (at probability level = 0.05), h=0 means differences are not statistically significant.

Overall, one of the most noteworthy observations is that the strength of regional differences between ground motions in the Northeast and S. California is highly dependent on frequency. Ground motions show similar amplitudes to those of S. California over all distances at low frequencies (0.33 and 1 Hz), although the attenuation trends appear to be more complex in the Northeast. At high frequency (PGA), however,

ground motions in the Northeast become higher than those in S. California over all distances. In the CUS, ground motion amplitudes are larger than those in S. California at both low and high frequencies at distances more than 100 km across all magnitudes available. At distances less than 100 km, CUS amplitudes are lower than those for S. California at frequencies greater than 1Hz. Interestingly, the PNW/BC amplitudes are systematically lower than those of S. California over all distances for the entire frequency range, except at low frequency (0.33 Hz) where the two regions show similar amplitudes. N. California shows similar amplitudes to S. California at low frequencies, and slightly lower amplitudes for PGA, over all distances. This appears to be the case for the entire magnitude range studied. This is an important observation, as it suggests that the earlier conclusion of Chiou et al. (2010) regarding a magnitude dependence of these differences may have been influenced by a paucity of data (the current study has much more data for N. California).

4.4 Influence of site effects

One of the significant factors that can lead to apparent regional differences in ground-motion amplitudes is regional variability in site amplification effects that are reflected in the average ground motions. This is certainly the case in North America. Most recordings in the Northeast are on rock sites, while those in the CUS and California are predominantly on soil sites. A convenient way of summarizing the expected effects is to consider the average horizontal to vertical component ratio. This is a good preliminary measure of average site amplification effects (Nakamura, 1989). Figure 4.16 shows the average value of log(H/V) versus hypocentral distance (in distance bins) for each region, at each frequency (averaged over all events within each distance bin); the average value of Vs30 (taken over all observations plotted) is also given. The ratio of H/V is systematically higher for the regions with softer site conditions predominating in the database (CUS, N. California, and S. California) than for the regions where the site category is hard rock (Northeast and PNW/BC). The ratio of H/V in the Northeast (average Vs30=1518 m/s) is near unity for all frequencies over all distances. For PNW/BC, with average Vs30 776 m/s, the H/V is about 0.2 log units, while for the other regions, where the average Vs30s is about 500 m/s, the H/V ratio is higher. With the

possible exception of S. California, H/V appears to be independent of distance over the range studied. In S. California, H/V decreases with increasing distance, with a negative slope being statistically significant at $p < 0.05$ for frequencies 0.33, 0.5, 1, 3.3, and 5 Hz. Figure 4.17 shows the log-averaged H/V in each region versus frequency over all distance bins. The average value of the site-correction factors used to correct the horizontal components to the equivalent B/C site condition is also plotted. CUS and Northeast show the highest and lowest H/V at all frequencies, respectively. This corresponds well with the average Vs30 in the two regions with CUS having the lowest (386 m/s) and Notheast the highest Vs30 (1518 m/s) among all regions. The average site-correction factor for the PNW/BC is nearly zero as the average Vs30 in this region is 776 m/s which is very close to the Vs30 for the B/C site condition (760 m/s). An interesting observation is that the H/V ratios tend to be larger than the average assumed site correction factors. This implies that there may be a bias in the applied site correction factors for the horizontal component, if H/V is indeed a good measure of site response.

4.5 Conclusions

Ground-motion amplitudes from earthquakes with **M** between 3.0 and 6.0 were studied in order to reveal regional differences in amplitudes across North America. Ratios of log-averaged ground-motion amplitudes (modified to B/C site condition for horizontal components) in each region to those in S. California were examined to decipher any dependency of the differences with magnitude, frequency and distance. The apparent geometric spreading coefficient at distances <50 km is significantly steeper than 1/R in all regions except possibly the CUS, and shows evidence of frequency dependence. The apparent geometric spreading coefficient in S. California tends to be steeper (more negative) overall than that in the Northeast, CUS, and PNW/BC while it is similar to that in N. California. The change in the slope of geometrical spreading (transition from direct waves to refracted waves) occurs at nearer distance in the Northeast (50 km) than that in other regions. In the Northeast, the strength of apparent differences in average amplitudes is highly dependent on frequency. At lower frequencies (1Hz), ground motions show similar to lower amplitudes than those in S. California over all distances. At higher frequencies (PGA), ground motions in the Northeast show higher amplitudes than those

in S. California over all distances. In the CUS, ground motions are higher than those in S. California at both low and high frequencies at distances more than 100 km for all magnitudes. Ground-motion amplitudes in the PNW/BC are lower than those in S. California over all distances for the entire frequency range at all magnitudes. Ground-motion amplitudes in N. California are similar to those in S. California at low frequencies and slightly lower than those in S. California at higher frequencies over all distances.

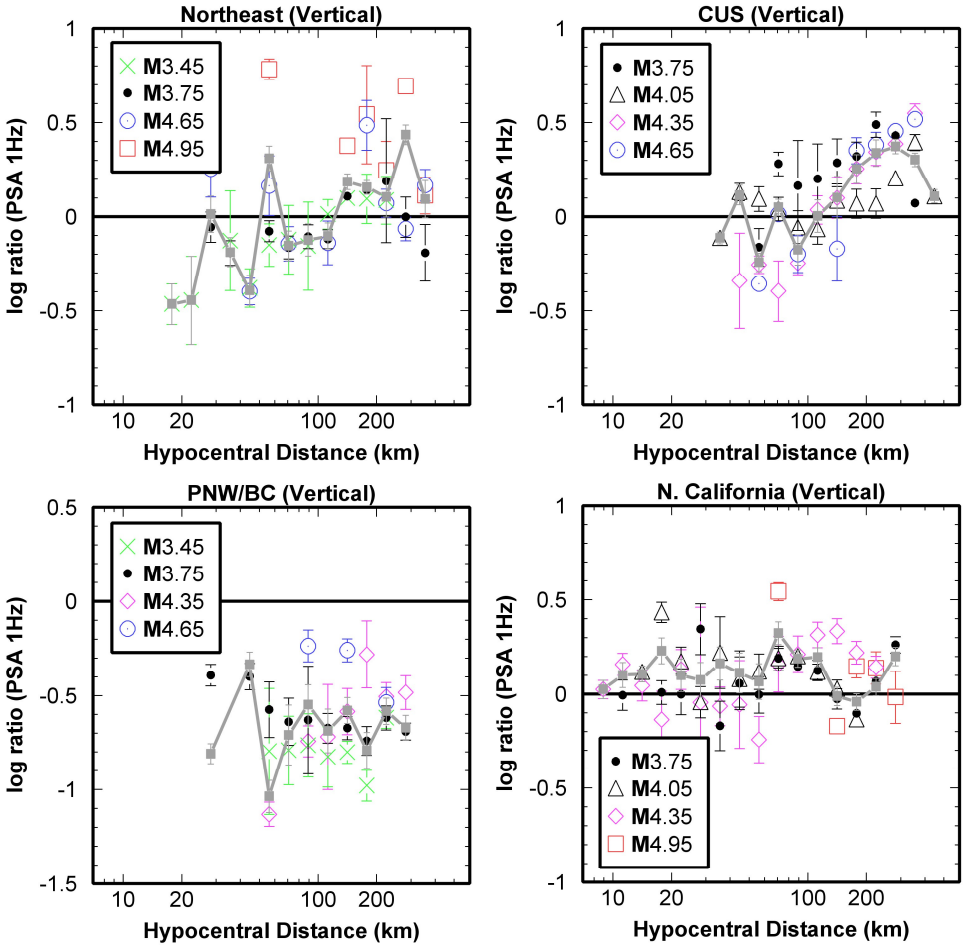

Figure 4.12 Ratios of log-averaged ground motions in each region (B/C site condition) with respect to those in S. California for PSA 1-Hz (vertical component). The error bars are the standard error from Equation 4.4. The solid line shows the weighted average of the ratios in each distance bins (for all magnitudes) with error bars showing weighted standard errors.

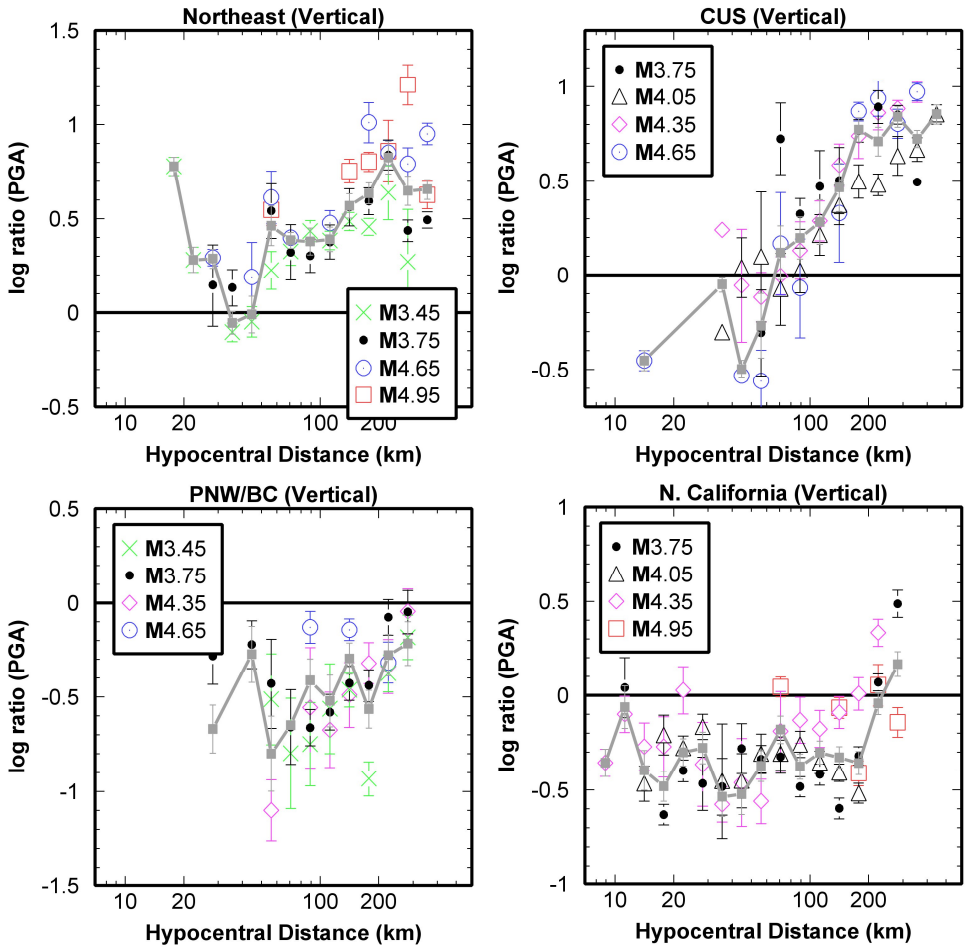

Figure 4.13 Ratios of log-averaged ground motions in each region (B/C site condition) with respect to those in S. California for PGA (vertical component). The error bars are the standard error from Equation 4. The solid line shows the weighted average of the ratios in each distance bins (for all magnitudes) with error bars showing weighted standard errors.

An important conclusion of this study is that, unlike a previous study by Chiou et al. (2010), we find little evidence for magnitude dependence in the observed differences in ground-motion amplitudes between northern and southern California. This suggests that small-magnitude data can be used to draw inferences regarding regional differences in ground motion processes that can then be applied to larger magnitudes. Noteworthy examples of such conclusions, on the basis of the observations of this study, are: (i) amplitudes in the Northeast and CUS are similar to those in California at low frequencies

(<= 1Hz) at distances out to about 150 km; (ii) amplitudes of ground motion at intermediate frequency (3.3 Hz) in the Northeast and CUS are larger than those in California, but differences are only pronounced at distances > 100 km; and (iii) PGA is higher in the Northeast and CUS than in California at all distances. These conclusions can be used to assess the relative differences that should be expected for GMPEs for the Northeast and CUS relative to GMPEs for California.

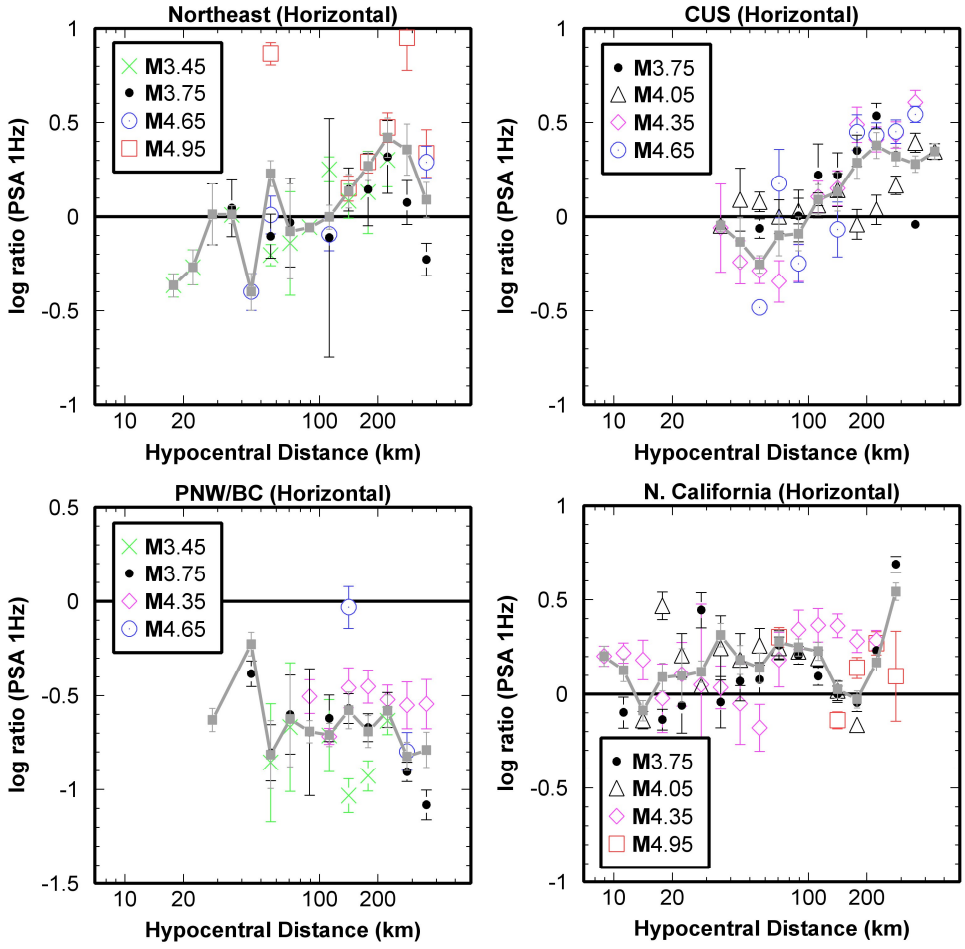

Figure 4.14 Ratios of log-averaged ground motions in each region (B/C site condition) with respect to those in S. California for PSA 1-Hz (geometric mean of horizontal components). The error bars are the standard error from Equation 4.4. The solid line shows the weighted average of the ratios in each distance bins (for all magnitudes) with error bars showing weighted standard errors.

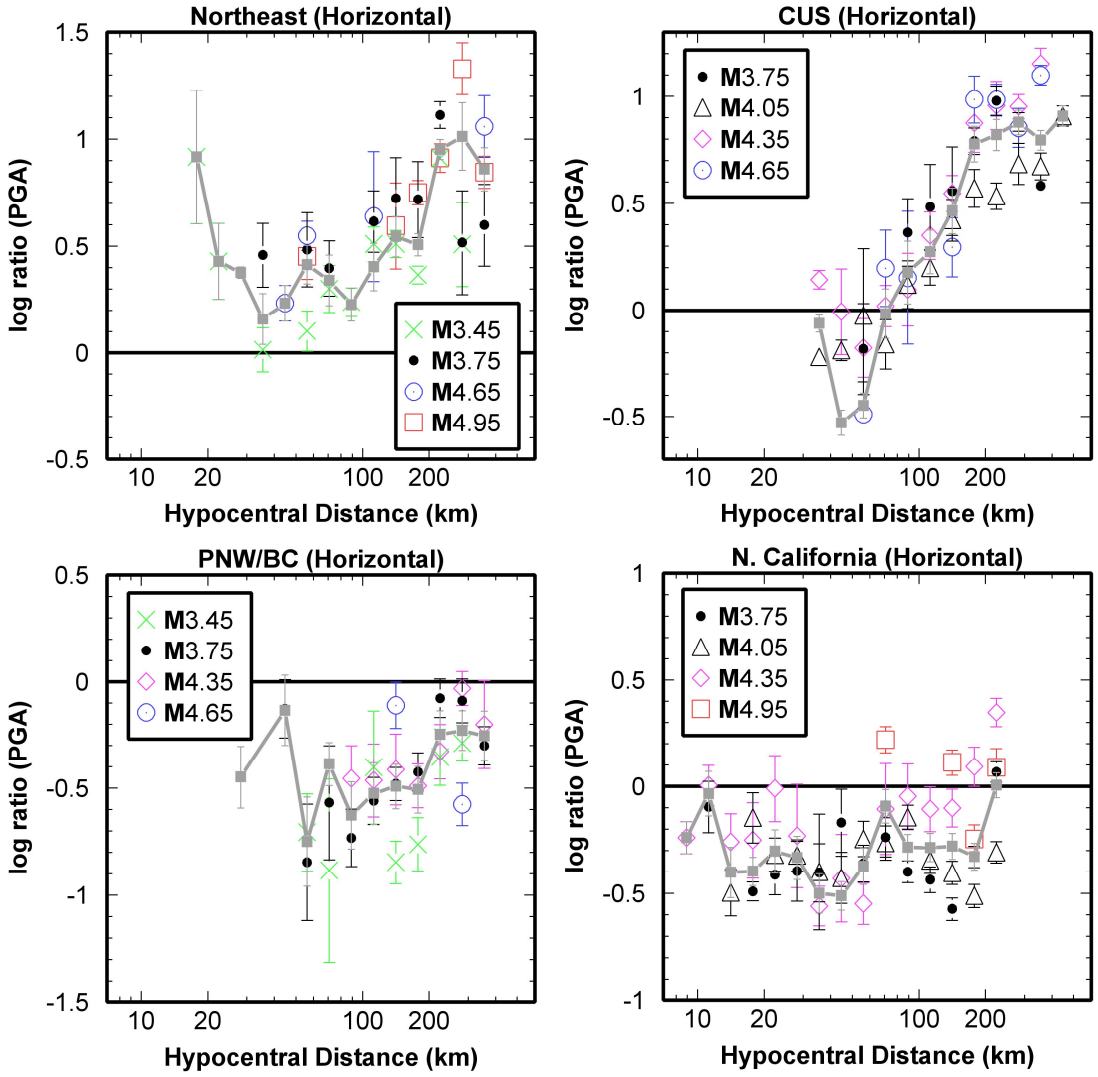

Figure 4.15 Ratios of log-averaged ground motions in each region (B/C site condition) with respect to those in S. California for PGA (geometric mean of horizontal component). The error bars are the standard error from Equation 4.4. The solid line shows the weighted average of the ratios in each distance bins (for all magnitudes) with error bars showing weighted standard errors.

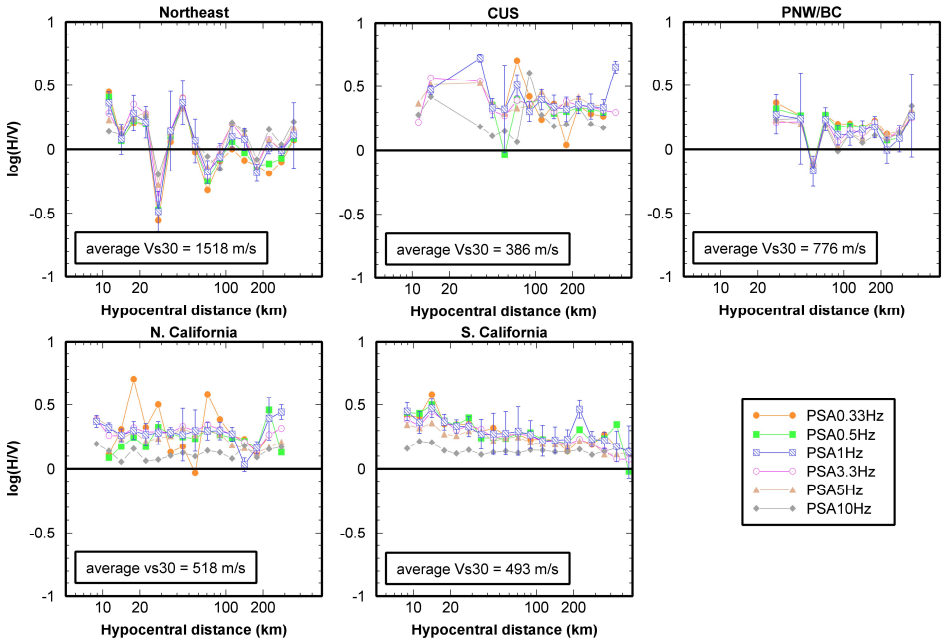

Figure 4.16 Plot of log(H/V) versus distance (averaged over all magnitude bins) in each region. Standard error of log(H/V) is plotted for 1 Hz.

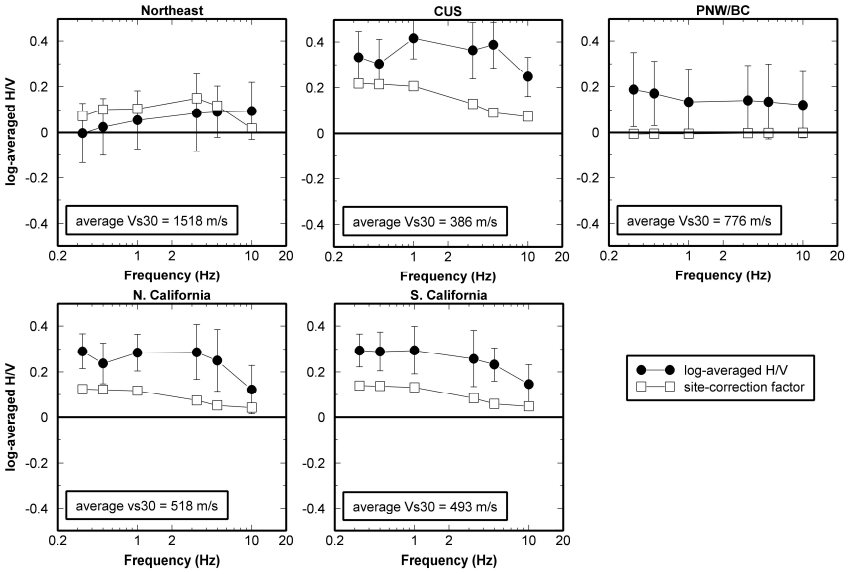

Figure 4.17 Plot of log-averaged H/V in each region versus frequency (averaged over all distance bins in Figure 4.16). The average value of site-correction factors used to correct the horizontal components to the equivalent B/C site condition is also plotted.

4.6 References

Atkinson, G. M. (2012). Evaluation of Attenuation Models for the Northeastern United States/Southeastern Canada, *Seim. Res. Lett,* **83,** 166-178.

Atkinson G. M. (2005). Ground Motions for Earthquakes in Southwestern British Columbia and Northwestern Washington: Crustal, In-Slab, and Offshore Events, *Bull. Seism. Soc. Am.* **95,** 1027-1044.

Atkinson, G. M. (2004). Empirical Attenuation of Ground-Motion Spectral Amplitudes in Southeastern Canada and the Northeastern United States, *Bull. Seism. Soc. Am.* **94,** 1079-1095.

Atkinson, G. M., and A. Babaie Mahani (2012). Estimation of Moment Magnitude from Ground Motions at Regional Distances. *Bull. Seism. Soc. Am*. (in press).

Atkinson, G. M., and D. M. Boore (2011). Modifications to Existing Ground-Motion Prediction Equations in Light of New Data, *Bull. Seism. Soc. Am.* **101,** 1121-1135.

Atkinson, G. M., and D. M. Boore (2006). Earthquake Ground-Motion Prediction Equations for Eastern North America, *Bull. Seism. Soc. Am.* **96,** 2181-2205.

Atkinson G. M., and T. C. Hanks (1995). A High-Frequency Magnitude Scale, *Bull. Seism. Soc. Am.* **85,** 825-833.

Atkinson, G. M., and R. Mereu (1992). The shape of Ground Motion Attenuation curves in Southeastern Canada, *Bull. Seism. Soc. Am.* **82,** 2014-2031.

Atkinson, G. M., and M. Morrison (2009). Observations on Regional Variability in Ground- Motion Amplitudes for Small-to-Moderate Earthquakes in North America, *Bull. Seism. Soc. Am.* **99**, 2393-2409.

Babaie Mahani, A., and G. M. Atkinson (2012). Evaluation of Functional Forms for the Attenuation of Small-to-Moderate-Earthquake Response Spectral Amplitudes in North America. *Bull. Seism. Soc. Am.* **102,** 2714-2726.

Benz, H., A. Frankel, and D. Boore (1997). Regional Lg attenuation for the continental United States, *Bull. Seism. Soc. Am.,* **87,** 606-619.

Boore, D. M., and G. M. Atkinson (2008). Ground-Motion Prediction Equations for the Average Horizontal Component of PGA, PGV, and 5%-Damped PSA at Spectral Periods between 0.01s and 10s, *Earthquake Spectra,* **24,** 99-138.

Chiou, B., R. Youngs, N. Abrahamson, and K. Addo (2010). Ground-Motion Attenuation Model for Small-To-Moderate Shallow Crustal Earthquakes in California and Its Implications on Regionalization of Ground-Motion Prediction Models, *Earthquake Spectra,* **26,** 907-926.

Dobry, R., R. D. Borcherdt, C. B. Crouse, I. M. Idriss, W. B. Joyner, G. R. Martin, M. S. Power, Rinne, and R. B. Seed (2000). New site coefficients and site classification system used in recent building seismic code provisions, *Earthquake Spectra*, **16,** 41-67.

Fatehi, A. and R. B. Herrmann (2008). High-Frequency Ground-Motion Scaling in the Pacific Northwest and in Northern and Central California, *Bull. Seism. Soc. Am.* **98,** 709-721.

Hanks, T. C., and H. Kanamori (1979). A Moment Magnitude Scale, J. Geophys. Res. 84 (B5): 2348–2350.

Lermo and Chávez-García (1993). Site effects evaluation using spectral ratios with only one station, *Bull. Seism. Soc. Am.,* **83,** 1574 – 1594.

Nakamura, Y. (1989). A Method for Dynamic Characteristics Estimation of Subsurface using Microtremor on the Ground Surface, *Quarterly Report of Railway Technical Research Institute (RTRI),* **30,** 1.

Nuttli, O. (1973). Seismic Wave Attenuation and Magnitude Relations for Eastern North America, J. Geophys. Res. 78, 876-885.

Wald, D. J., and T. I. Allen (2007). Topographic Slope as a Proxy for Seismic Site Conditions and Amplification, *Bull. Seism. Soc. Am.* **97,** 1379-1395.

Wong, I. G., K. H. Stokoe II, B. R. Cox, Y. Lin, and F. Menq (2011). Shear-wave velocity profiling of strong motion sites that recorded the 2001 Nisqually, Washington, earthquake, *Earthquake Spectra* **77,** 183-212.

Chapter 5

5 Conclusions and future studies

5.1 Summary and conclusions

In chapter 2 we examined thirty-two alternative combinations of linear, bi-linear and tri-linear attenuation shapes to assess their ability to describe the decay of amplitudes in 5 regions: Northeast, the CUS (including New Madrid), the PNW/BC, N. California and S. California. The residual plots for alternative shapes do not show any apparent significant differences between them, making it difficult to conclude which is the best model for each region. An AIC test was performed to see if statistical analyses reveal whether one model is superior to the others. The best AIC values are not consistent over frequency; nevertheless, we tabulate the best model on average (0.33 to 10 Hz) from each of the three trial forms of linear, bi-linear and tri-linear, for each region. We note that a simple linear form with geometric spreading ~1 in the East and ~1.3 in the West is a reasonable "first-order" description of the attenuation within 300 km across North America, and works as well as more complex models in describing regional attenuation. However, there may be advantages to using at least a bi-linear form to distinguish between direct-wave and surface-wave spreading regimes. Near-source geometric spreading under the bi-linear model appears to be in the range of $R^{-1.1}$ to $R^{-1.3}$ for most regions, with the CUS (including New Madrid) showing slower attenuation, and Southern California showing faster attenuation. Tri-linear models are a better fit to the data in some regions (Northeast), but may have no practical advantage over simpler models. These conclusions may be used to inform alternative choices for input attenuation forms in the development of ground-motion prediction models and other applications.

Estimation of moment magnitude was the subject of chapter 3. Moment magnitude can be estimated for events in North America of $\mathbf{M}<6$ from regional 1-Hz response spectral amplitudes (vertical component), with an uncertainty of <0.2 units (standard deviation of residuals) in most regions, using the relationships provided in Equations 3.2 to 3.5. The relationship between **M** and PSA_{1v} is robust and reliable for events having as few as 5

observations in the distance range from 100 to 400 km (100 to 300 km for Offshore and California; 100 to 400 km for PNW/BC; 150 to 400 km for Northeast and CUS). The empirical relationship for the Northeast and CUS is consistent with the predictions of a stochastic point-source model for a typical regional attenuation model for ENA.

Finally in chapter 4 we studied ground-motion amplitudes from earthquakes with **M** between 3.0 and 6.0 in order to reveal regional differences in amplitudes across North America. Ratios of log-averaged ground-motion amplitudes (modified to B/C site condition for horizontal components) in each region to those in S. California were examined to decipher any dependency of the differences with magnitude, frequency and distance. The apparent geometric spreading coefficient at distances <50 km is significantly steeper than 1/R in all regions except possibly the CUS, and shows evidence of frequency dependence. The apparent geometric spreading coefficient in S. California tends to be steeper (more negative) overall than that in the Northeast, CUS, and PNW/BC while it is similar to that in N. California. The change in the slope of geometrical spreading (transition from direct waves to refracted waves) occurs at nearer distance in the Northeast (50 km) than that in other regions. In the Northeast, the strength of apparent differences in average amplitudes is highly dependent on frequency. At lower frequencies (1Hz), ground motions show similar to lower amplitudes than those in S. California over all distances. At higher frequencies (PGA), ground motions in the Northeast show higher amplitudes than those in S. California over all distances. In the CUS, ground motions are higher than those in S. California at both low and high frequencies at distances more than 100 km at all magnitudes. Ground-motion amplitudes in the PNW/BC are lower than those in S. California over all distances for the entire frequency range at all magnitudes. Ground-motion amplitudes in N. California are similar to those in S. California at low frequencies and slightly lower than those in S. California at higher frequencies over all distances.

An important conclusion of this study is that, we find little evidence for magnitude dependence in the observed differences in ground-motion amplitudes between northern and southern California. This is in contrast to a previos conclusion by Chiou et al. (2010), who suggested that apparent regional differences in amplitude maybe magnitude

dependent. This suggests that small-magnitude data can be used to draw inferences regarding regional differences in ground motion processes that can then be applied to larger magnitudes. Noteworthy examples of such conclusions, on the basis of the observations of this study, are:

1) Amplitudes in the Northeast and CUS are similar to those in California at low frequencies (<= 1Hz) at distances out to about 150 km.

2) Amplitudes of ground motion at intermediate frequency (3.3 Hz) in the Northeast and CUS are larger than those in California, but differences are only pronounced at distances > 100 km.

3) PGA is higher in the Northeast and CUS than in California at all distances.

These conclusions can be used to assess the relative differences that should be expected for GMPEs for the Northeast and CUS relative to GMPEs for California.

5.2 Suggestions for future studies

Regional differences in earthquake ground motion amplitudes are dependent on several factors including magnitude, distance, frequency, and site condition or a combination of these. One of the challenges in the comparison of ground motion amplitudes is obtaining uniform databases for each region; therefore updating these databases for new earthquakes is a continuous task.

Information on site conditions for many stations is based on geological interpretation and indirect measure of Vs30. This is particularly the case in Eastern North America. Since site condition has significant effect on the amplitude of ground motions, determination of the amplification factors and resonance frequency for each site is a vital task in engineering seismology. Although direct measurements of Vs30 using active seismic methods are very costly, however, with the advantage of rapidly growing databases of ground motion amplitudes in Eastern North America, studying site effects using methods such as H/V can be a good compromise.

Stochastic simulations can be used to find simple models that would be in agreement with observations. Using these models we can develop consistent sets of GMPEs.

Appendices

Appendix A: Database of ground-motion amplitudes for each region.

Processing of the ground motion waveforms was performed in several steps. The waveforms were windowed from the event origin time to the end of the S-wave coda, then checked for instrumental glitches or trends. Glitches were considered as steps or spikes in a 20-point window. A cosine window with tapering width of 0.02 (fractional width relative to the length of the signal) was applied to the waveforms prior to the Fourier Transform. A 4^{th}-order Butterworth bandpass filter with low- and high-cut frequencies of 0.1 to 50 Hz, respectively, was applied in the frequency domain. Instrument correction of velocity data was performed in the frequency domain using the Seismotoolbox software (www.seismotoolbox.ca). We chose 50 Hz as the default high-cut frequency for filtering, since the majority of stations have a sampling rate of 100 samples per second; however the high-cut was reduced to the Nyquist frequency for those stations with lower sample rates. Peak Ground Acceleration (PGA), Peak Ground Velocity (PGV), and 5% damped PSA for 200 logarithmically distributed frequencies from 0.1 to 50 Hz were calculated. We restricted our focus in the analysis that follows to the frequency range from 0.33 Hz to 10 Hz (and the distance range of <400km), to mitigate the need to look carefully at each signal to judge the useable frequency range.

The ground motion databases used in this study can be found on the appended CD. The appended CD contains Excel datasheets for the Northeast, CUS, PNW/BC, and California. The following table is an extract from the databse tables to show format.

Event ID	Lat	Long	Mag	Mag type	Depth (km)	Network	Station ID	Lat	Long
1	45.77	-74.93	4.4	MN	16	CN	GAC	45.7033	-75.4783
2	46.3	-75.53	3.5	MN	16.3	CN	GAC	45.7033	-75.4783
3	45.26	-74.12	3.8	MN	8.1	CN	GAC	45.7033	-75.4783
4	46.46	-75.06	3.7	MN	14.5	CN	GAC	45.7033	-75.4783
5	45.19	-73.46	4.3		15.6	CN	GAC	45.7033	-75.4783
5	45.19	-73.46	4.3		15.6	CN	LMQ	47.5485	-70.3258

6	47.47	-70.16	3.5	MN	18	CN	LMQ	47.5483	-70.3267
7	46.49	-75.62	4.1	MN	18	CN	GAC	45.7033	-75.4783
8	47.45	-70.36	3.8	MN	6.2	CN	LMQ	47.5483	-70.3267
11	47	-66.6	4.1	MN	5	CN	LMN	45.852	-64.806
11	47	-66.6	4.1	MN	5	CN	LMQ	47.5485	-70.3258
12	47.77	-69.96	4.3	MN	17	CN	LMQ	47.5483	-70.3267
38	49.89	-66.29	3	MN	18	CN	LMQ	47.5483	-70.3267
38	49.89	-66.29	3	MN	18	CN	A16	47.4706	-70.0064
38	49.89	-66.29	3	MN	18	CN	A61	47.693	-70.09
38	49.89	-66.29	3	MN	18	CN	A64	47.8264	-69.8922
39	44.29	-70.54	3.2	MN	5	CN	LMQ	47.5483	-70.3267
39	44.29	-70.54	3.2	MN	5	CN	A16	47.4706	-70.0064
39	44.29	-70.54	3.2	MN	5	CN	A54	47.4567	-70.4125
39	44.29	-70.54	3.2	MN	5	CN	A61	47.693	-70.09
39	44.29	-70.54	3.2	MN	5	CN	A64	47.8264	-69.8922
40	47.44	-70.31	3	MN	10.8	CN	LMQ	47.5483	-70.3267
40	47.44	-70.31	3	MN	10.8	CN	A16	47.4706	-70.0064
40	47.44	-70.31	3	MN	10.8	CN	A21	47.7036	-69.6897
40	47.44	-70.31	3	MN	10.8	CN	A54	47.4567	-70.4125
40	47.44	-70.31	3	MN	10.8	CN	A61	47.693	-70.09
40	47.44	-70.31	3	MN	10.8	CN	A64	47.8264	-69.8922
41	45.92	-75.24	3	MN	10	CN	GAC	45.7033	-75.4783
42	45.9	-75.04	3.5	MN	18	CN	GAC	45.7033	-75.4783
42	45.9	-75.04	3.5	MN	18	CN	A54	47.4567	-70.4125
43	44.24	-74.43	3	MN	5	CN	GAC	45.7033	-75.4783
44	49.32	-66.67	3.1	MN	25.4	CN	LMQ	47.5483	-70.3267
44	49.32	-66.67	3.1	MN	25.4	CN	A11	47.2425	-70.1978
44	49.32	-66.67	3.1	MN	25.4	CN	A64	47.8264	-69.8922
45	49.15	-67.73	3.3	MN	15.4	CN	LMQ	47.5483	-70.3267
45	49.15	-67.73	3.3	MN	15.4	CN	A11	47.2425	-70.1978
45	49.15	-67.73	3.3	MN	15.4	CN	A16	47.4706	-70.0064

Appendix B: Supplementary materials.

Table B-1 Parameters of equation (4.3). a and b are the intercept and slope of the equation, respectively. L and U refer to the lower and upper bound of each parameter (%95 confidence interval).

Region	cut-off (km)	frequency (Hz)	a	b	L_a	U_a	L_b	U_b
CUS	40	0.33	-0.37	-0.26	-2.59	1.85	-1.90	1.38
	40	0.5	0.55	-0.88	-1.28	2.39	-2.25	0.48
	40	1	0.86	-0.71	-0.26	1.98	-1.54	0.12
	40	3.3	1.75	-0.69	0.68	2.82	-1.49	0.12
	40	5	2.53	-1.12	1.53	3.53	-1.88	-0.37
	40	10	3.16	-1.31	2.15	4.17	-2.11	-0.51
	50	0.33	-0.76	0.10	-2.91	1.38	-1.33	1.53
	50	0.5	0.26	-0.63	-1.40	1.92	-1.74	0.49
	50	1	0.61	-0.50	-0.40	1.62	-1.19	0.19
	50	3.3	1.70	-0.65	0.89	2.52	-1.21	-0.09
	50	5	2.30	-0.92	1.49	3.12	-1.48	-0.35
	50	10	3.09	-1.24	2.22	3.96	-1.85	-0.64
	60	0.33	0.06	-0.56	-1.93	2.04	-1.83	0.71
	60	0.5	0.55	-0.86	-0.91	2.02	-1.81	0.09
	60	1	1.12	-0.91	0.26	1.98	-1.46	-0.35
	60	3.3	2.10	-0.97	1.36	2.83	-1.45	-0.49
	60	5	2.50	-1.08	1.75	3.25	-1.58	-0.58
	60	10	3.20	-1.34	2.38	4.03	-1.90	-0.79
	70	0.33	0.27	-0.72	-1.61	2.15	-1.89	0.44
	70	0.5	0.79	-1.04	-0.56	2.14	-1.89	-0.20

	70	1	1.26	-1.01	0.42	2.10	-1.54	-0.48
	70	3.3	2.18	-1.03	1.50	2.86	-1.46	-0.61
	70	5	2.46	-1.04	1.76	3.16	-1.49	-0.60
	70	10	3.14	-1.29	2.38	3.90	-1.78	-0.80
	80	0.33	0.59	-0.96	-1.01	2.18	-1.91	0.00
	80	0.5	0.83	-1.07	-0.35	2.00	-1.78	-0.36
	80	1	1.48	-1.18	0.74	2.23	-1.63	-0.73
	80	3.3	2.22	-1.07	1.61	2.83	-1.44	-0.69
	80	5	2.48	-1.06	1.84	3.12	-1.46	-0.66
	80	10	3.14	-1.29	2.41	3.87	-1.75	-0.83
	90	0.33	0.90	-1.18	-0.56	2.37	-2.04	-0.32
	90	0.5	0.90	-1.12	-0.18	1.98	-1.77	-0.47
	90	1	1.59	-1.25	0.89	2.29	-1.67	-0.83
	90	3.3	2.21	-1.06	1.63	2.78	-1.40	-0.71
	90	5	2.41	-1.01	1.79	3.03	-1.39	-0.63
	90	10	3.05	-1.22	2.35	3.76	-1.67	-0.78
	100	0.33	1.02	-1.26	-0.29	2.34	-2.01	-0.50
	100	0.5	0.97	-1.17	0.01	1.93	-1.72	-0.61
	100	1	1.63	-1.28	1.01	2.25	-1.64	-0.92
	100	3.3	2.12	-0.99	1.60	2.64	-1.30	-0.69
	100	5	2.30	-0.93	1.74	2.86	-1.26	-0.59
	100	10	2.86	-1.08	2.20	3.52	-1.48	-0.67
	110	0.33	1.14	-1.33	-0.09	2.37	-2.03	-0.64
	110	0.5	1.01	-1.20	0.11	1.92	-1.71	-0.68

	110	1	1.78	-1.38	1.18	2.38	-1.72	-1.03
	110	3.3	2.22	-1.06	1.71	2.72	-1.35	-0.77
	110	5	2.41	-1.01	1.88	2.95	-1.32	-0.70
	110	10	2.94	-1.14	2.30	3.59	-1.53	-0.75
	120	0.33	1.25	-1.40	0.12	2.37	-2.03	-0.78
	120	0.5	1.06	-1.23	0.23	1.89	-1.69	-0.76
	120	1	1.83	-1.41	1.25	2.41	-1.74	-1.08
	120	3.3	2.22	-1.06	1.74	2.70	-1.34	-0.79
	120	5	2.43	-1.02	1.92	2.95	-1.32	-0.73
	120	10	3.00	-1.18	2.38	3.62	-1.55	-0.81
	130	0.33	1.21	-1.38	0.15	2.27	-1.96	-0.80
	130	0.5	0.99	-1.19	0.22	1.77	-1.61	-0.76
	130	1	1.74	-1.35	1.18	2.30	-1.66	-1.04
	130	3.3	2.21	-1.06	1.74	2.68	-1.32	-0.80
	130	5	2.46	-1.04	1.96	2.96	-1.33	-0.76
	130	10	3.05	-1.22	2.44	3.66	-1.58	-0.85
	140	0.33	1.44	-1.53	0.47	2.41	-2.04	-1.01
	140	0.5	1.06	-1.23	0.35	1.77	-1.61	-0.84
	140	1	1.71	-1.34	1.19	2.24	-1.62	-1.05
	140	3.3	2.18	-1.04	1.74	2.62	-1.28	-0.80
	140	5	2.46	-1.04	1.98	2.94	-1.31	-0.78
	140	10	3.03	-1.20	2.45	3.61	-1.54	-0.86
	150	0.33	1.34	-1.46	0.46	2.21	-1.92	-1.00
	150	0.5	0.97	-1.17	0.31	1.62	-1.51	-0.82

	150	1	1.54	-1.22	1.03	2.04	-1.49	-0.96
	150	3.3	2.02	-0.93	1.60	2.44	-1.16	-0.71
	150	5	2.30	-0.94	1.85	2.76	-1.18	-0.69
	150	10	2.96	-1.15	2.41	3.52	-1.48	-0.83
	160	0.33	1.17	-1.36	0.31	2.03	-1.80	-0.91
	160	0.5	0.85	-1.10	0.21	1.49	-1.43	-0.76
	160	1	1.43	-1.16	0.94	1.92	-1.41	-0.90
	160	3.3	1.95	-0.89	1.55	2.35	-1.10	-0.67
	160	5	2.21	-0.88	1.78	2.64	-1.11	-0.64
	160	10	2.98	-1.16	2.46	3.50	-1.46	-0.87
	170	0.33	1.01	-1.26	0.17	1.84	-1.69	-0.83
	170	0.5	0.77	-1.04	0.15	1.38	-1.36	-0.72
	170	1	1.32	-1.09	0.83	1.80	-1.34	-0.84
	170	3.3	1.92	-0.87	1.52	2.31	-1.07	-0.66
	170	5	2.18	-0.86	1.75	2.61	-1.08	-0.63
	170	10	2.95	-1.15	2.45	3.45	-1.43	-0.87
	180	0.33	0.98	-1.25	0.19	1.78	-1.65	-0.84
	180	0.5	0.67	-0.98	0.07	1.26	-1.29	-0.68
	180	1	1.30	-1.08	0.82	1.78	-1.33	-0.83
	180	3.3	1.90	-0.85	1.50	2.29	-1.06	-0.65
	180	5	2.16	-0.85	1.74	2.59	-1.07	-0.63
	180	10	2.87	-1.09	2.38	3.37	-1.37	-0.82
	190	0.33	0.87	-1.18	0.09	1.64	-1.57	-0.79
	190	0.5	0.50	-0.88	-0.10	1.09	-1.19	-0.58

	190	1	1.13	-0.98	0.66	1.61	-1.22	-0.74
	190	3.3	1.76	-0.77	1.37	2.14	-0.97	-0.57
	190	5	2.01	-0.75	1.59	2.44	-0.97	-0.53
	190	10	2.62	-0.92	2.13	3.11	-1.19	-0.66
	200	0.33	0.82	-1.15	0.07	1.57	-1.53	-0.78
	200	0.5	0.37	-0.81	-0.22	0.95	-1.10	-0.51
	200	1	0.98	-0.89	0.52	1.45	-1.13	-0.66
	200	3.3	1.58	-0.66	1.19	1.97	-0.86	-0.47
	200	5	1.84	-0.64	1.42	2.26	-0.86	-0.43
	200	10	2.42	-0.79	1.94	2.89	-1.04	-0.54
	210	0.33	0.52	-0.98	-0.18	1.23	-1.33	-0.64
	210	0.5	0.15	-0.68	-0.41	0.71	-0.95	-0.40
	210	1	0.79	-0.78	0.34	1.25	-1.01	-0.56
	210	3.3	1.47	-0.60	1.09	1.85	-0.78	-0.41
	210	5	1.74	-0.58	1.33	2.15	-0.79	-0.38
	210	10	2.36	-0.75	1.90	2.82	-0.99	-0.51
	220	0.33	0.56	-1.00	-0.12	1.24	-1.33	-0.68
	220	0.5	0.18	-0.69	-0.37	0.72	-0.96	-0.43
	220	1	0.79	-0.78	0.34	1.23	-0.99	-0.56
	220	3.3	1.49	-0.61	1.13	1.86	-0.79	-0.43
	220	5	1.79	-0.62	1.39	2.19	-0.81	-0.42
	220	10	2.36	-0.75	1.91	2.81	-0.99	-0.52
	230	0.33	0.58	-1.02	-0.08	1.24	-1.33	-0.70
	230	0.5	0.19	-0.70	-0.34	0.72	-0.96	-0.45

	230	1	0.78	-0.77	0.34	1.21	-0.98	-0.56
	230	3.3	1.50	-0.62	1.15	1.86	-0.79	-0.44
	230	5	1.80	-0.62	1.41	2.19	-0.81	-0.43
	230	10	2.36	-0.75	1.91	2.80	-0.98	-0.52
	240	0.33	0.59	-1.02	-0.05	1.22	-1.32	-0.72
	240	0.5	0.17	-0.69	-0.34	0.69	-0.94	-0.45
	240	1	0.71	-0.73	0.29	1.13	-0.93	-0.53
	240	3.3	1.45	-0.59	1.11	1.80	-0.75	-0.42
	240	5	1.76	-0.59	1.38	2.13	-0.78	-0.41
	240	10	2.25	-0.68	1.81	2.70	-0.91	-0.46
	250	0.33	0.48	-0.96	-0.13	1.09	-1.25	-0.67
	250	0.5	0.11	-0.66	-0.39	0.61	-0.89	-0.42
	250	1	0.66	-0.70	0.24	1.07	-0.90	-0.51
	250	3.3	1.39	-0.55	1.05	1.73	-0.71	-0.39
	250	5	1.68	-0.55	1.31	2.05	-0.73	-0.37
	250	10	2.19	-0.64	1.76	2.62	-0.86	-0.43
	260	0.33	0.41	-0.92	-0.19	1.01	-1.20	-0.64
	260	0.5	0.08	-0.64	-0.41	0.57	-0.87	-0.41
	260	1	0.62	-0.68	0.22	1.02	-0.87	-0.49
	260	3.3	1.39	-0.55	1.06	1.73	-0.71	-0.40
	260	5	1.67	-0.54	1.30	2.03	-0.71	-0.37
	260	10	2.16	-0.62	1.73	2.58	-0.84	-0.41
	270	0.33	0.40	-0.92	-0.19	1.00	-1.19	-0.65
	270	0.5	0.07	-0.64	-0.41	0.56	-0.86	-0.41

	270	1	0.65	-0.70	0.25	1.05	-0.88	-0.52
	270	3.3	1.45	-0.58	1.12	1.77	-0.74	-0.43
	270	5	1.73	-0.58	1.38	2.09	-0.75	-0.41
	270	10	2.10	-0.59	1.68	2.52	-0.80	-0.38
	280	0.33	0.30	-0.86	-0.28	0.88	-1.13	-0.60
	280	0.5	0.06	-0.63	-0.41	0.53	-0.85	-0.41
	280	1	0.62	-0.68	0.23	1.00	-0.86	-0.51
	280	3.3	1.44	-0.58	1.12	1.76	-0.73	-0.44
	280	5	1.72	-0.57	1.38	2.06	-0.73	-0.41
	280	10	2.06	-0.56	1.66	2.47	-0.76	-0.37
	290	0.33	0.28	-0.85	-0.29	0.84	-1.11	-0.59
	290	0.5	0.04	-0.62	-0.42	0.51	-0.83	-0.41
	290	1	0.61	-0.68	0.23	0.99	-0.85	-0.51
	290	3.3	1.46	-0.59	1.15	1.77	-0.74	-0.45
	290	5	1.76	-0.60	1.43	2.10	-0.75	-0.44
	290	10	2.09	-0.58	1.69	2.48	-0.77	-0.38
	300	0.33	0.20	-0.81	-0.35	0.76	-1.06	-0.56
	300	0.5	0.03	-0.61	-0.43	0.49	-0.82	-0.41
	300	1	0.57	-0.66	0.20	0.95	-0.83	-0.49
	300	3.3	1.44	-0.58	1.13	1.74	-0.72	-0.44
	300	5	1.75	-0.59	1.42	2.08	-0.74	-0.44
	300	10	2.08	-0.57	1.69	2.47	-0.76	-0.38
	310	0.33	0.18	-0.80	-0.36	0.72	-1.04	-0.56
	310	0.5	0.02	-0.61	-0.43	0.46	-0.81	-0.41

	310	1	0.55	-0.65	0.19	0.92	-0.81	-0.48
	310	3.3	1.45	-0.58	1.15	1.74	-0.72	-0.45
	310	5	1.75	-0.59	1.43	2.07	-0.74	-0.44
	310	10	2.09	-0.58	1.70	2.48	-0.77	-0.39
	320	0.33	0.19	-0.80	-0.34	0.71	-1.04	-0.57
	320	0.5	0.03	-0.61	-0.41	0.46	-0.81	-0.42
	320	1	0.57	-0.66	0.22	0.93	-0.82	-0.50
	320	3.3	1.48	-0.60	1.18	1.77	-0.73	-0.47
	320	5	1.76	-0.59	1.44	2.07	-0.74	-0.45
	320	10	2.11	-0.59	1.73	2.50	-0.78	-0.41
	330	0.33	0.19	-0.80	-0.33	0.71	-1.03	-0.57
	330	0.5	0.06	-0.63	-0.37	0.49	-0.82	-0.44
	330	1	0.61	-0.68	0.25	0.96	-0.83	-0.52
	330	3.3	1.55	-0.64	1.26	1.85	-0.77	-0.51
	330	5	1.82	-0.63	1.50	2.14	-0.77	-0.48
	330	10	2.13	-0.61	1.75	2.52	-0.79	-0.42
	340	0.33	0.19	-0.80	-0.32	0.70	-1.03	-0.58
	340	0.5	0.04	-0.62	-0.39	0.46	-0.81	-0.43
	340	1	0.61	-0.68	0.26	0.96	-0.83	-0.52
	340	3.3	1.61	-0.67	1.32	1.90	-0.80	-0.54
	340	5	1.87	-0.66	1.56	2.19	-0.80	-0.52
	340	10	2.13	-0.60	1.75	2.50	-0.78	-0.42
	350	0.33	0.19	-0.81	-0.32	0.70	-1.03	-0.58
	350	0.5	0.03	-0.62	-0.39	0.46	-0.80	-0.43

	350	1	0.60	-0.67	0.26	0.94	-0.82	-0.52
	350	3.3	1.61	-0.67	1.32	1.89	-0.80	-0.54
	350	5	1.87	-0.66	1.57	2.18	-0.79	-0.52
	350	10	2.12	-0.60	1.75	2.49	-0.77	-0.42
	360	0.33	0.12	-0.77	-0.38	0.63	-1.00	-0.55
	360	0.5	-0.01	-0.59	-0.43	0.41	-0.78	-0.41
	360	1	0.60	-0.67	0.26	0.93	-0.82	-0.52
	360	3.3	1.64	-0.69	1.36	1.93	-0.81	-0.56
	360	5	1.93	-0.69	1.63	2.24	-0.82	-0.55
	360	10	2.16	-0.62	1.79	2.53	-0.80	-0.45
	370	0.33	0.10	-0.76	-0.40	0.61	-0.98	-0.54
	370	0.5	-0.01	-0.60	-0.42	0.41	-0.78	-0.41
	370	1	0.58	-0.66	0.25	0.92	-0.81	-0.52
	370	3.3	1.65	-0.69	1.37	1.93	-0.81	-0.57
	370	5	1.95	-0.70	1.65	2.25	-0.83	-0.56
	370	10	2.11	-0.59	1.75	2.48	-0.77	-0.42
	380	0.33	0.11	-0.77	-0.39	0.61	-0.98	-0.55
	380	0.5	-0.01	-0.59	-0.42	0.40	-0.77	-0.41
	380	1	0.57	-0.66	0.24	0.90	-0.80	-0.51
	380	3.3	1.66	-0.70	1.38	1.94	-0.82	-0.58
	380	5	1.96	-0.70	1.66	2.26	-0.83	-0.57
	380	10	2.10	-0.59	1.74	2.47	-0.76	-0.42
	390	0.33	0.12	-0.77	-0.37	0.61	-0.98	-0.56
	390	0.5	-0.03	-0.58	-0.43	0.38	-0.76	-0.41

	390	1	0.53	-0.64	0.21	0.86	-0.78	-0.50
	390	3.3	1.65	-0.69	1.38	1.93	-0.81	-0.57
	390	5	1.97	-0.71	1.67	2.27	-0.84	-0.58
	390	10	2.08	-0.57	1.71	2.44	-0.75	-0.40
	400	0.33	0.03	-0.72	-0.46	0.51	-0.93	-0.52
	400	0.5	-0.12	-0.54	-0.52	0.29	-0.71	-0.37
	400	1	0.49	-0.62	0.17	0.81	-0.75	-0.48
	400	3.3	1.67	-0.70	1.40	1.94	-0.82	-0.58
	400	5	2.01	-0.73	1.72	2.30	-0.85	-0.60
	400	10	2.03	-0.55	1.67	2.39	-0.72	-0.38
Region	cut-off (km)	frequency (Hz)	a	b	L_a	U_a	L_b	U_b
	40	0.33	0.60	-1.02	-0.21	1.41	-1.62	-0.43
	40	0.5	1.16	-1.25	0.58	1.74	-1.67	-0.83
	40	1	1.92	-1.46	1.44	2.40	-1.80	-1.11
	40	3.3	3.04	-1.64	2.63	3.46	-1.93	-1.34
	40	5	3.45	-1.80	3.04	3.85	-2.10	-1.51
	40	10	3.54	-1.86	3.13	3.95	-2.15	-1.57
N. Cal	50	0.33	0.74	-1.13	0.01	1.46	-1.65	-0.62
	50	0.5	1.09	-1.20	0.60	1.59	-1.55	-0.85
	50	1	1.88	-1.43	1.49	2.27	-1.70	-1.16
	50	3.3	3.02	-1.62	2.68	3.36	-1.85	-1.39
	50	5	3.31	-1.70	2.97	3.65	-1.93	-1.46
	50	10	3.41	-1.76	3.08	3.75	-1.98	-1.53
	60	0.33	0.61	-1.04	-0.04	1.27	-1.49	-0.59

	60	0.5	0.89	-1.04	0.46	1.32	-1.33	-0.75
	60	1	1.75	-1.33	1.42	2.08	-1.55	-1.11
	60	3.3	2.86	-1.50	2.56	3.15	-1.69	-1.30
	60	5	3.14	-1.57	2.84	3.43	-1.76	-1.37
	60	10	3.20	-1.60	2.92	3.49	-1.79	-1.41
	70	0.33	0.59	-1.02	0.02	1.16	-1.40	-0.64
	70	0.5	0.77	-0.96	0.39	1.15	-1.20	-0.71
	70	1	1.55	-1.18	1.26	1.84	-1.37	-1.00
	70	3.3	2.60	-1.31	2.33	2.86	-1.47	-1.14
	70	5	2.89	-1.39	2.63	3.16	-1.55	-1.22
	70	10	2.97	-1.43	2.71	3.23	-1.60	-1.26
	80	0.33	0.36	-0.84	-0.19	0.91	-1.20	-0.49
	80	0.5	0.69	-0.89	0.33	1.04	-1.11	-0.67
	80	1	1.42	-1.09	1.15	1.69	-1.26	-0.92
	80	3.3	2.45	-1.20	2.21	2.70	-1.35	-1.05
	80	5	2.79	-1.31	2.55	3.04	-1.47	-1.16
	80	10	2.89	-1.37	2.65	3.13	-1.52	-1.22
	90	0.33	0.29	-0.79	-0.24	0.81	-1.12	-0.46
	90	0.5	0.67	-0.88	0.33	1.01	-1.09	-0.67
	90	1	1.35	-1.04	1.10	1.61	-1.20	-0.89
	90	3.3	2.38	-1.15	2.15	2.61	-1.29	-1.01
	90	5	2.71	-1.26	2.48	2.94	-1.40	-1.12
	90	10	2.82	-1.32	2.59	3.04	-1.46	-1.18
	100	0.33	0.49	-0.94	0.00	0.98	-1.25	-0.63

	100	0.5	0.75	-0.94	0.43	1.07	-1.13	-0.74
	100	1	1.34	-1.04	1.11	1.58	-1.18	-0.89
	100	3.3	2.39	-1.16	2.18	2.61	-1.29	-1.03
	100	5	2.72	-1.27	2.50	2.94	-1.40	-1.13
	100	10	2.83	-1.33	2.61	3.04	-1.46	-1.20
	110	0.33	0.54	-0.97	0.05	1.02	-1.27	-0.67
	110	0.5	0.81	-0.98	0.50	1.11	-1.16	-0.79
	110	1	1.30	-1.01	1.08	1.53	-1.14	-0.87
	110	3.3	2.37	-1.14	2.16	2.57	-1.26	-1.02
	110	5	2.70	-1.25	2.49	2.91	-1.38	-1.13
	110	10	2.81	-1.32	2.61	3.02	-1.44	-1.20
	120	0.33	0.56	-0.99	0.09	1.02	-1.27	-0.70
	120	0.5	0.80	-0.97	0.50	1.09	-1.15	-0.79
	120	1	1.32	-1.02	1.10	1.54	-1.15	-0.89
	120	3.3	2.41	-1.17	2.21	2.61	-1.29	-1.05
	120	5	2.76	-1.29	2.56	2.97	-1.41	-1.17
	120	10	2.87	-1.36	2.67	3.07	-1.48	-1.24
	130	0.33	0.63	-1.03	0.18	1.07	-1.30	-0.77
	130	0.5	0.83	-0.99	0.55	1.12	-1.16	-0.83
	130	1	1.30	-1.01	1.09	1.51	-1.13	-0.88
	130	3.3	2.38	-1.15	2.19	2.58	-1.27	-1.04
	130	5	2.75	-1.28	2.55	2.95	-1.40	-1.17
	130	10	2.84	-1.34	2.65	3.04	-1.45	-1.23
	140	0.33	0.66	-1.06	0.23	1.08	-1.31	-0.80

	140	0.5	0.81	-0.98	0.54	1.09	-1.14	-0.82
	140	1	1.26	-0.98	1.06	1.46	-1.10	-0.86
	140	3.3	2.37	-1.14	2.18	2.56	-1.25	-1.04
	140	5	2.74	-1.28	2.55	2.94	-1.39	-1.17
	140	10	2.83	-1.33	2.64	3.03	-1.44	-1.22
	150	0.33	0.66	-1.06	0.25	1.08	-1.30	-0.81
	150	0.5	0.81	-0.98	0.54	1.08	-1.14	-0.82
	150	1	1.25	-0.97	1.05	1.45	-1.09	-0.86
	150	3.3	2.37	-1.15	2.19	2.56	-1.25	-1.04
	150	5	2.76	-1.29	2.57	2.95	-1.40	-1.18
	150	10	2.83	-1.33	2.64	3.02	-1.44	-1.22
	160	0.33	0.68	-1.07	0.27	1.09	-1.31	-0.83
	160	0.5	0.80	-0.97	0.54	1.07	-1.13	-0.82
	160	1	1.29	-1.00	1.09	1.49	-1.11	-0.88
	160	3.3	2.41	-1.17	2.23	2.60	-1.28	-1.07
	160	5	2.80	-1.31	2.61	2.98	-1.42	-1.21
	160	10	2.86	-1.35	2.68	3.05	-1.46	-1.24
	170	0.33	0.78	-1.14	0.38	1.18	-1.38	-0.91
	170	0.5	0.86	-1.01	0.60	1.12	-1.16	-0.86
	170	1	1.31	-1.01	1.11	1.50	-1.12	-0.90
	170	3.3	2.43	-1.19	2.25	2.61	-1.29	-1.08
	170	5	2.82	-1.33	2.63	3.00	-1.43	-1.22
	170	10	2.88	-1.36	2.69	3.06	-1.46	-1.25
	180	0.33	0.81	-1.16	0.41	1.21	-1.39	-0.93

	180	0.5	0.89	-1.03	0.63	1.14	-1.18	-0.88
	180	1	1.32	-1.02	1.12	1.51	-1.13	-0.91
	180	3.3	2.44	-1.19	2.26	2.62	-1.29	-1.09
	180	5	2.83	-1.33	2.64	3.01	-1.44	-1.23
	180	10	2.88	-1.36	2.70	3.06	-1.47	-1.26
	190	0.33	0.77	-1.13	0.38	1.17	-1.36	-0.90
	190	0.5	0.87	-1.02	0.61	1.13	-1.17	-0.87
	190	1	1.30	-1.01	1.11	1.49	-1.11	-0.90
	190	3.3	2.43	-1.18	2.25	2.61	-1.28	-1.08
	190	5	2.82	-1.33	2.63	3.00	-1.43	-1.22
	190	10	2.87	-1.36	2.69	3.05	-1.46	-1.25
	200	0.33	0.73	-1.11	0.34	1.12	-1.33	-0.88
	200	0.5	0.88	-1.02	0.62	1.13	-1.17	-0.88
	200	1	1.33	-1.02	1.14	1.52	-1.13	-0.92
	200	3.3	2.44	-1.19	2.26	2.61	-1.29	-1.09
	200	5	2.82	-1.33	2.64	3.00	-1.43	-1.23
	200	10	2.86	-1.35	2.68	3.04	-1.45	-1.25
	210	0.33	0.76	-1.13	0.37	1.15	-1.35	-0.90
	210	0.5	0.91	-1.04	0.66	1.16	-1.19	-0.90
	210	1	1.36	-1.04	1.18	1.55	-1.15	-0.94
	210	3.3	2.45	-1.20	2.28	2.63	-1.30	-1.10
	210	5	2.83	-1.33	2.65	3.00	-1.43	-1.23
	210	10	2.86	-1.35	2.69	3.04	-1.45	-1.25
	220	0.33	0.73	-1.11	0.34	1.12	-1.33	-0.88

	220	0.5	0.86	-1.01	0.61	1.11	-1.16	-0.87
	220	1	1.32	-1.02	1.13	1.51	-1.12	-0.91
	220	3.3	2.42	-1.18	2.25	2.59	-1.27	-1.08
	220	5	2.79	-1.31	2.62	2.97	-1.41	-1.21
	220	10	2.82	-1.33	2.65	3.00	-1.42	-1.23
	230	0.33	0.69	-1.08	0.31	1.07	-1.30	-0.86
	230	0.5	0.82	-0.98	0.57	1.07	-1.13	-0.84
	230	1	1.28	-0.99	1.10	1.47	-1.10	-0.89
	230	3.3	2.38	-1.15	2.21	2.55	-1.25	-1.05
	230	5	2.76	-1.29	2.58	2.93	-1.39	-1.19
	230	10	2.78	-1.30	2.61	2.95	-1.40	-1.20
	240	0.33	0.64	-1.05	0.27	1.01	-1.26	-0.84
	240	0.5	0.78	-0.96	0.53	1.02	-1.10	-0.82
	240	1	1.23	-0.96	1.05	1.42	-1.07	-0.86
	240	3.3	2.33	-1.12	2.16	2.50	-1.22	-1.03
	240	5	2.71	-1.26	2.54	2.88	-1.36	-1.16
	240	10	2.72	-1.26	2.55	2.89	-1.36	-1.17
	250	0.33	0.60	-1.02	0.24	0.97	-1.23	-0.82
	250	0.5	0.74	-0.93	0.49	0.98	-1.07	-0.80
	250	1	1.18	-0.93	1.00	1.36	-1.03	-0.83
	250	3.3	2.28	-1.09	2.11	2.45	-1.19	-1.00
	250	5	2.67	-1.23	2.50	2.84	-1.33	-1.14
	250	10	2.67	-1.23	2.50	2.84	-1.33	-1.14
	260	0.33	0.56	-1.00	0.19	0.93	-1.20	-0.79

	260	0.5	0.70	-0.91	0.46	0.94	-1.05	-0.77
	260	1	1.15	-0.91	0.97	1.33	-1.01	-0.81
	260	3.3	2.25	-1.07	2.08	2.42	-1.17	-0.98
	260	5	2.64	-1.22	2.47	2.81	-1.31	-1.12
	260	10	2.64	-1.21	2.47	2.81	-1.30	-1.12
	270	0.33	0.56	-0.99	0.19	0.92	-1.20	-0.79
	270	0.5	0.71	-0.91	0.47	0.95	-1.05	-0.78
	270	1	1.14	-0.91	0.96	1.32	-1.01	-0.81
	270	3.3	2.24	-1.07	2.08	2.41	-1.16	-0.98
	270	5	2.63	-1.21	2.46	2.80	-1.31	-1.12
	270	10	2.62	-1.20	2.45	2.79	-1.30	-1.11
	280	0.33	0.56	-0.99	0.19	0.92	-1.20	-0.79
	280	0.5	0.71	-0.92	0.47	0.95	-1.05	-0.78
	280	1	1.13	-0.90	0.96	1.31	-1.00	-0.80
	280	3.3	2.23	-1.06	2.07	2.40	-1.15	-0.97
	280	5	2.62	-1.20	2.45	2.78	-1.30	-1.11
	280	10	2.61	-1.19	2.44	2.78	-1.29	-1.10
	290	0.33	0.56	-0.99	0.19	0.92	-1.20	-0.79
	290	0.5	0.71	-0.92	0.47	0.95	-1.05	-0.78
	290	1	1.13	-0.90	0.96	1.31	-1.00	-0.80
	290	3.3	2.23	-1.06	2.07	2.40	-1.15	-0.97
	290	5	2.62	-1.20	2.45	2.78	-1.30	-1.11
	290	10	2.61	-1.19	2.44	2.78	-1.29	-1.10
	300	0.33	0.56	-0.99	0.19	0.92	-1.20	-0.79

	300	0.5	0.71	-0.92	0.47	0.95	-1.05	-0.78
	300	1	1.13	-0.90	0.96	1.31	-1.00	-0.80
	300	3.3	2.23	-1.06	2.07	2.40	-1.15	-0.97
	300	5	2.62	-1.20	2.45	2.78	-1.30	-1.11
	300	10	2.61	-1.19	2.44	2.78	-1.29	-1.10
	310	0.33	0.55	-0.99	0.18	0.91	-1.19	-0.78
	310	0.5	0.71	-0.91	0.47	0.94	-1.05	-0.78
	310	1	1.13	-0.90	0.95	1.31	-1.00	-0.80
	310	3.3	2.23	-1.06	2.06	2.39	-1.15	-0.97
	310	5	2.61	-1.20	2.45	2.78	-1.29	-1.11
	310	10	2.60	-1.19	2.44	2.77	-1.28	-1.10
	320	0.33	0.55	-0.99	0.18	0.91	-1.19	-0.78
	320	0.5	0.71	-0.91	0.47	0.94	-1.05	-0.78
	320	1	1.13	-0.90	0.95	1.31	-1.00	-0.80
	320	3.3	2.23	-1.06	2.06	2.39	-1.15	-0.97
	320	5	2.61	-1.20	2.45	2.78	-1.29	-1.11
	320	10	2.60	-1.19	2.44	2.77	-1.28	-1.10
	330	0.33	0.55	-0.99	0.18	0.91	-1.19	-0.78
	330	0.5	0.71	-0.91	0.47	0.94	-1.05	-0.78
	330	1	1.13	-0.90	0.95	1.31	-1.00	-0.80
	330	3.3	2.23	-1.06	2.06	2.39	-1.15	-0.97
	330	5	2.61	-1.20	2.45	2.78	-1.29	-1.11
	330	10	2.60	-1.19	2.44	2.77	-1.28	-1.10
	340	0.33	0.55	-0.99	0.18	0.91	-1.19	-0.78

	340	0.5	0.71	-0.91	0.47	0.94	-1.05	-0.78
	340	1	1.13	-0.90	0.95	1.31	-1.00	-0.80
	340	3.3	2.23	-1.06	2.06	2.39	-1.15	-0.97
	340	5	2.61	-1.20	2.45	2.78	-1.29	-1.11
	340	10	2.60	-1.19	2.44	2.77	-1.28	-1.10
	350	0.33	0.54	-0.98	0.18	0.90	-1.19	-0.78
	350	0.5	0.70	-0.91	0.47	0.94	-1.04	-0.78
	350	1	1.12	-0.90	0.95	1.30	-0.99	-0.80
	350	3.3	2.23	-1.06	2.06	2.39	-1.15	-0.97
	350	5	2.61	-1.20	2.44	2.78	-1.29	-1.11
	350	10	2.60	-1.19	2.43	2.77	-1.28	-1.09
	360	0.33	0.54	-0.99	0.19	0.90	-1.19	-0.79
	360	0.5	0.70	-0.91	0.46	0.94	-1.04	-0.78
	360	1	1.12	-0.89	0.94	1.30	-0.99	-0.79
	360	3.3	2.22	-1.06	2.06	2.39	-1.15	-0.96
	360	5	2.61	-1.20	2.44	2.78	-1.29	-1.10
	360	10	2.60	-1.19	2.43	2.76	-1.28	-1.09
	370	0.33	0.54	-0.99	0.19	0.90	-1.19	-0.79
	370	0.5	0.70	-0.91	0.46	0.94	-1.04	-0.78
	370	1	1.12	-0.89	0.94	1.30	-0.99	-0.79
	370	3.3	2.22	-1.06	2.06	2.39	-1.15	-0.96
	370	5	2.61	-1.20	2.44	2.78	-1.29	-1.10
	370	10	2.60	-1.19	2.43	2.76	-1.28	-1.09
	380	0.33	0.54	-0.99	0.19	0.90	-1.19	-0.79

	380	0.5	0.70	-0.91	0.46	0.94	-1.04	-0.78
	380	1	1.12	-0.89	0.94	1.30	-0.99	-0.79
	380	3.3	2.22	-1.06	2.06	2.39	-1.15	-0.96
	380	5	2.61	-1.20	2.44	2.78	-1.29	-1.10
	380	10	2.60	-1.19	2.43	2.76	-1.28	-1.09
	390	0.33	0.54	-0.99	0.19	0.90	-1.19	-0.79
	390	0.5	0.70	-0.91	0.46	0.94	-1.04	-0.78
	390	1	1.12	-0.89	0.94	1.30	-0.99	-0.79
	390	3.3	2.22	-1.06	2.06	2.39	-1.15	-0.96
	390	5	2.61	-1.20	2.44	2.78	-1.29	-1.10
	390	10	2.60	-1.19	2.43	2.76	-1.28	-1.09
	400	0.33	0.54	-0.99	0.19	0.90	-1.19	-0.79
	400	0.5	0.70	-0.91	0.46	0.94	-1.04	-0.78
	400	1	1.12	-0.89	0.94	1.30	-0.99	-0.79
	400	3.3	2.22	-1.06	2.06	2.39	-1.15	-0.96
	400	5	2.61	-1.20	2.44	2.78	-1.29	-1.10
	400	10	2.60	-1.19	2.43	2.76	-1.28	-1.09
Region	cut-off (km)	frequency (Hz)	a	b	L_a	U_a	L_b	U_b
Northeast	40	0.33	1.07	-1.93	0.01	2.12	-2.72	-1.15
	40	0.5	1.03	-1.64	-0.04	2.09	-2.44	-0.85
	40	1	1.16	-1.37	0.00	2.31	-2.23	-0.51
	40	3.3	1.76	-1.01	0.62	2.91	-1.86	-0.16
	40	5	2.36	-1.17	1.28	3.44	-1.98	-0.36
	40	10	3.07	-1.40	2.10	4.03	-2.13	-0.68

	50	0.33	0.87	-1.77	-0.09	1.84	-2.46	-1.07
	50	0.5	0.88	-1.52	-0.10	1.85	-2.22	-0.81
	50	1	1.07	-1.30	0.04	2.11	-2.04	-0.55
	50	3.3	1.72	-0.97	0.70	2.73	-1.70	-0.24
	50	5	2.34	-1.15	1.40	3.29	-1.83	-0.47
	50	10	3.00	-1.35	2.15	3.85	-1.96	-0.73
	60	0.33	0.01	-1.07	-1.03	1.06	-1.78	-0.37
	60	0.5	0.12	-0.90	-0.92	1.16	-1.61	-0.20
	60	1	0.29	-0.66	-0.81	1.38	-1.40	0.08
	60	3.3	1.25	-0.59	0.27	2.23	-1.26	0.07
	60	5	1.85	-0.75	0.95	2.76	-1.36	-0.14
	60	10	2.43	-0.88	1.61	3.25	-1.44	-0.33
	70	0.33	-0.28	-0.84	-1.32	0.75	-1.52	-0.16
	70	0.5	-0.20	-0.66	-1.22	0.82	-1.33	0.01
	70	1	-0.04	-0.41	-1.09	1.02	-1.10	0.28
	70	3.3	0.93	-0.34	-0.04	1.90	-0.98	0.29
	70	5	1.54	-0.51	0.65	2.44	-1.10	0.08
	70	10	2.16	-0.68	1.36	2.96	-1.20	-0.15
	80	0.33	0.00	-1.05	-0.98	0.97	-1.68	-0.43
	80	0.5	0.12	-0.90	-0.84	1.07	-1.51	-0.28
	80	1	0.33	-0.68	-0.65	1.31	-1.31	-0.05
	80	3.3	1.27	-0.60	0.37	2.18	-1.18	-0.02
	80	5	1.80	-0.71	0.97	2.63	-1.24	-0.17
	80	10	2.35	-0.82	1.60	3.10	-1.30	-0.34

	90	0.33	0.23	-1.22	-0.69	1.14	-1.80	-0.65
	90	0.5	0.43	-1.12	-0.48	1.33	-1.69	-0.55
	90	1	0.77	-1.01	-0.17	1.71	-1.60	-0.41
	90	3.3	1.74	-0.95	0.86	2.62	-1.50	-0.39
	90	5	2.24	-1.03	1.43	3.05	-1.54	-0.52
	90	10	2.73	-1.10	1.99	3.46	-1.56	-0.64
	100	0.33	-0.26	-0.87	-1.23	0.72	-1.47	-0.27
	100	0.5	0.06	-0.86	-0.88	1.00	-1.43	-0.28
	100	1	0.49	-0.81	-0.45	1.44	-1.39	-0.23
	100	3.3	1.50	-0.78	0.62	2.38	-1.31	-0.24
	100	5	1.97	-0.84	1.15	2.79	-1.34	-0.34
	100	10	2.52	-0.95	1.77	3.26	-1.40	-0.49
	110	0.33	-0.32	-0.83	-1.24	0.60	-1.38	-0.28
	110	0.5	0.03	-0.84	-0.85	0.91	-1.36	-0.31
	110	1	0.50	-0.81	-0.39	1.38	-1.34	-0.29
	110	3.3	1.48	-0.76	0.66	2.29	-1.25	-0.27
	110	5	1.95	-0.82	1.18	2.71	-1.28	-0.36
	110	10	2.46	-0.91	1.76	3.16	-1.32	-0.49
	120	0.33	-0.51	-0.70	-1.43	0.41	-1.23	-0.16
	120	0.5	-0.13	-0.73	-1.01	0.75	-1.24	-0.21
	120	1	0.36	-0.72	-0.51	1.22	-1.22	-0.21
	120	3.3	1.37	-0.68	0.57	2.17	-1.15	-0.22
	120	5	1.85	-0.75	1.10	2.59	-1.19	-0.31
	120	10	2.35	-0.83	1.66	3.04	-1.23	-0.43

	130	0.33	-0.61	-0.63	-1.52	0.31	-1.15	-0.10
	130	0.5	-0.22	-0.66	-1.09	0.64	-1.16	-0.16
	130	1	0.27	-0.65	-0.57	1.11	-1.14	-0.17
	130	3.3	1.29	-0.63	0.52	2.06	-1.07	-0.18
	130	5	1.77	-0.70	1.05	2.50	-1.11	-0.28
	130	10	2.27	-0.77	1.60	2.93	-1.16	-0.39
	140	0.33	-0.61	-0.62	-1.50	0.28	-1.13	-0.11
	140	0.5	-0.24	-0.65	-1.09	0.61	-1.13	-0.16
	140	1	0.22	-0.62	-0.60	1.05	-1.10	-0.15
	140	3.3	1.27	-0.61	0.51	2.02	-1.04	-0.18
	140	5	1.75	-0.68	1.04	2.46	-1.09	-0.28
	140	10	2.24	-0.75	1.59	2.89	-1.13	-0.38
	150	0.33	-0.25	-0.86	-1.10	0.59	-1.34	-0.39
	150	0.5	0.08	-0.86	-0.72	0.88	-1.31	-0.42
	150	1	0.47	-0.79	-0.30	1.24	-1.22	-0.36
	150	3.3	1.47	-0.75	0.77	2.18	-1.15	-0.36
	150	5	1.93	-0.80	1.27	2.58	-1.17	-0.43
	150	10	2.43	-0.88	1.82	3.04	-1.22	-0.54
	160	0.33	-0.47	-0.72	-1.30	0.37	-1.18	-0.26
	160	0.5	-0.10	-0.74	-0.89	0.68	-1.18	-0.31
	160	1	0.33	-0.70	-0.42	1.08	-1.11	-0.28
	160	3.3	1.38	-0.69	0.70	2.06	-1.06	-0.31
	160	5	1.81	-0.72	1.17	2.45	-1.08	-0.37
	160	10	2.29	-0.79	1.70	2.87	-1.11	-0.46

	170	0.33	-0.46	-0.73	-1.26	0.34	-1.17	-0.29
	170	0.5	-0.10	-0.74	-0.86	0.65	-1.16	-0.33
	170	1	0.34	-0.71	-0.38	1.07	-1.10	-0.31
	170	3.3	1.37	-0.68	0.72	2.02	-1.04	-0.33
	170	5	1.81	-0.72	1.19	2.42	-1.06	-0.39
	170	10	2.29	-0.79	1.73	2.86	-1.10	-0.48
	180	0.33	-0.23	-0.88	-1.01	0.55	-1.30	-0.46
	180	0.5	0.12	-0.89	-0.62	0.85	-1.28	-0.49
	180	1	0.54	-0.83	-0.16	1.24	-1.21	-0.45
	180	3.3	1.52	-0.78	0.88	2.15	-1.12	-0.44
	180	5	1.95	-0.81	1.35	2.54	-1.13	-0.49
	180	10	2.41	-0.87	1.87	2.96	-1.17	-0.57
	190	0.33	-0.17	-0.91	-0.92	0.58	-1.31	-0.52
	190	0.5	0.18	-0.93	-0.53	0.89	-1.30	-0.55
	190	1	0.61	-0.88	-0.07	1.28	-1.24	-0.52
	190	3.3	1.58	-0.82	0.97	2.19	-1.14	-0.49
	190	5	2.02	-0.86	1.45	2.59	-1.17	-0.56
	190	10	2.48	-0.91	1.96	3.01	-1.20	-0.63
	200	0.33	-0.18	-0.91	-0.91	0.55	-1.30	-0.53
	200	0.5	0.16	-0.91	-0.53	0.85	-1.28	-0.55
	200	1	0.57	-0.85	-0.09	1.23	-1.20	-0.50
	200	3.3	1.54	-0.79	0.94	2.14	-1.11	-0.48
	200	5	1.99	-0.84	1.43	2.55	-1.14	-0.54
	200	10	2.45	-0.89	1.93	2.97	-1.17	-0.62

	210	0.33	-0.13	-0.94	-0.84	0.58	-1.31	-0.57
	210	0.5	0.18	-0.93	-0.49	0.86	-1.28	-0.58
	210	1	0.58	-0.86	-0.07	1.22	-1.20	-0.52
	210	3.3	1.54	-0.79	0.96	2.13	-1.10	-0.49
	210	5	2.00	-0.85	1.45	2.55	-1.14	-0.56
	210	10	2.45	-0.89	1.94	2.96	-1.16	-0.63
	220	0.33	-0.11	-0.95	-0.81	0.59	-1.32	-0.59
	220	0.5	0.21	-0.94	-0.46	0.87	-1.29	-0.60
	220	1	0.60	-0.87	-0.03	1.24	-1.21	-0.54
	220	3.3	1.58	-0.82	1.00	2.15	-1.12	-0.52
	220	5	2.02	-0.86	1.48	2.56	-1.14	-0.58
	220	10	2.46	-0.90	1.96	2.95	-1.16	-0.64
	230	0.33	0.00	-1.02	-0.66	0.66	-1.36	-0.68
	230	0.5	0.33	-1.02	-0.30	0.96	-1.34	-0.69
	230	1	0.73	-0.95	0.13	1.34	-1.27	-0.64
	230	3.3	1.68	-0.88	1.14	2.23	-1.16	-0.60
	230	5	2.11	-0.92	1.59	2.62	-1.18	-0.65
	230	10	2.51	-0.93	2.04	2.99	-1.17	-0.69
	240	0.33	0.03	-1.04	-0.61	0.67	-1.37	-0.72
	240	0.5	0.35	-1.03	-0.26	0.96	-1.34	-0.72
	240	1	0.75	-0.96	0.16	1.34	-1.26	-0.66
	240	3.3	1.69	-0.89	1.15	2.22	-1.16	-0.61
	240	5	2.12	-0.92	1.62	2.62	-1.18	-0.67
	240	10	2.54	-0.95	2.08	3.00	-1.18	-0.71

	250	0.33	0.02	-1.03	-0.61	0.65	-1.35	-0.71
	250	0.5	0.35	-1.03	-0.26	0.95	-1.34	-0.72
	250	1	0.73	-0.96	0.15	1.32	-1.25	-0.66
	250	3.3	1.69	-0.89	1.16	2.22	-1.15	-0.62
	250	5	2.13	-0.93	1.64	2.62	-1.18	-0.68
	250	10	2.54	-0.95	2.09	2.99	-1.18	-0.72
	260	0.33	0.09	-1.08	-0.53	0.71	-1.39	-0.77
	260	0.5	0.43	-1.08	-0.16	1.03	-1.38	-0.79
	260	1	0.83	-1.01	0.25	1.40	-1.30	-0.73
	260	3.3	1.77	-0.93	1.25	2.29	-1.19	-0.68
	260	5	2.20	-0.97	1.72	2.68	-1.21	-0.73
	260	10	2.59	-0.98	2.14	3.03	-1.20	-0.75
	270	0.33	0.09	-1.08	-0.51	0.69	-1.38	-0.78
	270	0.5	0.45	-1.10	-0.12	1.03	-1.38	-0.81
	270	1	0.86	-1.03	0.30	1.42	-1.31	-0.76
	270	3.3	1.81	-0.96	1.31	2.31	-1.21	-0.71
	270	5	2.26	-1.01	1.79	2.73	-1.24	-0.78
	270	10	2.67	-1.02	2.23	3.10	-1.24	-0.81
	280	0.33	0.11	-1.09	-0.48	0.69	-1.37	-0.80
	280	0.5	0.48	-1.11	-0.08	1.04	-1.38	-0.83
	280	1	0.90	-1.06	0.36	1.45	-1.32	-0.79
	280	3.3	1.86	-0.99	1.37	2.35	-1.23	-0.75
	280	5	2.33	-1.05	1.87	2.78	-1.27	-0.82
	280	10	2.74	-1.07	2.31	3.17	-1.28	-0.86

	290	0.33	0.16	-1.12	-0.41	0.72	-1.39	-0.84
	290	0.5	0.54	-1.15	0.00	1.09	-1.41	-0.89
	290	1	1.00	-1.11	0.47	1.53	-1.37	-0.86
	290	3.3	1.96	-1.05	1.48	2.44	-1.28	-0.81
	290	5	2.41	-1.10	1.97	2.86	-1.32	-0.88
	290	10	2.82	-1.12	2.40	3.24	-1.32	-0.92
	300	0.33	0.15	-1.12	-0.40	0.70	-1.38	-0.85
	300	0.5	0.56	-1.16	0.03	1.09	-1.41	-0.90
	300	1	1.03	-1.13	0.51	1.55	-1.38	-0.88
	300	3.3	1.99	-1.07	1.52	2.46	-1.30	-0.84
	300	5	2.45	-1.12	2.01	2.89	-1.33	-0.91
	300	10	2.87	-1.15	2.46	3.28	-1.34	-0.95
	310	0.33	0.10	-1.08	-0.44	0.64	-1.34	-0.83
	310	0.5	0.52	-1.13	-0.01	1.04	-1.38	-0.88
	310	1	1.00	-1.11	0.48	1.52	-1.36	-0.87
	310	3.3	1.99	-1.07	1.53	2.46	-1.29	-0.85
	310	5	2.44	-1.12	2.01	2.88	-1.33	-0.91
	310	10	2.86	-1.14	2.45	3.26	-1.33	-0.94
	320	0.33	0.08	-1.07	-0.45	0.60	-1.32	-0.82
	320	0.5	0.50	-1.12	-0.02	1.02	-1.37	-0.88
	320	1	0.98	-1.10	0.47	1.49	-1.35	-0.86
	320	3.3	1.98	-1.06	1.52	2.44	-1.28	-0.84
	320	5	2.44	-1.12	2.01	2.87	-1.32	-0.91
	320	10	2.85	-1.14	2.46	3.25	-1.33	-0.95

	330	0.33	0.01	-1.03	-0.52	0.54	-1.28	-0.78
	330	0.5	0.45	-1.09	-0.07	0.96	-1.34	-0.85
	330	1	0.95	-1.09	0.44	1.47	-1.33	-0.85
	330	3.3	1.97	-1.05	1.50	2.43	-1.27	-0.84
	330	5	2.44	-1.11	2.00	2.87	-1.32	-0.91
	330	10	2.86	-1.14	2.45	3.26	-1.33	-0.95
	340	0.33	0.01	-1.03	-0.51	0.53	-1.27	-0.79
	340	0.5	0.46	-1.10	-0.05	0.97	-1.34	-0.86
	340	1	0.99	-1.11	0.48	1.49	-1.35	-0.87
	340	3.3	2.00	-1.07	1.54	2.46	-1.29	-0.86
	340	5	2.47	-1.13	2.04	2.90	-1.33	-0.93
	340	10	2.88	-1.16	2.49	3.28	-1.34	-0.97
	350	0.33	-0.01	-1.02	-0.52	0.50	-1.26	-0.79
	350	0.5	0.45	-1.10	-0.04	0.95	-1.33	-0.87
	350	1	1.00	-1.12	0.51	1.50	-1.35	-0.89
	350	3.3	2.03	-1.09	1.58	2.49	-1.30	-0.88
	350	5	2.51	-1.15	2.08	2.93	-1.35	-0.96
	350	10	2.92	-1.18	2.53	3.31	-1.36	-0.99
	360	0.33	-0.07	-0.98	-0.57	0.43	-1.21	-0.75
	360	0.5	0.40	-1.07	-0.09	0.89	-1.29	-0.84
	360	1	0.98	-1.11	0.49	1.47	-1.33	-0.88
	360	3.3	2.03	-1.09	1.59	2.48	-1.30	-0.89
	360	5	2.51	-1.16	2.09	2.93	-1.35	-0.96
	360	10	2.93	-1.18	2.54	3.32	-1.36	-1.00

	370	0.33	-0.06	-0.99	-0.55	0.42	-1.21	-0.77
	370	0.5	0.42	-1.08	-0.06	0.90	-1.30	-0.86
	370	1	1.01	-1.12	0.53	1.50	-1.34	-0.90
	370	3.3	2.08	-1.12	1.64	2.52	-1.32	-0.92
	370	5	2.55	-1.18	2.13	2.96	-1.37	-0.99
	370	10	2.96	-1.20	2.57	3.34	-1.37	-1.02
	380	0.33	-0.13	-0.95	-0.61	0.36	-1.17	-0.74
	380	0.5	0.36	-1.05	-0.11	0.83	-1.26	-0.83
	380	1	0.97	-1.10	0.49	1.44	-1.31	-0.88
	380	3.3	2.05	-1.10	1.61	2.48	-1.30	-0.90
	380	5	2.52	-1.16	2.12	2.93	-1.35	-0.98
	380	10	2.94	-1.18	2.56	3.31	-1.36	-1.01
	390	0.33	-0.16	-0.93	-0.64	0.31	-1.15	-0.72
	390	0.5	0.33	-1.03	-0.14	0.79	-1.24	-0.82
	390	1	0.94	-1.08	0.47	1.41	-1.29	-0.87
	390	3.3	2.02	-1.09	1.59	2.45	-1.28	-0.89
	390	5	2.49	-1.15	2.09	2.90	-1.33	-0.97
	390	10	2.91	-1.17	2.54	3.28	-1.34	-1.00
	400	0.33	-0.16	-0.94	-0.62	0.31	-1.15	-0.73
	400	0.5	0.33	-1.03	-0.12	0.79	-1.23	-0.82
	400	1	0.94	-1.08	0.48	1.40	-1.29	-0.87
	400	3.3	2.01	-1.08	1.59	2.43	-1.27	-0.89
	400	5	2.49	-1.14	2.09	2.88	-1.32	-0.97
	400	10	2.91	-1.17	2.55	3.28	-1.34	-1.01

Region	cut-off (km)	frequency (Hz)	a	b	L_a	U_a	L_b	U_b
PNW/BC	40	0.33	-0.80	-0.43	-2.51	0.91	-1.71	0.85
	40	0.5	-0.93	-0.23	-2.63	0.77	-1.50	1.04
	40	1	-1.11	0.08	-2.87	0.64	-1.24	1.40
	40	3.3	-0.34	0.26	-2.19	1.52	-1.13	1.65
	40	5	0.03	0.29	-2.03	2.10	-1.26	1.83
	40	10	0.30	0.27	-1.85	2.44	-1.34	1.88
	50	0.33	-0.80	-0.42	-2.10	0.50	-1.32	0.47
	50	0.5	-0.87	-0.28	-2.13	0.39	-1.14	0.59
	50	1	-0.91	-0.09	-2.22	0.40	-0.99	0.81
	50	3.3	-0.12	0.08	-1.46	1.23	-0.84	1.00
	50	5	0.32	0.05	-1.11	1.74	-0.93	1.03
	50	10	0.67	-0.04	-0.81	2.15	-1.05	0.97
	60	0.33	-0.17	-0.91	-1.70	1.35	-1.92	0.10
	60	0.5	-0.20	-0.80	-1.72	1.32	-1.81	0.21
	60	1	-0.25	-0.61	-1.84	1.35	-1.66	0.45
	60	3.3	0.71	-0.56	-0.92	2.33	-1.64	0.52
	60	5	1.24	-0.67	-0.44	2.91	-1.78	0.44
	60	10	1.57	-0.74	-0.01	3.15	-1.79	0.31
	70	0.33	0.16	-1.16	-0.98	1.30	-1.85	-0.46
	70	0.5	0.23	-1.12	-0.95	1.41	-1.84	-0.40
	70	1	0.35	-1.06	-0.92	1.63	-1.84	-0.28
	70	3.3	1.49	-1.16	0.11	2.87	-2.00	-0.31
	70	5	2.07	-1.29	0.62	3.51	-2.18	-0.41

	70	10	2.16	-1.19	0.81	3.51	-2.01	-0.36
	80	0.33	0.05	-1.08	-0.99	1.10	-1.70	-0.46
	80	0.5	0.13	-1.05	-0.94	1.21	-1.69	-0.41
	80	1	0.23	-0.97	-0.93	1.40	-1.66	-0.28
	80	3.3	1.40	-1.09	0.17	2.63	-1.82	-0.36
	80	5	2.02	-1.26	0.75	3.29	-2.02	-0.51
	80	10	2.17	-1.19	0.96	3.38	-1.91	-0.48
	90	0.33	-0.09	-0.98	-1.04	0.86	-1.53	-0.43
	90	0.5	0.00	-0.96	-0.99	0.99	-1.53	-0.39
	90	1	0.11	-0.88	-0.98	1.19	-1.51	-0.26
	90	3.3	1.28	-1.01	0.15	2.41	-1.66	-0.36
	90	5	1.91	-1.18	0.74	3.08	-1.86	-0.51
	90	10	2.19	-1.21	1.04	3.35	-1.88	-0.55
	100	0.33	0.15	-1.14	-0.70	1.00	-1.61	-0.67
	100	0.5	0.23	-1.11	-0.65	1.11	-1.60	-0.63
	100	1	0.35	-1.05	-0.61	1.31	-1.58	-0.52
	100	3.3	1.47	-1.13	0.48	2.46	-1.68	-0.59
	100	5	2.03	-1.26	1.04	3.02	-1.81	-0.71
	100	10	2.29	-1.28	1.32	3.27	-1.81	-0.74
	110	0.33	0.11	-1.12	-0.71	0.93	-1.56	-0.67
	110	0.5	0.19	-1.09	-0.65	1.04	-1.55	-0.63
	110	1	0.33	-1.03	-0.60	1.25	-1.53	-0.53
	110	3.3	1.44	-1.11	0.47	2.40	-1.64	-0.59
	110	5	2.05	-1.28	1.10	3.00	-1.79	-0.76

	110	10	2.34	-1.31	1.43	3.26	-1.80	-0.81
	120	0.33	0.07	-1.09	-0.68	0.82	-1.49	-0.69
	120	0.5	0.16	-1.07	-0.61	0.94	-1.48	-0.66
	120	1	0.32	-1.03	-0.53	1.17	-1.48	-0.58
	120	3.3	1.40	-1.09	0.51	2.29	-1.56	-0.62
	120	5	1.98	-1.23	1.10	2.86	-1.70	-0.76
	120	10	2.30	-1.28	1.42	3.17	-1.74	-0.81
	130	0.33	0.16	-1.15	-0.56	0.88	-1.53	-0.77
	130	0.5	0.26	-1.13	-0.49	1.00	-1.52	-0.73
	130	1	0.41	-1.08	-0.40	1.22	-1.51	-0.66
	130	3.3	1.46	-1.13	0.62	2.30	-1.57	-0.68
	130	5	1.99	-1.24	1.16	2.82	-1.67	-0.80
	130	10	2.24	-1.24	1.42	3.07	-1.68	-0.81
	140	0.33	0.07	-1.09	-0.66	0.80	-1.47	-0.71
	140	0.5	0.16	-1.07	-0.59	0.91	-1.46	-0.68
	140	1	0.30	-1.02	-0.52	1.12	-1.45	-0.59
	140	3.3	1.38	-1.08	0.53	2.22	-1.52	-0.64
	140	5	1.95	-1.21	1.14	2.76	-1.64	-0.79
	140	10	2.16	-1.19	1.36	2.96	-1.61	-0.78
	150	0.33	0.02	-1.06	-0.68	0.72	-1.42	-0.70
	150	0.5	0.06	-1.01	-0.67	0.79	-1.38	-0.63
	150	1	0.17	-0.94	-0.65	0.98	-1.35	-0.52
	150	3.3	1.27	-1.01	0.45	2.10	-1.43	-0.59
	150	5	1.84	-1.15	1.04	2.64	-1.55	-0.74

	150	10	1.99	-1.09	1.22	2.76	-1.49	-0.70
	160	0.33	0.05	-1.08	-0.61	0.70	-1.41	-0.75
	160	0.5	0.07	-1.02	-0.62	0.77	-1.37	-0.67
	160	1	0.16	-0.94	-0.61	0.94	-1.33	-0.55
	160	3.3	1.31	-1.03	0.52	2.09	-1.43	-0.64
	160	5	1.92	-1.19	1.17	2.68	-1.57	-0.82
	160	10	2.22	-1.23	1.50	2.95	-1.59	-0.87
	170	0.33	0.13	-1.12	-0.51	0.77	-1.44	-0.81
	170	0.5	0.20	-1.09	-0.48	0.87	-1.42	-0.75
	170	1	0.34	-1.04	-0.41	1.09	-1.41	-0.66
	170	3.3	1.51	-1.15	0.74	2.28	-1.53	-0.77
	170	5	2.09	-1.29	1.35	2.82	-1.65	-0.92
	170	10	2.38	-1.32	1.68	3.07	-1.66	-0.97
	180	0.33	0.04	-1.07	-0.59	0.67	-1.39	-0.76
	180	0.5	0.11	-1.04	-0.55	0.77	-1.37	-0.71
	180	1	0.25	-0.98	-0.49	0.98	-1.35	-0.62
	180	3.3	1.45	-1.11	0.71	2.19	-1.48	-0.75
	180	5	2.01	-1.25	1.30	2.72	-1.60	-0.89
	180	10	2.33	-1.29	1.66	3.00	-1.62	-0.96
	190	0.33	-0.04	-1.03	-0.64	0.55	-1.32	-0.74
	190	0.5	0.02	-0.99	-0.60	0.65	-1.29	-0.68
	190	1	0.15	-0.93	-0.55	0.85	-1.27	-0.59
	190	3.3	1.29	-1.02	0.58	2.00	-1.37	-0.68
	190	5	1.81	-1.13	1.13	2.50	-1.47	-0.80

	190	10	2.12	-1.17	1.47	2.76	-1.49	-0.86
	200	0.33	-0.21	-0.94	-0.79	0.37	-1.22	-0.66
	200	0.5	-0.14	-0.90	-0.75	0.47	-1.19	-0.61
	200	1	-0.01	-0.84	-0.69	0.67	-1.17	-0.51
	200	3.3	1.08	-0.91	0.38	1.78	-1.25	-0.57
	200	5	1.60	-1.02	0.93	2.27	-1.35	-0.70
	200	10	1.93	-1.07	1.30	2.57	-1.38	-0.77
	210	0.33	-0.11	-0.99	-0.68	0.47	-1.27	-0.72
	210	0.5	-0.04	-0.95	-0.65	0.56	-1.24	-0.66
	210	1	0.07	-0.89	-0.60	0.75	-1.21	-0.56
	210	3.3	1.18	-0.96	0.49	1.87	-1.30	-0.63
	210	5	1.67	-1.06	1.01	2.33	-1.37	-0.74
	210	10	1.95	-1.08	1.32	2.57	-1.38	-0.78
	220	0.33	-0.18	-0.96	-0.73	0.38	-1.22	-0.69
	220	0.5	-0.09	-0.93	-0.67	0.49	-1.21	-0.65
	220	1	0.06	-0.88	-0.59	0.71	-1.19	-0.57
	220	3.3	1.15	-0.95	0.49	1.81	-1.26	-0.63
	220	5	1.62	-1.03	0.98	2.25	-1.33	-0.73
	220	10	1.83	-1.01	1.22	2.43	-1.30	-0.73
	230	0.33	-0.16	-0.96	-0.71	0.38	-1.22	-0.70
	230	0.5	-0.07	-0.94	-0.63	0.50	-1.21	-0.67
	230	1	0.10	-0.90	-0.53	0.73	-1.20	-0.60
	230	3.3	1.22	-0.98	0.57	1.86	-1.29	-0.68
	230	5	1.67	-1.06	1.05	2.29	-1.35	-0.76

	230	10	1.89	-1.05	1.30	2.48	-1.33	-0.77
	240	0.33	-0.23	-0.93	-0.76	0.30	-1.18	-0.68
	240	0.5	-0.14	-0.90	-0.69	0.42	-1.16	-0.64
	240	1	0.04	-0.87	-0.57	0.65	-1.16	-0.58
	240	3.3	1.14	-0.94	0.51	1.76	-1.24	-0.65
	240	5	1.58	-1.01	0.97	2.18	-1.29	-0.72
	240	10	1.78	-0.99	1.20	2.35	-1.26	-0.72
	250	0.33	-0.28	-0.90	-0.79	0.23	-1.14	-0.66
	250	0.5	-0.19	-0.87	-0.72	0.34	-1.12	-0.62
	250	1	-0.03	-0.84	-0.62	0.56	-1.11	-0.56
	250	3.3	1.11	-0.93	0.51	1.71	-1.21	-0.65
	250	5	1.55	-0.99	0.97	2.13	-1.26	-0.72
	250	10	1.74	-0.97	1.18	2.29	-1.23	-0.71
	260	0.33	-0.26	-0.91	-0.76	0.23	-1.14	-0.68
	260	0.5	-0.18	-0.88	-0.69	0.33	-1.12	-0.64
	260	1	-0.02	-0.84	-0.60	0.55	-1.10	-0.57
	260	3.3	1.09	-0.92	0.50	1.67	-1.19	-0.64
	260	5	1.53	-0.98	0.97	2.09	-1.24	-0.72
	260	10	1.68	-0.94	1.14	2.22	-1.19	-0.68
	270	0.33	-0.25	-0.92	-0.72	0.23	-1.14	-0.70
	270	0.5	-0.16	-0.89	-0.66	0.34	-1.12	-0.66
	270	1	-0.01	-0.85	-0.56	0.55	-1.10	-0.59
	270	3.3	1.11	-0.93	0.55	1.67	-1.19	-0.67
	270	5	1.54	-0.99	1.00	2.08	-1.24	-0.74

	270	10	1.67	-0.93	1.15	2.19	-1.17	-0.69
	280	0.33	-0.25	-0.92	-0.71	0.22	-1.13	-0.70
	280	0.5	-0.16	-0.89	-0.64	0.32	-1.11	-0.67
	280	1	0.00	-0.85	-0.54	0.54	-1.10	-0.60
	280	3.3	1.16	-0.95	0.61	1.71	-1.21	-0.70
	280	5	1.59	-1.01	1.06	2.12	-1.26	-0.77
	280	10	1.61	-0.90	1.10	2.12	-1.14	-0.67
	290	0.33	-0.21	-0.94	-0.67	0.25	-1.15	-0.73
	290	0.5	-0.12	-0.91	-0.60	0.36	-1.13	-0.69
	290	1	0.04	-0.87	-0.49	0.58	-1.12	-0.63
	290	3.3	1.18	-0.96	0.63	1.72	-1.21	-0.71
	290	5	1.60	-1.02	1.07	2.13	-1.26	-0.78
	290	10	1.58	-0.89	1.07	2.09	-1.12	-0.65
	300	0.33	-0.24	-0.92	-0.69	0.22	-1.13	-0.71
	300	0.5	-0.15	-0.90	-0.62	0.33	-1.11	-0.68
	300	1	0.02	-0.86	-0.51	0.55	-1.10	-0.62
	300	3.3	1.15	-0.95	0.60	1.69	-1.19	-0.70
	300	5	1.54	-0.99	1.02	2.06	-1.23	-0.75
	300	10	1.48	-0.84	0.98	1.99	-1.07	-0.60
	310	0.33	-0.20	-0.94	-0.64	0.25	-1.15	-0.74
	310	0.5	-0.08	-0.93	-0.55	0.38	-1.14	-0.72
	310	1	0.10	-0.90	-0.41	0.62	-1.14	-0.67
	310	3.3	1.23	-0.99	0.70	1.76	-1.23	-0.75
	310	5	1.60	-1.02	1.08	2.11	-1.25	-0.78

	310	10	1.49	-0.84	0.99	2.00	-1.07	-0.61
	320	0.33	-0.17	-0.96	-0.61	0.26	-1.15	-0.76
	320	0.5	-0.05	-0.95	-0.50	0.40	-1.15	-0.74
	320	1	0.14	-0.92	-0.36	0.65	-1.15	-0.69
	320	3.3	1.33	-1.04	0.81	1.85	-1.27	-0.80
	320	5	1.69	-1.06	1.19	2.19	-1.29	-0.84
	320	10	1.49	-0.84	1.00	1.98	-1.06	-0.62
	330	0.33	-0.26	-0.91	-0.69	0.17	-1.10	-0.72
	330	0.5	-0.13	-0.91	-0.57	0.31	-1.11	-0.71
	330	1	0.08	-0.89	-0.41	0.57	-1.11	-0.67
	330	3.3	1.27	-1.01	0.76	1.78	-1.24	-0.78
	330	5	1.65	-1.04	1.16	2.14	-1.27	-0.82
	330	10	1.45	-0.82	0.97	1.93	-1.04	-0.60
	340	0.33	-0.31	-0.89	-0.73	0.11	-1.08	-0.70
	340	0.5	-0.17	-0.89	-0.60	0.27	-1.08	-0.69
	340	1	0.06	-0.88	-0.42	0.54	-1.10	-0.66
	340	3.3	1.28	-1.01	0.78	1.77	-1.24	-0.79
	340	5	1.65	-1.05	1.17	2.13	-1.26	-0.83
	340	10	1.42	-0.80	0.94	1.89	-1.02	-0.59
	350	0.33	-0.33	-0.88	-0.74	0.08	-1.06	-0.69
	350	0.5	-0.18	-0.88	-0.61	0.24	-1.07	-0.69
	350	1	0.04	-0.87	-0.43	0.51	-1.08	-0.66
	350	3.3	1.23	-0.99	0.74	1.72	-1.21	-0.77
	350	5	1.57	-1.01	1.09	2.05	-1.22	-0.79

	350	10	1.30	-0.75	0.82	1.78	-0.96	-0.53
	360	0.33	-0.36	-0.86	-0.77	0.04	-1.04	-0.68
	360	0.5	-0.21	-0.87	-0.63	0.21	-1.05	-0.68
	360	1	0.02	-0.86	-0.44	0.49	-1.07	-0.65
	360	3.3	1.22	-0.98	0.73	1.70	-1.20	-0.77
	360	5	1.56	-1.00	1.09	2.03	-1.21	-0.79
	360	10	1.24	-0.71	0.76	1.71	-0.93	-0.50
	370	0.33	-0.46	-0.81	-0.85	-0.06	-0.99	-0.64
	370	0.5	-0.30	-0.82	-0.71	0.11	-1.01	-0.64
	370	1	-0.05	-0.82	-0.51	0.40	-1.03	-0.62
	370	3.3	1.17	-0.96	0.70	1.64	-1.17	-0.75
	370	5	1.52	-0.98	1.05	1.98	-1.19	-0.77
	370	10	1.19	-0.69	0.72	1.66	-0.90	-0.48
	380	0.33	-0.49	-0.80	-0.88	-0.10	-0.97	-0.62
	380	0.5	-0.32	-0.81	-0.73	0.08	-0.99	-0.63
	380	1	-0.07	-0.82	-0.52	0.38	-1.02	-0.62
	380	3.3	1.17	-0.96	0.71	1.64	-1.17	-0.75
	380	5	1.51	-0.97	1.05	1.97	-1.18	-0.77
	380	10	1.13	-0.66	0.67	1.60	-0.87	-0.45
	390	0.33	-0.50	-0.79	-0.88	-0.11	-0.96	-0.62
	390	0.5	-0.32	-0.81	-0.71	0.07	-0.99	-0.64
	390	1	-0.05	-0.82	-0.49	0.38	-1.02	-0.63
	390	3.3	1.23	-0.99	0.77	1.69	-1.19	-0.79
	390	5	1.52	-0.98	1.07	1.97	-1.18	-0.78

	390	10	1.08	-0.64	0.63	1.54	-0.84	-0.44
	400	0.33	-0.54	-0.77	-0.92	-0.16	-0.94	-0.61
	400	0.5	-0.36	-0.79	-0.75	0.03	-0.97	-0.62
	400	1	-0.09	-0.81	-0.52	0.34	-1.00	-0.62
	400	3.3	1.21	-0.98	0.76	1.66	-1.18	-0.78
	400	5	1.51	-0.97	1.06	1.95	-1.17	-0.78
	400	10	1.07	-0.63	0.63	1.52	-0.83	-0.43
Region	cut-off (km)	frequency (Hz)	a	b	L_a	U_a	L_b	U_b
S. Cal	40	0.33	0.92	-1.21	0.43	1.41	-1.56	-0.85
	40	0.5	1.41	-1.35	0.93	1.89	-1.70	-1.01
	40	1	2.36	-1.61	1.87	2.85	-1.97	-1.26
	40	3.3	3.22	-1.50	2.78	3.66	-1.81	-1.18
	40	5	3.27	-1.37	2.86	3.69	-1.67	-1.06
	40	10	3.43	-1.38	3.03	3.82	-1.67	-1.10
	50	0.33	0.97	-1.25	0.57	1.37	-1.52	-0.97
	50	0.5	1.53	-1.44	1.14	1.91	-1.71	-1.18
	50	1	2.31	-1.58	1.92	2.70	-1.84	-1.31
	50	3.3	3.18	-1.46	2.83	3.52	-1.70	-1.22
	50	5	3.30	-1.39	2.97	3.63	-1.61	-1.16
	50	10	3.45	-1.40	3.14	3.75	-1.61	-1.19
	60	0.33	1.12	-1.36	0.77	1.46	-1.59	-1.13
	60	0.5	1.69	-1.57	1.35	2.02	-1.79	-1.34
	60	1	2.38	-1.63	2.04	2.72	-1.85	-1.40
	60	3.3	3.27	-1.53	2.97	3.57	-1.73	-1.33

	60	5	3.41	-1.47	3.13	3.70	-1.66	-1.28
	60	10	3.56	-1.48	3.29	3.83	-1.66	-1.30
	70	0.33	1.13	-1.37	0.81	1.45	-1.57	-1.16
	70	0.5	1.69	-1.57	1.38	2.00	-1.76	-1.37
	70	1	2.49	-1.70	2.18	2.79	-1.90	-1.51
	70	3.3	3.41	-1.63	3.14	3.68	-1.80	-1.46
	70	5	3.56	-1.58	3.30	3.81	-1.74	-1.41
	70	10	3.71	-1.59	3.47	3.95	-1.74	-1.44
	80	0.33	1.22	-1.43	0.93	1.51	-1.62	-1.25
	80	0.5	1.74	-1.61	1.46	2.02	-1.78	-1.43
	80	1	2.46	-1.69	2.19	2.74	-1.86	-1.51
	80	3.3	3.37	-1.60	3.12	3.61	-1.75	-1.45
	80	5	3.53	-1.55	3.30	3.76	-1.70	-1.41
	80	10	3.64	-1.54	3.42	3.85	-1.67	-1.40
	90	0.33	1.19	-1.41	0.92	1.46	-1.58	-1.24
	90	0.5	1.72	-1.59	1.46	1.97	-1.74	-1.43
	90	1	2.44	-1.67	2.18	2.69	-1.82	-1.51
	90	3.3	3.32	-1.57	3.10	3.54	-1.71	-1.44
	90	5	3.51	-1.54	3.30	3.72	-1.67	-1.41
	90	10	3.59	-1.51	3.40	3.79	-1.63	-1.39
	100	0.33	1.09	-1.34	0.84	1.34	-1.49	-1.19
	100	0.5	1.63	-1.52	1.39	1.87	-1.67	-1.38
	100	1	2.37	-1.62	2.13	2.60	-1.76	-1.48
	100	3.3	3.25	-1.52	3.05	3.46	-1.65	-1.40

	100	5	3.44	-1.50	3.25	3.64	-1.62	-1.38
	100	10	3.52	-1.46	3.33	3.70	-1.56	-1.35
	110	0.33	1.05	-1.31	0.81	1.29	-1.45	-1.17
	110	0.5	1.58	-1.49	1.35	1.80	-1.62	-1.36
	110	1	2.31	-1.58	2.08	2.53	-1.71	-1.45
	110	3.3	3.20	-1.49	3.01	3.40	-1.61	-1.37
	110	5	3.40	-1.47	3.22	3.59	-1.58	-1.36
	110	10	3.46	-1.42	3.28	3.64	-1.52	-1.31
	120	0.33	1.00	-1.28	0.77	1.23	-1.42	-1.14
	120	0.5	1.53	-1.46	1.31	1.75	-1.59	-1.33
	120	1	2.26	-1.55	2.05	2.47	-1.67	-1.43
	120	3.3	3.17	-1.47	2.98	3.36	-1.58	-1.36
	120	5	3.38	-1.46	3.20	3.56	-1.56	-1.35
	120	10	3.44	-1.40	3.27	3.61	-1.50	-1.31
	130	0.33	0.98	-1.27	0.76	1.20	-1.39	-1.14
	130	0.5	1.49	-1.43	1.28	1.70	-1.55	-1.32
	130	1	2.21	-1.52	2.01	2.41	-1.63	-1.40
	130	3.3	3.16	-1.46	2.98	3.34	-1.57	-1.36
	130	5	3.39	-1.46	3.22	3.56	-1.56	-1.36
	130	10	3.45	-1.41	3.29	3.61	-1.50	-1.32
	140	0.33	0.91	-1.22	0.69	1.12	-1.34	-1.09
	140	0.5	1.42	-1.39	1.22	1.62	-1.50	-1.27
	140	1	2.13	-1.47	1.94	2.33	-1.58	-1.36
	140	3.3	3.12	-1.44	2.95	3.29	-1.53	-1.34

	140	5	3.34	-1.43	3.18	3.51	-1.52	-1.34
	140	10	3.41	-1.38	3.26	3.56	-1.47	-1.30
	150	0.33	0.87	-1.19	0.66	1.08	-1.31	-1.07
	150	0.5	1.41	-1.38	1.22	1.61	-1.49	-1.27
	150	1	2.15	-1.48	1.96	2.34	-1.58	-1.37
	150	3.3	3.15	-1.45	2.98	3.31	-1.55	-1.36
	150	5	3.38	-1.45	3.22	3.54	-1.54	-1.37
	150	10	3.45	-1.41	3.30	3.59	-1.49	-1.33
	160	0.33	0.83	-1.17	0.63	1.04	-1.28	-1.05
	160	0.5	1.36	-1.35	1.17	1.55	-1.46	-1.24
	160	1	2.14	-1.47	1.96	2.32	-1.57	-1.37
	160	3.3	3.15	-1.46	2.99	3.32	-1.55	-1.37
	160	5	3.40	-1.47	3.24	3.55	-1.55	-1.38
	160	10	3.48	-1.43	3.33	3.62	-1.51	-1.35
	170	0.33	0.78	-1.13	0.58	0.98	-1.24	-1.02
	170	0.5	1.26	-1.28	1.07	1.44	-1.38	-1.18
	170	1	2.04	-1.41	1.86	2.22	-1.51	-1.31
	170	3.3	3.10	-1.42	2.94	3.25	-1.51	-1.34
	170	5	3.35	-1.43	3.20	3.50	-1.52	-1.35
	170	10	3.45	-1.41	3.31	3.59	-1.49	-1.33
	180	0.33	0.74	-1.11	0.54	0.93	-1.21	-1.00
	180	0.5	1.22	-1.26	1.03	1.40	-1.36	-1.16
	180	1	2.00	-1.38	1.82	2.17	-1.48	-1.29
	180	3.3	3.07	-1.41	2.92	3.22	-1.49	-1.32

	180	5	3.33	-1.42	3.19	3.47	-1.50	-1.35
	180	10	3.44	-1.40	3.30	3.57	-1.48	-1.33
	190	0.33	0.71	-1.09	0.52	0.90	-1.20	-0.99
	190	0.5	1.19	-1.24	1.01	1.37	-1.34	-1.14
	190	1	1.97	-1.36	1.80	2.14	-1.46	-1.27
	190	3.3	3.05	-1.40	2.90	3.20	-1.48	-1.31
	190	5	3.32	-1.42	3.18	3.46	-1.49	-1.34
	190	10	3.43	-1.40	3.30	3.56	-1.47	-1.33
	200	0.33	0.72	-1.09	0.53	0.90	-1.20	-0.99
	200	0.5	1.17	-1.23	0.99	1.34	-1.32	-1.13
	200	1	1.95	-1.35	1.78	2.11	-1.44	-1.26
	200	3.3	3.05	-1.39	2.90	3.20	-1.47	-1.31
	200	5	3.32	-1.42	3.19	3.46	-1.49	-1.35
	200	10	3.44	-1.40	3.31	3.57	-1.47	-1.33
	210	0.33	0.73	-1.10	0.55	0.91	-1.20	-1.00
	210	0.5	1.15	-1.22	0.98	1.33	-1.31	-1.13
	210	1	1.93	-1.34	1.77	2.10	-1.43	-1.25
	210	3.3	3.05	-1.39	2.91	3.20	-1.47	-1.32
	210	5	3.34	-1.43	3.20	3.47	-1.50	-1.36
	210	10	3.46	-1.42	3.33	3.59	-1.48	-1.35
	220	0.33	0.68	-1.07	0.50	0.86	-1.17	-0.98
	220	0.5	1.10	-1.18	0.93	1.27	-1.27	-1.09
	220	1	1.89	-1.31	1.72	2.05	-1.40	-1.23
	220	3.3	3.03	-1.38	2.89	3.17	-1.45	-1.31

	220	5	3.32	-1.42	3.19	3.46	-1.49	-1.35
	220	10	3.46	-1.42	3.33	3.58	-1.48	-1.35
	230	0.33	0.68	-1.07	0.50	0.86	-1.17	-0.97
	230	0.5	1.06	-1.16	0.89	1.23	-1.25	-1.07
	230	1	1.84	-1.28	1.68	2.00	-1.37	-1.20
	230	3.3	3.01	-1.37	2.87	3.15	-1.44	-1.30
	230	5	3.32	-1.42	3.19	3.45	-1.48	-1.35
	230	10	3.46	-1.41	3.33	3.58	-1.48	-1.35
	240	0.33	0.66	-1.06	0.49	0.84	-1.15	-0.96
	240	0.5	1.05	-1.15	0.88	1.21	-1.24	-1.07
	240	1	1.82	-1.27	1.66	1.98	-1.36	-1.19
	240	3.3	3.00	-1.36	2.86	3.14	-1.43	-1.29
	240	5	3.31	-1.41	3.18	3.44	-1.48	-1.34
	240	10	3.45	-1.41	3.33	3.57	-1.47	-1.35
	250	0.33	0.65	-1.05	0.47	0.82	-1.14	-0.96
	250	0.5	1.01	-1.13	0.85	1.18	-1.22	-1.05
	250	1	1.79	-1.25	1.63	1.94	-1.34	-1.17
	250	3.3	2.98	-1.35	2.84	3.12	-1.42	-1.28
	250	5	3.30	-1.40	3.17	3.43	-1.47	-1.34
	250	10	3.44	-1.41	3.32	3.56	-1.47	-1.34
	260	0.33	0.63	-1.04	0.46	0.80	-1.13	-0.95
	260	0.5	0.98	-1.11	0.82	1.14	-1.20	-1.03
	260	1	1.75	-1.23	1.59	1.90	-1.31	-1.15
	260	3.3	2.96	-1.34	2.83	3.10	-1.41	-1.27

	260	5	3.29	-1.40	3.17	3.42	-1.47	-1.34
	260	10	3.44	-1.40	3.32	3.56	-1.47	-1.34
	270	0.33	0.63	-1.04	0.46	0.80	-1.13	-0.95
	270	0.5	0.96	-1.10	0.80	1.12	-1.18	-1.02
	270	1	1.72	-1.21	1.56	1.87	-1.29	-1.13
	270	3.3	2.95	-1.33	2.81	3.08	-1.40	-1.26
	270	5	3.28	-1.39	3.15	3.40	-1.46	-1.33
	270	10	3.42	-1.39	3.31	3.54	-1.46	-1.33
	280	0.33	0.60	-1.02	0.43	0.77	-1.11	-0.93
	280	0.5	0.93	-1.08	0.77	1.09	-1.16	-1.00
	280	1	1.69	-1.19	1.54	1.84	-1.27	-1.12
	280	3.3	2.93	-1.32	2.80	3.06	-1.39	-1.26
	280	5	3.27	-1.39	3.15	3.39	-1.45	-1.33
	280	10	3.42	-1.39	3.30	3.53	-1.45	-1.33
	290	0.33	0.57	-1.00	0.40	0.73	-1.09	-0.91
	290	0.5	0.90	-1.06	0.74	1.05	-1.14	-0.98
	290	1	1.65	-1.17	1.50	1.80	-1.25	-1.10
	290	3.3	2.91	-1.31	2.78	3.04	-1.38	-1.24
	290	5	3.26	-1.38	3.14	3.38	-1.44	-1.32
	290	10	3.40	-1.38	3.28	3.51	-1.44	-1.32
	300	0.33	0.55	-0.99	0.38	0.71	-1.07	-0.90
	300	0.5	0.86	-1.04	0.71	1.02	-1.12	-0.96
	300	1	1.62	-1.15	1.47	1.76	-1.23	-1.08
	300	3.3	2.90	-1.30	2.77	3.02	-1.37	-1.24

	300	5	3.25	-1.38	3.13	3.37	-1.44	-1.32
	300	10	3.39	-1.37	3.27	3.50	-1.43	-1.31
	310	0.33	0.53	-0.98	0.37	0.70	-1.07	-0.90
	310	0.5	0.84	-1.03	0.69	0.99	-1.11	-0.95
	310	1	1.60	-1.14	1.45	1.74	-1.22	-1.07
	310	3.3	2.89	-1.30	2.76	3.02	-1.36	-1.23
	310	5	3.25	-1.37	3.13	3.37	-1.44	-1.31
	310	10	3.38	-1.37	3.26	3.49	-1.42	-1.31
	320	0.33	0.51	-0.97	0.35	0.67	-1.05	-0.88
	320	0.5	0.81	-1.01	0.66	0.96	-1.09	-0.93
	320	1	1.57	-1.13	1.43	1.72	-1.20	-1.05
	320	3.3	2.88	-1.29	2.75	3.00	-1.35	-1.23
	320	5	3.24	-1.37	3.12	3.36	-1.43	-1.31
	320	10	3.36	-1.36	3.25	3.47	-1.41	-1.30
	330	0.33	0.51	-0.97	0.35	0.67	-1.05	-0.88
	330	0.5	0.80	-1.01	0.65	0.95	-1.09	-0.93
	330	1	1.57	-1.13	1.43	1.72	-1.20	-1.05
	330	3.3	2.88	-1.29	2.76	3.01	-1.36	-1.23
	330	5	3.25	-1.38	3.13	3.37	-1.43	-1.32
	330	10	3.36	-1.36	3.25	3.48	-1.42	-1.30
	340	0.33	0.50	-0.96	0.34	0.66	-1.04	-0.88
	340	0.5	0.79	-1.00	0.64	0.94	-1.08	-0.92
	340	1	1.56	-1.12	1.42	1.71	-1.20	-1.05
	340	3.3	2.88	-1.29	2.76	3.00	-1.36	-1.23

	340	5	3.25	-1.37	3.13	3.36	-1.43	-1.32
	340	10	3.36	-1.36	3.25	3.47	-1.41	-1.30
	350	0.33	0.49	-0.95	0.33	0.65	-1.04	-0.87
	350	0.5	0.78	-1.00	0.63	0.93	-1.07	-0.92
	350	1	1.56	-1.12	1.41	1.70	-1.19	-1.04
	350	3.3	2.88	-1.29	2.76	3.00	-1.36	-1.23
	350	5	3.25	-1.38	3.13	3.37	-1.43	-1.32
	350	10	3.36	-1.36	3.25	3.47	-1.41	-1.30
	360	0.33	0.47	-0.95	0.32	0.63	-1.03	-0.86
	360	0.5	0.77	-0.99	0.62	0.92	-1.07	-0.91
	360	1	1.55	-1.11	1.40	1.69	-1.18	-1.04
	360	3.3	2.88	-1.29	2.76	3.00	-1.35	-1.23
	360	5	3.25	-1.38	3.14	3.37	-1.43	-1.32
	360	10	3.36	-1.35	3.25	3.47	-1.41	-1.30
	370	0.33	0.47	-0.94	0.32	0.63	-1.03	-0.86
	370	0.5	0.77	-0.99	0.62	0.92	-1.06	-0.91
	370	1	1.54	-1.11	1.40	1.68	-1.18	-1.04
	370	3.3	2.88	-1.29	2.76	3.00	-1.35	-1.23
	370	5	3.25	-1.38	3.13	3.36	-1.43	-1.32
	370	10	3.35	-1.35	3.24	3.46	-1.41	-1.30
	380	0.33	0.46	-0.94	0.30	0.62	-1.02	-0.86
	380	0.5	0.75	-0.98	0.60	0.90	-1.05	-0.90
	380	1	1.53	-1.10	1.39	1.67	-1.17	-1.03
	380	3.3	2.88	-1.29	2.75	3.00	-1.35	-1.23

	380	5	3.25	-1.38	3.13	3.36	-1.43	-1.32
	380	10	3.35	-1.35	3.24	3.46	-1.41	-1.29
	390	0.33	0.45	-0.93	0.30	0.61	-1.01	-0.85
	390	0.5	0.75	-0.98	0.60	0.89	-1.05	-0.90
	390	1	1.53	-1.10	1.38	1.67	-1.17	-1.03
	390	3.3	2.88	-1.29	2.76	3.00	-1.35	-1.23
	390	5	3.25	-1.38	3.14	3.37	-1.43	-1.32
	390	10	3.35	-1.35	3.24	3.46	-1.41	-1.29
	400	0.33	0.45	-0.93	0.30	0.61	-1.01	-0.85
	400	0.5	0.75	-0.98	0.60	0.89	-1.05	-0.90
	400	1	1.52	-1.10	1.38	1.66	-1.17	-1.03
	400	3.3	2.88	-1.29	2.76	3.00	-1.35	-1.23
	400	5	3.25	-1.38	3.14	3.37	-1.44	-1.32
	400	10	3.35	-1.35	3.24	3.46	-1.41	-1.29

Table B-2 Log(base10)-averaged ground-motion amplitude ratios in each region to those in S. California. Dhypo is hypocentral distance, and err is the standard error of the log ratio in each distance bin (weighted average for the entire magnitude range). The log ratios are for the geometric mean of the horizontal components and equivalent site class B/C.

	Dhypo	PSA0.33	err	Dhypo	PSA1	err	Dhypo	PSA3.3	err	Dhypo	PGA	err
CUS	44.67	0.1984	0.05	35.48	-0.0498	0.03	35.48	-0.0358	0.04	35.48	-0.0624	0.04
	56.23	-0.1442	0.06	44.67	-0.1362	0.13	44.67	-0.1566	0.12	44.67	-0.5300	0.06
	70.79	0.5240	0.05	56.23	-0.2555	0.05	56.23	-0.7597	0.09	56.23	-0.4495	0.06
	89.13	-0.0881	0.07	70.79	-0.1002	0.11	70.79	-0.0761	0.05	70.79	-0.0169	0.12
	112.20	0.1194	0.11	89.13	-0.0919	0.09	89.13	0.1253	0.09	89.13	0.1760	0.15
	141.25	0.1114	0.13	112.20	0.0899	0.08	112.20	0.2699	0.09	112.20	0.2725	0.10
	177.83	0.2527	0.13	141.25	0.1331	0.10	141.25	0.3438	0.10	141.25	0.4644	0.11
	223.87	0.2662	0.09	177.83	0.2852	0.09	177.83	0.7128	0.08	177.83	0.7756	0.08
	281.84	0.3693	0.06	223.87	0.3777	0.07	223.87	0.6427	0.08	223.87	0.8188	0.07
	354.81	0.2330	0.07	281.84	0.3193	0.05	281.84	0.7977	0.06	281.84	0.8768	0.06
				354.81	0.2795	0.04	354.81	0.7535	0.05	354.81	0.7940	0.05
				446.68	0.3456	0.04	446.68	0.8147	0.06	446.68	0.9065	0.05
N. California	17.78	0.1530	0.20	8.91	0.2008	0.05	8.91	-0.0090	0.07	8.91	-0.2409	0.08
	22.39	0.2224	0.18	11.22	0.1266	0.06	11.22	-0.0208	0.10	11.22	-0.0350	0.10
	28.18	0.3719	0.04	14.13	-0.0895	0.05	14.13	-0.2574	0.12	14.13	-0.4031	0.12
	35.48	0.2195	0.10	17.78	0.0896	0.07	17.78	-0.3327	0.06	17.78	-0.3979	0.07
	44.67	-0.0663	0.07	22.39	0.0984	0.14	22.39	-0.0515	0.12	22.39	-0.3045	0.10
	56.23	0.1653	0.07	28.18	0.1183	0.06	28.18	-0.0361	0.11	28.18	-0.3345	0.10
	70.79	0.2697	0.09	35.48	0.3125	0.06	35.48	-0.0340	0.07	35.48	-0.5006	0.09

	89.13	0.1459	0.09	44.67	0.1808	0.08	44.67	-0.1171	0.07	44.67	-0.5124	0.07
	112.20	0.0962	0.09	56.23	0.1397	0.08	56.23	-0.0818	0.08	56.23	-0.3742	0.09
	141.25	0.0836	0.06	70.79	0.2762	0.06	70.79	0.1575	0.08	70.79	-0.0940	0.08
	177.83	0.0157	0.06	89.13	0.2472	0.05	89.13	-0.0171	0.06	89.13	-0.2862	0.06
	223.87	0.0459	0.12	112.20	0.2275	0.05	112.20	-0.0364	0.06	112.20	-0.2872	0.07
	281.84	0.8802	0.08	141.25	0.0240	0.05	141.25	-0.1843	0.06	141.25	-0.2810	0.06
				177.83	-0.0296	0.05	177.83	-0.2391	0.06	177.83	-0.3296	0.06
				223.87	0.1672	0.04	223.87	0.0271	0.06	223.87	0.0044	0.06
				281.84	0.5417	0.05	281.84	0.3679	0.07	281.84	0.3166	0.07
Northeast	17.78	-0.3097	0.11	17.78	-0.3676	0.06	17.78	-0.0951	0.03	17.78	0.9158	0.31
	22.39	-0.4076	0.16	22.39	-0.2709	0.09	22.39	-0.2282	0.18	22.39	0.4281	0.18
	28.18	0.0735	0.07	28.18	0.0116	0.16	28.18	-0.0096	0.10	28.18	0.3760	0.03
	35.48	-0.1671	0.07	35.48	0.0108	0.05	35.48	-0.0037	0.08	35.48	0.1582	0.12
	44.67	-0.3573	0.01	44.67	-0.4015	0.10	44.67	-0.1887	0.12	44.67	0.2321	0.08
	56.23	-0.2141	0.09	56.23	0.2294	0.07	56.23	0.0206	0.11	56.23	0.4128	0.09
	70.79	-0.0038	0.09	70.79	-0.0797	0.25	70.79	-0.0645	0.14	70.79	0.3394	0.12
	89.13	0.1679	0.07	89.13	-0.0587	0.01	89.13	-0.0332	0.07	89.13	0.2261	0.08
	112.20	0.0224	0.06	112.20	-0.0032	0.06	112.20	0.1866	0.05	112.20	0.4018	0.11
	141.25	-0.0386	0.11	141.25	0.1349	0.09	141.25	0.1714	0.08	141.25	0.5440	0.09
	177.83	0.1995	0.12	177.83	0.2696	0.08	177.83	0.1734	0.19	177.83	0.5060	0.05
	223.87	0.0985	0.05	223.87	0.4193	0.10	223.87	0.6012	0.08	223.87	0.9511	0.05
	281.84	0.3790	0.21	281.84	0.3562	0.14	281.84	0.4672	0.08	281.84	1.0111	0.16
	354.81	0.1216	0.14	354.81	0.0897	0.09	354.81	0.7762	0.11	354.81	0.8585	0.10
PNW/BC	28.18	0.0571	0.06	28.18	-0.6304	0.06	28.18	-0.7810	0.09	28.18	-0.4497	0.14

	44.67	0.2224	0.07	44.67	-0.2267	0.06	44.67	-0.3392	0.19	44.67	-0.1351	0.17
	56.23	-0.2268	0.08	56.23	-0.8154	0.18	56.23	-0.9551	0.23	56.23	-0.7505	0.21
	70.79	0.2356	0.08	70.79	-0.6253	0.26	70.79	-0.8568	0.08	70.79	-0.3876	0.10
	89.13	0.0123	0.07	89.13	-0.6931	0.06	89.13	-0.6772	0.10	89.13	-0.6282	0.16
	112.20	0.0102	0.16	112.20	-0.7101	0.06	112.20	-0.7586	0.11	112.20	-0.5262	0.14
	141.25	-0.1400	0.12	141.25	-0.5787	0.10	141.25	-0.6979	0.10	141.25	-0.4929	0.10
	177.83	-0.0418	0.09	177.83	-0.6931	0.09	177.83	-0.7712	0.10	177.83	-0.5081	0.11
	223.87	0.0738	0.06	223.87	-0.5832	0.09	223.87	-0.6580	0.09	223.87	-0.2487	0.11
	281.84	-0.1085	0.12	281.84	-0.8253	0.08	281.84	-0.6598	0.09	281.84	-0.2304	0.09
	354.81	0.0075	0.09	354.81	-0.7899	0.09	354.81	-0.6579	0.10	354.81	-0.2558	0.12

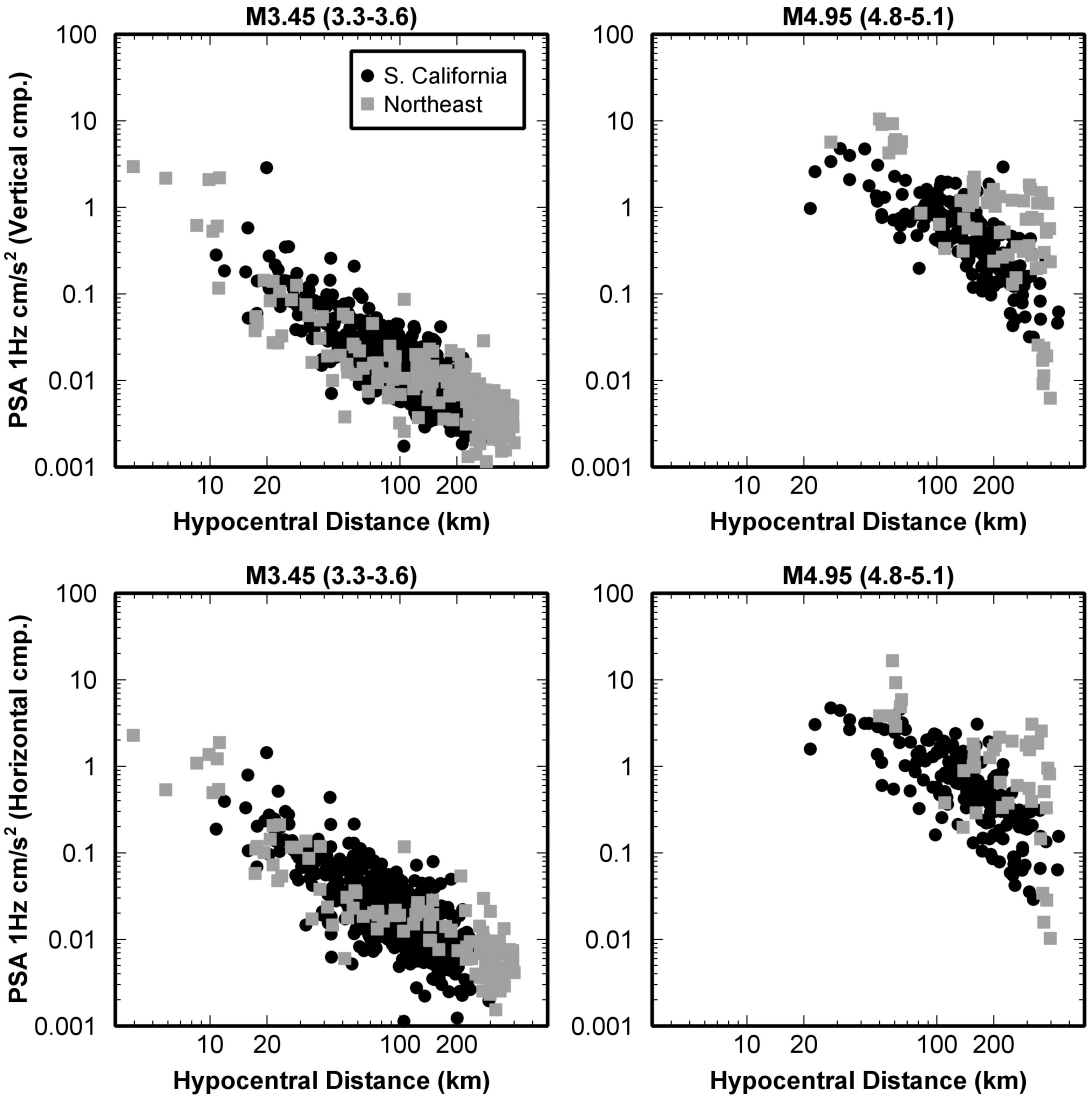

Figure B1 Plot of PSA-1Hz (cm/s^2) versus hypocentral distance for the vertical component and geometric mean of horizontal components in two magnitude bins, **M=** 3.45 and 4.95 for S. California and Northeast (all for B/C site condition).

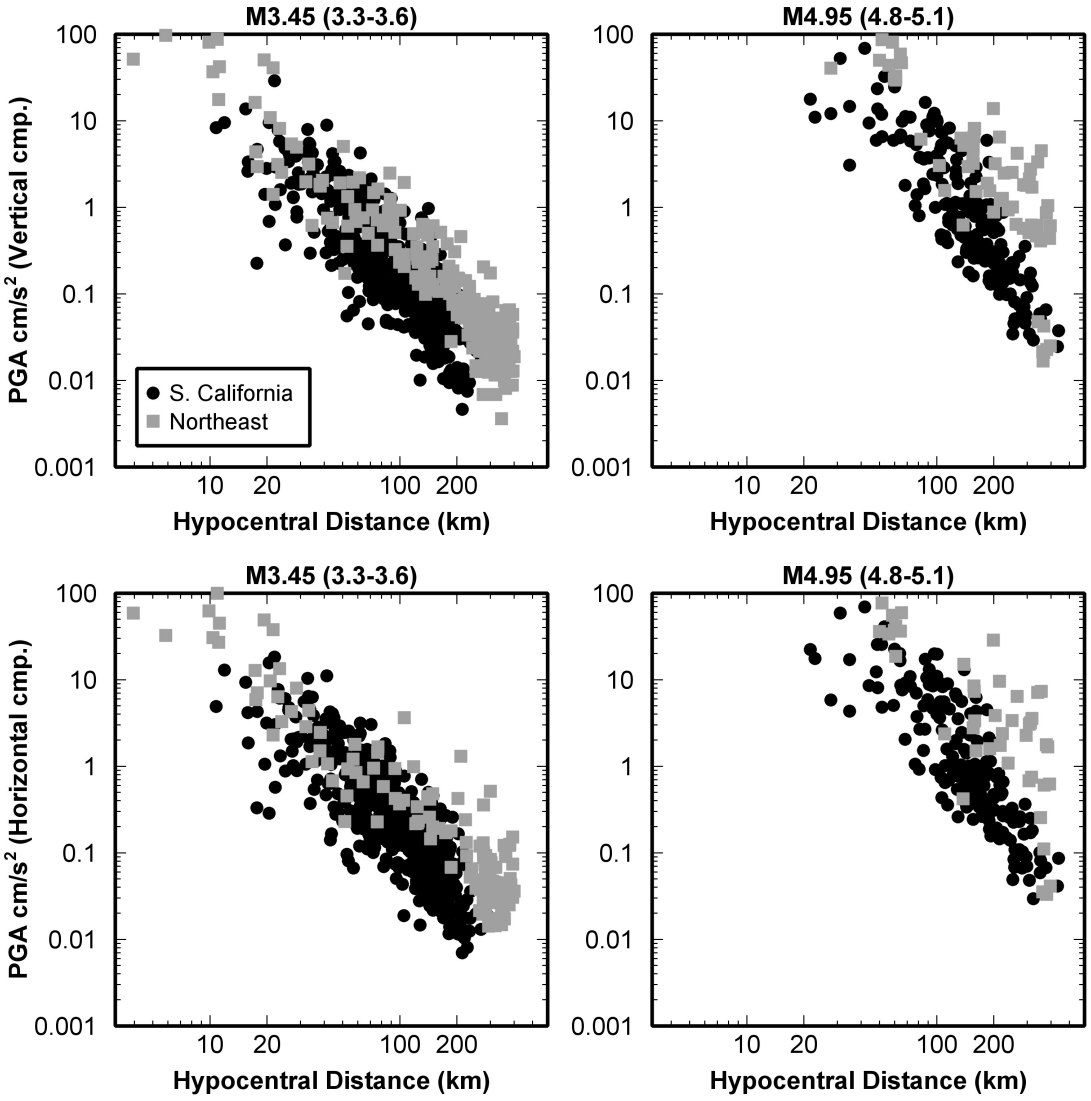

Figure B2 Plot of PGA (cm/s^2) versus hypocentral distance for the vertical component and geometric mean of horizontal components in two magnitude bins, **M**= 3.45 and 4.95 for S. California and Northeast (all for B/C site condition).

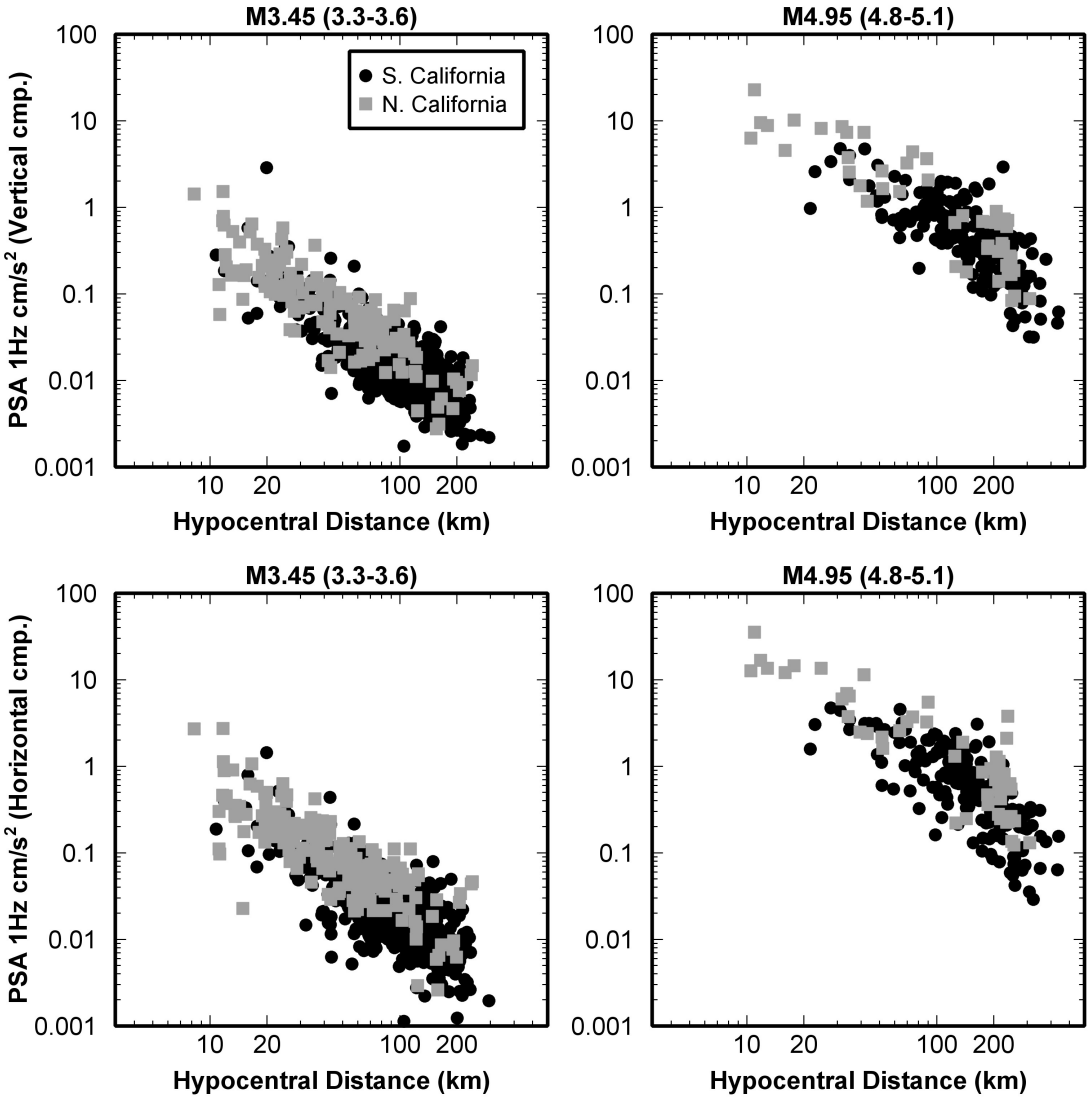

Figure B3 Plot of PSA-1Hz (cm/s^2) versus hypocentral distance for the vertical component and geometric mean of horizontal components in two magnitude bins, **M=** 3.45 and 4.95 for S. California and N. California (all for B/C site condition).

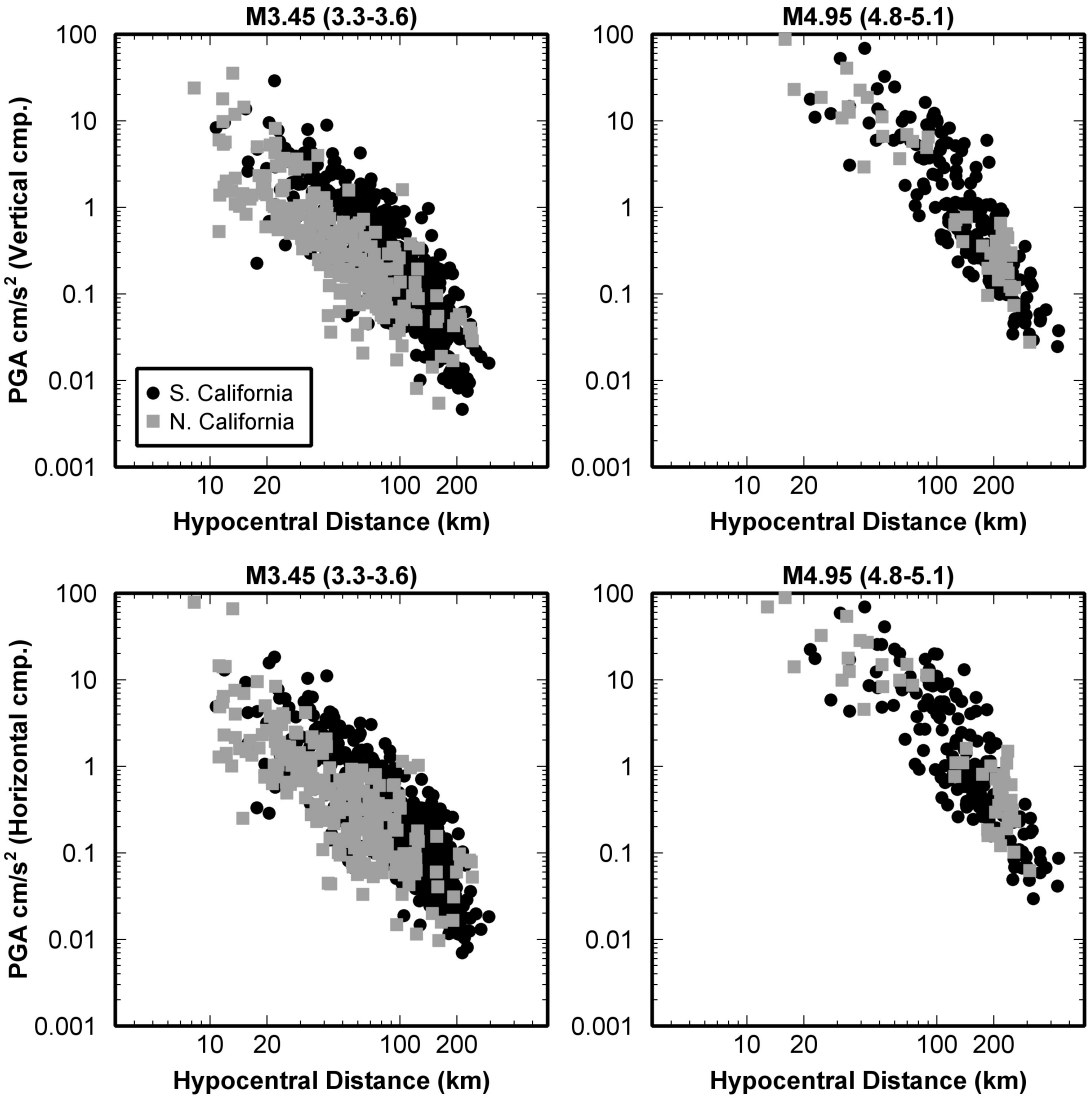

Figure B4 Plot of PGA (cm/s^2) versus hypocentral distance for the vertical component and geometric mean of horizontal components in two magnitude bins, **M**= 3.45 and 4.95 for S. California and N. California (all for B/C site condition).

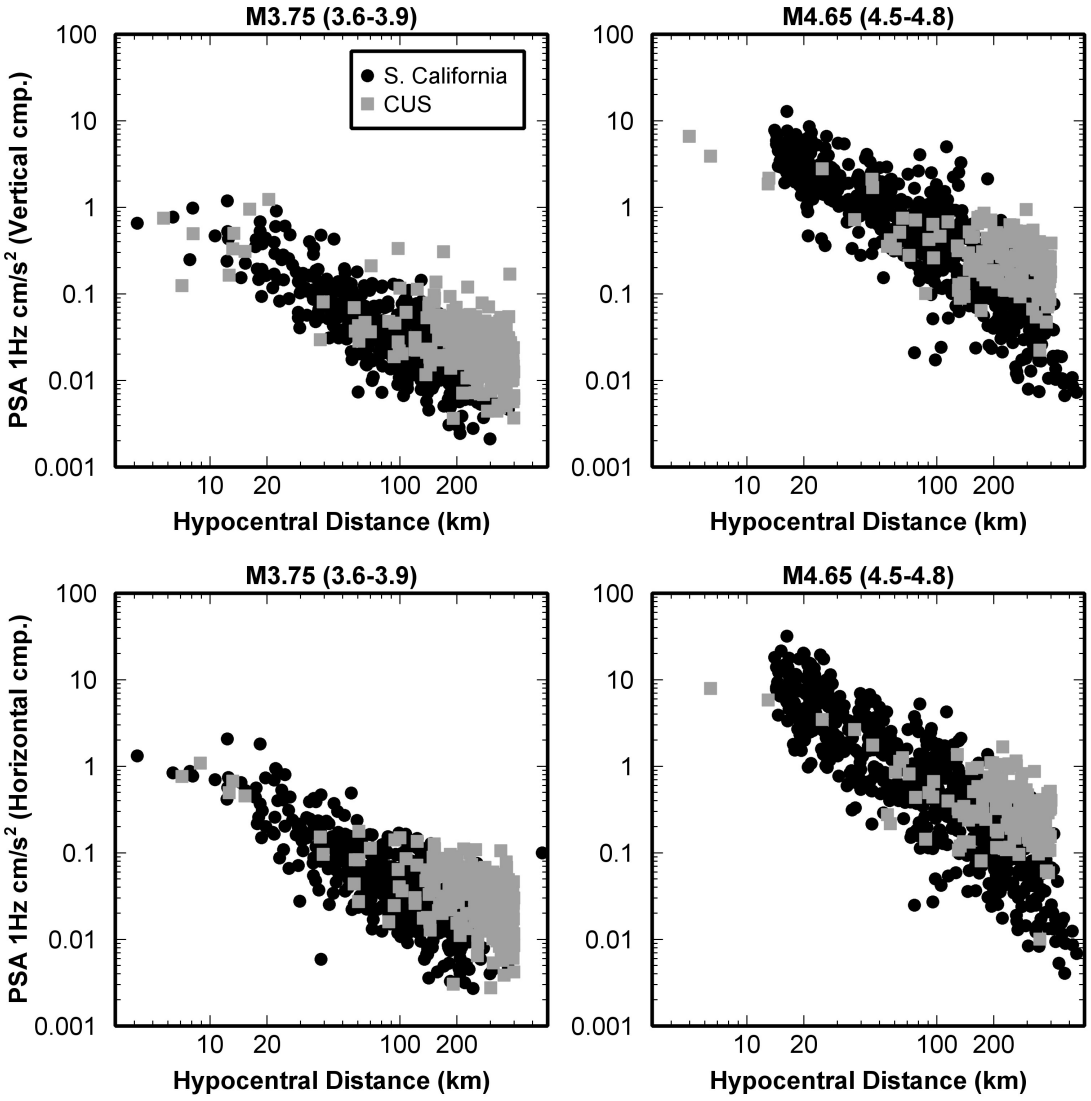

Figure B5 Plot of PSA-1Hz (cm/s^2) versus hypocentral distance for the vertical component and geometric mean of horizontal components in two magnitude bins, **M=** 3.75 and 4.65 for S. California and CUS (all for B/C site condition).

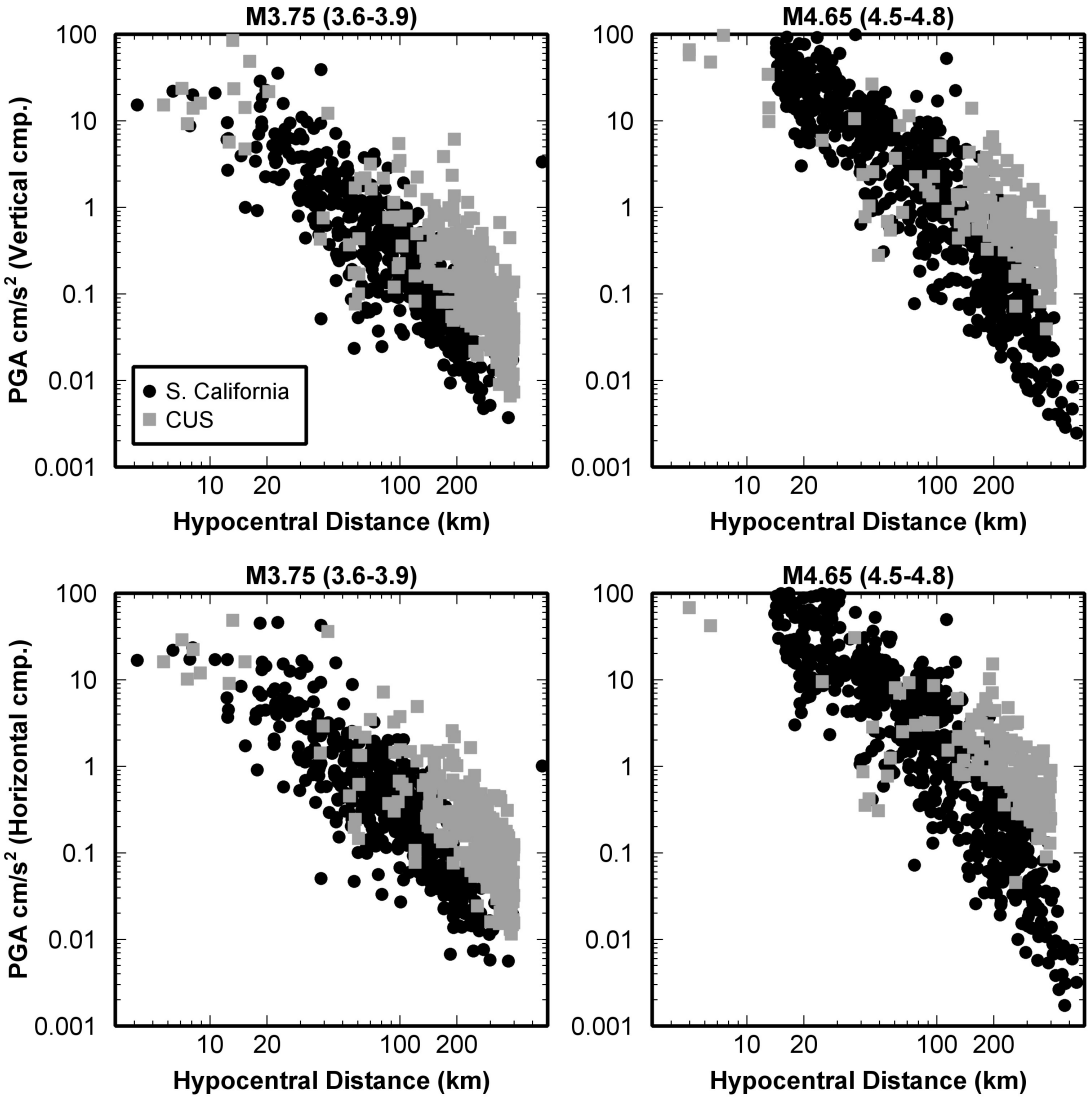

Figure B6 Plot of PGA (cm/s^2) versus hypocentral distance for the vertical component and geometric mean of horizontal components in two magnitude bins, **M**= 3.75 and 4.65 for S. California and CUS (all for B/C site condition).

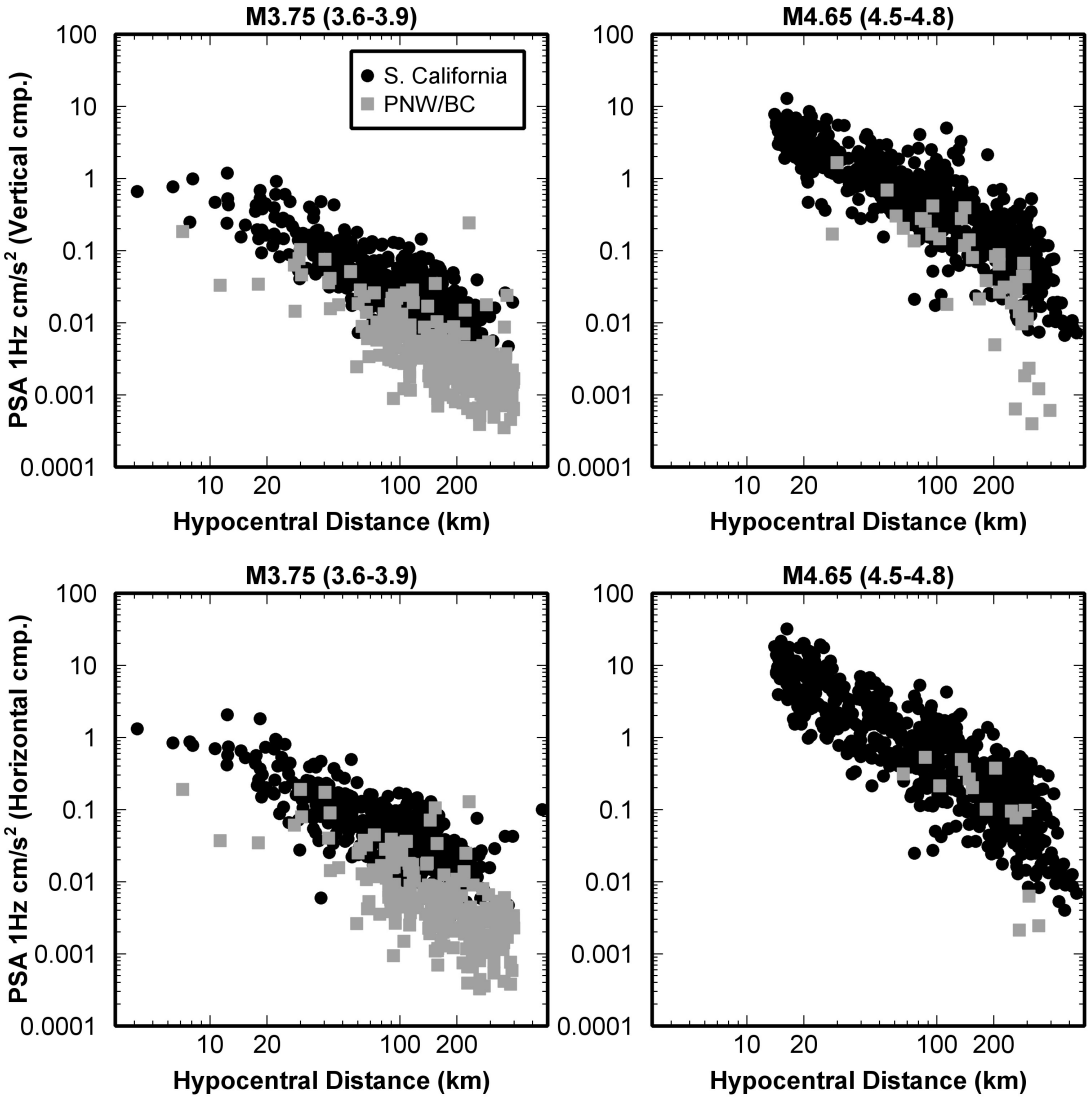

Figure B7 Plot of PSA-1Hz (cm/s^2) versus hypocentral distance for the vertical component and geometric mean of horizontal components in two magnitude bins, **M=** 3.75 and 4.65 for S. California and PNW/BC (all for B/C site condition).

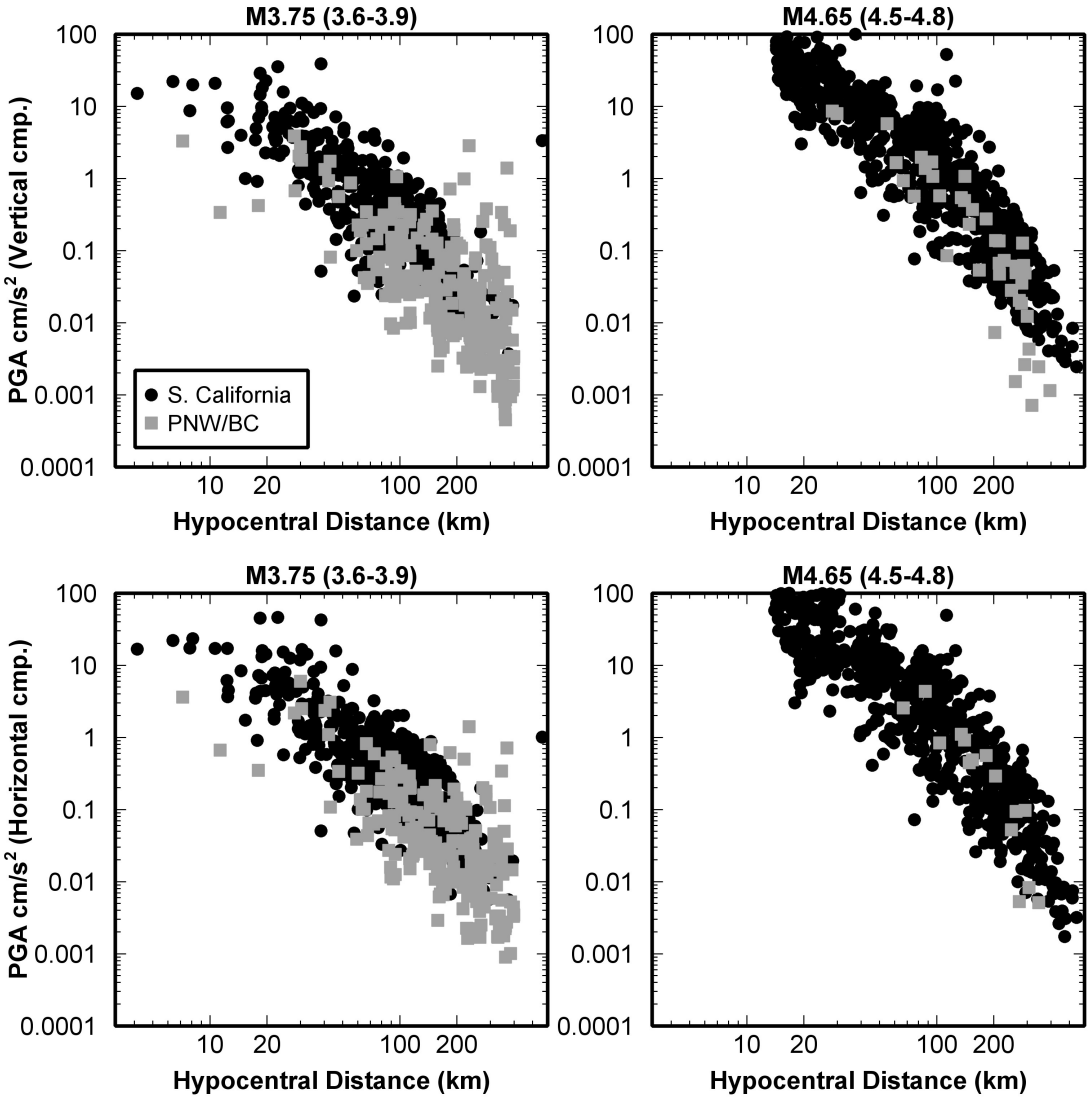

Figure B8 Plot of PGA (cm/s^2) versus hypocentral distance for the vertical component and geometric mean of horizontal components in two magnitude bins, **M**= 3.75 and 4.65 for S. California and PNW/BC (all for B/C site condition).

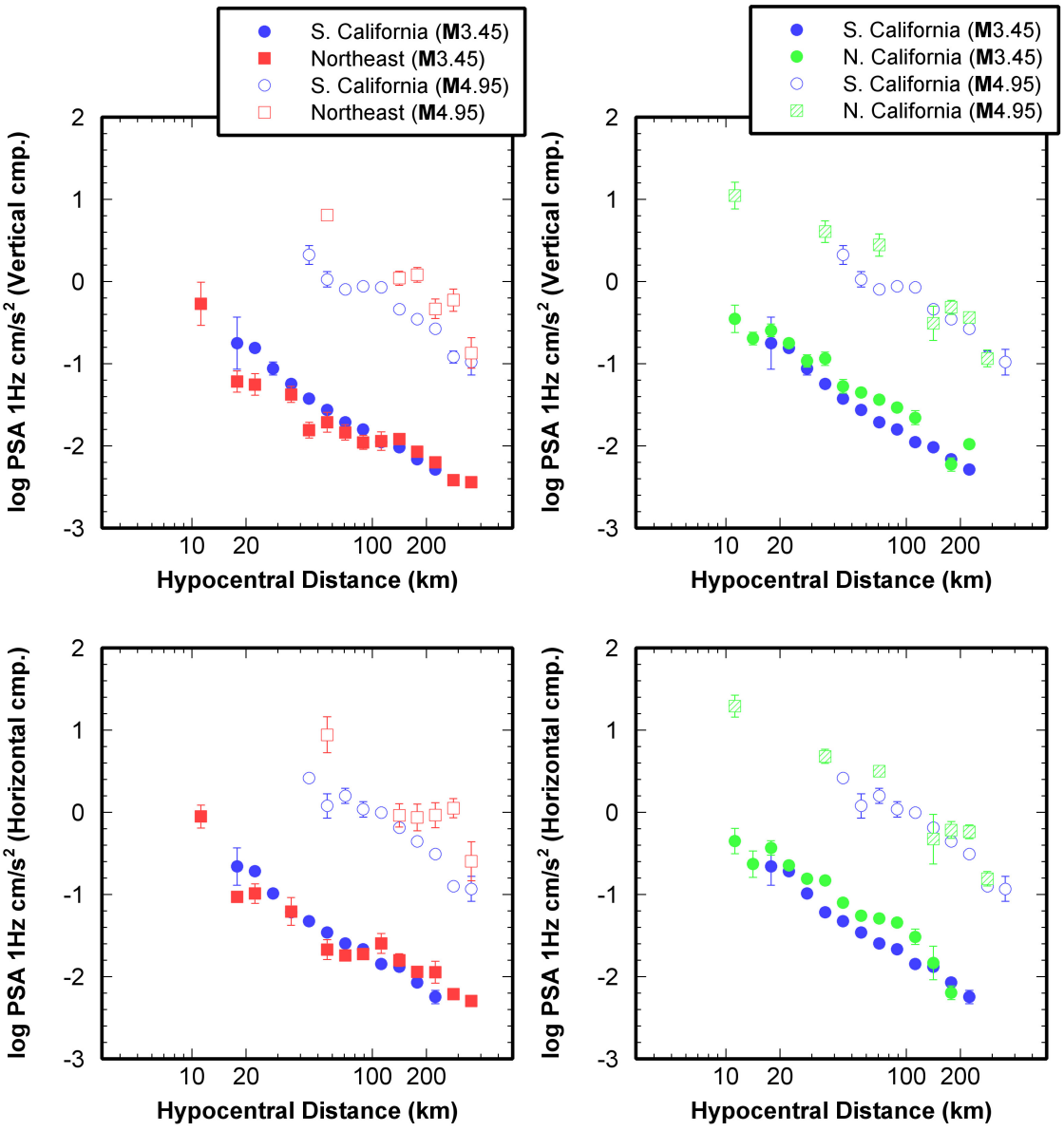

Figure B9 Plot of log-averaged PSA-1Hz (cm/s^2) versus hypocentral distance for the vertical component and geometric mean of the horizontal components in two magnitude bins, **M**= 3.45 and 4.95, for Northeast and N. California, in comparison to S. California. All amplitudes corrected to site class B/C. Error bars show the standard error of the average of ground motions in each magnitude-distance bin. Points are plotted only if at least 3 events, each of which has at least 3 records, are included in a bin.

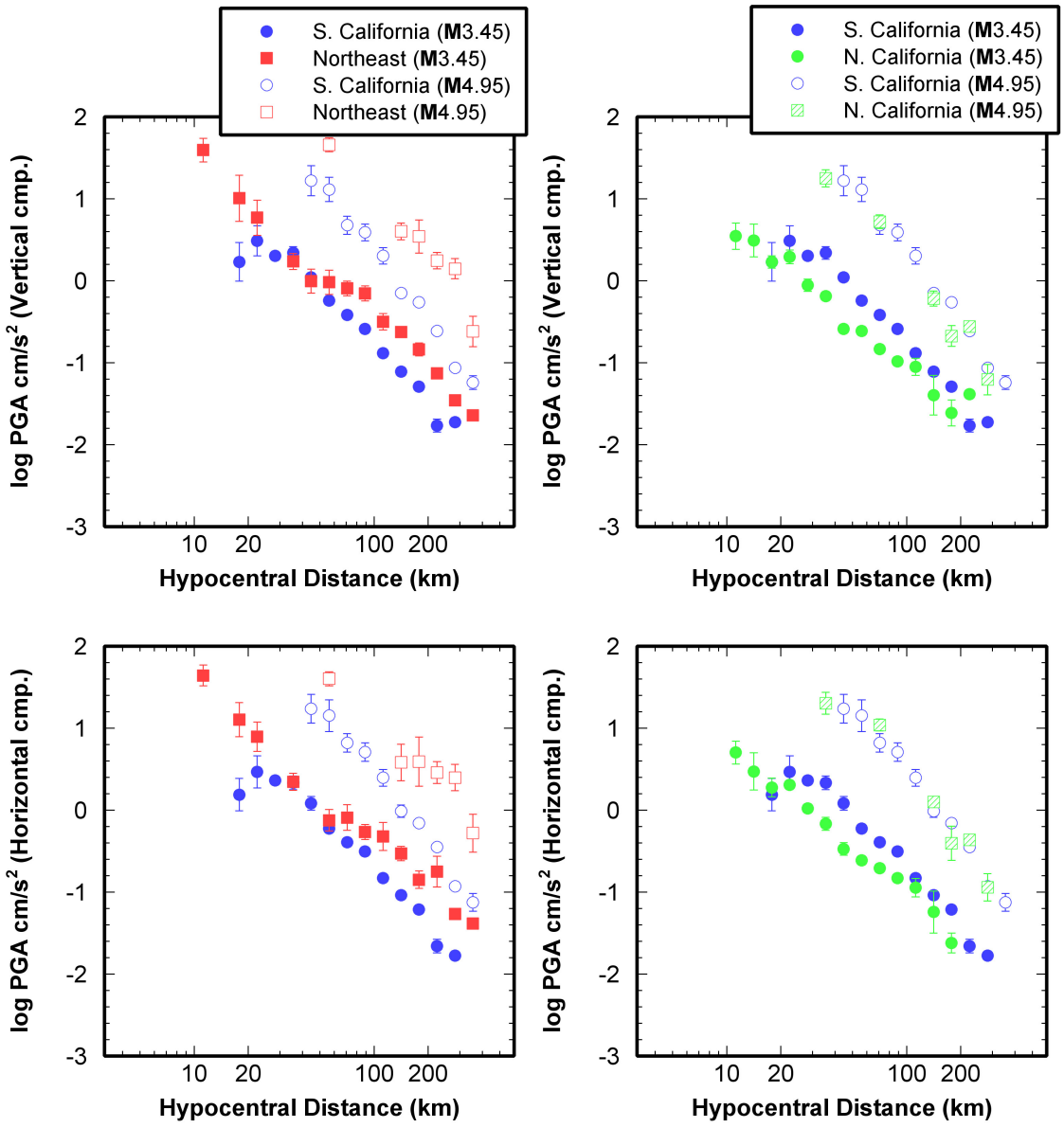

Figure B10 Plot of log-averaged PGA (cm/s^2) versus hypocentral distance for the vertical component and geometric mean of the horizontal components in two magnitude bins, **M=** 3.45 and 4.95 for Northeast and N. California, in comparison to S. California. All amplitudes corrected to site class B/C. Error bars show the standard error of the average of ground motions in each magnitude-distance bin. Points are plotted only if at least 3 events, each of which has at least 3 records, are included in a bin.

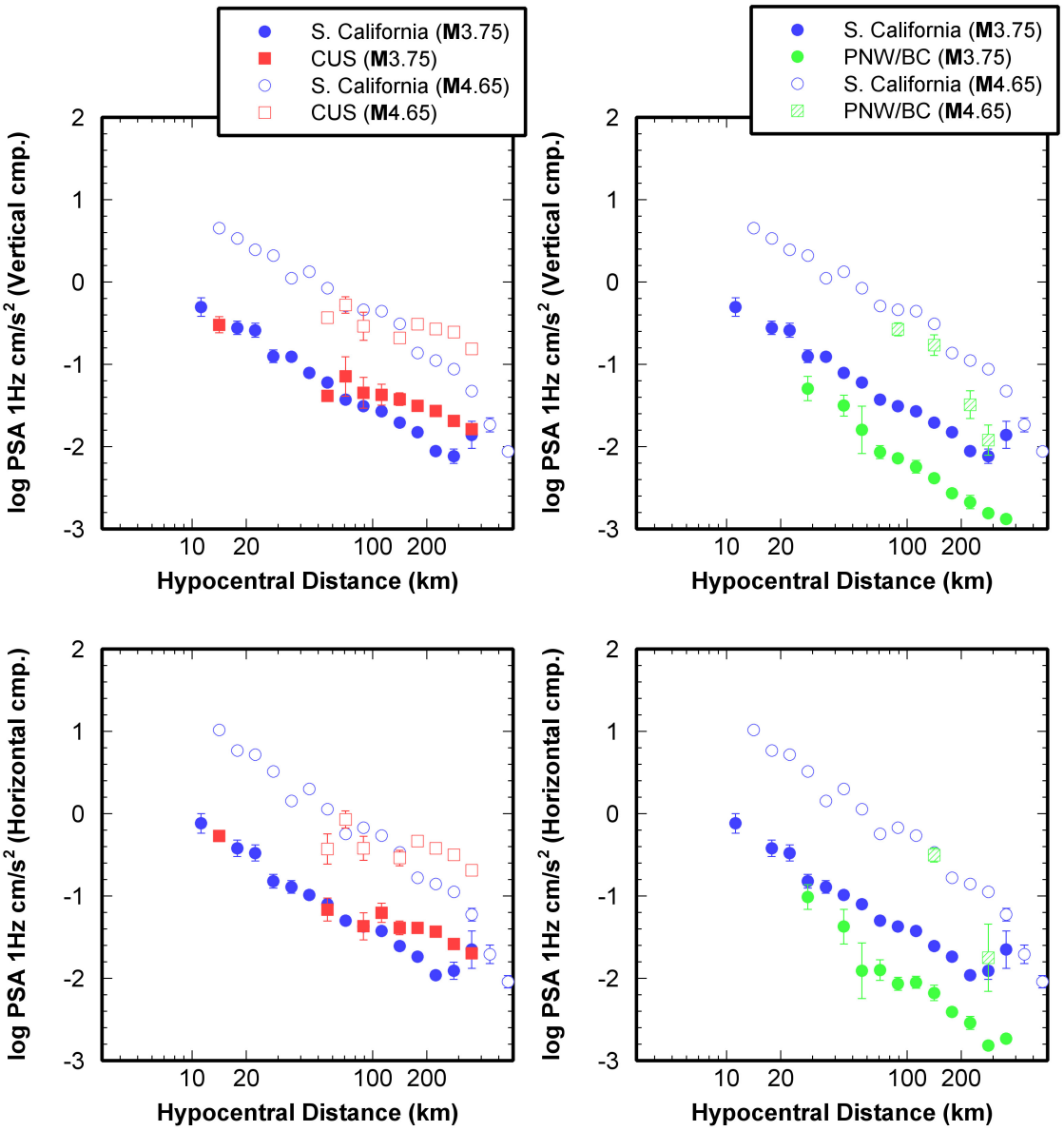

Figure B11 Plot of log-averaged PSA-1Hz (cm/s^2) versus hypocentral distance for the vertical component and geometric mean of the horizontal components in two magnitude bins, **M**= 3.75 and 4.65, for CUS and PNW/BC, in comparison to S. California. All amplitudes corrected to site class B/C. Error bars show the standard error of the average of ground motions in each magnitude-distance bin. Points are plotted only if at least 3 events, each of which has at least 3 records, are included in a bin.

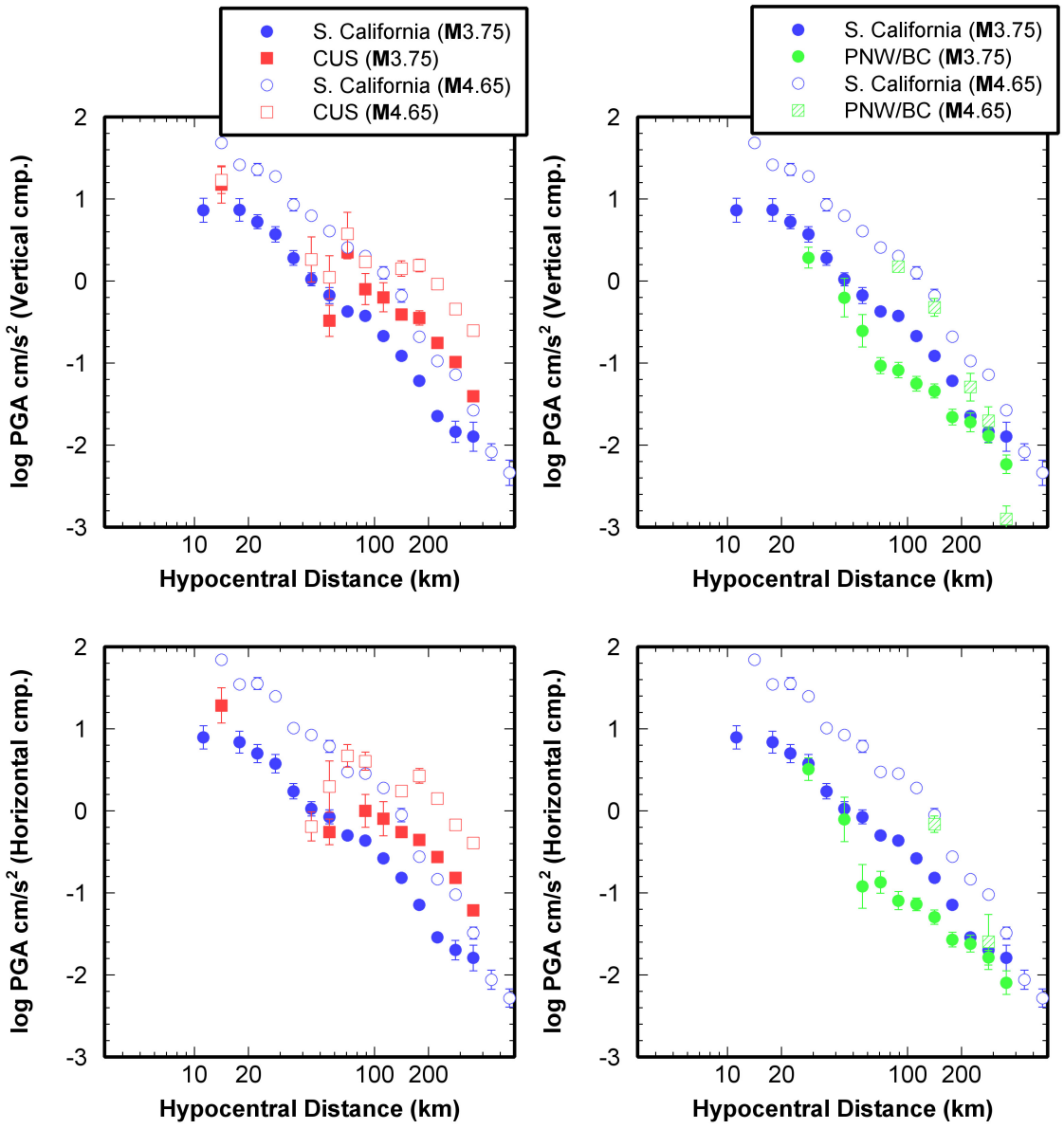

Figure B12 Plot of log-averaged PGA (cm/s^2) versus hypocentral distance for the vertical component and geometric mean of the horizontal components in two magnitude bins **M=** 3.75 and 4.65 for CUS and PNW/BC, in comparison to S. California. All amplitudes corrected to site class B/C. Error bars show the standard error of the average of ground motions in each magnitude-distance bin. Points are plotted only if at least 3 events, each of which has at least 3 records, are included in a bin.

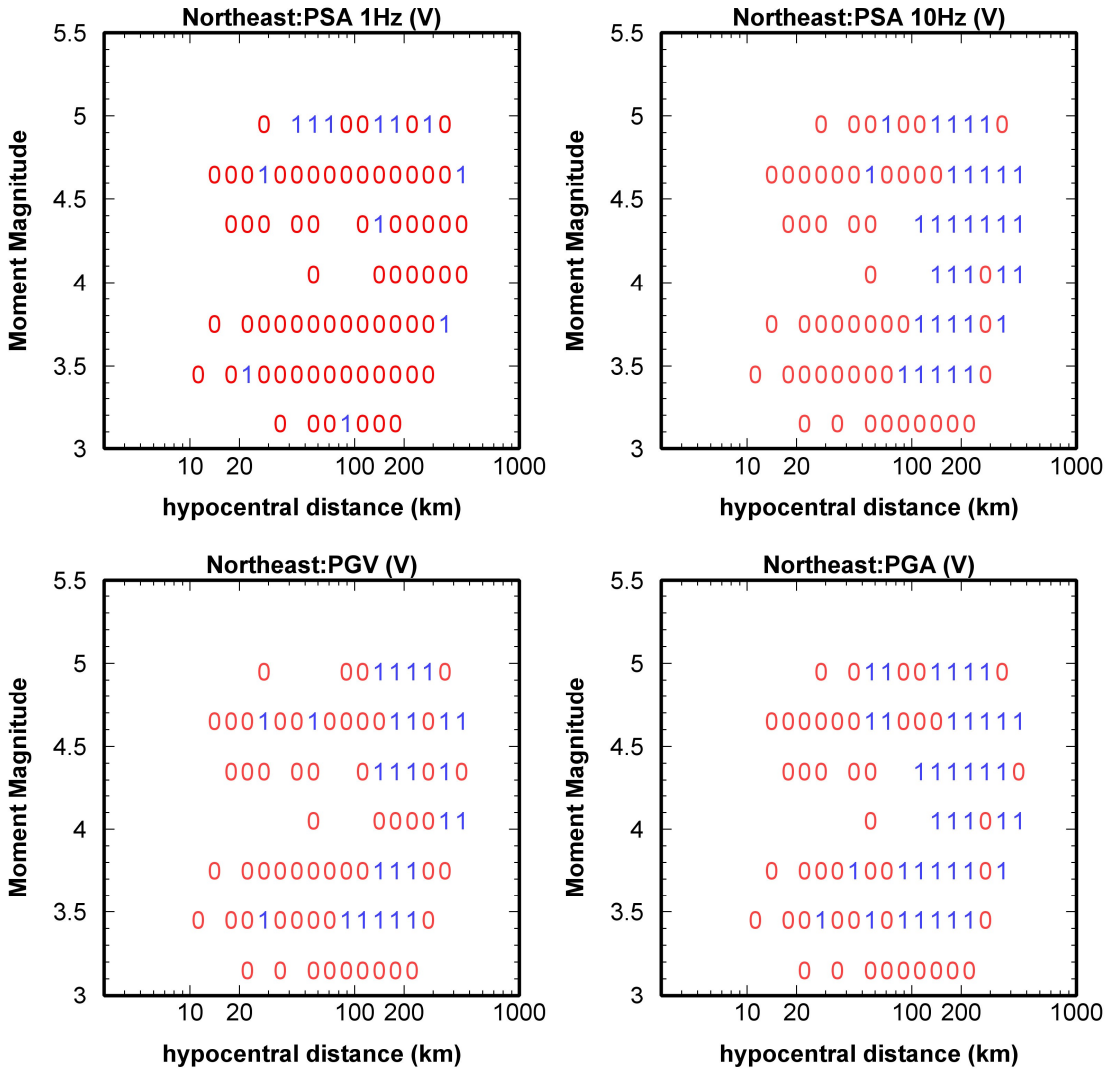

Figure B13 Results of statistical t-test for the binned vertical ground motions in Northeast and S. California. h = 1 is for the case where the difference in ground motions are statistically significant (at probability level = 0.05), h=0 means differences are not statistically significant.

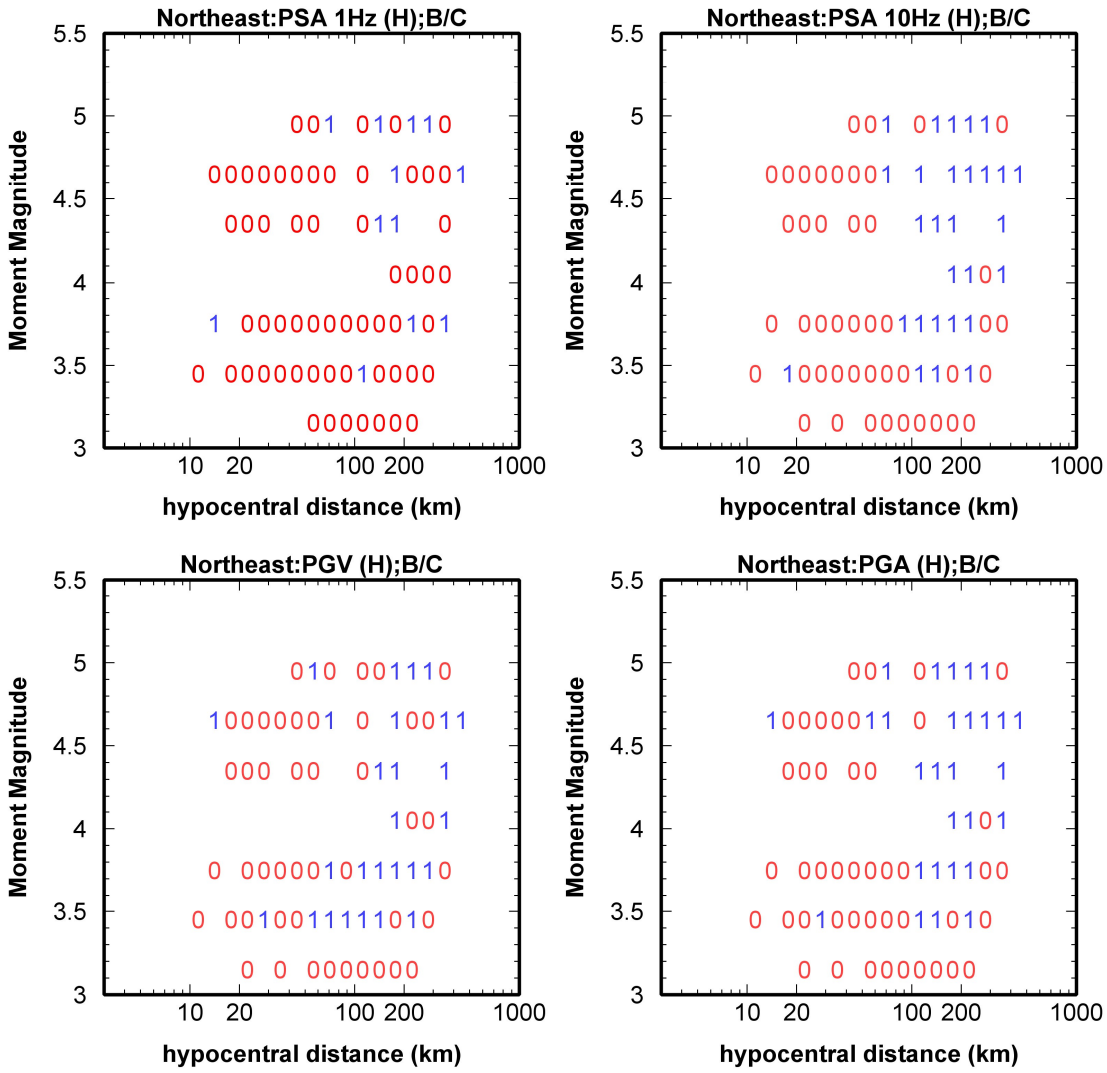

Figure B14 Results of statistical t-test for the binned horizontal ground motions (all records corrected to site class B/C) in Northeast and S. California. h = 1 is for the case where the difference in ground motions are statistically significant (at probability level = 0.05), h=0 means differences are not statistically significant.

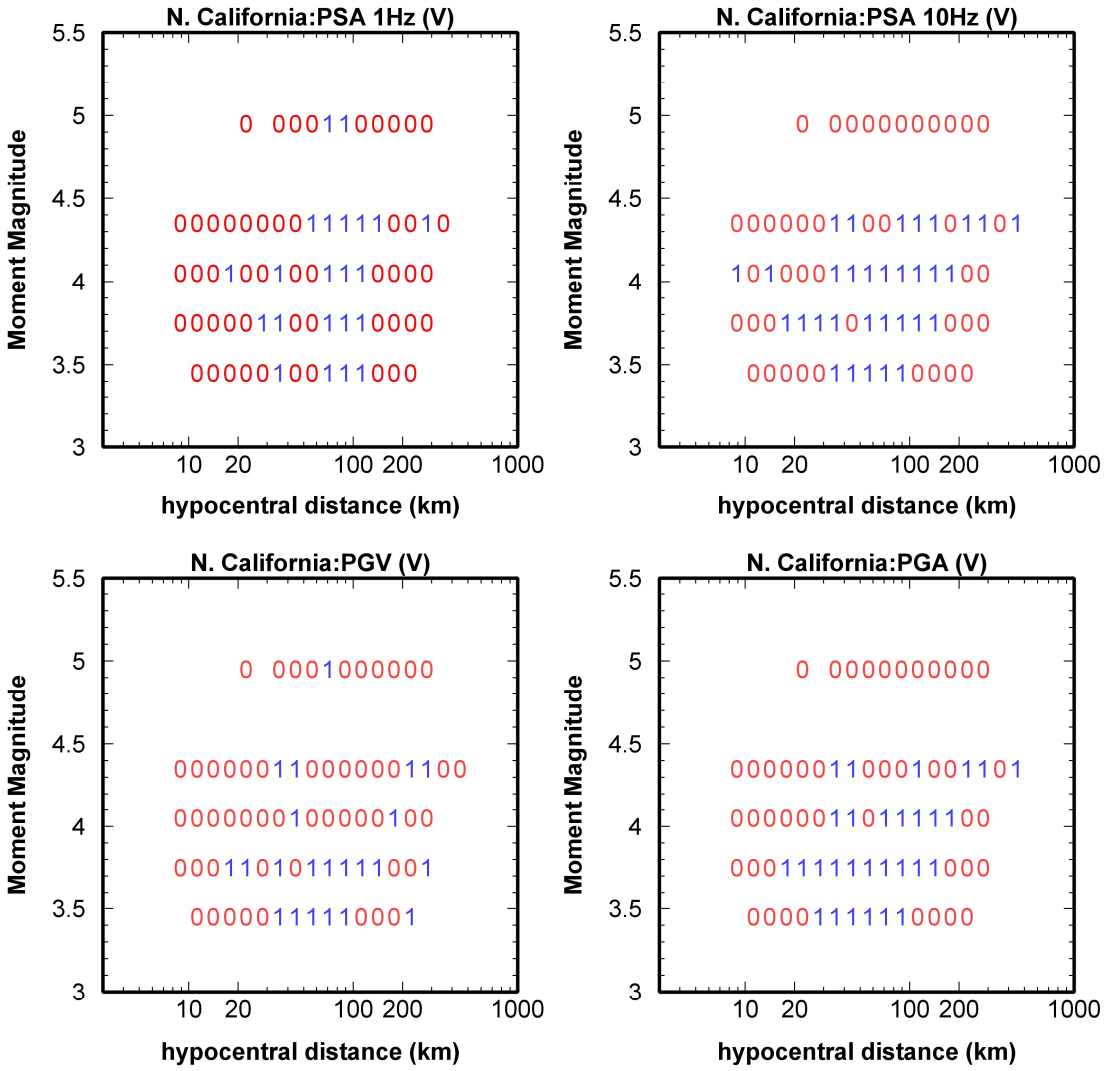

Figure B15 Results of statistical t-test for the binned vertical ground motions in N. California and S. California. h = 1 is for the case where the difference in ground motions are statistically significant (at probability level = 0.05), h=0 means differences are not statistically significant.

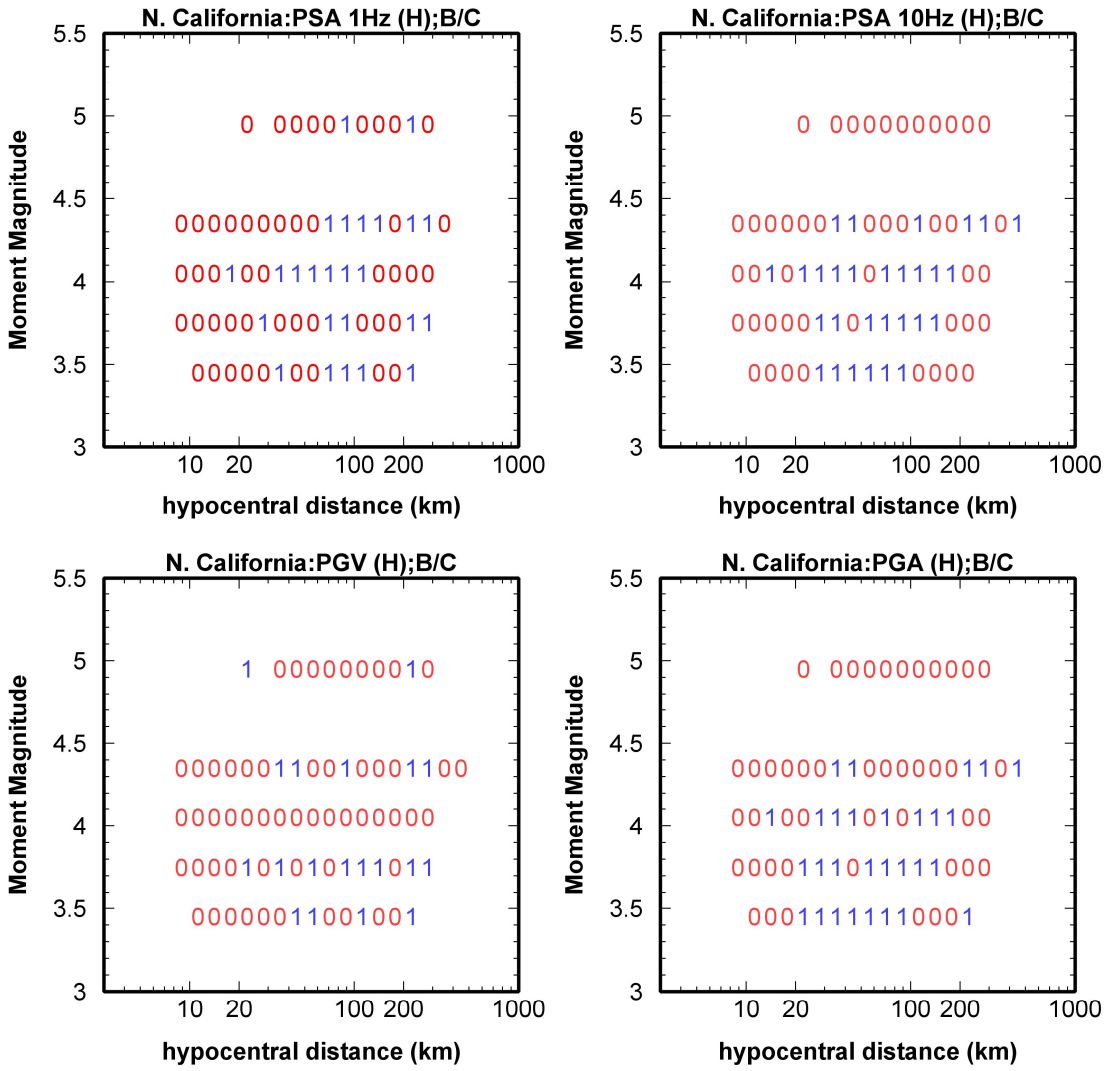

Figure B16 Results of statistical t-test for the binned horizontal ground motions (all records corrected to site class B/C) in N. California and S. California. h = 1 is for the case where the difference in ground motions are statistically significant (at probability level = 0.05), h=0 means differences are not statistically significant.

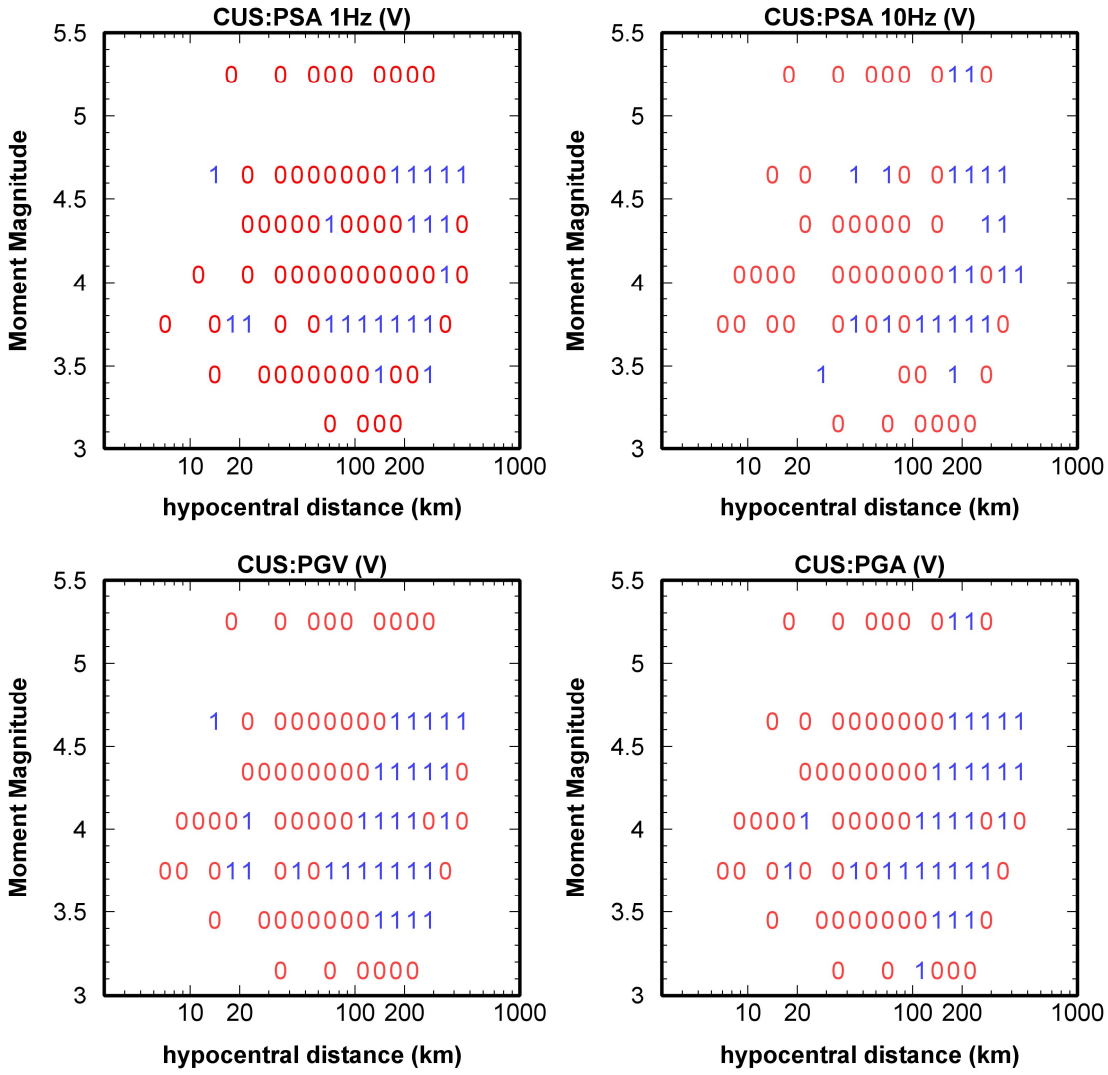

Figure B17 Results of statistical t-test for the binned vertical ground motions in CUS and S. California. h = 1 is for the case where the difference in ground motions are statistically significant (at probability level = 0.05), h=0 means differences are not statistically significant.

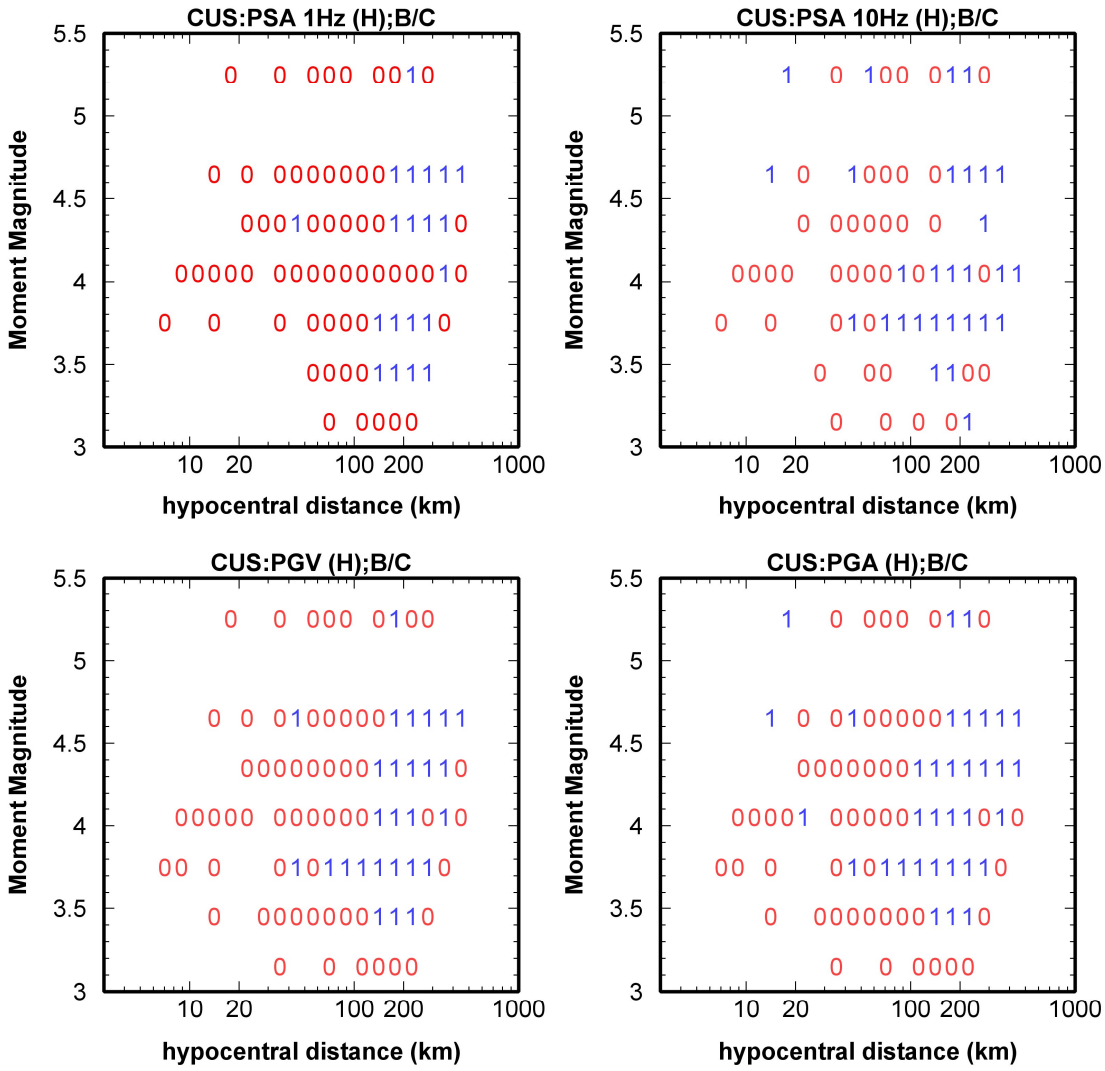

Figure B18 Results of statistical t-test for the binned horizontal ground motions (all records corrected to site class B/C) in CUS and S. California. h = 1 is for the case where the difference in ground motions are statistically significant (at probability level = 0.05), h=0 means differences are not statistically significant.

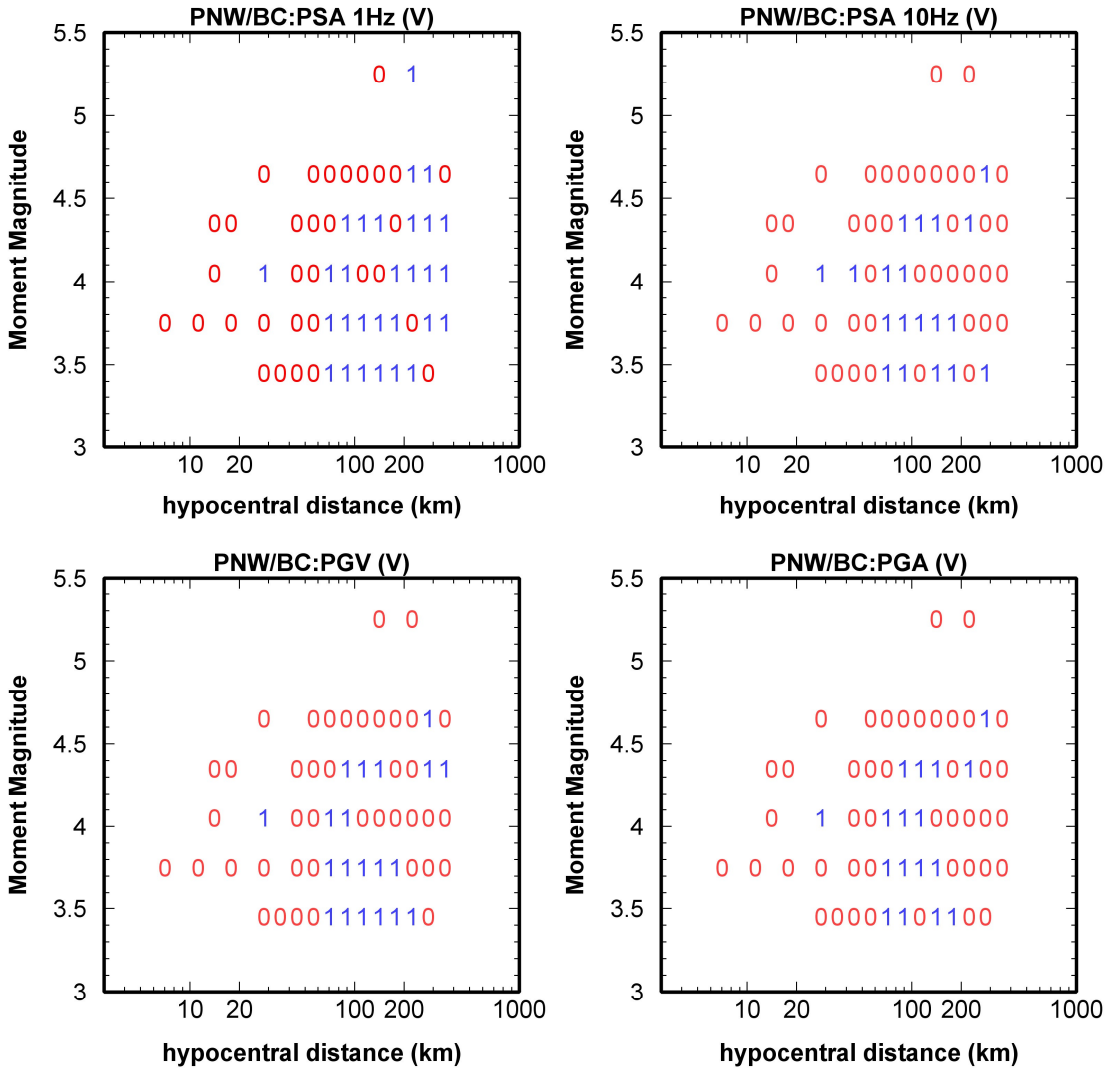

Figure B19 Results of statistical t-test for the binned vertical ground motions in PNW/BC and S. California. h = 1 is for the case where the difference in ground motions are statistically significant (at probability level = 0.05), h=0 means differences are not statistically significant.

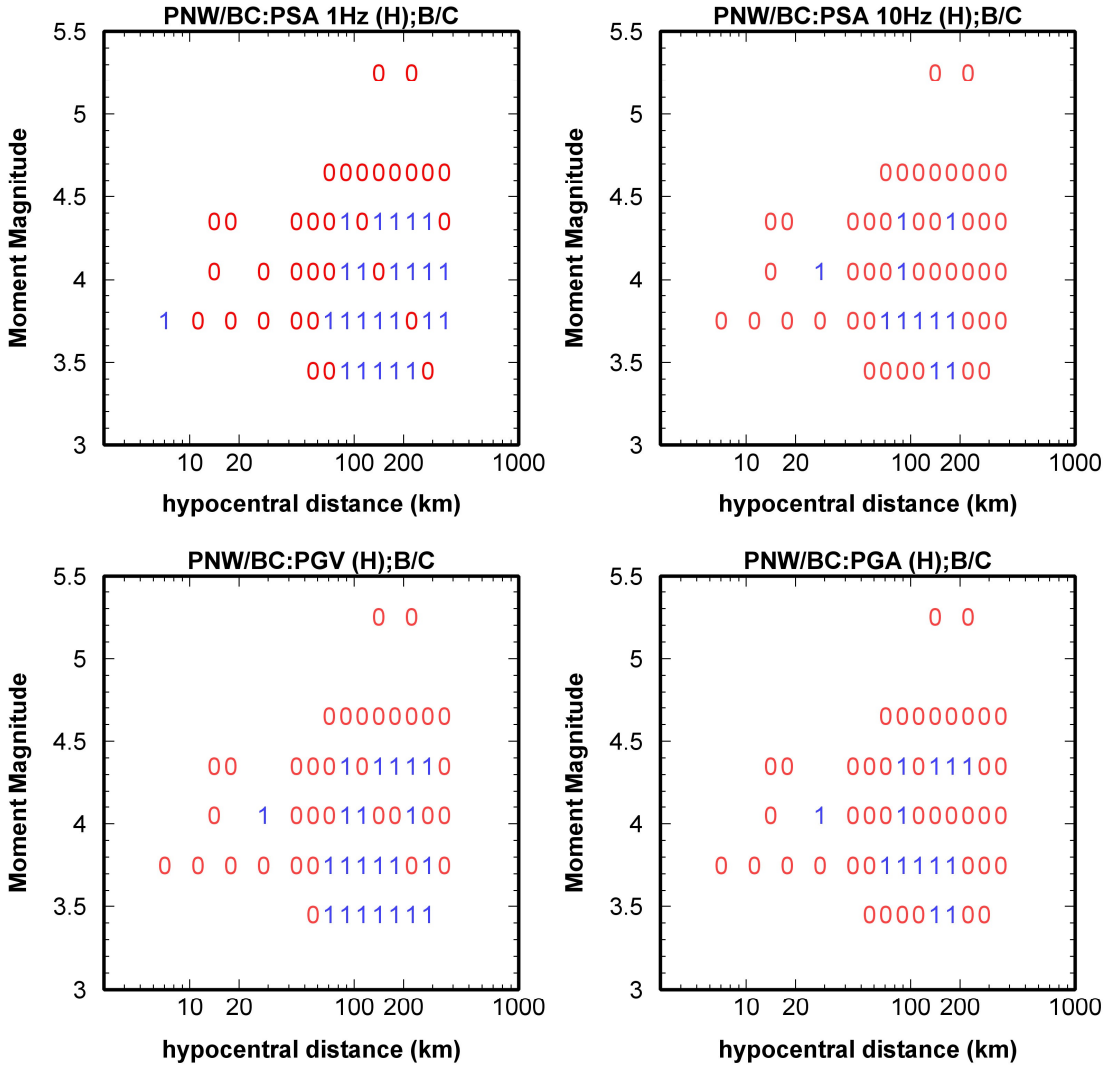

Figure B20 Results of statistical t-test for the binned horizontal ground motions (all records corrected to site class B/C) in PNW/BC and S. California. h = 1 is for the case where the difference in ground motions are statistically significant (at probability level = 0.05), h=0 means differences are not statistically significant.

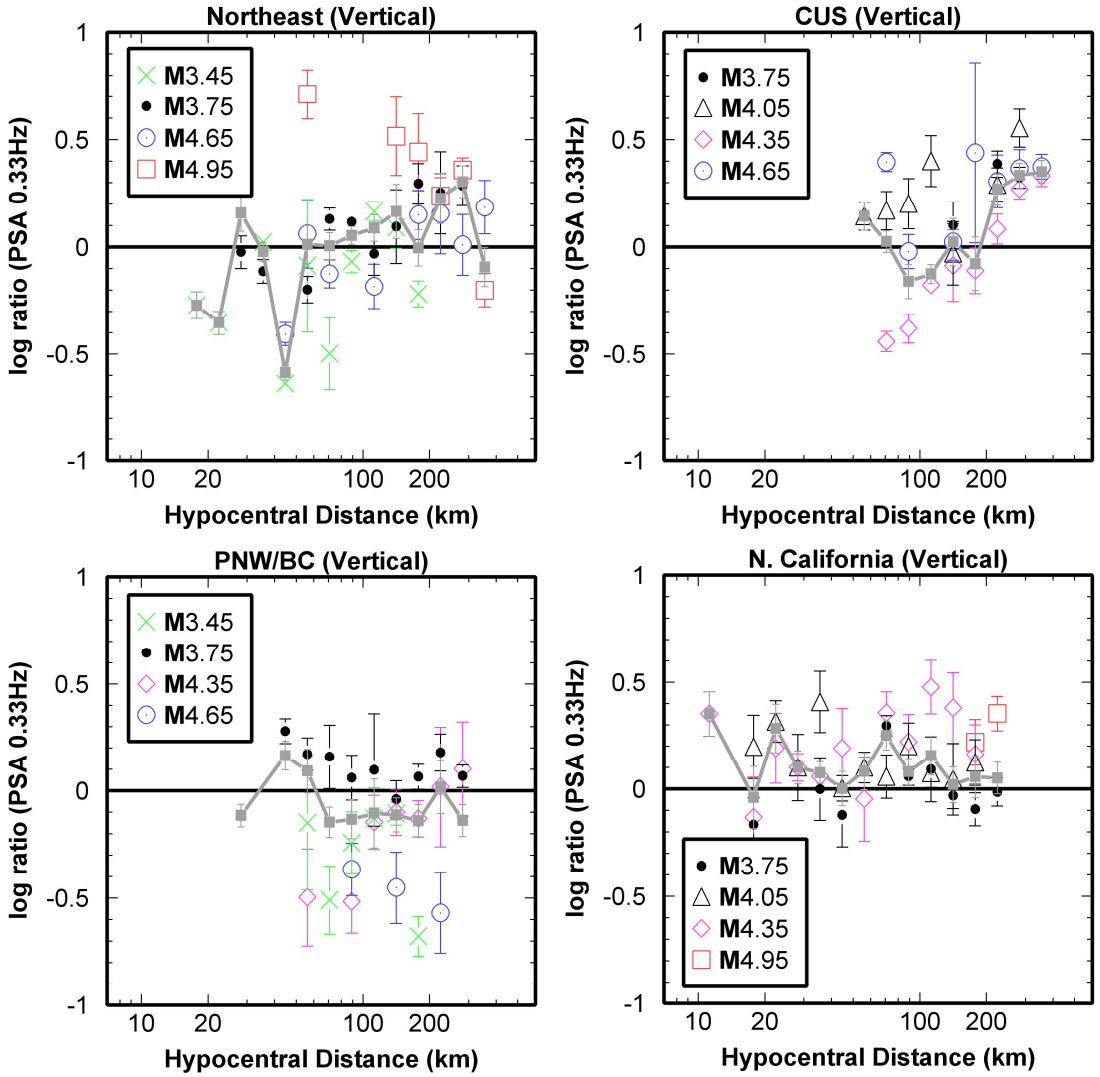

Figure B21 Ratios of log-averaged ground motions in each region with respect to those in S. California for PSA 0.33-Hz (vertical component). The error bars are the standard error from Equation 4.4. The solid line shows the weighted average of the ratios in each distance bins (for all magnitudes) with error bars showing weighted standard errors.

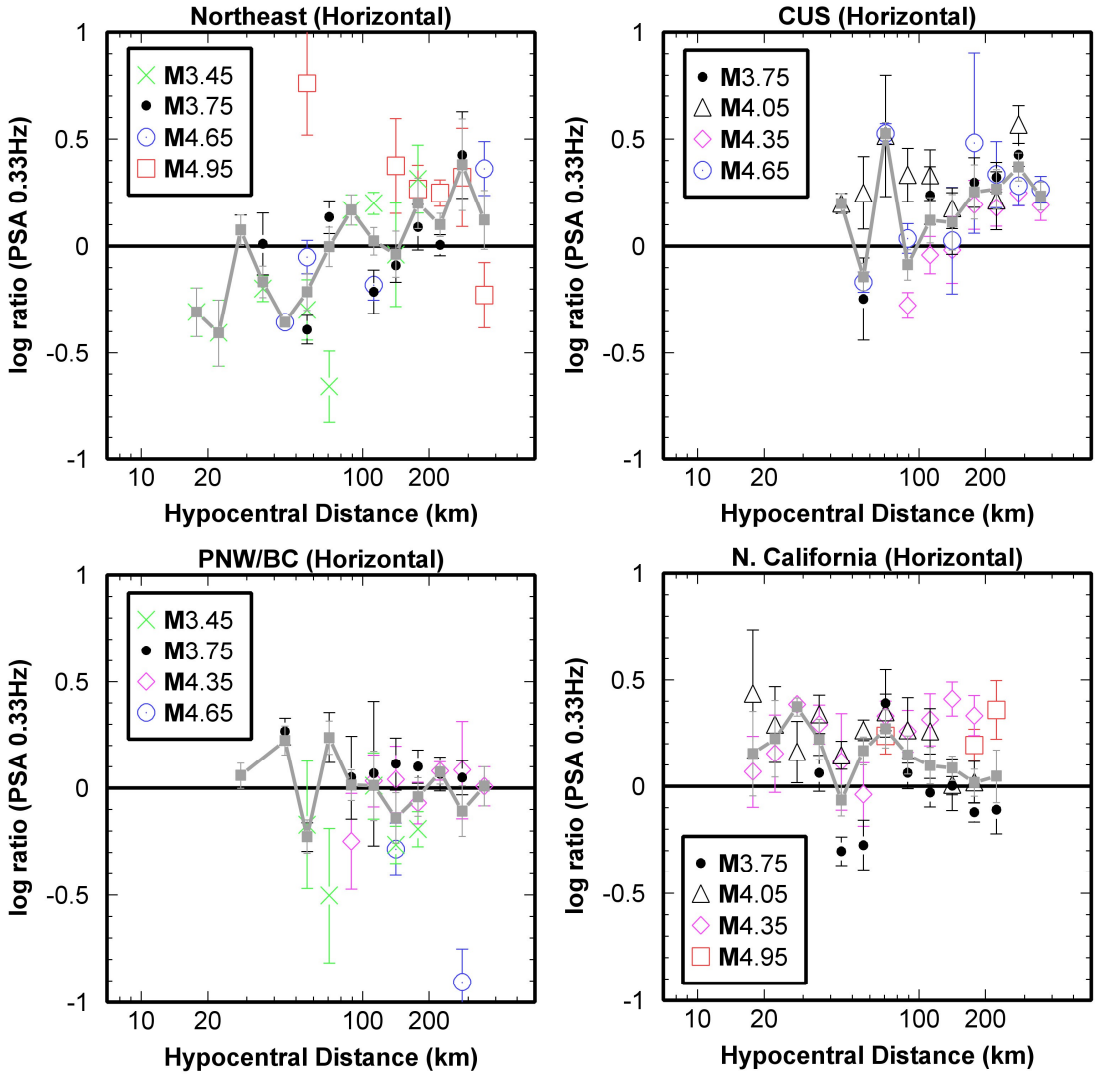

Figure B22 Ratios of log-averaged ground motions in each region (B/C site condition) with respect to those in S. California for PSA 0.33-Hz (geometric mean of horizontal components). The error bars are the standard error from Equation 4.4. The solid line shows the weighted average of the ratios in each distance bins (for all magnitudes) with error bars showing weighted standard errors.

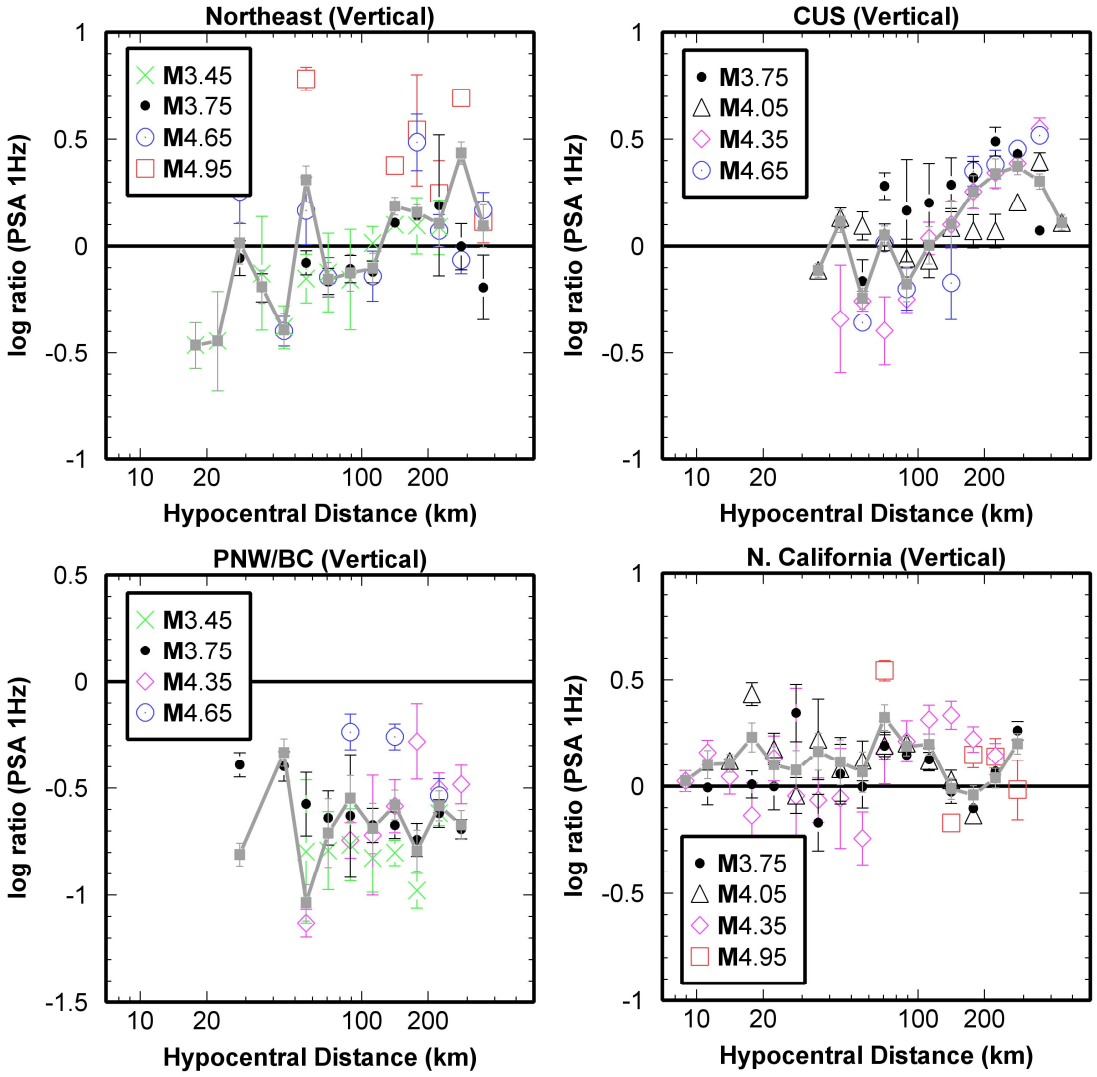

Figure B23 Ratios of log-averaged ground motions in each region with respect to those in S. California for PSA 1-Hz (vertical component). The error bars are the standard error from Equation 4.4. The solid line shows the weighted average of the ratios in each distance bins (for all magnitudes) with error bars showing weighted standard errors.

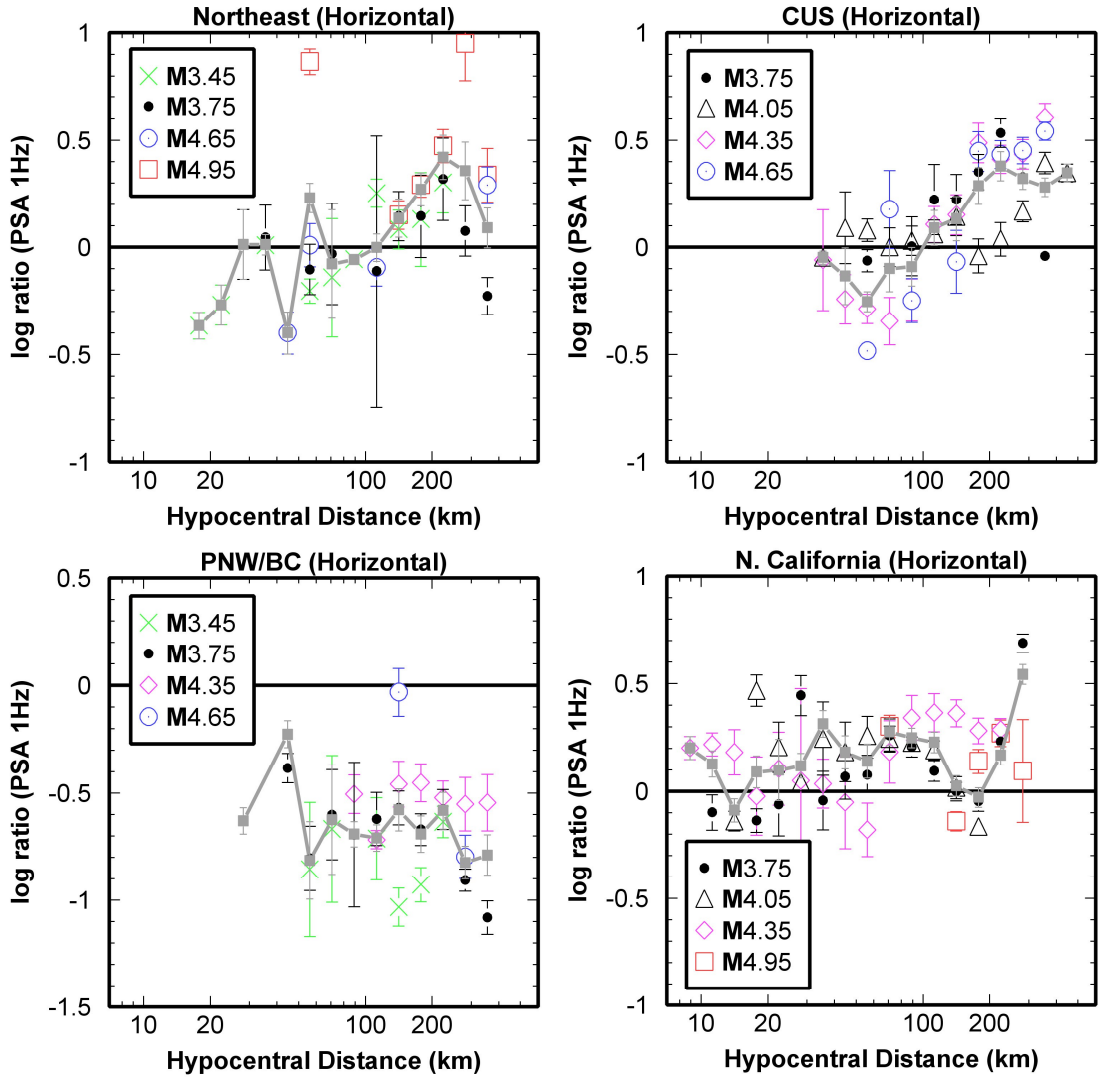

Figure B24 Ratios of log-averaged ground motions in each region (B/C site condition) with respect to those in S. California for PSA 1-Hz (geometric mean of horizontal components). The error bars are the standard error from Equation 4.4. The solid line shows the weighted average of the ratios in each distance bins (for all magnitudes) with error bars showing weighted standard errors.

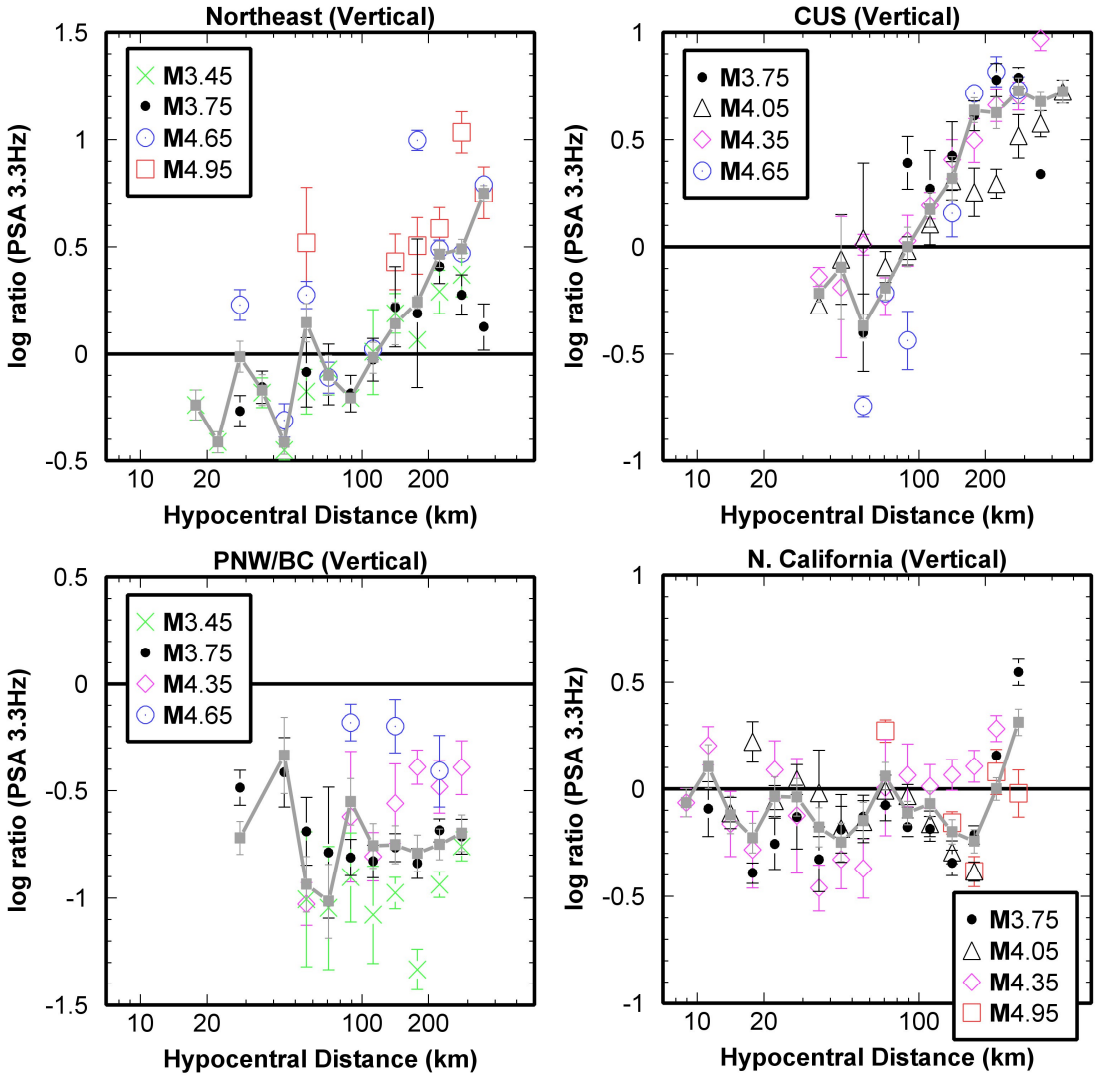

Figure B25 Ratios of log-averaged ground motions in each region with respect to those in S. California for PSA 3.3-Hz (vertical component). The error bars are the standard error from Equation 4.4. The solid line shows the weighted average of the ratios in each distance bins (for all magnitudes) with error bars showing weighted standard errors.

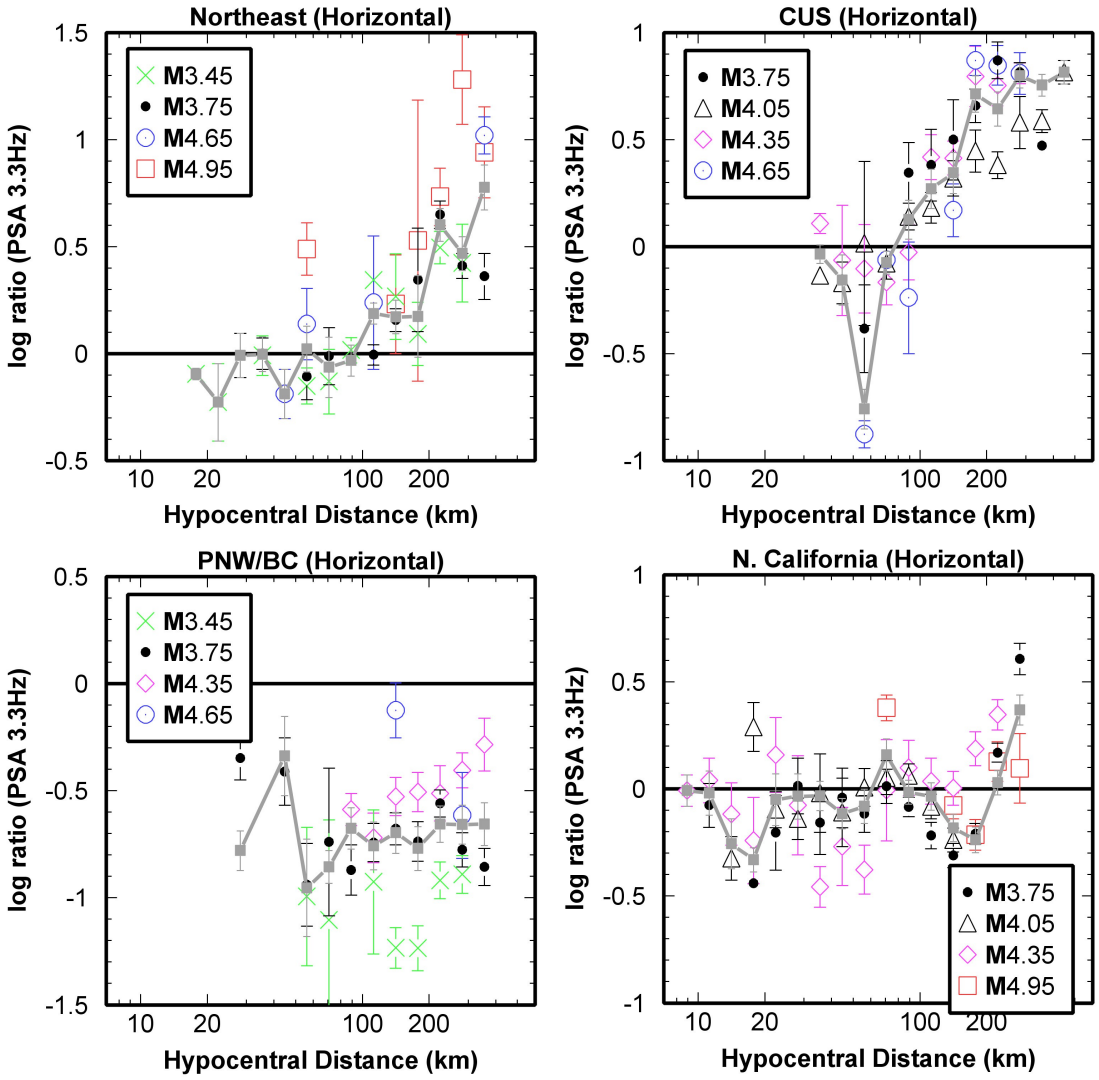

Figure B26 Ratios of log-averaged ground motions in each region (B/C site condition) with respect to those in S. California for PSA 3.3-Hz (geometric mean of horizontal components). The error bars are the standard error from Equation 4.4. The solid line shows the weighted average of the ratios in each distance bins (for all magnitudes) with error bars showing weighted standard errors.

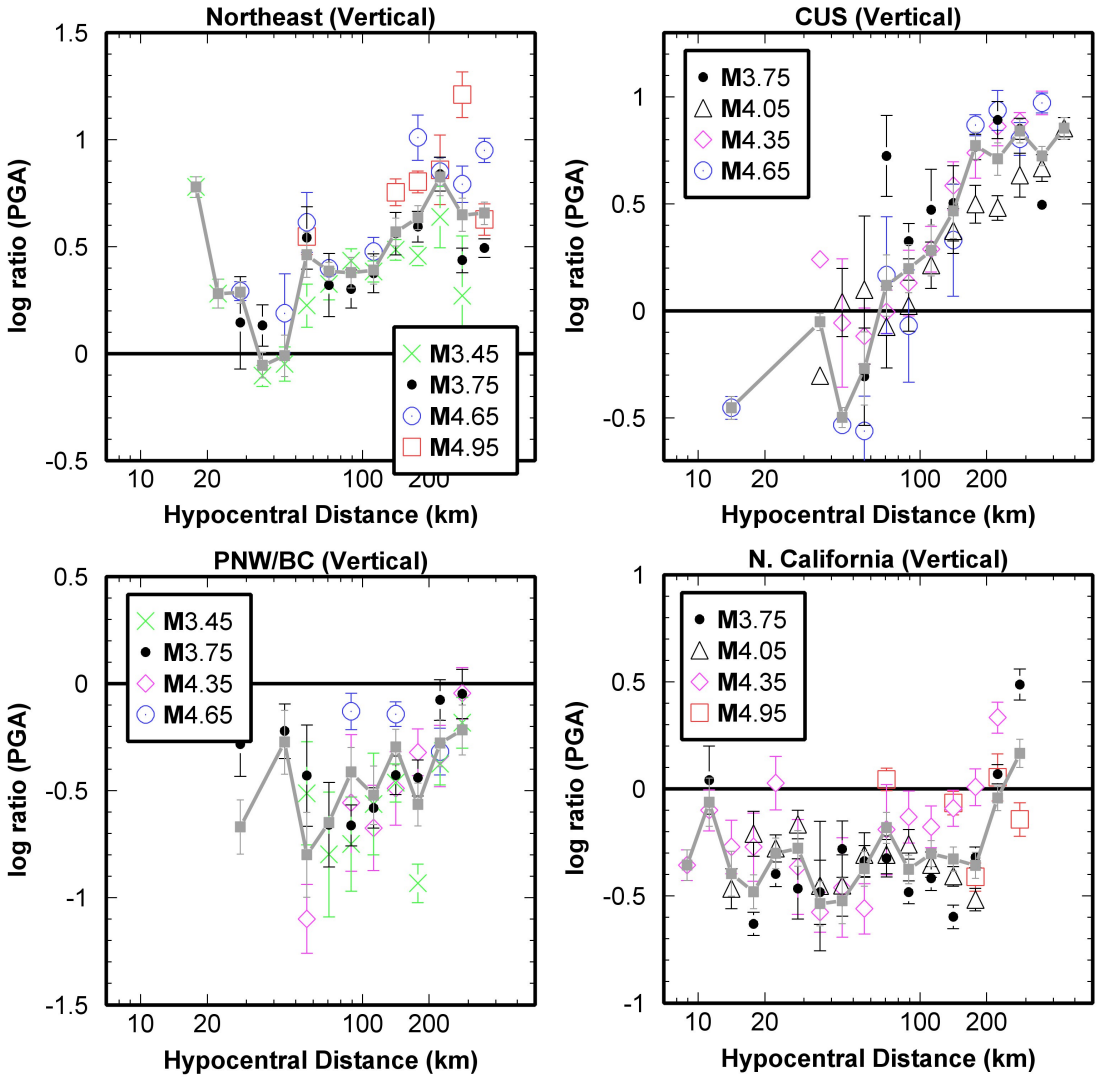

Figure B27 Ratios of log-averaged ground motions in each region with respect to those in S. California for PGA (vertical component). The error bars are the standard error from Equation 4.4. The solid line shows the weighted average of the ratios in each distance bins (for all magnitudes) with error bars showing weighted standard errors.

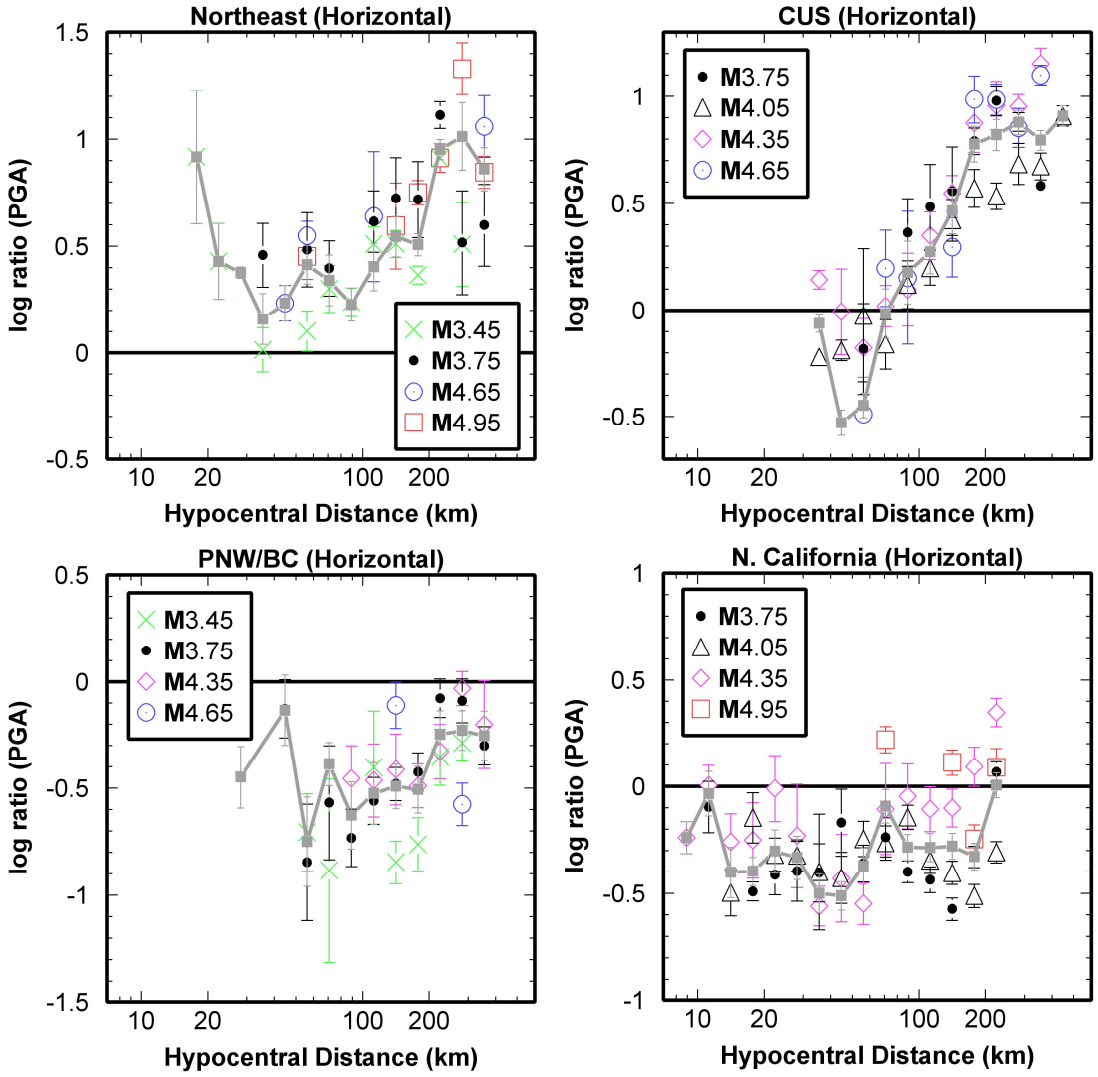

Figure B28 Ratios of log-averaged ground motions in each region (B/C site condition) with respect to those in S. California for PGA (geometric mean of horizontal components). The error bars are the standard error from Equation 4.4. The solid line shows the weighted average of the ratios in each distance bins (for all magnitudes) with error bars showing weighted standard errors.

Curriculum Vitae

Name:	Alireza Babaie Mahani
Post-secondary Education and Degrees:	Kerman University Kerman, Iran 2001-2005 B.Sc. University of Tehran Tehran, Iran 2005-2008 M.Sc. The University of Western Ontario London, Ontario, Canada 2008-2012 Ph.D.
Honors and Awards:	Western Graduate Research Scholarships (WGRS) 2008-2012 Canadian Geophysical Union Travel Award 2011
Related Work Experience	Teaching/Research Assistant The University of Western Ontario 2008-2012

Publications:

Atkinson, G. M., and **A. Babaie Mahani** (2013). Estimation of Moment Magnitude from Ground Motions at Regional Distances, *Bull. Seism. Soc. Am.* (in press).

Babaie Mahani, A., and G. M. Atkinson (2012). Regional Differences in Ground-Motion Amplitudes of Small-to-Moderate Earthquakes in North America, S*ubmitted to Bull. Seism. Soc. Am.*

Babaie Mahani, A., and G. M. Atkinson (2012). Evaluation of Functional Forms for the Attenuation of Small-to-Moderate-Earthquake Response Spectral Amplitudes in North America, *Bull. Seism. Soc. Am.* **102,** 2714-2726.